Dynamics and Control of T Follicular Helper Cell-Dependent and -Independent Responses to Influenza Virus Infection and Immunization

Wenbo Jiang

Submitted in total fulfilment of the requirements of the degree of

Doctor of Philosophy

February 2021

Department of Microbiology and Immunology

Faculty of Medicine, Dentistry and Health Sciences

The University of Melbourne

Abstract

Seasonal influenza viruses circulate globally and cause recurrent disease in humans. Worldwide, annual epidemics are estimated to cause 1 billion infections, with 3–5 million cases of severe illness and 290,000–650,000 deaths. Influenza viruses undergo rapid antigenic evolution allowing mutant viruses to escape from host immune responses acquired to parental virus strains. Current seasonal influenza vaccines are effective when vaccine strains are matched with circulating strains. However, there is little to no cross-protection against antigenic variants, emerging pandemic or zoonotic outbreak strains. There is therefore tremendous interest in the development of novel "universal" vaccines which induce potent, broad and durable antibody responses against most or all influenza viruses. T follicular helper (Tfh) cells are crucial for the generation of high-affinity antibodies and the maintenance of B cell memory. But relatively little is known about Tfh in important animal models of influenza. Insights gained from the study of Tfh cell responses will facilitate the design of next-generation vaccines against influenza.

In this thesis, we first developed an activation-induced marker (AIM) assay for the identification of antigen (Ag)-specific Tfh cells in mice after influenza virus infection and hemagglutinin (HA) protein immunization. We showed that the AIM assay was robust and sensitive for the detection of murine Ag-specific Tfh cells by quantifying the upregulation of surface CD154 or CD25/OX40 following either HA peptide pool or whole HA protein stimulation for 18 hours. This murine AIM assay makes it feasible to delineate Ag-specific Tfh cells in mice without the need for transgenic mice or MHC-II tetramers restricted to specific epitopes. Importantly, Ag-specific Tfh cells can be sorted for TCR sequencing or adoptive transfer since AIM assay is a live cell assay.

Ferrets are a well-established animal model for influenza research and are widely used to investigate the pathogenesis and transmission of influenza viruses and pre-clinically evaluate the efficacy of influenza vaccines. However, little is known about ferret Tfh cells due to the lack of ferret-reactive immunological reagents. To enable the study of ferret Tfh cells, we screened commercial markers of Tfh cells (anti-BCL6, CXCR5 and PD-1 antibodies) and found two anti-BCL6 antibodies had cross-reactivity with lymph node (LN) cells from influenza-infected ferrets. We also developed two murine monoclonal antibodies against ferret CXCR5 and PD-1 using a single B cell PCR-based method. We were able to clearly identify Tfh cells in LNs from influenza infected ferrets using these antibodies. The development of ferret Tfh marker antibodies and the identification of ferret Tfh cells will facilitate the assessment of vaccine-induced Tfh responses in the ferret model and the design of novel vaccines against influenza infection.

HA stem is an attractive target for the development of universal influenza vaccines due to its relatively conserved feature. However, HA stem is poorly immunogenic when administered alone in a soluble form. Immunogen multimerization can enhance the immunogenicity of poor immunogens even in the absence of the help of T cells, which serves as an alternative pathway to improve the immunogenicity of stem without the dependence on Tfh responses. We showed that chemically coupling a peptide derived from the head domain of PR8 HA (P35) with the weakly immunogenic HA stem protein caused aggregation of the HA stem which significantly enhanced stem-specific B cell responses independent of Tfh cell help in mice. P35 conjugation represents a new pathway to boost stem-specific antibody responses without introducing exotic carrier proteins which will elicit anti-carrier responses.

Collectively, we investigated Tfh responses to influenza virus infection and immunization in mice and ferrets and explored the effects of immunogen multimerization on humoral immunity in the context limiting Tfh responses to HA stem. An increased understanding of Tfh-dependent and -independent mechanisms to enhance humoral immune responses will assist developing novel vaccines to prevent the infection of influenza and other viruses.

Declaration

This is to certify that:

1. This thesis comprises my original work towards the Ph.D. except where indicated in the Preface.

2. Due acknowledgements have been made in the text to all other material used.

3. This thesis is less than 100,000 words in length, exclusive of tables, figures, references and appendices.

_____

Wenbo Jiang

Preface

Work for this thesis was performed in the Kent Laboratory, Department of Microbiology and Immunology, The University of Melbourne, at The Peter Doherty Institute for Infection and Immunity, Victoria, Australia. This was conducted under the supervision of Prof Stephen Kent, Dr Jennifer Juno and Dr Adam Wheatley. This PhD thesis contains a published research article and articles that have been submitted for publication:

Chapter 2 is included as a PDF file of the published manuscript:

- **Wenbo Jiang**, Kathleen M. Wragg, Hyon-Xhi Tan, Hannah G. Kelly, Adam K. Wheatley, Stephen J. Kent, Jennifer A. Juno. **Identification of murine antigen-specific T follicular helper cells using an activation-induced marker assay**. *J Immunol Methods.* 2019 Apr; 467:48-57.

  Author contributions: WJ designed the study, performed experiments, analysed data and drafted the manuscript. KMW provided assistance with mouse organ processing. HXT provided assistance with mouse infection and immunization. HGK provided assistance with mouse organ collection. Supervisors AKW, SJK and JAJ designed the study and edited the manuscript.

Chapter 3 is included as a PDF file of the published manuscript:

- Wenbo Jiang, Julius Wong, Hyon-Xhi Tan, Hannah G Kelly, Paul G Whitney, Ian G Barr, Daniel S. Layton, Stephen J Kent, Adam K Wheatley, Jennifer A Juno. **Screening**

and development of monoclonal antibodies for identification of ferret T follicular helper cells. *Sci Rep. 2021 Jan 21;11(1):1864.*

Author contributions: WJ designed the study, performed experiments, analysed data and drafted the manuscript. JW provided assistance with single cell PCR. HXT provided assistance with mouse immunization. HGK performed the experiment of macaque lymph node sample staining. PGW provided ferret samples and drafted the manuscript. IGB provided ferret samples. DSL provided ferret CD4 antibody. Supervisors SJK, AKW and JAJ designed the study and edited the manuscript.

Chapter 4 is included as a PDF file of the published manuscript:

- Wenbo Jiang, Emily H Pilkington, Hannah G Kelly, Hyon-Xhi Tan, Jennifer A Juno, Adam K Wheatley, Stephen J Kent. **Aggregation by peptide conjugation rescues poor immunogenicity of the HA stem**. *PLoS One. 2020 Nov 2;15(11):e0241649.*

  Author contributions: WJ designed the study, performed experiments, analysed data and drafted the manuscript. EHP performed the experiment involving dynamic light scattering and zeta potential and drafted the manuscript. HGK provided assistance with mouse organ collection and processing. HXT provided assistance with probe making. Supervisors JAJ, AKW and SJK designed the study and edited the manuscript.

Other publications during candidature (see Appendix for published manuscripts):

- Hannah G. Kelly, Hyon-Xhi Tan, Jennifer A. Juno, Robyn Esterbauer, Yi Ju, **Wenbo Jiang**, Verena C. Wimmer, Brigette C. Duckworth, Joanna R. Groom, Frank Caruso, Masaru Kanekiyo, Stephen J. Kent, and Adam K. Wheatley. **Self-assembling influenza nanoparticle vaccines drive extended germinal center activity and memory B cell maturation**. JCI Insight. 2020 May 21;5(10):136653.

  Author contributions: WJ assisted with the experiments involving mouse activation induced marker assay. This work does not form part of this thesis.

Acknowledgements

I'm grateful to all the people who have helped me in various ways during my PhD. First and foremost, I want to thank my supervisors Prof Stephen Kent, Drs Jennifer Juno and Adam Wheatley for their guidance for the projects. I am extremely grateful to Stephen for giving me the opportunity to do my PhD in Kent lab and helping with scholarship deferral when I was waiting for the Visa. During these years, his open-mindedness and inclusiveness have impressed me and are valuable intangible assets I gain from him. His knowledge and personality will continue to influence me in my future career no matter in academic field or industrial field. I am also thankful to Jen and Adam for imparting their superb T cell and B cell skills to me. I am lucky to have both a T cell expert and a B cell expert as co-supervisors who guide me working on projects at the interface of T and B cells. Without either of them, the projects would not be completed.

I would like to thank Wheatley and Juno group members, Hyon-Xhi, Hannah, Julius, Yi, Robyn, Kathleen, Isaac, Kirsty, Mai and Mingyang for their help in my experiments. Thank Hyon-Xhi and Hannah for helping me with mouse experiments. Thank Robyn, Hannah and Mingyang for helping me with protein purification. Thank Kathleen for helping me with flow cytometry. A special thank you to Julius, for helping me with PCR and all ferret works.

I also want to thank the lab management and maintenance team, Jane, Thakshila, Vinca, and Sriveni. Thank Jane for ordering reagents and supplies, managing funding and organising annual lab retreat. Thank Thakshila for general lab trainings, updating SOPs and managing safety issues. Thank Vinca and Sriveni for helping with lab maintenance and doing lab chores. All their work to keep the lab running smoothly allowed me and other people in the lab to focus on their research with minimal distraction.

I would also like to thank other members in Kent family, Emily, Wen Shi, Kevin, Worley, Amy, Ester, Timon, Sam, Ebene, Milla for all the parties, diners and games we have experienced together. All of the pleasant time we spend together will become wonderful memories of my life in Melbourne.

I am very grateful to our collaborators, without whom some of the aims of my thesis would not be achieved. I want to thank Dr Paul Whitney and Prof Ian Barr (WHO) for generously providing us with ferret samples. I also want to thank Dr Daniel Layton (CSIRO) for kindly providing us with ferret CD4 antibodies.

I also want to express my heartfelt appreciation to the members of my PhD committee, Prof Patrick Reading, Dr Linda Wakim and Dr Joanna Groom, for their insightful comments and constructive suggestions on my projects.

Finally, my gratitude goes to my friends and family. I want to thank my friends in Doherty Institute, Xiaoxiao, Huimeng, and Wuji for their company and encouragement throughout my PhD. A special thank you to my girlfriend, Yuwei, for cheering me up whenever I am depressed. Lastly, I want to express my deepest gratitude to my parents and brother for their constant love and support.

Table of Contents

Abstract ..... **I**

Declaration ..... **IV**

Preface ..... **V**

Acknowledgements ..... **VIII**

Table of Contents ..... **X**

List of Figures ..... **XV**

List of Tables ..... **XVII**

Abbreviation list ..... **XVIII**

Chapter 1: General Introduction **1**

1.1 Global burden of Influenza disease **2**

1.1.1 Seasonal influenza 2

1.1.2 Pandemic influenza 3

1.1.3 Zoonotic influenza 5

1.2 Influenza virus **6**

1.2.1 Classification and nomenclature 6

1.2.2 Genome structure and organisation 8

1.2.3 Antigenic drift and antigenic shift 11

1.3 Influenza vaccines **12**

1.3.1 Seasonal influenza vaccine 12

1.3.2 The quest for a universal influenza vaccine 14

1.4 Animal models to study human influenza infection **20**

1.4.1 Mice 20

1.4.2 Ferrets 21

1.4.3 Nonhuman Primates (NHP) 23

1.5 Humoral immune response to influenza virus infection and immunisation **26**

1.5.1 Antibodies against HA 26

1.5.2 Antibodies against NA 27

1.5.3 Antibodies against other proteins of influenza virus 27

1.5.4 Fc-mediated functions of antibodies 28

1.6 Germinal centre response and T follicular helper cells **29**

1.6.1 B cell activation 29

1.6.2 Germinal centre response 30

1.6.3 T follicular helper cells 34

1.7 Identification of Ag-specific Tfh cells **36**

1.8 Role of Tfh during immunisation **38**

1.8.1 Circulating Tfh 38

1.8.2 Tfh responses to immunisation 39

1.8.3 Linked recognition and conjugate vaccines 40

1.8.4 Tfh and immunogenicity 41

1.9 Unconventional T cells and T-cell independent B cell responses **42**

1.9.1 Unconventional T cells supporting B cell responses 42

1.9.2 T-cell independent B cell responses 43

1.10 Multimeric vaccine antigens **44**

1.10.1 Protein aggregates 44

1.10.2 Nanoparticles 46

1.11 Thesis overview **48**

Chapter 2: Identification of murine antigen-specific T follicular helper cells using an activation-induced marker assay **49**

Abstract **50**

Introduction **50**

Materials and methods **52**

Mouse infection and immunization 52

Antigen stimulations and cell culture 52

Antibodies and flow cytometry 53

Cell sorting and culture 55

Statistical analysis 55

Results **55**

Identification of Tfh cells in murine lymph node suspensions 55

Phenotype of Tfh cells following cell culture 55

Activation-induced marker expression to delineate Ag-specific Tfh cells 55

Kinetics of Ag-specific Tfh activation and viability 57

Maintenance of antigen-specific Tfh phenotype over time 57

CD154 and CD25/OX40 best identify Ag-specific Tfh cells 57

Detection of Ag-specific Tfh cells following whole protein stimulation 57

Discussion **57**

References **59**

Chapter 3: Screening and development of monoclonal antibodies for identification of ferret T follicular helper cells **60**

Abstract **61**

Introduction **61**

Results **62**

Screening of commercial anti-human or mouse BCL6, CXCR5 and PD-1 antibodies for 62

cross-reactivity with ferret lymph node cells 62

Homology analysis of ferret, human and mouse BCL6, CXCR5 and PD-1 62

Generation of mouse anti-ferret CXCR5 and PD-1 monoclonal antibodies 62

Validation of anti-ferret CXCR5 and PD-1 monoclonal antibodies by ELISA 62

Identification of Tfh cells in lymph node cells from influenza infected ferrets 62

Discussion **64**

Materials and methods **65**

Animals and ethics 65

Sequence analysis and recombinant protein generation 67

Sorting of ferret CXCR5 and PD-1 specific B cells 67

RT-PCR 67

Antibody generation 67

ELISA 68

FACS 68

References **69**

Chapter 4: Aggregation by peptide conjugation rescue poor immunogenicity of the HA stem **71**

Abstract **72**

Introduction **72**

Materials and Methods **74**

Mouse infection and immunization 74

Antigen stimulations and cell culture 74

Peptide and protein conjugation 74

Flow cytometry 74

ELISA 75

Dynamic light scattering and zeta potential 75

Statistical Analysis 75

Results **76**

P35-cysteine conjugation improves the immunogenicity of stem. 76

P35C improves the immunogenicity of stem in the absence of adjuvants. 76

P35C improves the immunogenicity of stem by an aggregation mechanism......79

Generalisability of the enhanced immunogenicity of P35C conjugations to other proteins......80

Discussion.....**82**

Reference.....**84**

Chapter 5: General Discussion.....**91**

5.1 Integrated findings of this thesis.....**92**

5.2 Summary of experimental studies.....**96**

5.3 Comparison of CD154 and CD25/OX40 as the makers for identifying Ag-specific Tfh cells.....**97**

5.4 The viability of Tfh cells during culture.....**103**

5.5 Ferret T cell responses to influenza virus infection and immunization.....**104**

5.6 Ferrets as a model for SARS-CoV-2.....**107**

5.7 Tfh dependent-enhancement of stem-specific antibody responses.....**109**

5.8 Tfh independent-enhancement of stem-specific antibody responses.....**111**

5.8.1 Boosting stem-specific antibody responses by ferritin nanoparticles.....111

5.8.2 Boosting stem-specific antibody responses by peptide conjugation.....111

5.9 Concluding remarks.....**113**

Reference.....**115**

Appendix.....**141**

List of Figures

Chapter 1

Figure 1.1 The History of Pandemic Influenza. 5

Figure 1.2 RNA segments of influenza A virus and their encoded proteins. 10

Figure 1.3 Schematic diagram of influenza A virus particles. 11

Figure 1.4 Cyclic re-entry model for affinity-based selection in the GC. 33

Figure 1.5 T follicular helper (Tfh) cell and Germinal center (GC) B cell. 37

Chapter 2

Figure 1. Identification of Tfh cells in mouse mediastinal lymph node (mLN). 51

Figure 2. Confirmation of Tfh phenotype following tissue culture. 52

Figure 3. Activation-induced marker expression following mitogenic or antigen-specific stimulation. 53

Figure 4. Kinetics of Tfh cell activation marker expression and Tfh cell viability in cell culture. 54

Figure 5. Comparison of PD-1 and activation marker expression on HA-stimulated Tfh cells over time. 55

Figure 6. Comparison of activation markers for identifying Ag-specific Tfh cells. 56

Figure 7. Modification of assay for whole protein stimulation. 58

Chapter 3

Figure 1. Cross-reactivity of commercial anti-human/mouse BCL6 antibodies with lymph node cells from influenza infected ferret. 63

Figure 2. Flow chart to develop mouse anti-ferret CXCR5 and PD-1 monoclonal antibodies. 64
Figure 3. Binding activity of anti-CXCR5 and PD-1 antibodies with autologous and control antigens. 65
Figure 4. Identification of Tfh cells in lymph node cells from influenza infected ferrets. 66
Figure 5. The nucleic acid sequences of variable domains of anti-ferret CXCR5 and PD-1 antibodies. 68

Chapter 4

Figure 1. Stem-specific B cell and serological responses in immunized mice. 77
Figure 2. Bulk GC B and Tfh cell responses in immunized mice. 78
Figure 3. P35C improves the immunogenicity of stem in the absence of adjuvants. 79
Figure 4. P35C improves the immunogenicity of stem by an aggregation mechanism. 80
Figure 5. HEL/OVA/gp120-specific B cell responses in immunized mice. 81
Supplementary Figure 1. Binding activity of anti-HA stem monoclonal antibodies with PR8 HA stem or P35C-stem. 88
Supplementary Figure 2. Activation-induced marker expression of mLN cells from influenza-infected mice following stimulation. 89

Chapter 5

Figure 1. Immunodominance hierarchy of Tfh responses and CD4 T cell responses. 94
Figure 2. Activation-induced CD154 and CD25/OX40 expression identifies both common and distinct populations of antigen-specific Tfh cells. 99
Figure 3. Activation-induced CD154 and CD25/OX40 expression following single peptide stimulation.....101

Figure 4. Tfh-dependent and -independent approaches to enhance stem immunogenicity. ..110

List of Tables

Chapter 1

Table 1.1 Cumulative number of human cases for avian influenza H5N1 and H7N9. 6

Table 1.2 Pros and cons of different animal models for influenza research. 25

Table 1.3 Commercially available and unavailable monoclonal antibodies for ferret immunological study. 25

Chapter 3

Table 1. Antigen homology of ferret, human and mouse BCL6, CXCR5 and PD-1. 64

Chapter 4

Supplementary Table 1. Biophysical characterisation of stem protein and P35C-stem conjugates. 90

Chapter 5

Table 5.1 Tfh/CD4 T cell epitopes of PR8 HA in C57BL/6 mice. 94

Abbreviation list

Ab	Antibody
ADCC	Antibody-dependent cellular cytotoxicity
ADP	Antibody-dependent phagocytosis
Ag	Antigen
AIM	Activation induced maker
APC	Antigen-presenting cells
BCL6	B-cell lymphoma 6
BCR	B cell receptor
CD	Cluster of differentiation
Con A	Concanavalin A
cTfh	Circulating T follicular helper
CXCR	C-X-C motif chemokine receptor
DC	Dendritic cell
GC	Germinal centre
HA	Hemagglutinin
HEL	Hen egg lysozyme
HI	Hemagglutination inhibition
HIV	Human immunodeficiency virus
HPAI	Highly pathogenic avian influenza
IAV	Influenza A virus
IBV	Influenza B virus
ICV	Influenza C virus
IDV	Influenza D virus

ICOS	Inducible costimulator
ICS	Intracellular cytokine staining
IgG	Immunoglobulin G
IFN	Interferon
IL	Interleukin
KLH	Keyhole limpet hemocyanin
LAIV	Live-attenuated influenza vaccine
mAb	Monoclonal antibody
MHC	Major histocompatibility complex
NA	Neuraminidase
NHP	Nonhuman primate
NK	Natural killer
OVA	Ovalbumin
PD-1	Programmed cell death protein 1
PD-L1	Programmed death-ligand 1
PMA	Phorbol 12-myristate 13-acetate
QIV	Quadrivalent influenza vaccine
TCR	T cell receptor
Tfh	T follicular helper
Tfr	T follicular regulatory
TIV	Trivalent influenza vaccine
TLR	Toll-like receptor
VLP	Virus-like particle

Chapter 1: General Introduction

Chapter 1: General Introduction

1.1 Global burden of Influenza disease

1.1.1 Seasonal influenza

Influenza is an infectious respiratory disease that is caused by influenza viruses. There are three broad threats to human health caused by influenza: seasonal (epidemic) influenza, pandemic influenza and sporadic cases of zoonotic influenza transmission from animal hosts[1]. Seasonal influenza viruses circulate in all geographical regions of the world and cause recurrent disease in humans. It is estimated that children under the age of 10 catch influenza once every two and a half years[2]. The frequency of infection declines initially with age, but it becomes steady after the age of 30, adult over 30 catching influenza approximately once every five years[2]. In temperate regions, seasonal influenza usually outbreaks in winter, whereas in tropical regions, influenza may irregularly outbreak throughout the year[3]. Worldwide, these annual epidemics are estimated to encompass 1 billion infections, with 3–5 million cases of severe illness and 290,000–650,000 deaths[4]. Although all age groups can be infected with influenza viruses, pregnant women, young children (<59 months old), older adults (>65 years old) and people with chronic diseases and immunosuppressed individuals are more prone to become severe cases after infection[3].

In addition to the substantial health burden, influenza causes a tremendous economic burden to humans, including medical care costs and productivity loss[5,6]. The estimated total economic burden of annual influenza epidemics to the healthcare system and society was $11.2 billion in United States alone, with $3.2 billion of direct medical costs to the healthcare system and $8.0 billions of indirect costs due to productivity loss[5].

1.1.2 Pandemic influenza

An influenza pandemic occurs when a novel influenza virus, previously not circulating among humans, emerges and spreads rapidly around the world due to a lack of pre-existing immunity within the population [7]. Four pandemics have occurred in the past century[1].

In 1918, an H1N1 influenza strain emerged and caused more than 40 million deaths (Figure 1.1)[8,9]. It killed more people than World War I and is the worst pandemic in recorded history[8]. The origin of the 1918 pandemic has been subject to debate and the most likely origin of the pandemic was Haskell County, Kansas[10,11]. In the spring of 1918, a mild respiratory disease started in military camps at Fort Funston, Kansas[10]. The disease spread throughout the United States and then transported by troopships to Europe and the rest of the world[10]. In Spain, a neutral country in World War I without news censorship, the outbreak was widely reported by news media and was soon referred to as the "Spanish flu"[10,11]. It is proposed that the 1918 pandemic virus is a reassortant of an avian and a mammalian influenza virus and it seems that the reassortant circulated in a mammalian host for a few years before it transmitted to humans[9,10]. However, others propose that the 1918 pandemic virus was directly transmitted from birds to humans[12].

About forty years later, in February 1957, a new pandemic outbroke in the Guizhou province of southern China before reaching Hong Kong and further spread around the world[10,13]. This pandemic was known as the Asian flu, and it caused more than one million deaths worldwide[9,10]. In May 1957, a virus of H2N2 the subtype which caused the outbreak was isolated in Japan[10]. Genetic and biochemical analyses revealed that the 1957 pandemic virus was a reassortant of

human and avian viruses[10]. Three gene segments (HA, NA, and PB1) of avian virus origin had moved into the previous H1N1 virus, thus producing the new H2N2 subtype[10,13].

History repeated itself around a decade later. A virus of the H3N2 subtype was isolated in Hong Kong in July 1968, which soon spread around the world[10]. This new pandemic was known as the Hong Kong flu. Again, the virus caused this pandemic originated from reassortment between human and avian viruses, with the HA and PB1-coding genes coming from an avian source[13]. The Hong Kong flu is estimated to have caused approximately one million deaths worldwide, and the variants of the H3N2 virus are still circulating in humans[8,9].

The most recent pandemic, also known as Swine flu, likely emerged from Mexico in April 2009[8]. In mid-April, genetically similar H1N1 influenza A viruses of swine origin were almost simultaneously detected in specimens collected in southern California and Mexico[10]. The new pandemic virus spread rapidly between humans across different continents and claimed more than 200,000 lives, and the variants of this pandemic virus are still circulating in humans as a seasonal influenza virus[9]. Sequence and phylogenetic analyses indicated that the pandemic virus was a quadruple reassortant of North American avian virus (PB2 and PA genes), human H3N2 virus (PB1 gene), classic swine virus (HA, NP, and NS genes) and Eurasian avian-like swine virus (NA and M genes)[10].

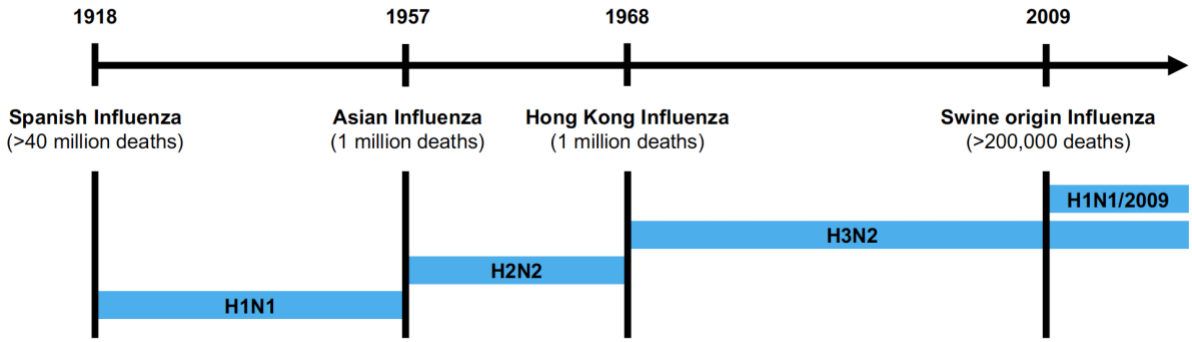


Figure 1.1 The History of Pandemic Influenza. In 1918, "Spanish Influenza" caused by a H1N1 strain emerged and resulted in more than 40 million deaths. About forty years later, in 1957, a H2N2 pandemic called "Asian Influenza" outbroke and caused more than one million deaths. A virus of the H3N2 subtype was isolated in Hong Kong in July 1968, which soon spread around the world. The "Hong Kong Influenza" is estimated to have caused approximately one million deaths. The most recent pandemic, also known as Swine Influenza, likely emerged from Mexico in April 2009. The new pandemic claimed more than 200,000 lives.

1.1.3 Zoonotic influenza

In addition to pandemics and annual seasonal epidemics, there are irregular and unpredictable local outbreaks caused by zoonotic influenza viruses transmitted from animal to humans. Humans can be infected with avian-origin (such as H5N1 and H7N9) and swine (such as H1N1v and H3N2v) influenza viruses[14]. (When influenza viruses normally circulating in swine are detected in humans, such viruses are called "variant" viruses, with a "v" placed after the subtype of the virus, e.g. H1N1v or H3N2v, in order to differentiate them from antigenically and genetically distinct human seasonal influenza H1N1 and H3N2 viruses[15].) These zoonotic influenza viruses have resulted in about 3000 cases of human infection to date[16,17]. The vast majority of these infections were caused by H5N1 and H7N9 viruses, both of which have

mortality rates above 30%[18]. The first known human infection with H5N1 dated back to 1997 when H5N1 outbroke in the live poultry markets in Hong Kong[19,20]. Since then, H5N1 continues to circulate in healthy duck populations and intermittently causes outbreaks in humans[19,20]. It has resulted in 455 deaths out of 861 cases in 17 different countries as of February 2020, with a case fatality rate of 53% (Table 1.1)[16]. The emergence of human infection with H7N9 was first reported in March 2013 in eastern China[19,21]. From then on, H7N9 has caused seasonal waves of zoonotic infections and has led to hundreds of lethal human infections in China[19,21]. At the end of December 2019, it has resulted 616 deaths from 1,568 human cases in China, with a case fatality rate of 39%[17]. These zoonotic influenza viruses pose a great threat to human health and have the potential to become next pandemic due to a lack of pre-existing immunity in human population. Thus, an increased understanding of the humoral and cellular immune responses to these influenza viruses is required to guide the development of novel influenza vaccines to combat the next pandemic.

Table 1.1 Cumulative number of human cases for avian influenza H5N1 and H7N9.

Subtype	H5N1	H7N9
Year	1997-2020*	2013-2020*
Areas affected	Asia, Africa and North America	China, Malaysia, Canada
Deaths	455	616
Cases	861	1568
Fatality rate	53%	39%

*Information updated to April 2020[16,17]

1.2 Influenza virus

1.2.1 Classification and nomenclature

Influenza viruses are members of the Orthomyxoviridae family of enveloped, negative-sense, single-strand RNA viruses with segmented genomes[10]. Based on the sequence and antigenicity

of nucleoprotein (NP), influenza viruses are classified to 4 types, influenza A virus (IAV), influenza B virus (IBV), influenza C virus (ICV) and influenza D virus (IDV)[3].

IAV are further divided into different subtypes according to the sequence and antigenicity of the viral HA and NA. To date, 18 subtypes of HA and 11 subtypes of NA have been identified[22,23]. 18 subtypes of HA can be classified into two phylogenetically distinct groups. Group 1 consists of H1, H2, H5, H6, H8, H9, H11, H12, H13, H16, H17, and H18, and group 2 comprises H3, H4, H7, H10, H14, and H15[22]. Except for H17N10 and H18N11, which were recently isolated from bats [23], the other 16 HAs and 9 NAs were isolated from wild aquatic birds which are considered the natural reservoir of IAV[24]. There are currently about 103 known subtypes of influenza A virus out of the theoretically possible 144 HA-NA combinations circulating among wild aquatic birds[25].

IBV are broken down into two antigenically distinct lineages, B/Victoria/2/1987 lineage and B/Yamagata/16/1988 lineage[3]. ICV and IDV are not classified into different subtypes or lineages[3]. Approximately 75% of all human seasonal influenza cases result from IAV infection, and the remaining 25% of infection is caused by IBV [26]. Although IBV can cause severe disease, it does not pose a pandemic threat to humans due to the lack of an animal reservoir. Currently, influenza A/H1N1, A/H3N2, B/ Victoria and B/ Yamagata viruses are co-circulating in humans every year. Other subtypes of IAV which have been documented to cause human infections include H2, H5, H6, H7, H9 and H10 [27]. Human ICV infection is generally mild or asymptomatic, and thus, it does not present a substantial public health concern[3]. IDV primarily infects cattle and no case of human infection with IDV has been reported so far[3]. This thesis focusses primarily on IAV since all known pandemics to date and most seasonal epidemics are caused by IAV.

Current nomenclature for the designation of influenza viruses was revised by the WHO in 1980[28,29]. The strain designation for influenza viruses contains information on 1) the antigenic type of the virus (A, B, C or D, based on the antigenic specificity of the nucleoprotein), 2) the host of origin (for strains isolated from non-human sources), 3) geographical origin, 4) strain number, 5) year of isolation and 6) the subtype the HA and of the NA antigens (for influenza A viruses)[28,29]. For example, a type A virus isolated in 2013 in Shanghai with a strain number of 2 and an H7N9 subtype is designated: A/Shanghai/2/2013 (H7N9).

1.2.2 Genome structure and organisation

IAV and IBV possess eight RNA segments: polymerase basic 2 (PB2), polymerase basic 1 (PB1), polymerase acid (PA), hemagglutinin (HA), nucleoprotein (NP), neuraminidase (NA), matrix/membrane protein (M), non-structural protein (NS), whereas ICV and IDV contain seven RNA segments (PB2, PB1, polymerase 3 (P3), hemagglutinin-esterase-fusion (HEF), NP, M and NS[4,10,30].

The three largest RNA segments of IAV encode the three polymerases: PB2 (segment 1), PB1 (segment 2), and PA (segment 3) which form RNA polymerase complex and are responsible for viral RNAs (vRNAs) transcription and replication (Figure 1.2)[10,13]. PB1 segment also encodes another two proteins: PB1-F2 (a proapoptotic factor) and PB1-N40 (function unknown) using alternative open reading frames[10,13]. Segments 4, 5, and 6 encode HA, NA and NP, respectively. NP binds to the vRNA segments along with three polymerase proteins and plays a central role in the nuclear import of ribonucleoprotein (RNP) complex[10,13]. HA is the most important glycoprotein on the virion surface, which binds to sialic acid-containing receptors on host cells and mediates viral entry into host cells[10,13]. NA, another major glycoprotein on

the surface of virus particles, cleaves sialic acid on the surface of host cells during virus release[10,13]. Matrix protein (M1) which is the most abundant protein forming the matrix of virion is translated from the un-spliced mRNA of segment 7 while the membrane ion channel protein (M2) which is crucial for the uncoating of the virion is translated from the spliced mRNA of segment 7[4,10,13]. Unlike the M2 protein of IAV, BM2 protein of IBV is expressed by a stop-start mechanism[31]. The un-spliced mRNA of segment 8 encodes the multifunctional protein NS1 which has IFN antagonist activity whereas the spliced mRNA of segment 8 encodes nuclear export protein (NEP/NS2) which directs the nuclear export of RNPs[10,13].

The proteins encoded by IBV genome is similar to those of IAV genome except for segment 6. On top of NA, segment 6 of IBV encodes an additional protein NB which is an accessory protein dispensable for virus growth in cell culture[13,32]. In addition, the ion channel protein of IBV is called BM2 which functions similar to IAV M2 protein[13,32]. ICV and IDV contain one less RNA segment than IAV and IBV. However, the fourth RNA segment of ICV and IDV codes for the hemagglutinin-esterase-fusion (HEF) protein which combines the functions of the HA and NA[10]. The third polymerase protein of ICV and IDV is named P3 because it does not display acid charge features at neutral pH[10]. In addition, the ion channel proteins of ICV and IDV are called CM2 which are structurally analogous to to IAV M2 protein and IBV BM2 proteins[10,30].

The virion of influenza A virus consists of three sub-viral components: 1) an outermost envelope harbouring three transmembrane proteins HA, NA and M2 which project from the surface of the virus particle; 2) a middle layer formed by M1; and 3) an innermost component of RNP complex which is made up of viral RNA segments, the polymerase proteins (PB1, PB2, and PA), NP protein and minor amounts of NEP protein (Figure 1.3)[13,33]. The structure of IBV,

ICV and IDV virions is similar to that of IAV. IBV virions possess four proteins decorated in their envelope: HA, NA, NB, and BM2 while ICV and IDV virions have two proteins inserted in their envelope: HEF and CM2[10].

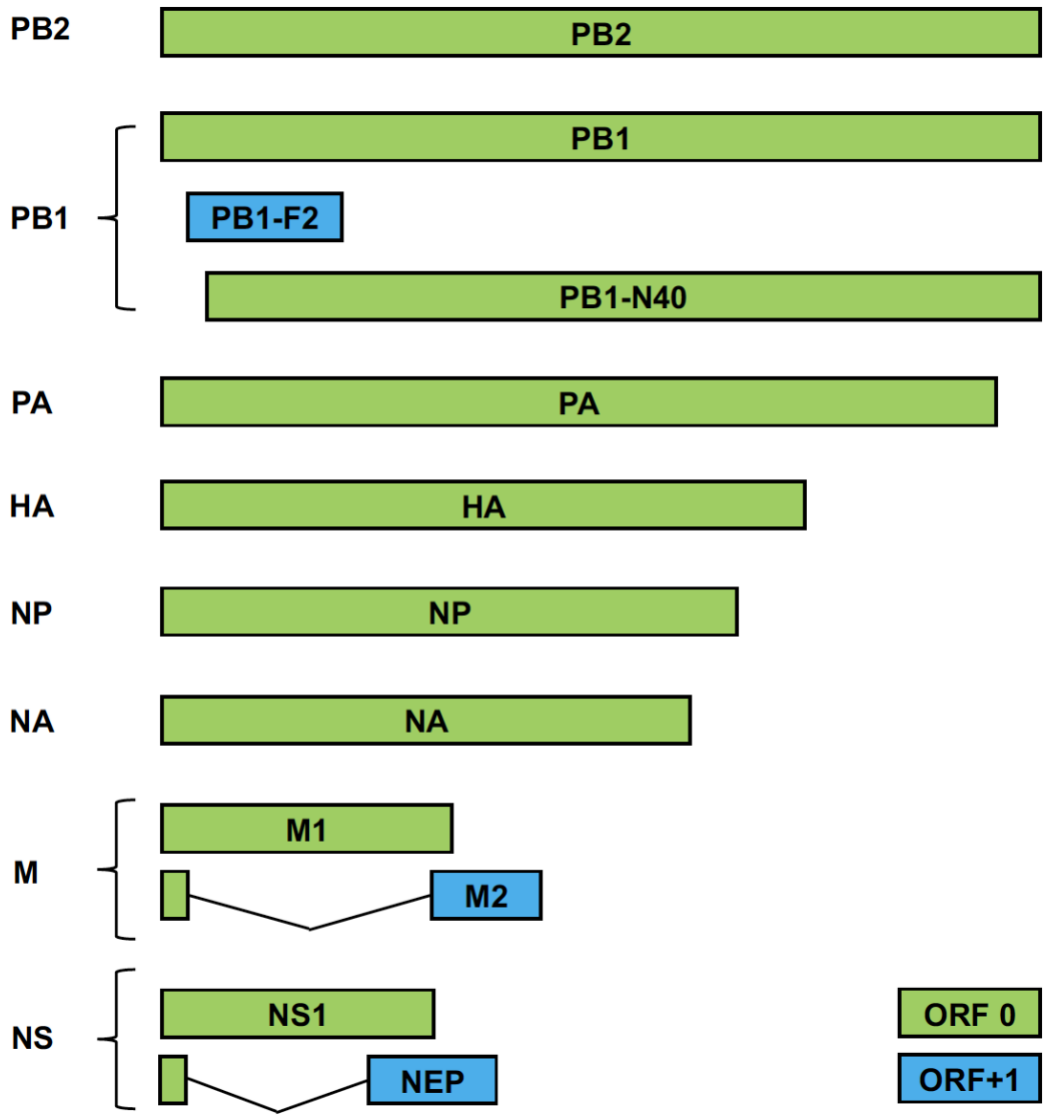


Figure 1.2 RNA segments of influenza A virus and their encoded proteins. The PB2, PA, HA, NP and NA segments contain one open reading frame (ORF) each and encode one protein. The PB1 segment possesses a second ORF generating the PB1-F2 protein and a third ORF generating the PB1-N40 protein. The M2 and NEP proteins are encoded by spliced mRNAs.

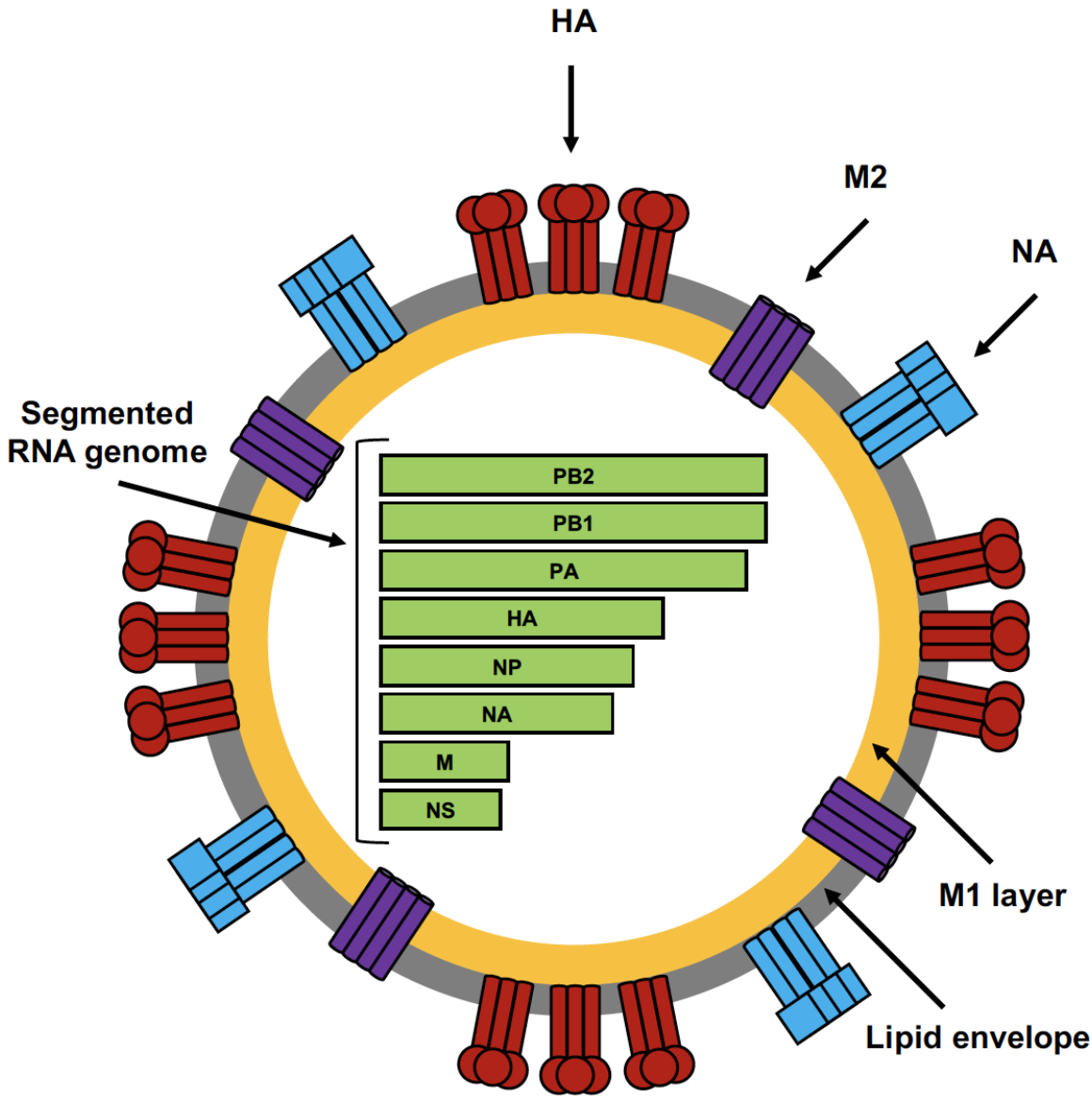


Figure 1.3 Schematic diagram of influenza A virus particles. The lipid envelope, HA, NA and M2 proteins form the outermost layer. M1 proteins form the middle layer. Viral RNA segments which are coated with PB2, PB1, PA and NP proteins form the innermost layer.

1.2.3 Antigenic drift and antigenic shift

The HA and NA genes of influenza viruses constantly mutate to evade host immune responses. Influenza viruses have two different ways of antigenic evolution: antigenic drift and antigenic

shift[10]. Antigenic drift results from accumulation of point mutations caused by the error-prone nature of RNA-dependent RNA polymerase in the HA or NA over time, which is a slow and gradual process[10]. Antigenic drift variants cannot be or are only inefficiently neutralized by antibodies against the "parental" virus strains, thus escaping host immunity[10]. Antigenic shift occurs as a consequence of reassortment between a circulating strain and a new virus with antigenically different HA and/or NA segment(s)[10,13]. Antigenic shift is usually concomitant with the emergence of a novel subtype of virus[10]. Since there is a lack of pre-existing population immunity to the new strain, antigenic shift causes pandemic with very high infection rates[10,13].

1.3 Influenza vaccines

1.3.1 Seasonal influenza vaccine

Currently, two broad types of influenza vaccine are commercially available: a live-attenuated influenza vaccine (LAIV), and an inactivated vaccine[34]. Inactivated vaccines can be further divided into three categories: whole inactivated (WIV), split, and subunit vaccines[34]. These vaccines are typically trivalent or quadrivalent formulations which contain antigen components derived from recently isolated strains (A/H1N1, A/H3N2, B/Victoria-like and/or B/Yamagata-like) that are thought most likely to circulate in the coming season[35].

Attenuated vaccine strains (LAIV) are generated by reverse genetic method, namely transfecting mammalian cells with two plasmids encoding the HA and NA of currently circulating strains and six plasmids encoding internal proteins of an attenuated cold-adapted strain[35]. The resulting recombinant virus has limited replicative ability in the human upper respiratory tract and is usually administered intranasally[35]. Intranasal administration of LAIV simulates the natural route of influenza infection, and induces strong local mucosal immunity,

cellular immunity and humoral immunity which can protect against following influenza infection[35,36]. However, LAIV is not recommended for use in children under 2 years, adults over 49 years, pregnant women, and people with a compromised immune system because the vaccine viruses may replicate to higher titres in these individuals, causing adverse effects[6,36,37]. In addition, US suspended the use of LAIV during the 2016–2017 and 2017–2018 seasons due to the lack of effectiveness against A(H1N1) pdm09 infection[38]. Although LAIV had been reinstated for use in the US in 2018-2019 season[38], it is hard to predict its effectiveness. More efforts should be put into the surveillance of circulating strain and the selection of vaccine strain to achieve better vaccine effectiveness[38]. Early inactivated vaccines comprise whole inactivated viruses (WIV) and this type of vaccines had been used until 1970s[35]. However, WIV administration usually results in both local and systemic reactogenicity[36]. WIV have been replaced with split virion vaccines which are considered to be less reactogenic[36]. Split vaccines are generated from inactivated influenza virions which are further disrupted by diethyl ether or detergent treatment[36]. Owing to their adequate immunogenicity and rare reactogenicity, split vaccines are the most widely used vaccines in global market at present[35]. Subunit vaccines are also now becoming frequently used in trivalent influenza vaccines (TIVs) or quadrivalent influenza vaccines (QIVs) formulations. The components of subunit vaccines are more defined and contain only HA and NA proteins[36]. The extra purification step makes subunit vaccines purer, but it also appears to make them less immunogenic. Therefore, adding adjuvants to subunit vaccine formulation is commonly needed to acquire adequate immunogenicity, particularly in the aged[36]. Although most influenza vaccines are administered unadjuvanted, Alum, MF59 and AS03 adjuvants are currently in use in human influenza vaccines[39]. These adjuvants improve antibody responses, and adjuvanted influenza vaccines are commonly used in vulnerable groups who generate poorer immune responses to unadjuvanted vaccines[39].

1.3.2 The quest for a universal influenza vaccine

The mechanism of protection of current seasonal influenza vaccines relies mainly on the induction of neutralizing antibody responses against immunodominant but highly variable HA head domain[40,41]. These vaccines are strain-specific and need to reformulate every year to maximize the protection efficacy since the HA genes of circulating strains are constant evolving[35]. The vaccine effectiveness largely depends on the extensive surveillance and accurate predictions of circulating strains[35]. Vaccination of these vaccines provides healthy adults with 70–90% protection when vaccine strains are well-matched with circulating strains[35,42]. However, the vaccine seed viruses are selected more than half a year before each epidemic season since vaccine production usually takes at least 6 months. As a result, mismatch between circulating strains and vaccine stains occurs occasionally[6,40,43]. The protection efficacy of these vaccines is low in years when there is a mismatch[35,42]. The vaccine efficacy against seasonal influenza virus infection is approximately 40% - 60% in recent years[44]. Furthermore, the majority of currently licensed vaccines are produced in egg-based vaccine platform[35,40]. Virus propagation in eggs sometimes results in adaptive mutations of the virus, which can exacerbate the antigenic mismatches[6,41].

Finally, these seasonal vaccines have an inherent limitation that they cannot protect against antigenically novel pandemic or zoonotic outbreak strains[40]. There is therefore growing interest in the development of novel universal vaccines that would provide broader and more durable protection against currently circulating and emerging pandemic or zoonotic outbreak influenza viruses. To address the shortcomings of current influenza virus vaccines, universal influenza vaccine development combines the strategy of redirecting the immune response toward conserved viral epitopes and the use of novel vaccine production platforms[41]. During the last

decade, two broad approaches have been used to develop universal influenza vaccines: one is a T cell-based approach, the other is an antibody-based approach.

1.3.2.1 T cell based universal influenza vaccines

The first approach is T cell based, which targets conserved internal proteins like NP and M1 to induce cross-reactive T cell responses[45]. Internal proteins (PB2, PB1, PA, NP, M1, NS1, NS2) of influenza virus are more conserved than surface proteins (HA, NA, M2), which makes them potential targets for a universal vaccine[41,46]. Antibodies to internal proteins are relatively ineffective in mediating protective immunity because they are generally not presented on the surface of virus particles or host cells[41]. However, internal proteins are abundant in infected cells where they are processed and presented on MHC molecules to T cells, which elicits T cell responses[41]. T cell responses play an important role in combating influenza disease[45]. Although T cells cannot prevent host cells from initially being infected, they are able to eliminate infected cells and ameliorate disease outcomes during infection[41]. A few T cell-based universal influenza vaccine candidates are in clinical development and display promising results[47]. Berthoud and Lillie et al. showed that Modified Vaccinia virus Ankara (MVA) vector encoding NP and M1 proteins (MVA-NP+M1) boosted robust T cell responses and provided protection against influenza virus challenge in adults and the elderly [48,49]. Pleguezuelos et al. demonstrated that FLU-v, a universal influenza vaccine candidate composed of 4 synthetic peptides from conserved epitopes of NP, M1 and M2 of IAV and IBV, elicited strong and long-lasting cellular immune responses and reduced clinical influenza symptoms in a phase IIb challenge study[50]. Despite tremendous efforts and progresses have been made, developing a T cell based universal influenza vaccine that provides broad coverage to individuals with diverse HLA haplotypes is still challenging[51,52].

1.3.2.2 Antibody based universal influenza vaccines

The other approach is antibody based, which targets conserved epitopes in the extracellular domain of surface proteins like HA, NA and M2 to elicit cross-protective antibodies[46]. Although vaccines can induce both antibody and cell-mediated immune responses, most current licensed vaccines confer protection against subsequent infection by eliciting protective antibodies.

1.3.2.2.1 M2 based universal influenza vaccines

Natural influenza infection can elicit antibodies to M2 proteins[10]. The M2 protein is a tetrameric ion channel which is crucial for the uncoating of the virion[10]. The M2 ectodomain (M2e), twenty-three amino acids on the N terminus which are exposed extracellularly, is highly conserved among influenza viruses[41]. Antibodies to M2e are generally not neutralizing and do not prevent infection, but they can mitigate disease outcome[41,53]. The mechanism of protection is in part due to Fc receptor mediate elimination of influenza virus-infected cells (discussed in more detail in section 1.5.4)[54]. M2e has become an attractive target for a universal influenza vaccine due to its conserved feature and the protection efficacy of M2e-targeting antibodies[41,46]. Many M2e-based vaccines have been evaluated in animal models and clinical trials[41,46]. Kim et al. designed a virus-like particle (VLP) vaccine displaying five tandem copies of the M2e (M2e5x) from human and zoonotic influenza viruses[55]. They found that M2e5x VLP vaccination elicited broadly cross-reactive antibody responses and provided full protection against lethal challenge of H1N1 and H3N2 viruses in mice[55]. Turley et al. demonstrated a fusion protein with four tandem copies of the M2e linking to a TLR5 ligand elicited high levels of M2e-specific antibodies and were safe and well tolerated in healthy adults[56].

1.3.2.2.2 NA based universal influenza vaccines

NA is the second major glycoprotein on the surface of virus particles, which facilitates virus release from the host cell by enzymatically cleaving the terminal sialic acids from glycans of host cell surface proteins[46]. As with HA, NA also undergoes antigenic changes, but it drifts more slowly than HA[41,46]. Antibodies against NA can reduce the duration of influenza symptoms in animals[46]. The protection mechanism is likely owing to the ability of anti-NA antibodies to inhibit NA enzymatic activity and reduce the spread of viruses[46]. These features make NA a potential target for a universal influenza vaccine[41]. Recently, several NA-targeting universal vaccine candidates have been developed and tested in animal models[46]. Broecker et al. generated a recombinant influenza virus with extended NA stalk domain in an attempt to overcome the HA immunodominance[57]. They found that formalin-inactivated viruses expressing stalk extended NA induced significantly higher anti-NA IgG responses than the inactivated wild-type viruses[57]. Kim et al. expressed a virus-like particle containing N1 NA (N1 VLP) and compared its immunogenicity and cross protective efficacy with inactivated split influenza vaccine in mice[58]. N1 VLP vaccination induced cross-reactive NA-inhibiting antibodies against H1N1, H5N1 and H3N2 viruses and conferred protection against challenge with H1N1, H5N1, and H3N2 viruses[58]. While NA-based universal influenza vaccines are attracting more attentions recently, many problems remain to be solved[59,60]. One major problem is the lack of reagents and functional assays for reliable evaluation of antibody responses to NA[59,60]. Although multiple studies showed that anti-NA antibodies contributed to protection against influenza in humans, the antibody titres which correlate with protection remain to be determined[59].

1.3.2.2.3 HA stem-based universal influenza vaccines

HA is the most important surface glycoprotein which mediates viral entry into host cells[10,13]. Influenza HA can be divided into two domains based on their functions[61]. The head domain contains the receptor-binding site via which the virus binds sialic acid receptors of the target cell, while the stem domain contains fusion peptide which mediates fusion between the viral envelope and the endosomal membrane of the host cell[10]. Unlike head domain which is highly variable, stem domain is relatively conserved among influenza viruses[61]. Additionally, anti-stem antibodies have been shown to provide cross-protection against both heterologous and heterosubtypic strains in mice[41,62]. The mechanisms of protection include direct inhibition of HA-mediated membrane fusion or elimination of virus infected cells by Fc receptor-mediated ADCC activity[63,64]. All these factors make stem domain an attractive target for universal influenza vaccine. However, stem domain is immune-subdominant compared with head domain[41]. Antibodies are mainly generated against the immunodominant HA head domain in the context of full-length HA[46]. Two different strategies have been proposed in an attempt to subvert the immunodominance of HA head domain[41].

The first strategy is to express headless stem protein[41]. Initial attempts were largely unsuccessful because it is not a natural protein and may not fold correctly[65]. In 2015, two groups successfully expressed correctly folded H1 stem trimer[66] and self-assembled H1 stem-containing ferritin nanoparticle vaccine by sophisticated structural approaches[65]. The H1 stem trimer vaccine conferred mice full protection against lethal challenge of H5 virus and also mitigated influenza disease in cynomolgus monkeys following sublethal challenge[66]. Similarly, the H1 stem-containing ferritin nanoparticle vaccine conferred full protection in mice and partial protection in ferrets against lethal challenge of H5 virus[65]. The safety and

immunogenicity of an H1 stem-containing ferritin nanoparticle vaccine are currently being evaluated in early phase clinical trials in healthy adults[67].

Another strategy is to sequential immunize animals with chimeric HA (cHA) in which heads from different HA subtypes were fused with a common stem to reduce anti-head domain antibodies and serially boost the antibody responses targeting stem domain[46]. Mice sequentially vaccinated with cHA containing a common H1 stem were protected against H5 and H6 (group 1) virus challenge, while mice sequentially immunized with cHA containing a common H3 stem were protected against H7 (group 2) virus challenge[68,69]. cHA-based universal influenza vaccine candidates have been evaluated in a phase 1 clinical trial[70]. The authors showed that cHA-based inactivated and live-attenuated vaccines immunization elicited cross-reactive serum IgG antibodies that targeted the stem domain and were tolerable in healthy adults[70].

In addition to the aforementioned strategies, another approach termed computationally optimized broadly reactive antigen (COBRA) has been used to develop universal influenza vaccines[71]. This approach uses an algorithm of multiple rounds of consensus generation to design an antigen which are able to induce broadly reactive immune responses[71]. Recently, Reneer et al. showed that H2 HA COBRA antigens induced broad neutralizing antibody responses against most H2 strains and conferred mice better protection against lethal challenge of H2 viruses compared to H2 HA wild-type antigens[71]. In another study, COBRA vaccine strategies tested in ferrets have shown that H5 HA COBRA antigens conferred full protection against lethal challenge of a heterologous H5N1 virus[72].

Despite progress in developing universal influenza vaccines, candidates are still being tested in pre-clinical or early stage clinical trials and none of them have been licensed yet[73]. The

breadth, potency and longevity of the immune responses induced by these vaccine candidates remain to be improved. The ultimate aim of developing a truly universal influenza vaccine may be achieved by combining two or more strategies discussed above.

1.4 Animal models to study human influenza infection

Animal models are essential for the investigation of the transmissibility of influenza viruses and pre-clinical evaluation of novel influenza vaccine candidates. Mice, ferrets and nonhuman primates are the most frequently used animal models in influenza virus research. Each of these species has its advantages and disadvantages (Table 1.2).

1.4.1 Mice

1.4.1.1 Susceptibility to influenza viruses and signs of disease

Several influenza strains (such as the 2009 H1N1 pandemic strains, highly pathogenic avian influenza (HPAI) H5N1 strains and several H7 strains) are able to directly infect laboratory mice[74-76]. However, most seasonal H1 and H3 IAVs and IBV human influenza isolates do not naturally infect laboratory mouse strains without prior adaptation[74-76]. Adaptation of the virus involves repeated passage in mouse lungs, which usually results in a number of mutations, increased replication ability and virulence in mice[75]. The drawback of this process is that the lab-adapted virus may be antigenically or phenotypically distinct from the "parental" strain[75]. Unlike humans, mice do not cough, sneeze or manifest high fever after influenza virus infection[74]. Typical clinical signs of mice following influenza virus infection include weight loss, ruffled fur, hunched posture and lethargy[74]. Of note, weight loss is an important quantitative readout for evaluating the vaccine efficacy in vaccination and challenge experiments[75,76].

1.4.1.2 Evaluation of influenza vaccines

Mice are used extensively as an animal model for studying influenza vaccine efficacy and immunological mechanisms that mediate protection against influenza virus due to their low cost, broadly available reagents and well-established techniques for genetic manipulation[75,76]. In particular, the ready access to specialised lymphoid organs permits the detailed study of immunity that is more difficult or expensive in larger animal models or humans. Overall, mice are an extremely useful model for primary screening of promising vaccine candidates and elucidating the immunological mechanisms of protection[75]. However, the predictive value of mouse models for successful vaccination of humans has been questioned[76]. Therefore, promising vaccine candidates should be examined in an additional animal model prior to further assessment in clinical trials[75,76].

1.4.2 Ferrets

1.4.2.1 Susceptibility to influenza viruses and signs of disease

The application of ferrets for studying influenza virus was first demonstrated by Wilson Smith in 1933 when the first human influenza virus was isolated[74,75]. Ever since, ferrets have been widely considered the best small-medium sized animal model to investigate the pathogenicity and transmissibility of influenza viruses[74,75]. Unlike mice, ferrets are naturally susceptible to most of human influenza isolates without prior adaptation, including seasonal A/H1N1, A/H3N2 and IBV[74,75]. This is due to similar lung physiology and distribution of sialic acid containing receptors in the respiratory tract of humans and ferrets[75,77]. These features enable accurate characterization of human isolates without adaptation-caused antigenic or phenotypic changes in ferrets[75]. Importantly, ferrets possess the ability to transmit viruses from infected animals to naive individuals via either direct contact or respiratory droplets[75,78]. Although most

ferret challenge studies use intranasal inoculation, natural transmission studies can also be employed for pathogenesis, treatment and vaccine studies in ferrets[74]. Furthermore, ferrets display human-like clinical symptoms which include fever, sneezing, nasal discharge, anorexia and lethargy upon infection with seasonal influenza viruses[74,75].

1.4.2.2 Evaluation of influenza vaccines

Ferrets have also been widely used for assessing the efficacy of influenza vaccines[75]. Recent efficacy studies of stem-based universal influenza vaccines in the ferret model demonstrated that ferrets are capable of generating cross-protective antibody responses to the HA stem domain[75,79]. Currently, the evaluation of the immune responses after influenza infection or immunization is limited to serological analysis, such as hemagglutination-inhibition (HI) assay and microneutralization (MN) assay[76].

Despite the inherent advantages of ferrets for influenza virus research, the in-depth study of their immunological response in the context of infection and vaccination has been hampered owing to a lack of commercially available ferret-specific reagents[80-84]. Screening of antibodies originally developed for other species for their cross-reactivity with ferret immune cell markers and cytokines gained limited success[85,86]. Currently, ferret-reactive CD3, CD4, CD8 and IFN-γ antibodies are commercially available (Table 1.3), which makes it feasible to study ferret CD4 and CD8 T cell responses. However, characterisation of various subsets of ferret CD4 T cells is not practicable since antibodies for the markers of different CD4 T cell subsets are not available. In particular, it has not been possible to date to resolved ferret T-follicular helper (Tfh) cells with current reagents. Since Tfh are critical to the induction of effective antibody responses, as shown in both humans and other animal models[87-90] (explored in further detail in section 1.8.2 below), this represents a significant gap in the utility of the ferret model.

Furthermore, while ferret cross-reactive CD79a and CD20 antibodies that can be used to identify ferret B cells are commercially available, no antibodies for ferret IgD (naïve B cell marker), CD27 (memory B cell marker) and CD138 (plasma cell marker) have been reported. Thus, characterisation of different subsets of ferret B cells and plasms cells is still not feasible at the moment. There is therefore an urgent need to develop ferret immunological reagents to interrogate immune responses following influenza virus infection and vaccination.

Importantly, ferrets serve as an animal model for the study of other viruses, including severe acute respiratory syndrome coronavirus 2 (SARS-CoV-2)[91]. This will be discussed in further detail in section 5.5, Chapter 5 (General Discussion).

1.4.3 Nonhuman Primates (NHP)

1.4.3.1 Susceptibility to influenza viruses and signs of disease

Non-human primates can be naturally infected with influenza viruses[92] and have been experimentally inoculated with most of the human influenza isolates, including seasonal A/H1N1, A/H3N2, pandemic A/H1N1, HPAI A/H5N1 and LPAI A/H7N9[74,75]. Of note, macaques do not commonly exhibit obvious signs of illness upon experimental infection with seasonal influenza viruses[74,75]. However, inoculation of macaques with highly virulent strains (such as A/H5N1 and 1918 A/H1N1) induces noticeable symptoms of disease including fever, cough, lethargy, bronchopneumonia and bronchiolitis[74,75].

1.4.3.2 Evaluation of influenza vaccines

Since the immune system of macaques is physiologically and anatomically similar to that of humans, macaques are regarded one of the best model for evaluation of the efficacy of human

influenza vaccines[75]. A few universal influenza vaccine candidates have been assessed in this model[75]. Although the immunogenicity data of human influenza vaccines obtained in macaques will be highly predictive, the high cost, complicated husbandry conditions and ethical issues make this model the least accessible model for influenza research[75,76].

Table 1.2 Pros and cons of different animal models for influenza research.

Species	Pros	Cons
Mice	• Low cost • Homogeneous responses • Good availability of immunological and biological reagents • Allows mechanistic studies (genetically modified mice)	• Majority of seasonal influenza viruses need to be adapted • Respiratory tract receptor distribution distinct from humans • Not suitable for transmission studies • Predictive value for vaccines is not always clear
Ferrets	• Human influenza virus isolates infection without adaptation • Human-like clinical signs and pathogenesis of disease • Respiratory tract receptor distribution analogous to humans • Suitable for transmission experiments	• Relatively expensive • Not easy to obtain specific pathogen free ferrets • Poor availability of immunological and biological reagents
NHP	• Susceptible to non-adapted human influenza virus isolates • Respiratory tract receptor distribution analogous to humans • Immune system similar to humans • Good availability of immunological and biological reagents • High predictive value of vaccine efficacy	• Very expensive • Ethical issues • Not easy to obtain specific pathogen free NHP • Lack of clinical signs upon seasonal influenza virus infection • Need of experienced personnel

Table 1.3 Commercially available and unavailable monoclonal antibodies for ferret immunological study.

Cell type	Antigen	Antibody clone	Source	Specificity	Cross-reactivity with ferret	Reference
T	CD3	CD3-12	Abcam	Human/Mouse	Yes	76
T	CD4	CSIRO	CSIRO	Ferret	Ferret specific	77
T	CD8	OKT8	Thermo	Human	Yes	78
T	IFNg	MTF14	Mabtech	Ferret	Ferret specific	78
T	PD-1	Many	Many	Human/Mouse	Unknown	Chapter 3 of this thesis
T/B	CXCR5	Many	Many	Human/Mouse	Unknown	Chapter 3 of this thesis
T/B	BCL6	K112-91	BD	Human/Mouse	Unknown	Chapter 3 of this thesis
B	CD79a	HM47	BioLegend	Human	Yes	78
B	CD20	71	Sino Biological	Ferret	Ferret specific	78
B	IgA/G/M	Polyclonal	LSBio	Ferret	Ferret specific	78
Innate	CD11b	M1/70	BioLegend	Human/Mouse	Yes	78

1.5 Humoral immune response to influenza virus infection and immunisation

1.5.1 Antibodies against HA

HA and NA are two major spike proteins on the virion surface and they are more accessible to B cell receptors compared with other viral proteins[13,93]. Therefore, most of the antibodies elicited by natural influenza virus infection are against HA and NA[10,13,93].

Antibodies to HA are widely viewed as the most important for virus neutralization[4]. Antibodies against HA head domain typically inhibit the binding between the viral HA and sialic acid-containing receptor of the host cell[93]. This type of antibodies can neutralize the virus before infection is initiated[93]. The neutralizing titre of these antibodies can be measured by microneutralization (MN) assay[13,93].

Antibodies against HA stem domain bind to HA on the surface of virus particles but normally do not prevent viral entry into the host cell[93]. Some anti-stem antibodies block the fusion of viral envelope and the endosomal membrane of the host cell and subsequent uncoating[10,93]. Of note, some anti-head antibodies that do not have hemagglutination-inhibition (HI) activity also function through this mechanism[93]. Furthermore, another type of stem-targeting antibodies binds to the cleavage site of HA0 and prevent host proteases from cleaving immature HA0 to mature HA1/HA2, which results in non-infectious virions[10,93].

Of note, there is a type of neutralizing antibodies targeting head domain do not have HI activity[93]. There also is a type of neutralizing antibodies targeting stem domain do not inhibit fusion or HA0 cleavage[93]. The neutralization mechanisms of these two types of antibodies are

not fully clear and possibly because the binding of these antibodies to HA causes steric hindrance to NA and prevents NA from releasing nascent virions from host cells[93,94].

1.5.2 Antibodies against NA

Antibodies to NA also have direct antiviral activity, although the level of NA-specific antibodies is lower than that of HA-specific antibodies[93]. NA antibodies can inhibit the enzymatic activity of NA[93]. This causes the inhibition of NA-mediated cleavage of sialic acids-containing mucins overlying the respiratory tract epithelium, thus preventing virus access to host cells[13,93]. This also results in the inhibition of NA-mediated removal of sialic acid from the cell surface, thus interfering the release of progeny virus[13,93]. By inhibiting these processes, anti-NA antibodies reduce viral replication efficiency and the spread of nascent virions for infection of neighbouring cells and finally mitigate disease severity[13].

1.5.3 Antibodies against other proteins of influenza virus

M2 is the third viral protein on the virion surface. Natural influenza infection can also induce M2-specific antibodies, although the titres are typically low[10]. M2-targeting antibodies do not neutralize influenza viruses, but they can ameliorate disease severity in animals[41,53]. In addition, antibodies against NP have been detected in individuals after natural virus infection[10]. Animal studies have shown that passive immunization of naïve mice with NP-specific polyclonal sera from recombinant NP protein immunized mice conferred protection against homosubtypic and heterosubtypic influenza viruses challenge[13]. Antibodies to M1 have also been reported in individuals following natural infection with H3N2 virus[93].

Although antibodies to different proteins of influenza virus are induced following infection or immunization, anti-HA head antibodies are the most potent for virus neutralization and anti-HA stem antibodies are the most broad-spectrum for cross-neutralization.

1.5.4 Fc-mediated functions of antibodies

On top of direct antiviral activity, some HA targeting antibodies have indirect antiviral effects mediated by the Fc portion of the antibody, including antibody-dependent cell mediated cytotoxicity (ADCC) and antibody-dependent cellular phagocytosis (ADCP) and complement mediated lysis[93]. Some HA head targeting antibodies that do not possess HI activity have Fc-mediated functions[93]. In contrast, it has been suggested that HA head targeting antibodies that possess HI activity have been argued little Fc-mediated functions since they block the binding between HA and the sialic acid receptor on effector cells, which is a second binding point required for optimal Fc-mediated effector functions of HA targeting antibodies[93,95-97]. Antibodies to NA have also been reported to have ADCC activity. Furthermore, anti-M2 antibodies was shown to protect mice from influenza virus challenge through Fc mediated effector functions[54]. Recently, Vanderven et al. demonstrated that antibodies to NP and M1 could also activate nature killer cells[98].

In summary, multiple proteins of influenza viruses can elicit antibody responses to different extent. An improved understanding of the initiation and control of humoral responses will accelerate the development of next generation vaccines against a wider range of influenza viruses.

1.6 Germinal centre response and T follicular helper cells

1.6.1 B cell activation

To initiate humoral immune responses, antigens have to be transported from the sites of infection or vaccination to the B cell areas of secondary lymphoid organs[99]. B cell activation is initiated by specific B cell recognition of antigen through the B cell receptor (BCR) complex which is composed of membrane Ig molecules and the associated Igα/Igβ proteins[99,100]. Igα/Igβ proteins contain immunoreceptor tyrosine activation motifs (ITAMs) which transmit transmembrane signalling[100]. Antigen binding results in BCR cross-linking and Src family kinase–mediated phosphorylation of the ITAM motifs, which is followed by the activation of intracellular signalling cascade required for B cell proliferation and differentiation[99,100].

In addition, the BCR can internalize the bound antigen into endosomal vesicles[99]. If the antigen is a protein, it is processed into peptides, loaded onto the MHC class II molecules, and presented on the B cell surface[99]. The peptide: MHC II complexes are recognized by cognate helper T cells which then upregulate surface CD154 (CD40L) expression[100]. The CD154 activates CD40 expressed by B cells, which serves as the second signal for B cell complete activation[101].

Although the signalling induced by antigen-BCR engagement is able to initiate B cell activation, by itself it appears inadequate to stimulate significant B cell proliferation and differentiation[99]. A second signal is needed for full B cell responses to be induced[101]. For thymus-dependent antigens (TD Ag), such as protein antigens, the second signal is provided by helper T cells as described above[101]. For thymus-independent antigens (TI Ag), such as the polysaccharides of bacterial cell walls, the second signal is derived from direct recognition of a microbial constituent such as LPS that can activate TLR signalling in the B cell[101]. Of note,

antibodies induced by TI Ag tend to have low affinity and be short-lived. However, TD Ag can induce high affinity antibodies through a process of affinity maturation which happens in the germinal centre with the help of helper T cells[101].

1.6.2 Germinal centre response

The germinal centre (GC) is a highly-specialised compartment that develops in secondary lymphoid organs after infection or vaccination when antigen activated B and T cells co-migrate to the B cell follicle[102-104]. The GC is the site of somatic hypermutation and affinity-based selection[102]. This selection ultimately leads to a GC with B cells have a higher affinity for the antigen[102]. Anatomically, GC is divided into two distinct compartments, dark zone (DZ) and light zone (LZ). DZ mainly comprises B cells which proliferate extensively while LZ consists of follicular dendritic cells (FDCs), Tfh cells and sparse B cells[102,105].

According to the cyclic re-entry model (Figure 1.4), affinity maturation is the outcome of repetitive Darwinian-like selection, and T follicular helper (Tfh) cells are the limiting factor driving affinity based selection[102]. B cells compete for Tfh help in a contact-dependent manner[106,107]. The contact is characterized by a short duration and extensive contact area, and the area of contact depends on levels of antigen presentation and ICOS co-stimulation[106]. B cell clones that possess a BCR with higher affinity capture more antigens and present more peptides on MHCII to Tfh cells[106]. Thus, the higher-affinity B cells are able to engage more stably with Tfh cells[106]. In the meantime, ICOS costimulatory signalling enhances calcium fluxes that drive CD154 (CD40L) externalization from an intracellular store to the surface of Tfh cells[106]. In turn, CD40 signalling drives B cell upregulation of ICOSL, which enhances its capability to entangle with Tfh cells in subsequent encounters[106]. As a result, higher affinity B

cells acquire more contact-dependent help in the light zone, then re-enter dark zone and undergo more cycles of proliferation in the dark zone[106].

Recently, Kennedy et al. identified two functionally distinct B cell populations that located at different areas in the DZ: proliferating DZ (DZp) cells and differentiating DZ (DZd) cells[108,109]. According to this new model, B cells that pass the selection in the LZ moved to canonical DZ, undergo proliferation and become DZp, the DZp then migrated to larger DZ to become DZd prior to re-entering the LZ[108,109].

B cells that survive the GC reaction ultimately exit from the light zone and differentiate into either plasma cells or memory cells[101,102]. Plasma cells are terminally differentiated B cells which secrete antibody into serum and secretions[99]. The master regulator of plasma cell differentiation is BLIMP-1[102]. BLIMP-1 is a transcriptional suppressor that shut down genes related to affinity maturation, which promotes the commitment of GC B cells to a plasma cell fate[101]. Some plasma cells downregulate CXCR5, upregulate CXCR4 and home to the bone marrow[99,101]. Plasma cells in bone marrow are maintained by BAFF-family cytokines that interact with membrane receptor BCMA, which allows them to survive for long periods[99]. These plasma cells can continue to secrete antibodies for decades even the antigen is no longer present[99]. Although mature plasma cells do not recirculate, secreted antibodies enter the circulation and mucosal secretions, and these antibodies can provide immediate protection when the pathogen invades again[99].

The signals that control memory B cell differentiation are still poorly understood[102]. Current data on GC B cell fate decisions suggest that higher-affinity B cells are more likely to be selected into the plasma cell pools while relatively low-affinity B cells that survive apoptosis

tend to be selected into memory or recycling GC B cell pools[102]. Memory B cell differentiation seems to occur to low or intermediate-affinity GC B cells which receive medium-level help signals from Tfh cells[105]. Memory B cells express surface immunoglobulin but secrete little or no antibody[101]. However, they are able to rapidly differentiate into plasma cells and then secret large quantities of high-affinity antibodies upon re-exposure to antigen[102].

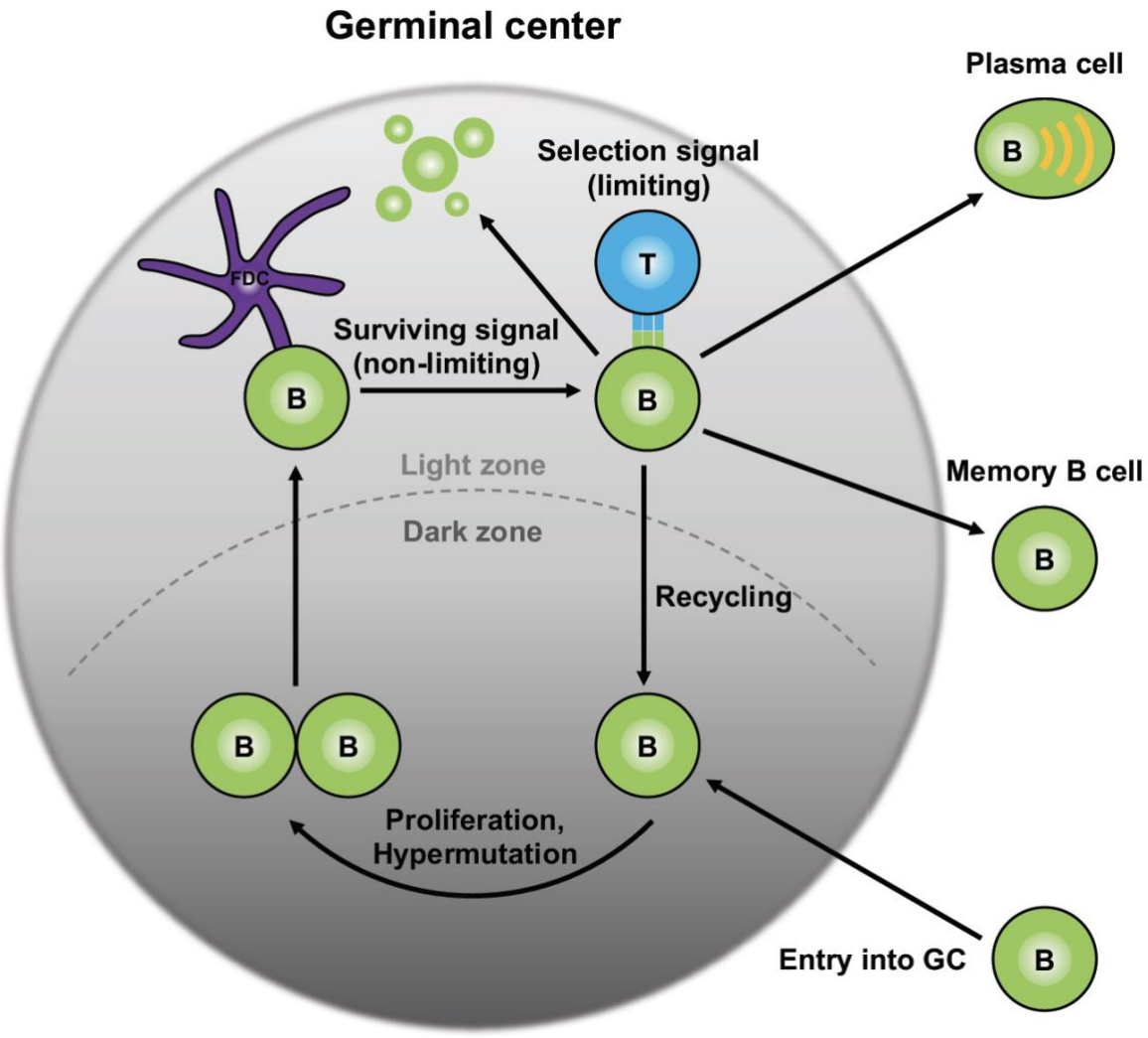


Figure 1.4 Cyclic re-entry model for affinity-based selection in the GC. After activation by antigens, B cells migrate to GC and proliferate with hypermutation in the dark zone. After one or more cycles of proliferation/hypermutation, B cells migrate to light zone. In light zone, B cells uptake antigens in immune complexes on FDCs and present antigens to a limiting number of Tfh cells. B cell clones that possess a BCR with higher affinity capture more antigens and present more peptides on MHCII to Tfh cells. Thus, the higher-affinity B cells are able to get more help signal from Tfh cells and are more likely to survive. By contrast, lower-affinity B cells tend to die due to lack of help signal from Tfh cells. Surviving B cells can then follow three potential fates: re-entry into dark zone for further proliferation/hypermutation; differentiate into plasma cells; or differentiate into memory B cells.

1.6.3 T follicular helper cells

Tfh cells are a subset of CD4 T cells that provide help with B cells for high-affinity antibody production in germinal centres[110-112]. These specialised cells are crucial for the formation of GC, affinity maturation and maintenance of B cell memory[110]. Tfh differentiation is complicated and tightly regulated process[110]. It starts with the priming of a naive CD4 T cell by a dendritic cell (DC)[105,110]. Several classes of DCs can prime Tfh differentiation, but monocyte-derived DCs are more effective than conventional DCs[110]. However, DC priming is necessary but not sufficient for Tfh differentiation, full Tfh differentiation usually requires the cooperation of another APC, B cells[105]. DCs are normally required for early Tfh differentiation, whereas B cells are needed for later events[105].

BCL6 is the master transcription factor for Tfh differentiation[113-115]. It is upregulated by the signalling of CD28 or STAT1/STAT3 activation[110]. BCL6 antagonizes BLIMP1, a transcription factor which promotes the formation of other effector T cells[110]. BCL 6 represses genes encoding proteins (CCR7, CCR6, EBI2, PSGL1, S1PR1) that control T cell migration toward non-follicle zone[110]. Upregulation of CXCR5 is also necessary for proper positioning and functions of Tfh cells[110]. Of note, ASCL2 induces CXCR5 upregulation during early stages of CD4 T cell activation and BCL6 sustains CXCR5 expression[110]. The combination of CXCR5 upregulation and CCR7 downregulation allows Tfh migrating to the T-B border[105]. Importantly, proper migration of Tfh cells and their interaction with B cells depend on ICOS: ICOSL signalling[105]. The function of ICOS for Tfh differentiation is important and complex, it serves as both a migration receptor and a costimulatory molecule for Tfh cells[105]. Tfh cells will not be recruited to B cell follicles without B cell–expressed ICOSL[110]. Also, ICOSL on B cells seems to be crucial for the maintenance of Tfh phenotype[110]. In turn, Tfh cells provide

signals, such as IL-21 and CD154 (CD40L), required for B cell proliferation and differentiation as well as affinity maturation[105]. These feedback loops are crucial for appropriate regulation of humoral immune responses[105].

Human and mouse Tfh cells in secondary lymphoid tissues are analogous in terms of surface protein marker phenotype and gene-expression profile[105]. However, the two species seem to largely differ in cytokines related to Tfh differentiation[105]. In mice, IL-6 and IL-21 are crucial for Tfh cell differentiation[110]. IL-6 is a potent inducer of murine IL-21 expression and Tfh cell differentiation[105]. IL-6 is secreted by a variety of cells, including DCs and B cells, whereas IL-21 is mostly produced by Tfh and Th17 cells[110]. Binding of IL-21 to its receptor IL-21R results in phosphorylation of STAT3 and STAT1[110]. In humans, IL-12, IL-23 and TGF-β are the most important cytokines for Tfh differentiation[110]. IL-12 is the most potent inducer of human IL-21 expression and Tfh differentiation predominantly in a STAT3-dependent manner[105,110]. IL-23 functions similar to IL-12[105,110]. Surprisingly, TGF-β also promotes Tfh cell formation in humans via STAT3 and STAT4, synergizing with IL-12 and IL-23[110]. (In mice, TGF-β inhibits Tfh cell fate in mice, both in vitro and in vivo.[110]) Although cytokines related to Tfh differentiation are different between mouse and human, there is a common inhibitory cytokine for two species. IL-2 is the most potent inhibitor of human and mouse Tfh differentiation[105,110]. Mechanistically, IL-2-dependent activation of STAT5 upregulates BLIMP1 which inhibits Tfh cell formation and promotes the differentiation of non-Tfh effector cells by antagonizing BCL6 functions[110].

1.7 Identification of Ag-specific Tfh cells

Interactions between Tfh (Figure 1.5 A) and GC B cells (Figure 1.5 B) are mediated via T cell receptor (TCR) recognition of cognate peptides presented by B cells upon MHC class II[116], which leads to the activation and proliferation of antigen-specific Tfh cells. Classical intracellular cytokine staining (ICS) assays have been extensively employed to identify Ag-specific CD4+ T cells in blood[117]. Typically, ICS assays have measured IFN-γ, IL-2 and TNF-α, which are produced in sufficient amounts intracellularly to be readily detected by flow cytometry. However, analogous detection of Ag-specific Tfh cells via ICS is difficult because Tfh cells mainly provide contact dependent, selective help to GC B cells as opposed to wholesale cytokine secretion which would probably be counterproductive to the competitive affinity-maturation of GC B cells[118]. Since it is challenging to detect IL-21 from Tfh cells following stimulation with antigen-derived peptides, most studies have used strong, non-specific PMA/ionomycin stimulation to detect IL-21 from Tfh cells[118].

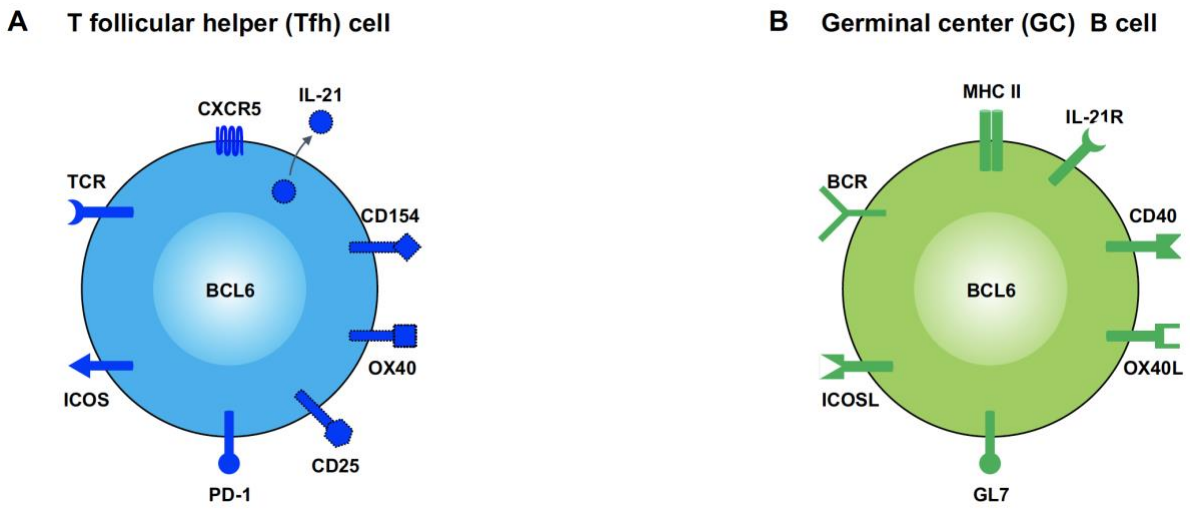


Figure 1.5 T follicular helper (Tfh) cell and Germinal center (GC) B cell. (A) BCL6 is the master transcription factor for Tfh cell differentiation. Distinguishing phenotypic markers of Tfh cells include the high expression of CXCR5, PD-1, and ICOS. IL-21and CD154 are crucial effector molecules produced by Tfh cells to help GC B cells proliferation and differentiation. Tfh cells also upregulate CD25 and OX40 upon activation. (B) BCL6 is the master transcription factor for GC B cell differentiation. Distinguishing phenotypic markers of GC B cells are the high expression of GL7. GC cells express CD40, OX40L, ICOSL and IL-21R to interact with CD154, OX40, ICOS and IL-21 expressed or secreted by Tfh cells.

An alternative to ICS assays was developed to detect antigen-specific CD4 T cells; this technique identifies Ag-specific Tfh based on the upregulation of surface activation markers, such as CD25 and OX40 (CD134)[118-123]. The CD25/OX40 assay was initially used to identify human Ag-specific CD4 T cells in peripheral blood[119], and has subsequently been extended to both human and macaque lymph node samples[118,121]. Compared with ICS, the AIM assay identified 85-fold or 10-fold more Ag-specific Tfh cells in humans[118] or macaques[121], respectively, highlighting the increased sensitivity of this approach. However, use of a similar approach has not yet been validated for mouse and ferret Ag-specific Tfh cells. Mouse Ag-specific Tfh cell responses to influenza virus infection and immunization are explored in

Chapter 2 of this thesis and ferret Ag-specific Tfh cell responses following influenza virus infection are investigated in Chapter 3 of this thesis.

1.8 Role of Tfh during immunisation

1.8.1 Circulating Tfh

Our understanding of GC Tfh cells substantially comes from mouse studies[124]. Knowledge about human GC Tfh is limited due to the difficult access to healthy human lymphoid tissue. To circumvent this problem, peripheral blood CXCR5+ CD4+ T cells which are called circulating Tfh (cTfh) have been employed as a surrogate to study human Tfh cell biology[110,112,125]. cTfh cells express CXCR5, PD-1 and ICOS, and share phenotypic and functional properties with GC Tfh[125]. Although there is an agreement that cTfh are closely related to GC Tfh cells, the lack of information on the ontogeny of cTfh arouses the controversy over the existence of real Tfh cells in blood[126]. Recently, Vella et al. showed that a subset of cTfh cells indeed originated in lymph nodes and trafficked into the blood via the thoracic duct by analysing phenotype, transcriptome, epigenetic profile and T cell receptor clonotype[124,127]. This study is of great significance because it provides the link between Tfh cells in lymph nodes, thoracic duct and peripheral blood[124].

cTfh cells are heterogeneous, consisting of different subsets with distinct phenotype and functions[124,125]. According to the expression of CXCR3 and CCR6, cTfh cells can be classified into three subsets: CXCR3+CCR6− cTfh1, CXCR3−CCR6− cells cTfh2, CXCR3−CCR6+ cTfh17[112,125]. In addition to surface CXCR3 and CCR6 expression, three subsets of cTfh cells resemble Th1, Th2 and Th17 in transcription factor expression profile, with cTfh1, cTfh2 and cTfh17 expressing T-bet, GATA3 and RORγt, respectively[125,128].

1.8.2 Tfh responses to immunisation

Tfh responses to immunisation and their influence on the humoral immune responses to vaccines have been extensively investigated in the context of seasonal influenza vaccine immunizations[105,128]. Bentebibel et al. demonstrated a temporary increase of ICOS+CXCR3+CXCR5+ cTfh1 cells in the blood of subjects immunized with a trivalent inactivated influenza vaccine. The increased level of activated cTfh1 cells in blood on day 7 following immunization correlated with the enhancement of antibody responses[87]. In addition, the specificity of these cTfh1 cells was determined, with up to 60% of these cTfh1 cells specific for influenza antigens[87]. Herati et al. showed that successive annual influenza vaccination induced a recurrent oligoclonotypic memory response in a population of ICOS+CD38+ cTfh cells, and this population included HA-specific cells identified by tetramer staining and AIM assay[88].

Tfh responses to immunisation in animals have also been widely explored. Moon et al. demonstrated that immunization of a malaria nanoparticle vaccine elicited strong Tfh responses in mice[89]. The specificity of Tfh cells elicited by OVA-containing nanoparticle vaccine was determined using OT-II mice[89]. Recently, Pardi et al. showed that Single intradermal immunization of nucleoside-modified mRNA encoding HIV envelope, influenza virus HA, or zika virus pre-membrane and envelopes proteins encapsulated in lipid nanoparticles induced potent Tfh responses in mice and nonhuman primates[90]. The specificity of induced Tfh responses in rhesus macaques immunized with HIV envelope-encoding mRNA was verified by AIM assay which revealed that 4–8% of Tfh cells were Env-specific[90].

Recently, Juno et al. in our group investigated the Ag-specific cTfh responses in humans following mild to moderate SARS-CoV-2 infection using AIM assay[129]. Strong cTfh responses

to SARS-CoV-2 spike protein were detected in convalescent subjects, with a median of 0.92% of cTfh cells exhibiting spike specificity[129]. In comparison, only weak cTfh responses were detected to the much small receptor binding domain (RBD) of spike, with a median of 0.12% RBD-specific cTfh cells[130]. Furthermore, they found that plasma neutralizing activity positively correlated with the proportion of spike-specific cTfh1 (CCR6−CXCR3+) and cTfh2 (CCR6−CXCR3−), but negatively correlated with the frequency of spike-specific cTfh17 (CCR6+CXCR3−)[130]. Increased frequency of CXCR3+ cTfh1 cells and their positive correlation with neutralizing antibody titres were also observed recently in patients with HCV and HIV infection[131,132].

1.8.3 Linked recognition and conjugate vaccines

T-cell dependent humoral immune responses require the interaction of B cells and Tfh cells that recognize the same antigen; this is termed linked recognition[101,133]. Of note, the epitope recognized by the Tfh cell is likely to be different from the epitope recognized by the B cell[101]. Linked recognition also apply to two physically associated molecules, with one molecule (hapten) providing B cell epitopes and the other molecule (carrier) having T-cell epitopes[133]. Haptens are small chemical groups which are unable to induce antibody responses by themselves[101]. But covalent linking hapten to a carrier protein makes it immunogenic, this is known as hapten carrier effect[101]. This is because T cells that are activated by peptides derived from the carrier protein can become Tfh cells and augment the antibody response to the hapten[101]. Keyhole limpet hemocyanin (KLH) and bovine serum albumin (BSA) are commonly used carrier proteins.

The concept of linked recognition has been applied to the design of vaccines against some bacterial infections in which the target antigens are capsular polysaccharides[99]. Capsular

polysaccharides, consisting of many repeating units of simple sugars, are type II T cell-independent antigens[134]. They are capable of inducing antibody responses, but incapable of inducing T cell responses[99]. Vaccines composed of purified polysaccharides against meningococcus and pneumococcus were partially immunogenic in adults[134]. However, these polysaccharide vaccines were non-immunogenic in infants and children younger than 2 years who are unable to generate strong T cell-independent humoral immune responses against TI-2[101,134]. The problem was solved with the invention of conjugate vaccines which are composed of bacterial polysaccharides chemically conjugated to protein carriers[101,134]. The mode of action of conjugate vaccines is similar to that of hapten-carrier conjugates[99,135]. The carrier protein provides peptides that can be recognized by Tfh cells[101]. Thus, conjugate vaccines are more easily to elicit high-affinity antibodies and memory B cells than polysaccharide vaccines without coupled proteins[99]. During the last three decades, various conjugate vaccines have been developed to prevent the infection of Haemophilus influenzae type b (Hib), pneumococcus and meningococcus, which used to cause more than a million deaths annually[134].

1.8.4 Tfh and immunogenicity

Numerous studies in human and animals have convincingly demonstrated the correlates between Tfh responses and antibody responses in recent years[136-138]. Importantly, a few animal studies have provided more relevant evidence on the contribution of Tfh cells to immunogenicity. Tan et al. showed that HA stem vaccination induced poor stem-specific Tfh and antibody responses in C57BL/6 mice, but stem-specific antibody responses could be rescued by conjugation to either the HA head domain or a KLH carrier protein, both of which could elicit Tfh cell responses[139]. He et al. found that extracellular matrix protein 1 (ECM1) promoted Tfh cell differentiation and antibody production[140]. They showed that ECM1 deficient mice exhibited impaired Tfh cell development, GC formation, and KLH-specific

antibody production compared with wild type mice upon KLH immunization[140]. In contrast, administration of ECM1 protein in wild-type mice improved Tfh development, neutralizing antibody production and promoted protective immune responses against PR8 influenza virus infection[140]. Another evidence comes from Hollister and colleagues' work which used conditional BCL6 knock-out mouse model where Bcl6 was conditionally deleted in T cells ($Bcl6^{fl/fl}$ Cre^{CD4} mice)[141]. The authors found that $Bcl6^{fl/fl}$ Cre^{CD4} mice had an almost complete loss of Tfh cells and sharply reduced antigen-specific serum IgG titre in comparison to control mice following sheep RBCs immunization[141].

1.9 Unconventional T cells and T-cell independent B cell responses

1.9.1 Unconventional T cells supporting B cell responses

In addition to Tfh cells, there are also several other types of T cells, such as invariant natural killer T follicular helper (iNKTfh) and gamma delta T cells which play important roles in antibody responses[142,143]. Natural killer T (NKT) cells (also called CD1d-restricted T cells), recognize the antigen-presenting molecule CD1d which binds lipids and glycolipids[144,145]. NKT cells are classified into two types: type I NKT cells, also called invariant natural killer T (iNKT) cells, express a TCR consisting of an invariant α-chain paired with a limited set of β-chains[144,145]. In contrast, type II NKT cells have more diverse αβTCR pairings[144,145]. iNKT cells recognize glycolipids, such as αGalCer, whereas type II NKT cells respond to sulfatide, not to αGalCer[144,145]. Upon activation by glycolipid antigens, a proportion of iNKT cells differentiate to follicular helper iNKT (iNKTfh) cells in a BCL6-dependent manner[144]. iNKTfh cells can support antibody responses by cognate interactions with B cells presenting glycolipid antigens on CD1d. iNKT cells can also provide non-cognate help for the generation of long-lasting antibody responses against protein antigens[145]. iNKT-licensed DCs

(noncognate help) can activate Tfh cells, which in turn support B cells to differentiate to long-lived plasma cells and memory B cells[146].

γδ (gamma delta) T cells express a TCR that is composed of γ chain and δ chain. The γ chain is structurally equivalent to the β chain of α β TCR, and the δ chain is more similar to the α chain of α β TCR[147-149]. γδ T cells are distributed in circulation blood and tissues. Unlike α β T cells, γδ TCR–mediated antigen recognition is MHC-unrestricted. In addition, γδ T cells are a functionally heterogeneous population. Thus, γδ T are able to rapidly recognize and respond to a variety of unconventional antigens (ligands) associated with either stress or infection, contributing to many early immune responses[147]. Apart from innate receptor expression, γδ T cells also play a critical role in antigen presentation, cytotoxicity, and cytokine production[147]. Furthermore, γδ T cells involve in antibody response by promoting GC formation, somatic hypermutation, isotype switching and plasma cell differentiation[150]. Recently, Rezende et al. demonstrated that γδ T cells modulate antibody response by inducing Tfh cell differentiation in mice[150]. CFA immunization in mice induced a population of CXCR5+ γδ T cells (Vγ1) in the draining lymph nodes[150]. CXCR5+ γδ T cells released Wnt ligands that promote Tfh cell differentiation[150].

1.9.2 T-cell independent B cell responses

According to the requirement for T cell help in eliciting antibody responses, antigens are categorized as T cell dependent antigen (TD-Ag) and T cell independent antigen (TI-Ag) as noted earlier in section 1.6.1[151]. The typical TD-Ags are proteins or peptides that require help signal from MHC II-restricted T cells to induce antibody responses. Antigens that induce antibody responses without the help signal from MHC II-restricted T cells are TI-Ags[151,152].

TI-Ags are more diverse and subdivided into type I (TI-1 Ag) and type II (TI-2 Ag), depending on whether they can induce antibody responses in neonatal mice or in CBA/N (xid/xid) mice

that have B cells with immature features[151,152]. TI-1 Ags can induce antibody responses both in mature B cells and in immature neonatal B cells or B cells from CBA/N (xid/xid) mice. In contrast, TI-2 Ags can only stimulate antibody responses in mature B cells. TI-1 Ags, such as LPS, CpG, or poly-IC, are potent B-cell mitogens which non-specifically or polyclonally activate B cells[153]. Bacterial polysaccharides and viral capsids are typical examples of TI-2 Ags which possesses characteristics of large molecular weight and highly repetitive epitopes[151,154].

B cells express both BCR and TLR (TLR7 and TLR9)[155]. It is generally accepted that TI-2 Ags can stimulate strong BCR signalling or synergetic BCR and TLR signalling, which can bypass the need of T cell help for B cell proliferation[154]. Many studies have demonstrated that TLR signalling can promote B cell proliferation and antibody responses to viruses and VLPs[154]. Raval et al. demonstrated that T cell-deficient mice with persistent polyomavirus infection generated durable IgG responses and the maintenance of this sustained IgG responses needs MyD88 signalling in the host[156]. Liao et al. showed that bacteriophage Qβ derived VLP (Qβ-VLPs) induced T-independent antibody responses and isotype-switched, somatically mutated memory B cells in TCRβδ KO mice (T cell receptor β and δ chain knockout mice)[154]. Follow-up studies demonstrated that B cell–intrinsic MyD88 signalling promotes initial cell proliferation and differentiation to enhance the germinal centre response to Qβ-VLPs[157].

1.10 Multimeric vaccine antigens

1.10.1 Protein aggregates

Recombinant protein vaccines are becoming popular and taking a bigger share of the vaccine market in recent years due to their well-defined antigenic components and low reactogenicity[158]. However, most soluble protein vaccines elicit poor protective immune responses in vivo[159].

One particularly effective strategy for enhancing the immunogenicity of protein antigens is the multimerization (particulation or aggregation) of soluble proteins[160]. Multimeric antigens which display antigens as a repetitive array are known to be more efficient in eliciting antibody responses than the monomeric soluble antigens[161-163]. This is likely due to improved lymphatic trafficking, enhanced antigen uptake by antigen presenting cells and increased B cell activation through cross-linking of B cell receptors[164,165]. Multimeric antigens can be classified into two major types: amorphous protein aggregates and highly ordered nanoparticles.

Protein aggregates are high molecular weight proteins composed of multimers of native or denatured monomers[161]. Although the effect of protein aggregates on the immunogenicity of protein antigens has been assessed in a limited number of literatures, studies conducted in mice have demonstrated that multimeric protein aggregates are more immunogenic than the monomeric forms[166-168]. Hermeling et al. generated recombinant human interferon alpha2a/b (rhIFNα2) aggregates by metal-catalyzed oxidation and showed that aggregated form of recombinant human interferon alpha2a/b (rhIFNα2) increased rhIFNα2-specific antibody response in wild-type FVB/N mice compared with native form of rhIFNα2[167]. They also found that rhIFNα2-specific serum IgG titre is dependent on the level of aggregation[167]. Ilyinskii et al. fused a weakly immunogenic model antigen GFP with long polyglutamine (polyQ) domain that triggers protein aggregation and immunized BALB/c mice with plasmids encoding polyQ-GFP or GFP alone[168]. They found that plasmids encoding polyQ-GFP elicited significant higher anti-GFP antibody titre and anti-GFP CTL activity than plasmids encoding GFP alone[168].

Aluminium, are the most widely used vaccine adjuvants, also enhances antigen immunogenicity by promoting the formation of antigen aggregates[169]. Aluminium adjuvants do not exist as monolithic particles but form fibrous loose aggregates of aluminium

nanocrystals[169,170]. Adsorption of antigens to aluminium aggregates enhances vaccine induced immune response[171]. Although aluminium adjuvants have been in continuous use in human vaccines for nearly 100 years, their mechanism of action remains elusive[172]. Current explanations for their mechanism include: (1) aggregate or particle formation enabling prolonged release of antigens within the site of injection (depot effect); (2) formation of aggregates or particles that promotes phagocytosis of antigens by antigen-presenting cells (pro-phagocytic effect); and (3) activation of NLRP3 inflammasome signalling pathway (pro-inflammatory effect)[171-174].

Some peptides can also aggregate to form larger polypeptides[175]. However, use of the conjugate of an aggregating peptide and a soluble protein as an aggregate based vaccine has not been reported and this is explored in Chapter 4 of this thesis.

1.10.2 Nanoparticles

Nanoparticles are a wide class of particulate substances which vary in size, shape and chemical composition[165]. Nanoparticles used as vaccines are usually defined as non-replicative, organized structures with size 1–1000 nm, which are produced by either recombinant expression or chemical synthesis[165,176]. The ability that nanoparticles enhance the immunogenicity of protein antigens has been demonstrated by myriad studies[164]. Commonly used nanoparticle vaccine platforms for multivalent antigen display include virus-like particles, liposomes and self-assembling protein nanoparticles[177].

1.10.2.1 Virus-like particles

Virus-like particles (VLPs) have viral capsid (and envelope sometimes) but do not have viral genomes[177]. The virus-like structure makes VLPs as immunogenic as traditional live attenuated

or inactivated vaccines, and the non-infectious property makes VLPs a safer vaccine platform compared with traditional live virus-based vaccine platforms[177]. The first VLP vaccine was licenced in 1986 to prevent the infection of hepatitis B virus[178]. The successful licensure of another VLP vaccine against human papilloma virus (HPV) in 2006 has spurred great efforts on development of VLP based vaccines[178]. 5 years later, another VLP vaccine against hepatitis E virus (HEV) was licensed[179]. Currently, a number of VLP-based vaccines against a wide range of pathogens are in preclinical and clinical development[165,179].

1.10.2.2 Liposomes

Liposomes are sphere-shaped vesicles made of one or more concentric phospholipid bilayers[177]. Liposomes can be modified to incorporate antigens into the phospholipid bilayer for surface display or encapsulate antigens within the cavity for delivery[177,178]. On the basis of this principle, researchers developed virosomes. Virosomes are in vitro assembled viral envelopes with viral phospholipids and envelope proteins derived from the parental viruses[180]. Two virosome vaccines against hepatitis A virus (HAV) and seasonal influenza viruses were launched in 1994 and 1997, respectively[180]. The successful industrial application of these virosome vaccines stimulates the interest in these vesicles as a versatile vaccine platform[180]. A few vaccine candidates based on second-generation virosomes against Malaria, Hepatitis C virus (HCV) and HIV are currently under clinical trials[180].

1.10.2.3 Self-assembling protein nanoparticles

Self-assembling proteins are promising vaccine carriers for displaying antigens to mimic a natural microbe architecture[178]. Ferritin is typical example of these self-assembling proteins which has been widely used in vaccine development. Ferritins are globular iron storage proteins which naturally self-assemble into hollow nanoparticles with an internal and external diameter

of 8 and 12 nm, respectively[163,178]. A ferritin nanoparticle consists of 24 copies of the same subunit, which forms an octahedron composed of eight trimeric units[163,177]. The 3-fold symmetry allows the correct presentation of a variety of trimeric antigens, such as influenza virus HA and HIV envelope proteins[163,177]. Sliepen et al. showed that ferritin nanoparticle vaccine presenting HIV-1 envelope protein trimers elicited significantly higher humoral immune responses than soluble trimers in mice and rabbits[181]. Kanekiyo and colleagues demonstrated that ferritin nanoparticle vaccines displaying full-length HAs or HA stems elicited broader antibody responses and exhibited superior protective efficacy compared to traditional inactivated vaccine in mice and ferrets[65,67,182].

1.11 Thesis overview

There is a growing interest in developing universal influenza vaccines that elicit broad and durable antibody responses against diverse influenza viruses. Tfh cells play a crucial role in the generation of high-affinity and long-lived antibodies[110]. Characterisation of Tfh cell responses will facilitate the design of novel Tfh-targeting influenza vaccine. On the other hand, immunogen multimerization can enhance antibody responses independent of Tfh cell help[161,162], which serves as an alternative pathway to augment humoral immunity overcoming limiting Tfh responses. This thesis investigates Tfh responses to influenza virus infection and immunization in mice and ferrets and explores the effects of immunogen multimerization on humoral immunity in the context of limiting Tfh responses to HA stem. Specific aims of this thesis are: 1) Develop and validate assays to characterize influenza-specific Tfh cells in mice; 2) Develop ferret-specific Tfh reagents and characterize Tfh responses in the ferret model of human influenza virus infection; 3) Explore the effects of immunogen multimerization on humoral immunity.

Chapter 2: Identification of murine antigen-specific T follicular helper cells using an activation-induced marker assay

Journal of Immunological Methods 467 (2019) 48–57

Contents lists available at ScienceDirect

Journal of Immunological Methods

journal homepage: www.elsevier.com/locate/jim

Research paper

Identification of murine antigen-specific T follicular helper cells using an activation-induced marker assay

Wenbo Jiang[a], Kathleen M. Wragg[a], Hyon-Xhi Tan[a], Hannah G. Kelly[a], Adam K. Wheatley[a], Stephen J. Kent[a,b,c,*], Jennifer A. Juno[a,*]

[a] Department of Microbiology and Immunology, Peter Doherty Institute for Infection and Immunity, University of Melbourne, Melbourne, Victoria, Australia
[b] Melbourne Sexual Health Clinic and Infectious Diseases Department, Alfred Hospital, Monash University Central Clinical School, Carlton, Victoria, Australia
[c] ARC Centre for Excellence in Convergent Bio-Nano Science and Technology, University of Melbourne, Melbourne, Australia

ARTICLE INFO

Keywords:
T follicular helper cell
Influenza
CD154
CD25
OX-40
Activation induced marker

ABSTRACT

Protective antibody (Ab) responses induced by natural infection or vaccination play a central role in defense against invasive pathogens. Germinal centers (GCs) are the sites of Ab affinity maturation and T follicular helper (Tfh) cells are a critical factor for driving GC formation and B cell selection. Therefore characterization of antigen (Ag)-specific Tfh cells is increasingly essential to define the mechanistic basis of protective antibody responses. However, since Tfh are weak producers of cytokines it is difficult to detect Ag-specific Tfh cells using conventional intracellular cytokine staining (ICS). Here, we report an assay identifying mouse Ag-specific Tfh cells by assessing the upregulation of surface activation-induced markers (AIM). Murine lymph node (LN)-derived Tfh cells largely retained CXCR5 and PD-1 expression following 18-hour cell culture. After influenza infection or influenza hemagglutinin (HA) protein vaccination of mice, stimulation of lymph node cell suspensions with peptide pools or whole protein drove upregulation of CD25, OX40 (CD134), ICOS (CD278) and CD154 on Tfh cells. Upregulation of either CD154 or CD25/OX40 proved a sensitive method for delineating HA-specific Tfh cells. This assay provides the opportunity to quantify antigen-specific Tfh cells in mice without the need for transgenic models or MHC-II tetramer reagents restricted to specific epitopes.

1. Introduction

Vaccination is widely acknowledged as one of the most cost-effective preventive measures for fighting infectious diseases. Although immunogens can induce both antibody and cell-mediated immune responses, most current licensed vaccines confer protection against subsequent infection by eliciting protective antibodies. Generation of protective antibodies with high affinity requires co-ordinated activation and differentiation of antigen-specific B and T lymphocytes, a process which takes place in secondary lymphoid organs (SLO) (Victora and Nussenzweig, 2012).

T follicular helper (Tfh) cells are a subset of CD4+ T cells which localize in the germinal centres (GCs) of SLO (Crotty, 2011; Linterman and Hill, 2016; Qi, 2016; Vinuesa et al., 2016). These specialized cells are crucial for the formation of GC, affinity maturation and the maintenance of B cell memory (Gatto and Brink, 2010; Victora et al., 2010; Victora and Nussenzweig, 2012; Liu et al., 2015). BCL6 is the master transcription factor for Tfh differentiation (Johnston et al., 2009; Nurieva et al., 2009; Yu et al., 2009), and distinguishing phenotypic markers of Tfh cells include the high expression of CXCR5, PD-1, and ICOS. IL-21, IL-4, and CD40L are crucial effector molecules produced by Tfh cells to help GC B cell proliferation and differentiation (Vinuesa et al., 2016).

Interactions between GC B cells and Tfh are mediated via TCR recognition of cognate peptides presented by B cells upon MHC class II (Tangye et al., 2015), which leads to the activation and proliferation of antigen-specific Tfh cells. Classical intracellular cytokine staining (ICS) assays have been extensively employed to identify Ag-specific CD4+ T cells in blood (Phetsouphanh et al., 2015). Typically, ICS assays have measured IFN-γ, IL-2 and TNF-α, which are produced in sufficient amounts to be readily detected by flow cytometry. However, analogous detection of Ag-specific Tfh cells via ICS is difficult because Tfh cells mainly provide contact dependent, selective help to GC B cells as opposed to wholesale cytokine secretion (Dan et al., 2016). Recently, an alternative to ICS assays was developed; this technique identifies Ag-specific Tfh based on the upregulation of surface activation markers,

* Corresponding authors at: Department of Microbiology and Immunology, Peter Doherty Institute for Infection and Immunity, University of Melbourne, Melbourne, Victoria, Australia.
E-mail addresses: skent@unimelb.edu.au (S.J. Kent), jennifer.juno@unimelb.edu.au (J.A. Juno).

https://doi.org/10.1016/j.jim.2019.02.008
Received 14 December 2018; Received in revised form 20 February 2019; Accepted 21 February 2019
Available online 22 February 2019
0022-1759/ © 2019 Elsevier B.V. All rights reserved.

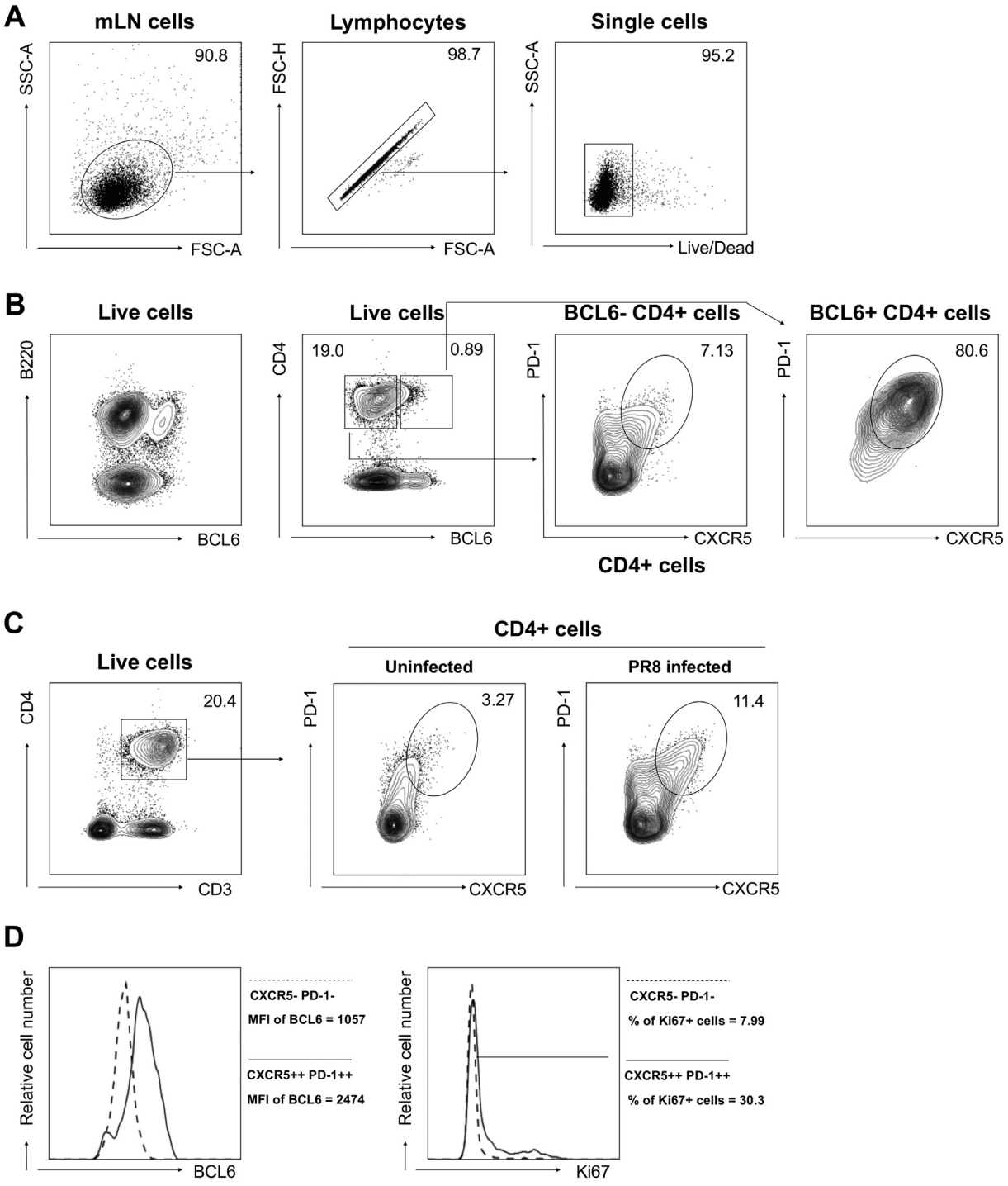


Fig. 1. Identification of Tfh cells in mouse mediastinal lymph node (mLN).
(A) Gating strategy to identify live lymphocytes in the mLN. Lymphocytes were identified by forward scatter area (FSC-A) and side-scatter area (SSC-A). Doublets were excluded by gating on single cells as determined by FSC-A versus FSC-H, and live cells were identified by viability dye exclusion. For each step, the parental population is indicated above the plot. (B) BCL6 expression among B220 + B cells was used as a gating guide to identify BCL6- and BCL6 + CD4 + T cells. Subsequent plots show the representative expression of CXCR5 and PD-1 within the CD4 + BCL6- and CD4 + BCL6 + T cell populations, which was used to generate a CXCR5 + + PD-1 + + gate to identify Tfh cells. Numbers indicate the proportion of the parent gate within the CXCR5 + + PD-1 + + gate. (C) Using the Tfh surface marker gate determined in B, Tfh cells were identified within the CD4 + T cell population of naïve versus influenza infected mice (at day 14 post-infection). (D) Representative histograms depicting the expression of BCL6 (median fluorescent intensity, MFI) and Ki67 (% positive) among Tfh and non-Tfh cells from influenza-infected mice.

such as CD25, PD-L1 (CD274) and OX40 (CD134) (Zaunders et al., 2009; Keoshkerian et al., 2012; Dan et al., 2016; Havenar-Daughton et al., 2016; Reiss et al., 2017; Bowyer et al., 2018). The CD25/OX40 assay was initially used to identify human Ag-specific CD4 T cells in peripheral blood (Zaunders et al., 2009), and has subsequently been extended to both human and macaque lymph node samples (Dan et al., 2016; Havenar-Daughton et al., 2016). Compared with ICS, the AIM assay identified 85-fold or 10-fold more Ag-specific Tfh cells in humans (Dan et al., 2016) or macaques (Havenar-Daughton et al., 2016), respectively, highlighting the increased sensitivity of this approach. Here,

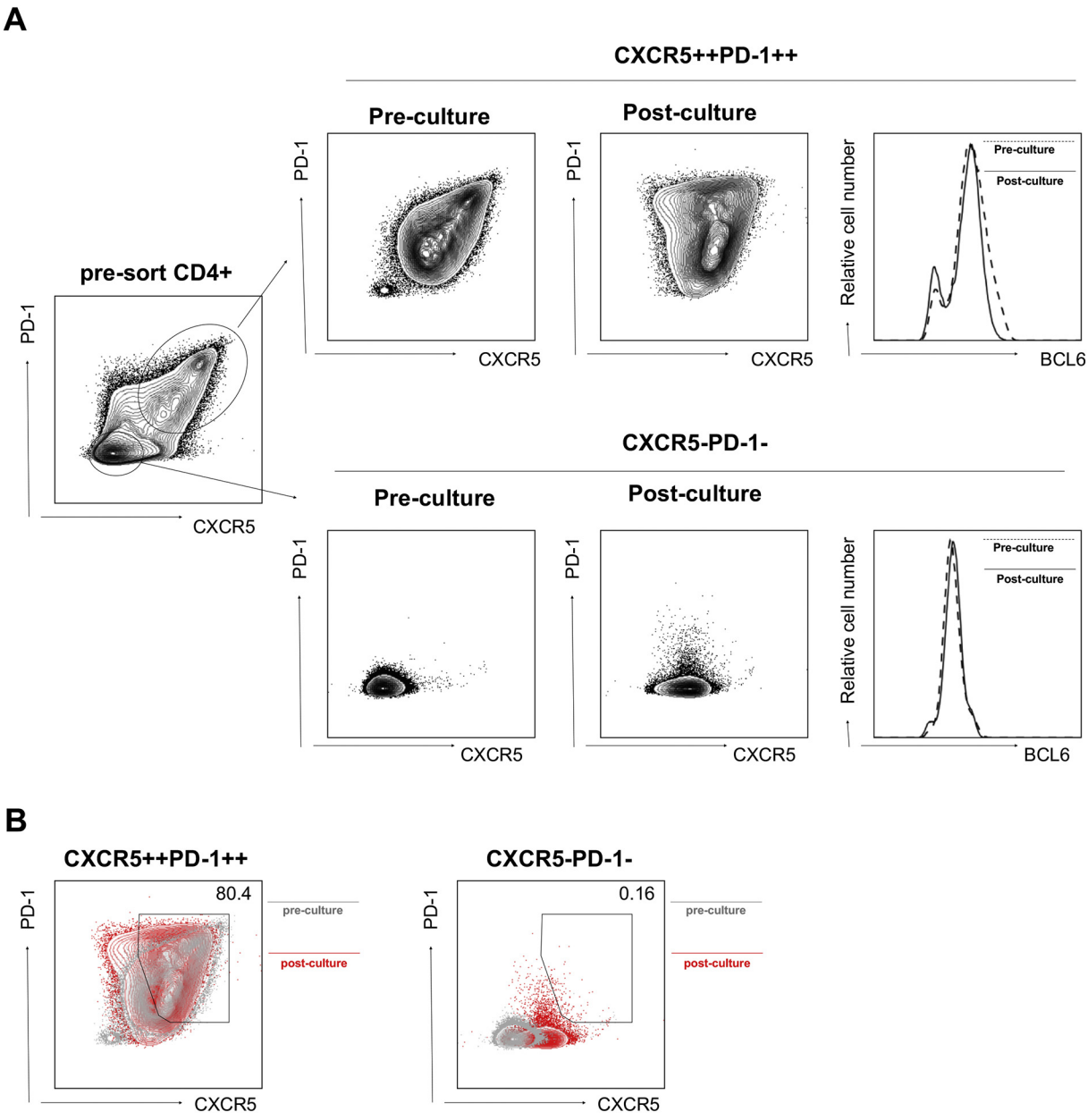


Fig. 2. Confirmation of Tfh phenotype following tissue culture.
(A) Tfh (CD4 + CXCR5 + + PD-1 + +, upper row) and non-Tfh (CD4 + CXCR5-PD-1-, lower row) cells were sorted from the mLN cells of influenza-infected mice (day 14 post-infection). Immediately post-sort, both populations were stained for intracellular BCL6 expression and analyzed for BCL6, CXCR5 and PD-1 expression (pre-culture plots). Tfh and non-Tfh cells were cultured separately for 18 h, and stained for expression of CXCR5, PD-1 and BCL6 (post-culture plots). Histograms show a comparison of BCL6 expression in each population before (dashed line) and after (solid line) culture. Results are representative of two independent experiments. (B) A gate to identify Tfh cells following cell culture using CXCR5 and PD-1 expression was determined by comparing the phenotype of Tfh and non-Tfh cells pre- (grey) and post-culture (red). (For interpretation of the references to color in this figure legend, the reader is referred to the web version of this article.)

we present an AIM assay to identify mouse Ag-specific Tfh cells, validated in the context of influenza infection and vaccination.

2. Materials and methods

2.1. Mouse infection and immunization

Mouse studies and related experimental procedures were approved by the University of Melbourne Animal Ethics Committee (#1714193). Female C57BL/6 mice (6–8 weeks old) were anesthetized by isoflurane inhalation prior to infection or immunization. For intranasal infections, mice were instilled with 50 µL of 50 $TCID_{50}$ of A/Puerto Rico/8/34 (PR8). For intramuscular vaccinations, 5 µg of PR8 HA protein with Addavax (1:1 ratio; InvivoGen) were injected into both hind quadriceps using a 29G needle. 14 days post infection or vaccination, draining lymph nodes (mediastinal lymph nodes (mLN) for infected animals, inguinal lymph nodes (inLN) and iliac lymph nodes (ilLN) for vaccinated animals) and spleen were collected.

2.2. Antigen stimulations and cell culture

Draining lymph nodes from flu-infected or HA-vaccinated mice were mashed into single cell suspensions and either pooled or cultured individually in RPMI 1640 supplemented with 10% fetal calf serum and penicillin/streptomycin (RF10). To identify antigen-specific Tfh cells using peptide stimulation, cell suspensions were stimulated for 18 h in

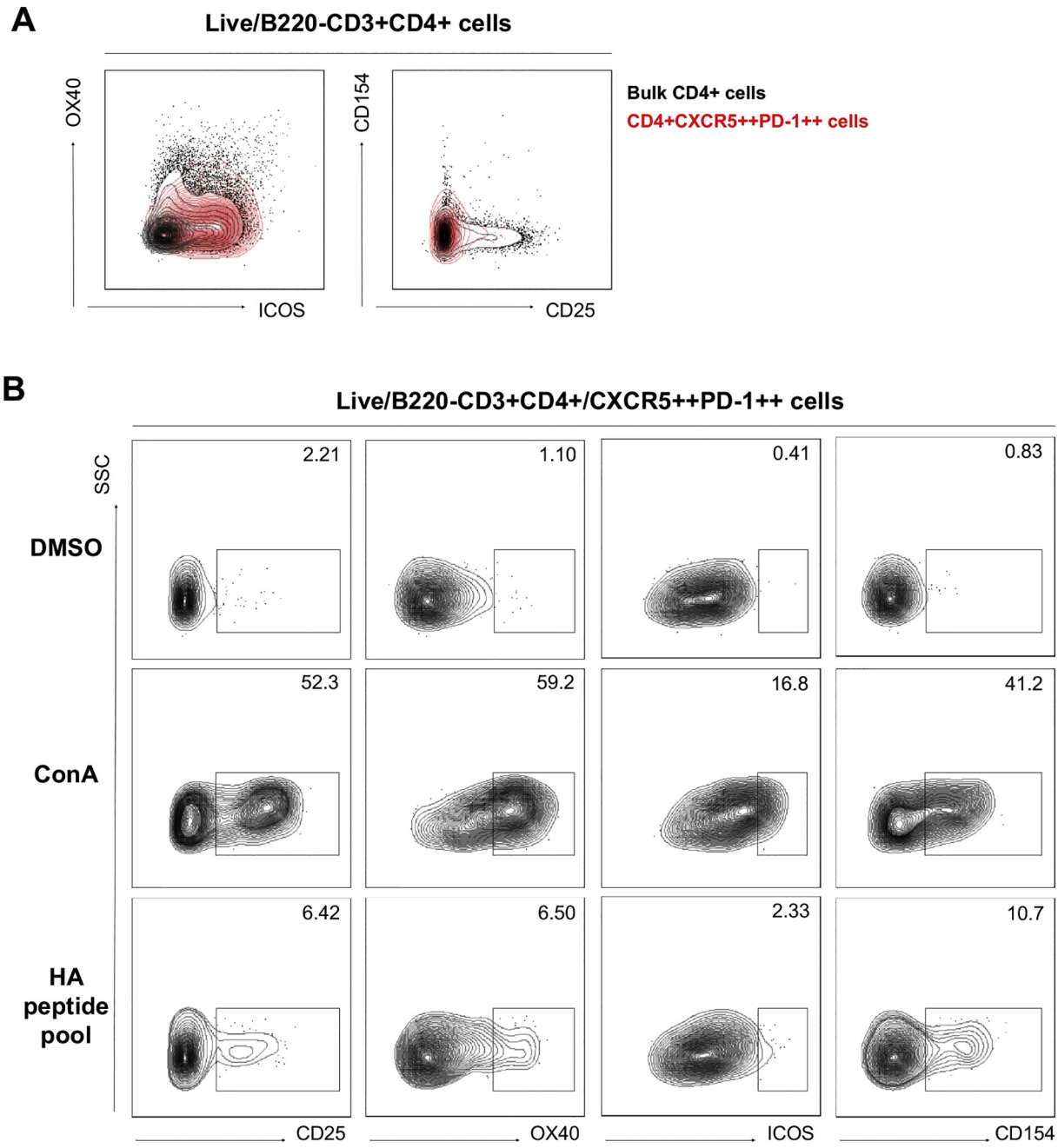


Fig. 3. Activation-induced marker expression following mitogenic or antigen-specific stimulation.
(A) Expression of ICOS, OX40, CD25 and CD154 in unstimulated CD4 + (black) and Tfh cells (red) following culture. (B) Representative expression of CD25, OX40, ICOS and CD154 expression on Tfh cells after 18 h of stimulation with DMSO, ConA or HA peptide pool. Gates for ICOS and OX40 indicate ICOS + + and OX40 + + cells, as determined by baseline ICOS and OX40 expression. Cells were derived from pooled mLN samples of n = 10 influenza-infected mice. Results are representative of 3 independent experiments. (For interpretation of the references to color in this figure legend, the reader is referred to the web version of this article.)

RF10 with a PR8 HA peptide pool (2 μg/peptide/mL, 93 peptides of 17mers overlapping by 11 amino acids, BEI resources), Concanavalin A (ConA, 5 μg/mL, Sigma) or a vehicle (DMSO) control. Cells were cultured in a 48-well plate in 500 μl at a concentration ranging from 2 to 8 million cells/ml. At the time of stimulation, anti-CD154 BV650 mAb (MR1; BD Biosciences) was added to all culture conditions. For kinetics experiments, mLN single cell suspensions from 5 mice were pooled together and 2 million cells were seeded into each well. For other experiments, LN single cell suspensions from individual mice were analyzed.

To identify antigen-specific Tfh cells using protein stimulation, freshly isolated LN single cell suspensions were either cultured alone in 96-well U-bottom plate in 200 μL RF10 or labelled with CellTrace Yellow (Thermo Fisher) and co-cultured with unlabeled splenocytes (1:10 ratio of splenocytes:LN cells) in a 48-well plate in 500 μL RF10. Cells were stimulated with HA protein (5 μg/mL), or a negative protein control (BSA, 5 μg/mL). At the time of stimulation, anti-CD154 BV650 mAb (MR1; BD Biosciences) was added to all culture conditions.

2.3. Antibodies and flow cytometry

For detection of Tfh cells ex vivo, freshly isolated LN cell suspensions were stained with the following panel: Live/dead Red (Thermo Fisher), B220 BV605 (RA3-6B2; BD Biosciences), CD3 BV510 (145-

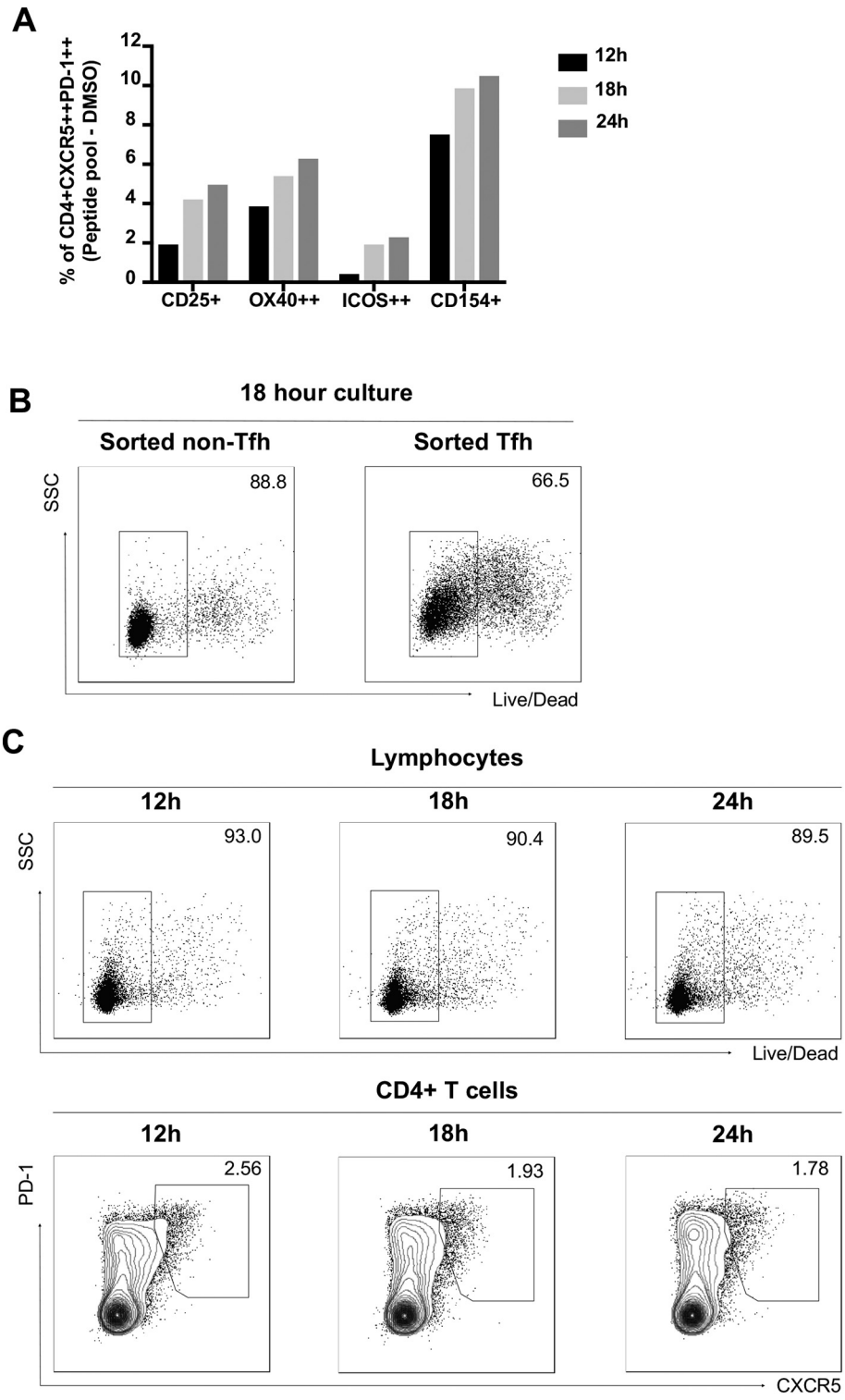


Fig. 4. Kinetics of Tfh cell activation marker expression and Tfh cell viability in cell culture.
(A) Kinetics of CD25, OX40, ICOS and CD154 upregulation on Tfh cells after 12 h, 18 h or 24 h of stimulation with HA peptide pool. Data is background subtracted based on the DMSO control. (B) Viability of sorted non-Tfh (CD4 + CXCR5-PD-1-) and Tfh (CD4 + CXCR5+ +PD-1+ +) cells from influenza-infected mice after culture for 18 h. (C) Plots indicate the viability of the bulk mLN lymphocyte population and the proportion of Tfh cells (within the CD4+ T cell population) after 12, 18 or 24 h of cell culture in influenza-infected mice.

2C11; BioLegend), CD4 BUV737 (RM4-5; BD Biosciences), CXCR5 BV421 (L138D7; BioLegend), PD-1 BV786 (29F.1A12; BioLegend), BCL6 AF647 (IG191E/A8; BioLegend), Ki67 BUV395 (B56; BD Biosciences). For BCL6 and Ki67 staining, cells were fixed, permeabilized, and stained using the BD Transcription Factor Buffer kit (BD Biosciences) according to the manufacturer's instructions.

For Ag-specific Tfh identification, cells were cultured as described above and then stained with the following panel: Live/dead Blue (Thermo Fisher), B220 BV605 (RA3-6B2; BD), CD3 BV510 (145-2C11; BioLegend), CD4 BUV737 (RM4-5; BD), CXCR5 BV421 (L138D7;

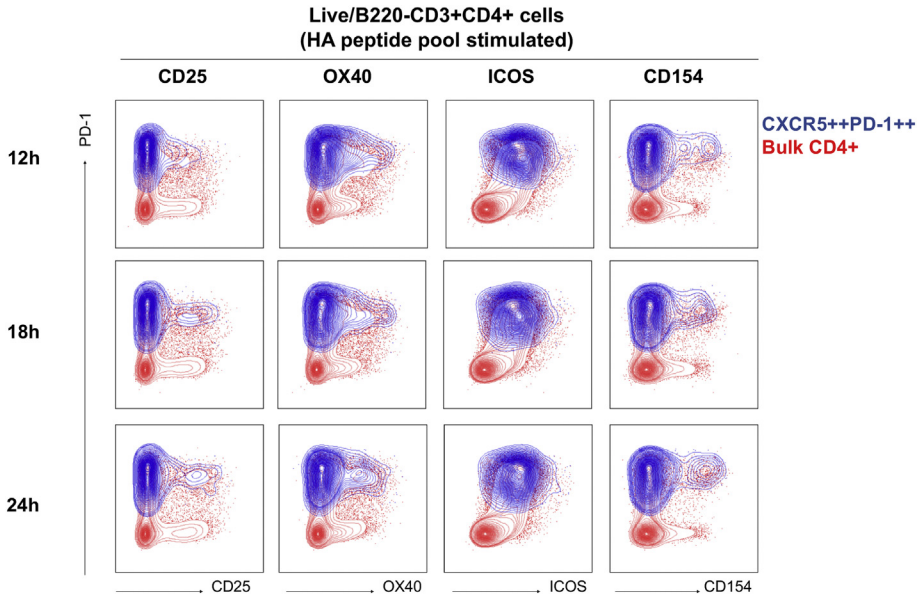


Fig. 5. Comparison of PD-1 and activation marker expression on HA-stimulated Tfh cells over time. mLN-derived cells were stimulated with HA peptide pool for 12, 18 or 24 h. Plots show bulk CD4 + T cells (red) or CXCR5 + +PD-1 + + Tfh cells (blue). (For interpretation of the references to colour in this figure legend, the reader is referred to the web version of this article.)

BioLegend), PD-1 BV786 (29F.1A12; BioLegend), CD25 BB515 (PC61; BD), OX40 PeCy7 (OX-86; BioLegend), ICOS PerCP-eFluor710 (15F9; Thermo Fisher), BCL6 AF647 (IG191E/A8; BioLegend).

All samples were acquired on a BD LSR Fortessa using BD FACS Diva and data was analyzed in FlowJo v10.

2.4. Cell sorting and culture

For cell sorting, freshly isolated mediastinal lymph nodes (mLN) from influenza infected mice were mashed into single cell suspensions, pooled together and stained with the following panel: Live/dead Red (Thermo Fisher), B220 BV605 (RA3-6B2; BD), CD3 BV510 (145-2C11; BioLegend), CD4 FITC (RM4-5; BioLegend), CXCR5 BV421 (L138D7; BioLegend), PD-1 BV786 (29F.1A12; BioLegend). Cells were sorted on a BD Aria III. After sorting, a portion of the sorted cells were intracellularly stained with BCL6 AF647 (IG191E/A8; BioLegend) and acquired on a BD LSR Fortessa. The remaining cells were cultured for 18 h in RF10 and then stained with the aforementioned panel of antibodies and acquired on a BD LSR Fortessa.

2.5. Statistical analysis

Data is presented as mean ± standard deviation and produced using GraphPad Prism version 7 (GraphPad Software, La Jolla California USA).

3. Results

3.1. Identification of Tfh cells in murine lymph node suspensions

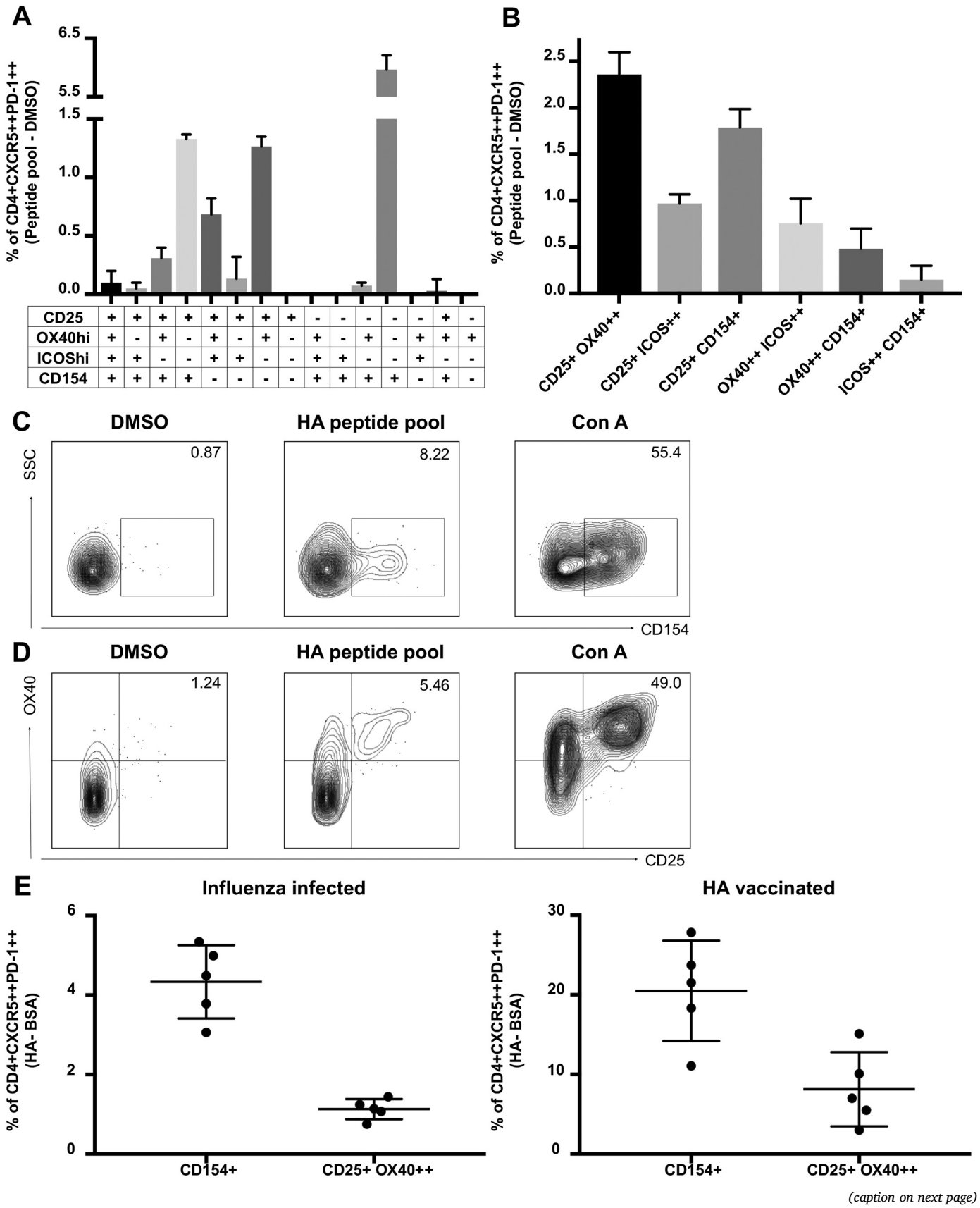
BCL6 expression is the canonical marker to distinguish Tfh cells from other CD4 + T cells (Johnston et al., 2009; Nurieva et al., 2009; Yu et al., 2009). However, many studies use high expression of CXCR5 and PD-1 as surrogate surface markers for the Tfh population in murine lymphoid tissues (Meli and King, 2015). We first validated a flow cytometric panel to allow Tfh identification in mice experimentally infected with influenza. C57BL/6 mice were intranasally inoculated with a sublethal dose of influenza virus and 14 days post-infection, lung-draining mediastinal lymph nodes (mLN) were harvested, stained with a panel of antibodies, and analyzed by flow cytometry (Fig. 1A). Using the BCL6 + GC B cell population (B220 + CD3- cells) as a guide, we identified BCL6 + CD4 + T cells (Fig. 1B). The majority (over 80%) of BCL6 + CD4 + T cells were CXCR5 + +PD-1 + +, enabling the definition of a gated population that were predominantly Tfh cells (Fig. 1C). In naive mice, this population was relatively infrequent compared to influenza-exposed mice (Fig. 1C). Relative to non-Tfh cells (CD4 + CXCR5-PD-1-), Tfh cells (CD4 + CXCR5 + +PD-1 + +) displayed elevated expression of both BCL6 and the proliferation marker Ki67 (Fig. 1D). We therefore used this analysis to set the CXCR5/PD-1 gate used for subsequent identification and sorting of murine Tfh cells ("ex vivo Tfh gate").

3.2. Phenotype of Tfh cells following cell culture

Determining the antigen specificity of T cells often requires re-stimulation in vitro, which could cause changes to Tfh surface phenotype. We therefore assessed the stability of CXCR5 and PD1 expression on Tfh and non-Tfh CD4 + T cell populations following culture. Using the ex vivo Tfh gate, Tfh and non-Tfh cells were sorted from pooled mLN cell suspensions of influenza-infected mice at day 14 post-infection and were analyzed immediately post-sort, or after 18 h of culture. The Tfh cells exhibited some downregulation of PD-1 expression during culture (Fig. 2A). We also observed minor changes in CXCR5 expression after culture, with a degree of downregulation observed in Tfh cells, and a minor upregulation in non-Tfh cells (Fig. 2A). There was a minor loss of BCL6 expression in the Tfh population, but no change in the non-Tfh cells (Fig. 2A). Despite the slight changes in PD-1 and CXCR5 expression, clear differentiation of non-Tfh and Tfh populations using PD-1 and CXCR5 remained possible. A new PD1 + +CXCR5 + + gate was generated to selectively identify Tfh cells post-culture ("post-culture" Tfh gate, Fig. 2B), which was applied to all antigen stimulation experiments.

3.3. Activation-induced marker expression to delineate Ag-specific Tfh cells

We next assessed whether previously reported activation markers were induced on murine Tfh cells following antigen stimulation. mLN cell suspensions from influenza-infected mice at day 14 post-infection were stimulated with DMSO, a HA peptide pool or ConA for 18 h. Due to the reported transient upregulation of CD40L during T cell activation (Chattopadhyay et al., 2005; Frentsch et al., 2005), anti-CD40L (CD154) antibody was added to the culture media for the duration of the stimulation. Cells were stained for activation markers CD25, OX40 and ICOS and compared to DMSO unstimulated controls. Baseline expression (stimulation with DMSO) of ICOS and OX40 upon Tfh was high, with low levels of CD25 and CD154 observed (Fig. 3A). As a



(caption on next page)

Fig. 6. Comparison of activation markers for identifying Ag-specific Tfh cells.
(A) mLN-derived cells were stimulated with DMSO, HA peptide pool or ConA for 18 h. Boolean gating was used to identify the phenotypes of antigen-specific Tfh cells expressing any combination of CD25, OX40, ICOS or CD154. Error bars indicate mean ± SD from 2 replicates. (B) Boolean-gated populations were combined to determine the combination of two activation markers that best identified antigen-specific Tfh cells. Error bars indicate mean ± SD from 2 replicates. (C) Representative plots of CD154+ expression on Tfh cells after DMSO, HA peptide pool or ConA stimulation for 18 h. (D) Representative plots identifying CD25 + OX40++ Tfh cells after DMSO, HA peptide pool or ConA stimulation for 18 h. All results are representative of 3 independent experiments. (E) Quantification of Ag-specific Tfh cells measured by the proportion of CD154+ or CD25 + OX40++ cells after background subtraction in individual influenza infected or HA vaccinated mice. N = 5 mice in each group. All results are representative of 2 independent experiments.

result, we assessed activation defined by CD25 or CD154 expression, or the proportion of cells with an OX40++ or ICOS++ phenotype. Stimulation with ConA confirmed that all four markers were upregulated upon Tfh cell activation. Stimulation with the HA peptide pool similarly resulted in the upregulation of the activation markers (Fig. 3B), confirming that these markers have utility for identifying Ag-specific Tfh populations in mice.

3.4. Kinetics of Ag-specific Tfh activation and viability

To optimise the detection of Ag-specific Tfh, we next determined the kinetics of Tfh cell activation marker expression following HA peptide stimulation. Overall, the expression of all four markers increased as the stimulation time increased from 12 to 18 to 24 h (Fig. 4A). We noted, however, that recovery of sufficient Tfh cells for analysis was a limiting variable following cell culture. Analysis of sort-purified Tfh and non-Tfh CD4+ T cells confirmed that Tfh cells died more readily than non-Tfh cells during culture (Fig. 4B). Thus, although the viability of the bulk population of mLN lymphocytes changed little from 12 h to 24 h of culture (93% live cells at 12 h versus 89.5% at 24 h), approximately 30% of the Tfh population was lost during this time period (2.56% of bulk CD4+ T cells at 12 h versus 1.78% at 24 h, Fig. 4C). We therefore selected a stimulation time of 18 h in order to achieve a balance between Tfh cell loss and upregulation of surface activation markers.

3.5. Maintenance of antigen-specific Tfh phenotype over time

Given the changes in sort-purified Tfh surface phenotype after 18 h of cell culture (Fig. 2A), and the progressive loss of Tfh cells in MLN cultures from 12 to 24 h (Fig. 4C), we sought to determine whether HA-specific Tfh cells progressively downregulated PD-1 expression over this time period. A comparison of PD-1 and activation marker expression among Tfh cells at 12, 18 and 24 hours post-HA stimulation revealed that antigen-specific Tfh cells consistently maintained a high level of PD-1 expression, regardless of the timepoint examined (Fig. 5). This data suggests that antigen-specific Tfh cells do not exhibit preferential loss of PD-1 expression over time, and that their loss from bulk MLN cultures is largely attributable to cell death.

3.6. CD154 and CD25/OX40 best identify Ag-specific Tfh cells

While all four markers examined demonstrated dynamic expression upon Tfh in response to stimulation, we used Boolean gating to identify combinations of markers that most robustly identified Ag-specific Tfh cells (Fig. 6A). Considering all 15 four-marker combinations, CD154 single-positive cells represented the highest proportion of influenza-specific Tfh cells following infection (Fig. 6A). When analyzed using combinations of two markers, the CD25 + OX40++ phenotype identified the highest proportion of Ag-specific cells (Fig. 6B). We therefore focused on CD154+ cells and CD25 + OX40++ cells. CD154 upregulation alone detected approximately 60% of the total influenza-specific Tfh identified by AIM expression, while the CD25 + OX40++ phenotype identified 23% of total Ag-specific cells. We therefore conclude that detection of CD154 with a monoclonal antibody during cell culture (Fig. 6C) and/or quantification of CD25 + OX40++ cells following 18 h of peptide stimulation (Fig. 6D) provide the greatest sensitivity for identifying Ag-specific Tfh cells in mice.

Using this assay, we found that a mean of 4.32% (3.06–5.34, ± 0.92) of Tfh cells identified by CD154+ or 1.13% (0.75–1.44, ± 0.25) of Tfh cells identified by CD25 + OX40++ are HA-specific following influenza infection across individual mice (Fig. 6E). In comparison, HA vaccination results in a mean of 20.49% (11.07–20.84, ± 6.30) HA-specific Tfh cells measured by CD154+ or 8.14% (3.00–15.10, ± 4.66) HA-specific Tfh cells measured by CD25 + OX40++ (Fig. 6E). The assay was reliable and reproducible across different experiments, using either pooled LN suspensions or LN suspensions from individual mice.

3.7. Detection of Ag-specific Tfh cells following whole protein stimulation

In situations where peptide pools are impractical to obtain or produce, whole proteins may be required as the antigen source for Tfh re-stimulation. While Ag-specific Tfh cells can be readily identified following peptide stimulation in 500 µL RF10 using 48-well plates, we found that whole proteins elicited relatively poor responses under the same conditions. Therefore, we modified the assay to detect Ag-specific Tfh cells following whole protein stimulation. We found that using 96-well U-bottom plates and a culture volume of 200 µL RF10 induced robust upregulation of AIM markers with LN suspensions from both influenza-infected and HA-vaccinated mice (Fig. 7A). Stimulation with whole HA protein facilitated the identification of a mean of 4.66% (3.21–6.49, ± 1.31) or 3.83% (2.60–5.10, ± 1.11) of HA-specific Tfh cells based upon CD154+ or CD25 + OX40++ upregulation respectively (Fig. 7B). By comparison, following HA vaccination we observed a mean of 3.17% (0.66–7.60, ± 2.94) HA-specific Tfh cells measured by CD154+ or 23.29% (16.77–28.90, ± 4.33) HA-specific Tfh cells measured by CD25 + OX40++ (Fig. 7B). As an alternative, we obtained similar results by co-culturing LN suspensions with autologous splenocytes (LN cells: splenocytes = 10:1) in a 48-well plate in 500 µl RF10 (Fig. 7C). Using this method, 4.01% (detected by CD154+) or 3.10% (detected by CD25 + OX40++) of Tfh cells were HA-specific for influenza-infected mice and 1.22% (detected by CD154+) or 5.84% (detected by CD25 + OX40++) of Tfh cells are HA-specific for HA-vaccinated mice (Fig. 7C). Notably, the discrepancy between the CD154+ and CD25 + OX40++ readouts suggest that the CD25 + OX40++ phenotype may be a more robust marker of Ag-specific Tfh following re-stimulation with whole protein. Taken together, these data show that Ag-specific Tfh cells could be detected following whole protein stimulation either using LN suspensions alone in 96-well U-bottom plates or co-culture of LN suspensions with splenocytes in 48-well plates.

4. Discussion

Characterization of Ag-specific Tfh cells can greatly assist providing an immunological rationale for the design of novel vaccines against infectious pathogens. However, it is difficult to detect Ag-specific GC Tfh cells by conventional ICS, and methods to study Ag-specific Tfh in mice are lacking. The use of CD25/OX40 for identification of human and macaque Ag-specific Tfh cells has been reported (Dan et al., 2016; Havenar-Daughton et al., 2016), but not validated in mice. Considering the crucial role of CD154 plays in the interaction between Tfh and GC B

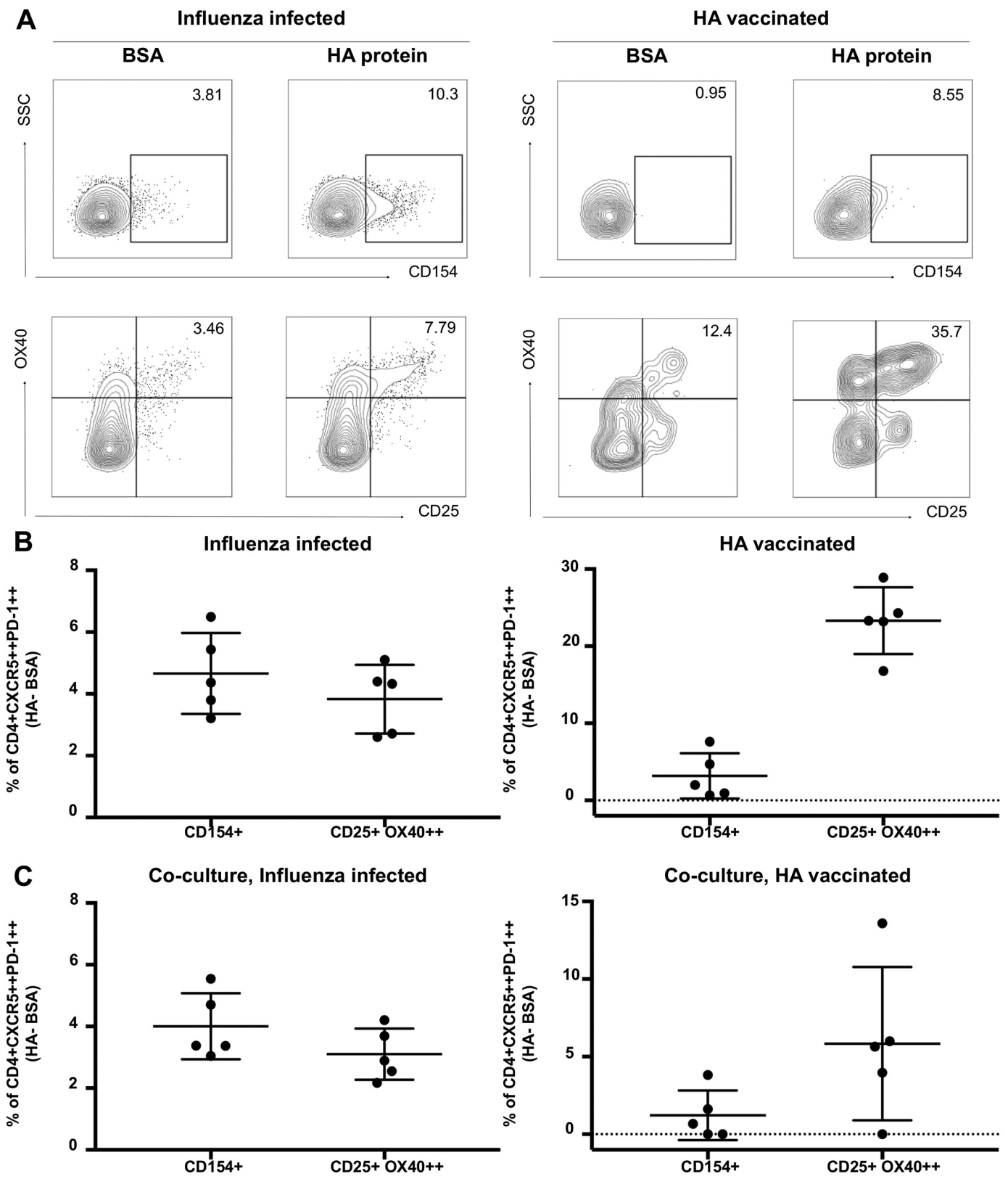


Fig. 7. Modification of assay for whole protein stimulation.

Draining lymph nodes were harvested from mice 14 days post-infection or HA vaccination. (A) LN suspensions were cultured in 200uL of RF10 in 96-well U-bottom plates for 18 h and stimulated with 5 μg/mL HA protein or BSA. Plots show representative CD154 or CD25/OX40 staining following stimulation in individual influenza infected or HA vaccinated mice (representative of n = 5). (B) Quantification of Ag-specific Tfh cells measured by the proportion of CD154 + or CD25 + OX40 + + cells after background subtraction. N = 5 mice in each group. (C) LN suspensions were co-cultured with autologous splenocytes (LN cells: splenocytes = 10:1) in 500 μL RF10 and stimulated with HA protein or BSA. Graph shows proportion of Ag-specific Tfh as defined by CD154 + or CD25 + OX40 + + cells. N = 5 mice in each group.

cells, we also tested it as a candidate activation marker. In this study, we adapted an AIM assay to identify mouse Ag-specific Tfh cells and confirmed that these cells were best detected by quantifying the upregulation of CD154 and CD25/OX40.

Previous studies have highlighted that GC Tfh cells are highly susceptible to apoptosis due to expression of Fas (CD95) (Breitfeld et al., 2000; Marinova et al., 2006; Bentebibel et al., 2011). Once removed from the GC environment, cell culture of this population can be challenging. A primary consideration in the development of a murine AIM assay was therefore ensuring the viability and recovery of Tfh cells following extended cell culture. Although the upregulation of all activation markers studied was greatest at 24 h post stimulation, the Tfh population was prone to cell death and continually declined as the cell culture time increased. Thus, an 18 h stimulation presented the optimal balance of sensitivity and cell viability. While we cannot fully exclude the possibility that a small proportion of antigen-specific Tfh cells downregulate CXCR5 and PD-1 to such an extent that they are no longer captured in the post-culture Tfh gate, the antigen-specific Tfh population maintained high levels of PD-1 expression with no observable downregulation throughout 12–24 h of cell culture and HA peptide stimulation.

Transgenic mice (such as OT II mice) are a powerful tool to study the Ag-specific Tfh cell response to model antigens (such as OVA). Similarly, MHC-II tetramers are insightful reagents to identify Ag-specific Tfh cells in wild-type mice for antigens with defined CD4 T cell epitopes. However there is a critical need for a robust assay to assess Tfh responses to complex antigens in mice, not restricted by a given MHC haplotype. Our AIM-based method for identifying Ag-specific Tfh cells provides a starting point to broaden investigations into Tfh activity and phenotype in mice. In particular, Ag-specific Tfh cells could be sorted for downstream applications, such as TCR sequencing or adoptive transfer experiments. We demonstrated that Ag-specific Tfh cells could restimulated with wither peptide or whole proteins, with comparable frequencies of HA-specific Tfh detected after infection using either approach. The ability to use whole protein stimulation is a tremendous asset that reduces experimental complexity and extends the utility of this our approach to situations where peptide pools are unavailable due to size or cost considerations. In summary, we developed a sensitive assay for identifying mouse Ag-specific Tfh cells using CD154 or CD25/OX40 upregulation that preserves both cell viability and Tfh phenotype.

Acknowledgements

This work was supported by NHMRC grants APP1052979 and GNT112909. WJ is supported by a Melbourne International Research Scholarship and Melbourne International Fee Remission Scholarship. JAJ and SJK are supported by NHMRC fellowships.

References

Bentebibel, S.E., Schmitt, N., Banchereau, J., Ueno, H., 2011. Human tonsil B-cell lymphoma 6 (BCL6)-expressing CD4+ T-cell subset specialized for B-cell help outside germinal centers. Proc. Natl. Acad. Sci. U. S. A. 108, E488–E497.

Bowyer, G., Rampling, T., Powlson, J., Morter, R., Wright, D., Hill, A.V.S., Ewer, K.J., 2018. Activation-induced markers detect vaccine-specific CD4(+) T cell responses not measured by assays conventionally used in clinical trials. Vaccines (Basel) 6.

Breitfeld, D., Ohl, L., Kremmer, E., Ellwart, J., Sallusto, F., Lipp, M., Forster, R., 2000. Follicular B helper T cells express CXC chemokine receptor 5, localize to B cell follicles, and support immunoglobulin production. J. Exp. Med. 192, 1545–1552.

Chattopadhyay, P.K., Yu, J., Roederer, M., 2005. A live-cell assay to detect antigen-specific CD4(+) T cells with diverse cytokine profiles. Nat. Med. 11, 1113–1117.

Crotty, S., 2011. Follicular helper CD4 T cells (TFH). Annu. Rev. Immunol. 29, 621–663.

Dan, J.M., Lindestam Arlehamn, C.S., Weiskopf, D., da Silva Antunes, R., Havenar-Daughton, C., Reiss, S.M., Brigger, M., Bothwell, M., Sette, A., Crotty, S., 2016. A cytokine-independent approach to identify antigen-specific human germinal center T follicular helper cells and rare antigen-specific CD4+ T cells in blood. J. Immunol. 197, 983–993.

Frentsch, M., Arbach, O., Kirchhoff, D., Moewes, B., Worm, M., Rothe, M., Scheffold, A., Thiel, A., 2005. Direct access to CD4(+) T cells specific for defined antigens according to CD154 expression. Nat. Med. 11, 1118–1124.

Gatto, D., Brink, R., 2010. The germinal center reaction. J. Allergy Clin. Immunol. 126, 898–907 (quiz 908-9).

Havenar-Daughton, C., Reiss, S.M., Carnathan, D.G., Wu, J.E., Kendric, K., Torrents de la Pena, A., Kasturi, S.P., Dan, J.M., Bothwell, M., Sanders, R.W., Pulendran, B., Silvestri, G., Crotty, S., 2016. Cytokine-independent detection of antigen-specific germinal center T follicular helper cells in immunized nonhuman primates using a live cell activation-induced marker technique. J. Immunol. 197, 994–1002.

Johnston, R.J., Poholek, A.C., DiToro, D., Yusuf, I., Eto, D., Barnett, B., Dent, A.L., Craft, J., Crotty, S., 2009. Bcl6 and Blimp-1 are reciprocal and antagonistic regulators of T follicular helper cell differentiation. Science 325, 1006–1010.

Keoshkerian, E., Helbig, K., Beard, M., Zaunders, J., Seddiki, N., Kelleher, A., Hampartzoumian, T., Zekry, A., Lloyd, A.R., 2012. A novel assay for detection of hepatitis C virus-specific effector CD4(+) T cells via co-expression of CD25 and CD134. J. Immunol. Methods 375, 148–158.

Linterman, M.A., Hill, D.L., 2016. Can follicular helper T cells be targeted to improve vaccine efficacy? F1000Res 5.

Liu, D., Xu, H., Shih, C., Wan, Z., Ma, X., Ma, W., Luo, D., Qi, H., 2015. T-B-cell entanglement and ICOSL-driven feed-forward regulation of germinal centre reaction. Nature 517, 214–218.

Marinova, E., Han, S., Zheng, B., 2006. Human germinal center T cells are unique Th cells with high propensity for apoptosis induction. Int. Immunol. 18, 1337–1345.

Meli, A.P., King, I.L., 2015. Identification of mouse T follicular helper cells by flow cytometry. Methods Mol. Biol. 1291, 3–11.

Nurieva, R.I., Chung, Y., Martinez, G.J., Yang, X.O., Tanaka, S., Matskevitch, T.D., Wang, Y.H., Dong, C., 2009. Bcl6 mediates the development of T follicular helper cells. Science 325, 1001–1005.

Phetsouphanh, C., Zaunders, J.J., Kelleher, A.D., 2015. Detecting antigen-specific T cell responses: from bulk populations to single cells. Int. J. Mol. Sci. 16, 18878–18893.

Qi, H., 2016. T follicular helper cells in space-time. Nat Rev Immunol 16, 612–625.

Reiss, S., Baxter, A.E., Cirelli, K.M., Dan, J.M., Morou, A., Daigneault, A., Brassard, N., Silvestri, G., Routy, J.P., Havenar-Daughton, C., Crotty, S., Kaufmann, D.E., 2017. Comparative analysis of activation induced marker (AIM) assays for sensitive identification of antigen-specific CD4 T cells. PLoS One 12, e0186998.

Tangye, S.G., Brink, R., Goodnow, C.C., Phan, T.G., 2015. SnapShot: interactions between B cells and T cells. Cell 162.

Victora, G.D., Nussenzweig, M.C., 2012. Germinal centers. Annu. Rev. Immunol. 30, 429–457.

Victora, G.D., Schwickert, T.A., Fooksman, D.R., Kamphorst, A.O., Meyer-Hermann, M., Dustin, M.L., Nussenzweig, M.C., 2010. Germinal center dynamics revealed by multiphoton microscopy with a photoactivatable fluorescent reporter. Cell 143, 592–605.

Vinuesa, C.G., Linterman, M.A., Yu, D., MacLennan, I.C., 2016. Follicular helper T cells. Annu. Rev. Immunol. 34, 335–368.

Yu, D., Rao, S., Tsai, L.M., Lee, S.K., He, Y., Sutcliffe, E.L., Srivastava, M., Linterman, M., Zheng, L., Simpson, N., Ellyard, J.I., Parish, I.A., Ma, C.S., Li, Q.J., Parish, C.R., Mackay, C.R., Vinuesa, C.G., 2009. The transcriptional repressor Bcl-6 directs T follicular helper cell lineage commitment. Immunity 31, 457–468.

Zaunders, J.J., Munier, M.L., Seddiki, N., Pett, S., Ip, S., Bailey, M., Xu, Y., Brown, K., Dyer, W.B., Kim, M., de Rose, R., Kent, S.J., Jiang, L., Breit, S.N., Emery, S., Cunningham, A.L., Cooper, D.A., Kelleher, A.D., 2009. High levels of human antigen-specific CD4+ T cells in peripheral blood revealed by stimulated coexpression of CD25 and CD134 (OX40). J. Immunol. 183, 2827–2836.

Chapter 3: Screening and development of monoclonal antibodies for identification of ferret T follicular helper cells

scientific reports

Check for updates

OPEN

Screening and development of monoclonal antibodies for identification of ferret T follicular helper cells

Wenbo Jiang[1], Julius Wong[1], Hyon-Xhi Tan[1], Hannah G. Kelly[1], Paul G. Whitney[2], Ian Barr[2], Daniel S. Layton[3], Stephen J. Kent[1,4,5], Adam K. Wheatley[1]✉ & Jennifer A. Juno[1]✉

The ferret is a key animal model for investigating the pathogenicity and transmissibility of important human viruses, and for the pre-clinical assessment of vaccines. However, relatively little is known about the ferret immune system, due in part to a paucity of ferret-reactive reagents. In particular, T follicular helper (Tfh) cells are critical in the generation of effective humoral responses in humans, mice and other animal models but to date it has not been possible to identify Tfh in ferrets. Here, we describe the screening and development of ferret-reactive BCL6, CXCR5 and PD-1 monoclonal antibodies. We found two commercial anti-BCL6 antibodies (clone K112-91 and clone IG191E/A8) had cross-reactivity with lymph node cells from influenza-infected ferrets. We next developed two murine monoclonal antibodies against ferret CXCR5 (clone feX5-C05) and PD-1 (clone fePD-CL1) using a single B cell PCR-based method. We were able to clearly identify Tfh cells in lymph nodes from influenza infected ferrets using these antibodies. The development of ferret Tfh marker antibodies and the identification of ferret Tfh cells will assist the evaluation of vaccine-induced Tfh responses in the ferret model and the design of novel vaccines against the infection of influenza and other viruses, including SARS-CoV2.

Ferrets (Mustela putorius furo) are a well-established animal model for influenza research and are widely used to investigate the pathogenesis and transmission of influenza viruses and pre-clinically evaluate the efficacy of influenza vaccines[1,2]. In addition, ferrets serve as an animal model for the study of other viruses, including human respiratory syncytial virus (HRSV)[3], human metapneumovirus (HMPV)[4], Hendra virus (HeV)[5], Nipah virus (NiV)[5], different species of ebolavirus[6] and severe acute respiratory syndrome coronavirus (SARS-CoV)[7]. Martina et al. demonstrated that ferrets are susceptible to experimental infection by SARS-CoV, and that the virus is efficiently transmitted to animals living with them[8]. It has now been shown that ferrets are similarly susceptible to the pandemic virus severe acute respiratory syndrome coronavirus 2 (SARS-CoV-2), and that the virus replicates efficiently in the upper respiratory tract of ferrets[9,10]. Ferrets are therefore a useful model in which to assess neutralizing antibody responses to viral challenge and to test novel vaccine candidates[11].

Characterization of the ferret immune response following infection and/or vaccination is informative for developing vaccines and anti-viral therapies. However, a diverse range of ferret-specific immunological reagents are not currently available. One major gap is the lack of reagents to study T follicular helper (Tfh) cells, which are critical for the generation and maturation of the antibody response. Tfh cells are a subset of CD4 T cells that provide help with B cells for high-affinity antibody production in germinal centres (GC)[12–14]. These specialised cells are crucial for the formation of GC, affinity maturation and maintenance of B cell memory. BCL6 is the master transcription factor for Tfh differentiation. Distinguishing phenotypic markers of Tfh cells include the high expression of CXCR5, PD-1, and ICOS[12]. High CXCR5 expression facilitates Tfh cells migration to B cell follicles where its ligand, CXCL13 is produced abundantly by follicular stromal cells. PD-1 and ICOS are required

[1]Department of Microbiology and Immunology, Peter Doherty Institute for Infection and Immunity, University of Melbourne, Melbourne, VIC, Australia. [2]WHO Collaborating Centre for Reference and Research On Influenza, Peter Doherty Institute for Infection and Immunity, University of Melbourne, Melbourne, VIC, Australia. [3]CSIRO Health and Biosecurity, Australian Animal Health Laboratories, Geelong, VIC, Australia. [4]Melbourne Sexual Health Clinic and Infectious Diseases Department, Alfred Hospital, Monash University Central Clinical School, Carlton, VIC, Australia. [5]ARC Centre for Excellence in Convergent Bio-Nano Science and Technology, University of Melbourne, Melbourne, Australia. ✉email: a.wheatley@unimelb.edu.au; jennifer.juno@unimelb.edu.au

to engage with their respective ligands, PD-L1/PDL-2 and ICOSL, which are expressed by GC B cells to support the development of Tfh cells[12].

Here, we describe the screening and development of ferret Tfh marker monoclonal antibodies and identification of ferret Tfh cells using these antibodies. We first identified two commercial anti-human/mouse BCL6 antibodies which had cross-reactivity with ferret lymph node (LN) cells. We next developed mouse anti-ferret CXCR5 and PD-1 monoclonal antibodies using single cell PCR-based method. Finally, we detected Tfh cells in lymph nodes from influenza infected ferrets using these antibodies.

Results

Screening of commercial anti-human or mouse BCL6, CXCR5 and PD-1 antibodies for cross-reactivity with ferret lymph node cells. BCL6 expression is the canonical transcription factor that distinguishes Tfh cells from other CD4+ T cells in human and mouse[15–17]. However, high co-expression of CXCR5 and PD-1 serves as surrogate or confirmatory surface markers for the Tfh population in human and mouse lymphoid tissues[18]. Commercial anti-human/mouse BCL6 antibodies were screened for cross-reactivity against ferrets by staining LN cell suspensions recovered from influenza infected ferrets. The gating strategy to identify live lymphocytes in the ferret LN is shown in Fig. 1a. We found that clones K112-91 and IG191E/A8, originally developed for human BCL6[15,16], showed cross-reactivity with ferret cLN cells (Fig. 1b). The BCL6+ B cell (CD79a+) population represents a putative GC B cell population, while BCL6+ CD4+ cells are likely to mark Tfh cells although additional markers are needed.

We next screened commercial antibodies raised against mouse or human CXCR5 (clones L138D7 and RF8B2) and PD-1 (clones 29F.1A12 and EH12.2H7) for ferret cross-reactivity. Unfortunately, all screened murine and human antibodies showed no cross-reactivity with ferret lymph node cells (data not shown) although they showed good reactivity with mouse or human lymph node cells. Thus, we initiated the generation of ferret CXCR5 and PD-1-specific monoclonal antibodies.

Homology analysis of ferret, human and mouse BCL6, CXCR5 and PD-1. Comparison of amino acid homology of ferret, human and mouse BCL6, CXCR5 and PD-1 confirmed ferret BCL6 was a highly conserved, with high homology to both human BCL6 (95.47%) and mouse BCL6 (93.78%) (Table 1). In contrast, ferret CXCR5 had only moderate homology with human CXCR5 (84.22%) and mouse CXCR5 (87.43%) and ferret PD-1 had low homology with both human (67.24%) and mouse PD-1 (54.48%), consistent with the lack of ferret cross-reactivity of commercially available CXCR5 and PD-1-specific monoclonal antibodies.

Generation of mouse anti-ferret CXCR5 and PD-1 monoclonal antibodies. Due to the low sequence conservation, we initiated the de novo development of anti-ferret PD1 and CXCR5 monoclonal antibodies for flow cytometric use (workflow in Fig. 2). The cDNA sequence of the ectodomains of ferret CXCR5 and PD-1 were identified using a NGS dataset (Wong et al. in press). These genes were synthesized and cloned into a mammalian expression vector containing human IgG1 Fc tag used for protein purification. Recombinant proteins were expressed by Expi293 cells and purified by protein A agarose. Next, we immunized C57BL/6 mice with recombinant ferret CXCR5 or PD-1 proteins. At day 21 post-immunization, we isolated draining lymph nodes from the mice, stained lymph node cell suspensions with a panel of antibodies as well as immunogen probes. The murine GC B cells binding to the fluorescent ferret CXCR5 or PD-1 probes were single-cell-sorted into 96-well PCR plates. The BCR sequences of sorted B cells were then recovered by single cell PCR with mouse IgG heavy or light chain primers[19]. The variable domains genes of heavy or kappa chains from clonally expanded families of B cells were synthesized and cloned into mammalian expression vectors containing mouse IgG1 or kappa chain constant domain gene. Antibodies were expressed in Expi293 and purified by protein G agarose.

Validation of anti-ferret CXCR5 and PD-1 monoclonal antibodies by ELISA. The binding specificity of the putative mouse anti-ferret CXCR5 and PD-1 antibodies was first assessed by ELISA. An irrelevant antigen with the same Fc tag as recombinant ferret CXCR5 or PD-1 proteins was used as a control. Anti-ferret CXCR5 clone A09 (feX5-A09), B04 (feX5-B04), C05 (feX5-C05) and E04 (feX5-E04) showed high binding activity with ferret CXCR5 proteins with an EC50 of 0.0109 µg/ml, 0.0036 µg/ml, 0.0027 µg/ml, 0.0033 µg/ml, respectively (Fig. 3a). Anti-ferret PD-1 clone CL1 (fePD-CL1) similarly displayed high binding activity with ferret PD-1 proteins with an EC50 of 0.0052 µg/ml while clone CL2 (fePD-CL2) showed no binding activity with ferret PD-1 proteins by ELISA (Fig. 3b). All antibodies showed no binding with control proteins, demonstrating that the antibodies were not targeted against Fc tag region of the recombinant proteins.

Identification of Tfh cells in lymph node cells from influenza infected ferrets. The ability of mAb feX5-C05 (anti-CXCR5) and fePD-CL1 (anti-PD1) to stain ferret lymphocytes was examined using flow cytometry. Single cell suspensions from the LN of influenza infected ferrets were stained with a panel consisting of anti-BCL6, CD4 and CD79a antibodies and anti-CXCR5 (feX5-C05) and anti-PD1 (fePD-CL1) conjugated to biotin and PE, respectively (gating in Fig. 4a). CXCR5++ PD-1++ CD4 T cells display elevated expression of BCL6 relative to non-Tfh cells (CD4+ CXCR5− PD−1−), consistent with a Tfh cell identity (Fig. 4b). Furthermore, the CXCR5 and PD-1 expression pattern of ferret CD4 T cells is similar to that of mouse and macaque CD4 T cells (Fig. 4c). In addition to CD4 T cells, CXCR5 is highly expressed by mouse and macaque B cells (Fig. 4d). Consistent with mouse and macaque data, we found that ferret CD79a+ B cells were also predominately CXCR5+ (Fig. 4d). Taken together, these data show that ferret Tfh cells are detected by our in-house developed anti-ferret CXCR5 and PD-1 antibodies or combination with a commercial cross-reactive anti-BCL6 antibody.

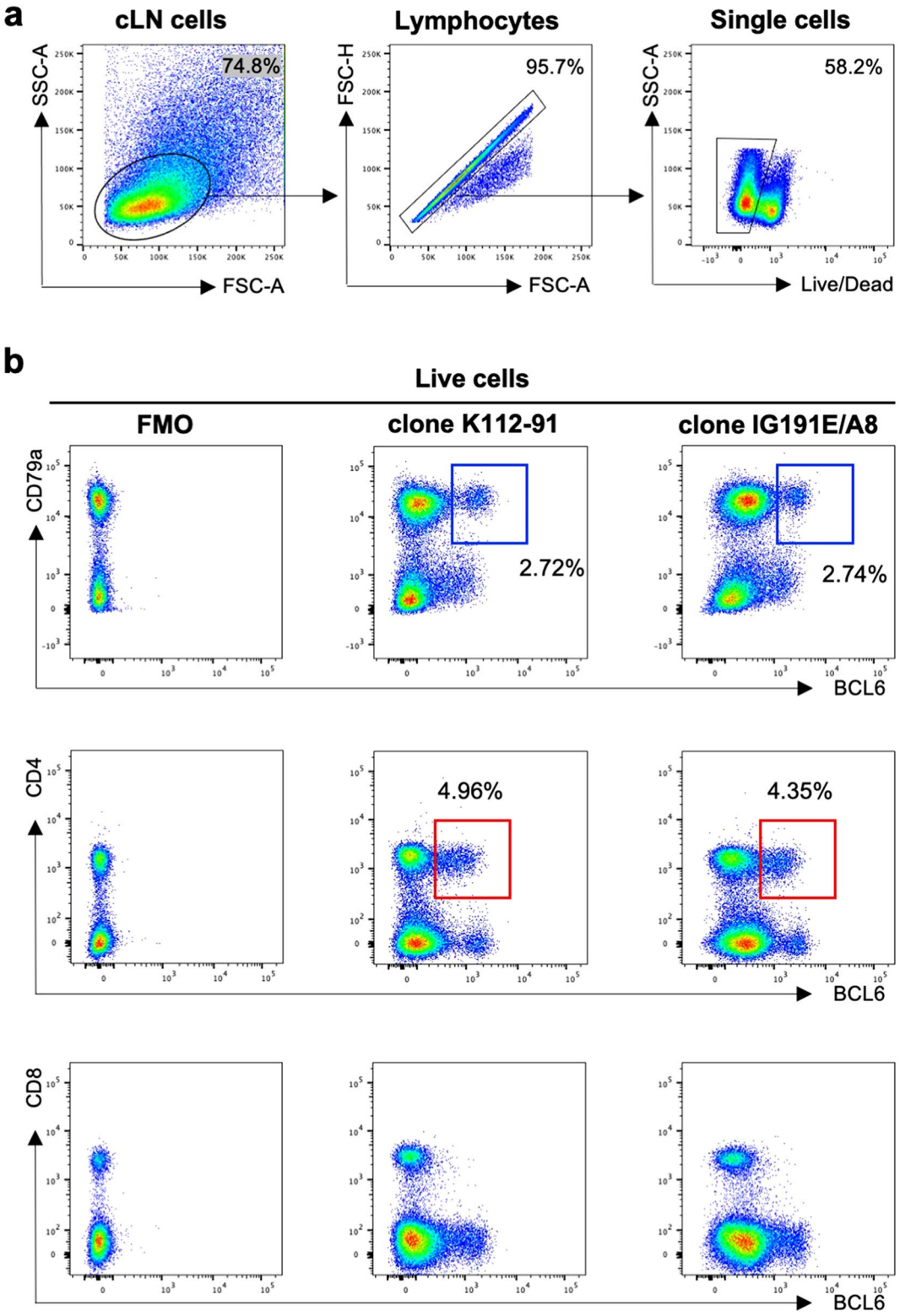


Figure 1. Cross-reactivity of commercial anti-human/mouse BCL6 antibodies with lymph node cells from influenza infected ferret. (**a**) Gating strategy to identify live lymphocytes in the ferret LN. Lymphocytes were identified by forward scatter area (FSC-A) and side-scatter area (SSC-A). Doublets were excluded by gating on single cells as determined by FSC-A versus FSC-H, and live cells were identified by viability dye exclusion. For each step, the parental population is indicated above the plot. (**b**) Representative plots of influenza-infected ferret lymph node cells stained with anti-BCL 6 (clone K112-91 and clone IG191E/A8), CD79a, CD4 and CD8 antibodies. The parental population is indicated above the plot. Blue box indicates GC B cells (BCL6+CD79a+) and red box indicates Tfh cells (BCL6+CD4+).

Antigen	Antigen homology (%)		
	Ferret vs human	Ferret vs mouse	Human vs Mouse
BCL6	95.47	93.78	94.63
CXCR5	84.22	87.43	83.16
PD-1	67.24	54.48	59.31

Table 1. Antigen homology of ferret, human and mouse BCL6, CXCR5 and PD-1.

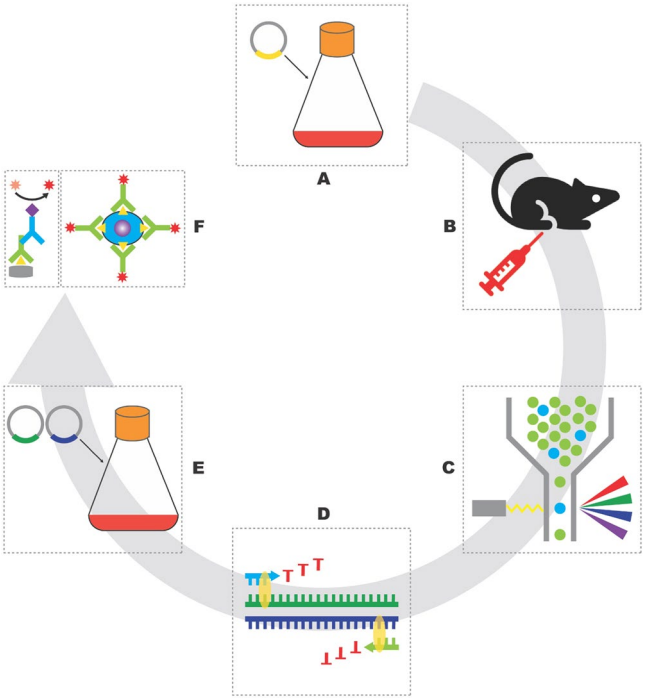


Figure 2. Flow chart to develop mouse anti-ferret CXCR5 and PD-1 monoclonal antibodies. Antigens were expressed by transiently transfection of Expi293 cells (**a**), C57BL/6 mice were intramuscularly immunized with purified antigens (**b**), antigen-specific B cells were single-cell-sorted by Aria III (**c**), the sequences of heavy and light chain variable domains of BCR were recovered by single cell PCR (**d**), candidate antibody clones were expressed by transiently transfection of Expi293 cells with heavy and light chain plasmids (**e**), purified antibodies were validated by ELISA and FACS (**f**). Illustration was drawn using Adobe Illustrator 2020.

Discussion

Protective antibody responses induced by vaccination play a central role in defense against virus infection[14]. Ferrets are a useful animal model for studying the pathogenicity and transmissibility of several human viruses and for pre-clinical evaluation of the in vivo protective efficacy of vaccines. The help signal provided by Tfh cells is a critical factor which determines the magnitude and quality of antibody responses[20]. Identification of Tfh cells in ferrets could greatly assist providing an immunological rationale for the design of novel vaccines against the infection of influenza and other viruses, including SARS-CoV2. However, key immunological reagents, such as ferret reactive Tfh marker monoclonal antibodies, were lacking until this report.

In the present study, we developed ferret-specific CXCR5 and PD-1 monoclonal antibodies and identified Tfh cells in ferrets. Identification of Tfh cells by surface CXCR5 and PD-1 staining is of great utility if live Tfh cell staining is needed (such as for antigen induced activation or RNA studies) since intranuclear BCL6 staining involves cell fixation and permeabilization. In addition, CXCR5 could be a surrogate surface B cell marker if intracellular staining is not warranted or wanted since the currently available marker for ferret B cells (a commercial cross-reactive CD79a antibody) requires intracellular staining. Furthermore, anti-ferret PD-1 antibody can be useful for studies of non-TFH T cell activation or exhaustion in this animal model (as demonstrated in Fig. 4), thereby increasing the complexity and detail of immunophenotype studies.

Ferret Tfh responses remain largely unexplored, and basic questions, such as what the magnitude and quality of ferret Tfh responses are in the context of virus infection or vaccination, and how Tfh responses correlate with antibody responses following vaccination, remain to be answered. With these ferret-specific CXCR5 and PD-1 antibodies, these questions can be investigated, including longitudinal tracking of Tfh activity following virus infection. Results from ferret Tfh response studies can provide useful insights regarding how Tfh cells influence

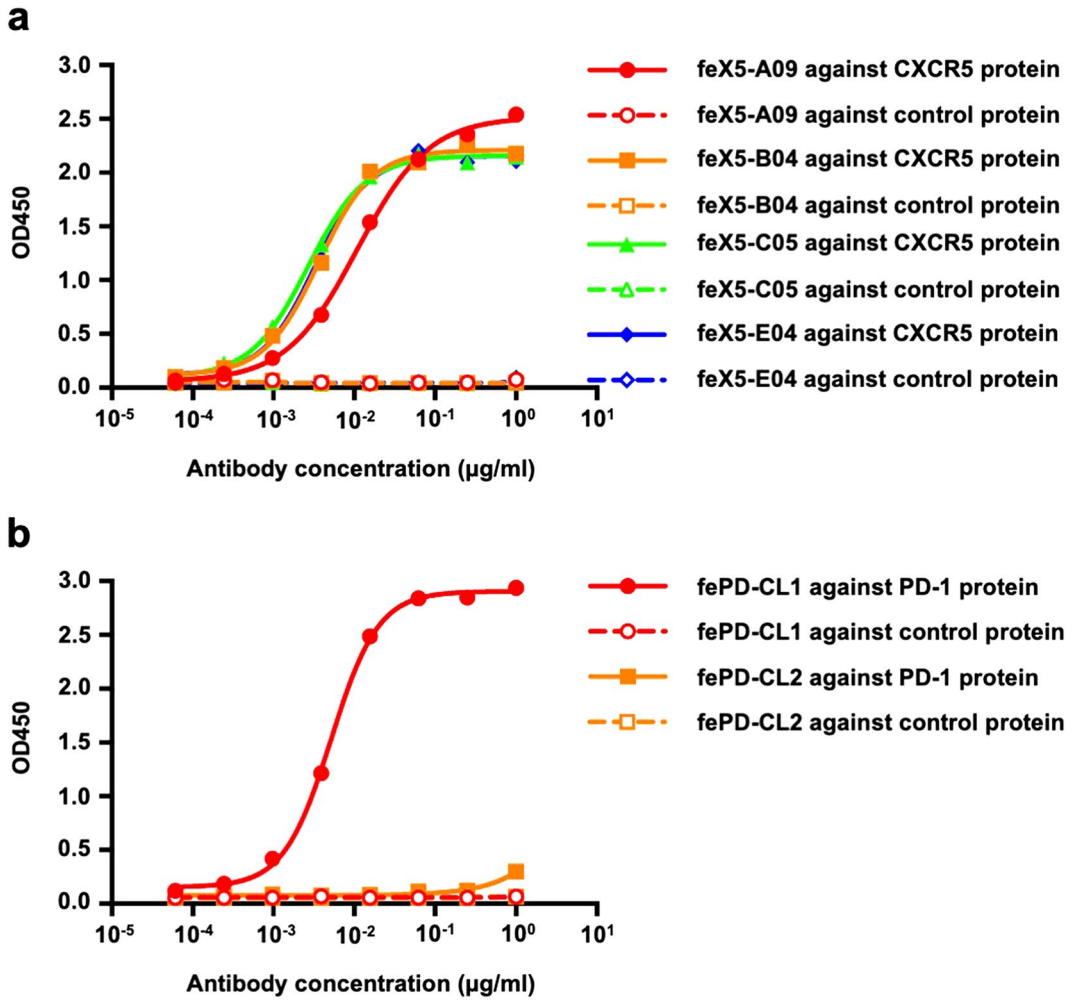


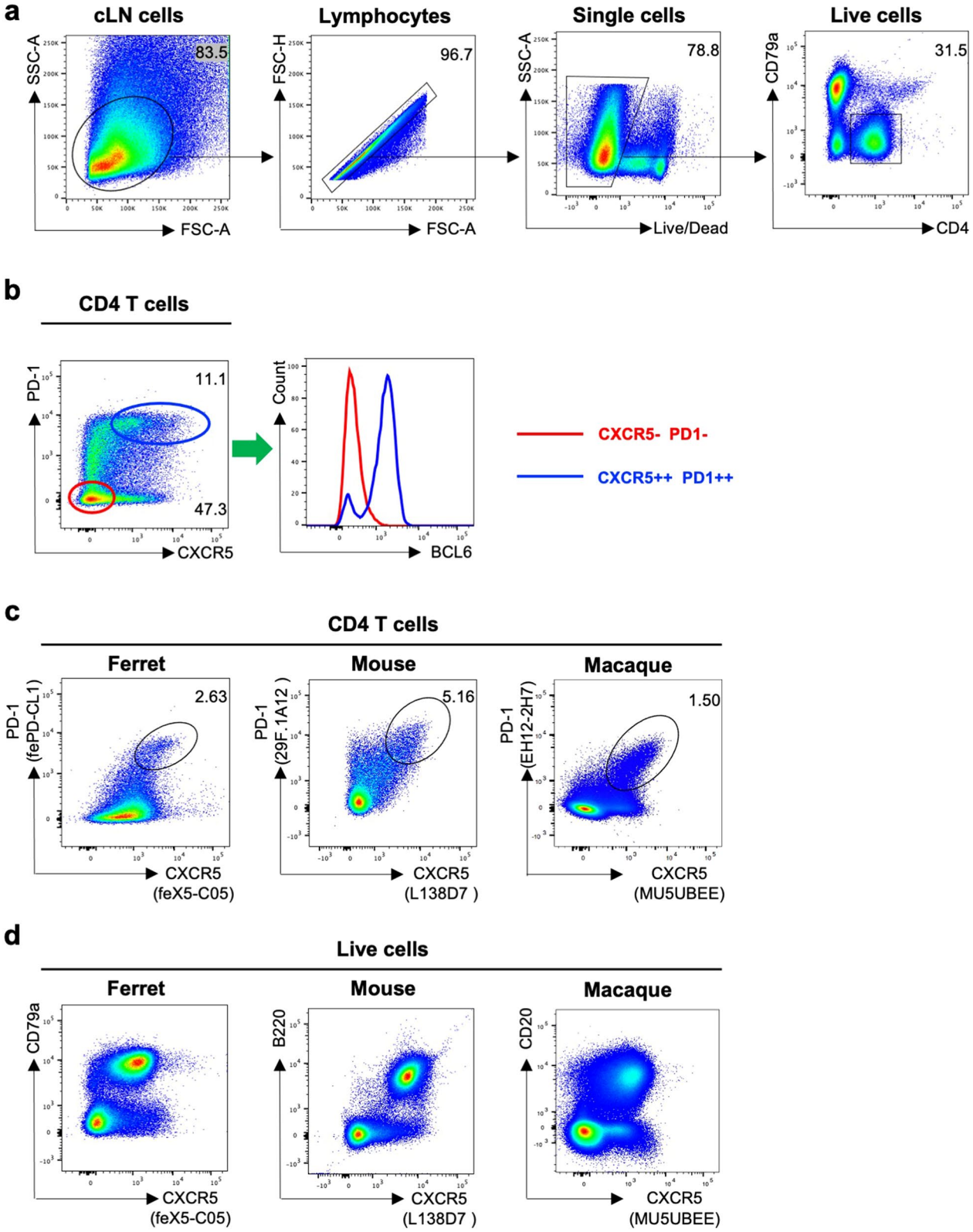
Figure 3. Binding activity of anti-CXCR5 and PD-1 antibodies with autologous and control antigens. (**a**) Binding activity of anti-ferret CXCR5 clone A09 (feX5-A09), B04 (feX5-B04), C05 (feX5-C05) and E04 (feX5-E04) against recombinant ferret CXCR5 protein or an irrelevant control protein with the same Fc tag. (**b**) Binding activity of anti-ferret PD-1 clone CL1 (fePD-CL1) and CL2 (fePD-CL2) against recombinant ferret PD-1 protein or an irrelevant control protein with the same Fc tag.

vaccine immunogenicity. These insights will assist the design and evaluation of novel Tfh-targeting vaccines against the infection of influenza and other viruses in ferrets, as they have for other animal models. Considering the current situation with coronavirus disease (COVID-19) pandemic, these reagents will be helpful in evaluation of the Tfh responses induced by COVID-19 vaccines in ferret model and accelerate the development of vaccines against SARS-CoV2 infection[9,10].

In summary, we developed ferret-specific CXCR5 and PD-1 monoclonal antibodies which were next used for detection of ferret Tfh cells. As these reagents identify surface-expressed antigens, they are compatible with live cell sorting and downstream RNA sequencing analysis, which can be challenging with antibodies requiring cell permeabilization and intracellular staining. The sequences of the heavy and light chain variable domains of anti-ferret CXCR5 and PD-1 antibodies are provided (Fig. 5) so that the field can use these reagents to advance the study of ferret Tfh. Recombinant antibodies can be expressed in a short time frame by transiently transfection of mammalian Expi293 cells. These ferret specific CXCR5 and PD-1 antibodies provide a starting point to allow in-depth study of the Tfh responses to viral infections, such as influenza and SARS-CoV2. Further reagents (such as anti-ferret CD154 monoclonal antibody) that are in critical need to identify antigen-specific Tfh are under development and will be made publicly available in the future.

Materials and methods

Animals and ethics. Mouse studies and related experimental procedures were approved by the University of Melbourne Animal Ethics Committee (#1914874) and were conducted in accordance with the Prevention of Cruelty to Animals Act (1986), the Australian National Health and Medical Research Council Code of Practice for the Care and Use of Animals for Scientific Purposes (1997) and the ARRIVE guidelines. Female C57BL/6 mice (6–8 weeks old) were immunized with 10 μg of recombinant ferret CXCR5 or PD-1 proteins with Addavax


a
cLN cells
Lymphocytes
Single cells
Live cells
SSC-A
FSC-A
83.5
FSC-H
96.7
78.8
Live/Dead
CD79a
CD4
31.5
b
CD4 T cells
PD-1
CXCR5
11.1
47.3
Count
BCL6
CXCR5- PD1-
CXCR5++ PD1++
c
CD4 T cells
Ferret
Mouse
Macaque
PD-1 (fePD-CL1)
CXCR5 (feX5-C05)
2.63
PD-1 (29F.1A12)
CXCR5 (L138D7)
5.16
PD-1 (EH12-2H7)
CXCR5 (MU5UBEE)
1.50
d
Live cells
Ferret
Mouse
Macaque
CD79a
CXCR5 (feX5-C05)
B220
CXCR5 (L138D7)
CD20
CXCR5 (MU5UBEE)

◂**Figure 4.** Identification of Tfh cells in lymph node cells from influenza infected ferrets. (**a**) Gating strategy to identify CD4 T cells in the ferret LN. Lymphocytes were identified by forward scatter area (FSC-A) and side-scatter area (SSC-A). Doublets were excluded by gating on single cells as determined by FSC-A versus FSC-H, live cells were identified by viability dye exclusion, CD4 T cells were identified as CD4+ CD79a−. For each step, the parental population is indicated above the plot. (**b**) Representative plots of ferret CD4 T cells stained with anti-BCL 6 (clone K112-91), anti-ferret CXCR5 (clone feX5-C05) and anti-ferret PD-1 (clone fePD-CL1) antibodies. The BCL6 expression of CXCR5++ PD-1++ CD4 T cells (Tfh, blue oval) were compared with CXCR5− PD-1− CD4 T cells (non-Tfh, red oval) cells. The parental population is indicated above the plot. (**c**) Representative plots of CD4 T cells from influenza-infected ferret, mouse and macaque LNs stained with species-appropriate CXCR5 and PD-1 antibodies (mouse, clones L138D7 and 29F.1A12 respectively; macaque, MU5UBEE and EH12.2H7 respectively). The parental population is indicated above the plot. (**d**) Representative plots of live lymphocytes from influenza-infected ferret, mouse and macaque LNs stained with their respective CXCR5 antibodies as well as CD79, B220 and CD19 antibodies. The parental population is indicated above the plot.

(1:1 ratio; InvivoGen) at both hind quadriceps using 29G needles. 21 days post vaccination, draining lymph nodes (inguinal lymph nodes (inLN) and iliac lymph nodes (ilLN)) were collected and mashed into single cell suspension using 70 µm strainer (Miltenyi Biotec) for staining.

Ferret specimens were collected from culled animals that were involved in experiments approved by The University of Melbourne Animal Ethics Committee (AEC 1714183) and were conducted in accordance with the Prevention of Cruelty to Animals Act (1986) and the Australian National Health and Medical Research Council Code of Practice for the Care and Use of Animals for Scientific Purposes (1997). Male ferrets were intranasally infected with between 1×10^4 to 1×10^6 TCID50 in 0.5 ml of A/Perth/265/2009. At day 14 post-infection, paratracheal lymph nodes from influenza-infected ferrets were removed, cut into small pieces and passing through a 70 µm strainer (Miltenyi Biotec). Single cell suspensions were then frozen in freezing media (90% fetal calf serum with 10% DMSO) and stored in liquid nitrogen.

As a comparator for pan-species expression of CXCR5 on T and B cell population, we assessed macaque Tfh and B cell phenotypes from lymph node samples. The macaque samples used in this were obtained from a macaque influenza vaccination trial and were processed as described previously[21].

Sequence analysis and recombinant protein generation. The nucleic acid sequences of ferret, human and mouse BCL6, CXCR5 and PD-1 were extracted from Ensembl website[22] and Centre for Biotechnology Information (NCBI). Amino acid homology of ferret, human and mouse BCL6, CXCR5 and PD-1 were compared using Geneious.

The ectodomain of ferret CXCR5 and PD-1 were identified using the NGS dataset (Wong et al. manuscript submitted). The gene sequence of ectodomains of ferret CXCR5 and PD-1 were codon-optimized and synthesized (GeneArt) and cloned into mammalian expression vector containing human IgG1 Fc tag. Plasmids were extracted using NucleoBond Xtra Midi Plus plasmid DNA kit (MACHEREY-NAGEL). Recombinant ferret CXCR5 and PD-1 proteins were expressed by transient transfection of Expi293 (Thermo) suspension cultures with 2.7 µl ExpiFectamine (Thermo) and 1ug DNA/ml cell culture. At day 5 post-transfection, proteins in culture supernatant were purified by protein A agarose affinity chromatography and gel filtration.

Sorting of ferret CXCR5 and PD-1 specific B cells. Recombinant ferret CXCR5 and PD-1 proteins were conjugated with APC or PE (Abcam) according to the manufacturer's instructions. The resulting fluorescent proteins were designated as probes. Cell suspension of draining lymph nodes from ferret CXCR5 and PD-1 immunized mice were stained with probes and the following panel: live/dead Aqua (Thermo Fisher), CD45 APC-Cy7 (30-F11; BD), CD3 BV785 (145-2C11; BioLegend), F4/80 BV785 (BM8; BioLegend), Streptavidin BV785 (BD), B220 BV650 (RA3-6B2; BD), IgD PerCP-Cy5.5 (11-26c.2a, BD), CD38 PE-Cy7 (90; BioLegend), GL7 AF488 (GL7; BioLegend). Probe-binding GC B cells were single-cell-sorted to 96-well PCR plates a BD Aria III.

RT-PCR. The BCR sequences of sorted ferret CXCR5 or PD-1 specific B cells were recovered as previously described[19]. Briefly, the mRNA of sorted single B cells was reversely transcribed into cDNA using SuperScript III reverse transcriptase (Thermo) and random hexamer primers (Bioline). The sequences of heavy and light chain variable domains were then amplified by nested PCR using HotStarTaq DNA polymerase (Qiagen) and mouse immunoglobulin heavy and light chain primers[19]. PCR products were sequenced in Macrogen.

Antibody generation. The gene of heavy or kappa chain variable domain was synthesized (GeneArt) and cloned into mammalian expression vector containing mouse IgG1 or kappa chain constant domain. Heavy and kappa chain plasmids were extracted using NucleoBond Xtra Midi Plus plasmid DNA kit (MACHEREY-NAGEL). Antibodies were expressed by transient transfection of Expi293 (Thermo) suspension cultures with 2.7 µl ExpiFectamine (Thermo) and 1ug DNA (heavy: kappa = 1:1)/ml cell culture. At day 5 post-transfection, antibodies in culture supernatant were purified by protein G agarose affinity chromatography. For flow cytometric application, antibodies were conjugated to biotin or PE using biotin or PE conjugation kit (Abcam).

a

feX5-05 heavy chain

CAGGTGCAGCTGCAGGAGTCTGGAGCTGAGCTGGCGAGGCCTGGGGCTTCAGTGAAGCTGCCCTGCAAGGTTTCT
GGCTACACCTTCATAAGCTATGGTATAAGCTGGGTGAAGCAGACAACTGGACAGGGCCTTGAGTGGATTGGAGAC
ATTTATCCTAGAAGTGGTAATACTTACTACAATGAGAAGTTCATGGGCAGGGCCACACTGACTGCAGACAAATCC
TCCAGCACAGCGTACATGGAGCTCCGCAGCCTGACATCTGAGGACTCTGCGGTCTACTTCTGTGCAAGGAGGAAC
CTAACTTTTGACTACTGGGGCCAAGGCACCACTTTCACAGTCTCCTCA

b

feX5-05 kappa chain

GATATTGTGGTGACCCAGTCTTACAAATTCATGTCCACATCAGTAGGAGACAGGGTCAGCATCACCTGCAAGGCC
AGTCAGGATGTGACTACTGCTGTAGCCTGGTATCAACAAAAACCAGGGCAATCTCCTAAACTACTGATTTACTGG
GCATCCACCCGGCACACTGGAGTCCCTGATCGCTTCGCAGGCAGTGGATCTGGGACAGATTATACTCTCACCATC
AGCAGTGTGCAGGCTGAAGACCTGGCACTTTATTACTGTCAGCAACATTATAGCGCTCCGTGGACGTTCGGTGGA
GGCACCAAGCTGGAAATCAAA

c

fePD-CL1 heavy chain

GAGGTGCAGCTGCAGGAGTCTGGGGGAGGCTTAGTGAAGCCTGGAGGGTCCCTGAAATTTTCCTGTACAGCCTCT
GGATTCACTTTCCGTAATTATGGAATGAACTGGGTTCGTCAGGCCCCAGAGAGGGGACTGGAGTGGGTTGCATAT
ATTAGTCGTGGCAGTACTACCATCTACTATGCAGACACAGTGGAGGGCCGATTCACCATCTCCAGAGACAATGAC
AAGAACACCCTGTTCCTGCAAATGACCAGTCTGAGGTCTGAGGACACGGCCATATATTACTGTGCAAGGCATGAA
TACGACGGCCTTGACTACTGGGGCCAAGGCACCACTCTCACAGTCTCCTCA

d

fePD-CL1 kappa chain

GACATCCAGATGACACAGTCTCCAGCCTCCCTATCTGTATCTGTGGGAGAAACTGTCACCATCACATGTCGAGCA
AGTGAGAATATTTACAGTGATTTAGCCTGGTATCAGCAGAAACAGGGAAAATCTCCTCAGCTCCTGGTCCATGCT
GCAACAAACTTAGCAGATGGTGTGCCGTCAAGGTTCAGTGGCAGTGGATCAGGCACACAGTTTTCCCTCAAGATC
AAAAGCCTGCAGTCTGAGGATTTTGGGACTTATTACTGTCAGCATTTTTGGGGTACTCCGTGGACGTTCGGTGGA
GGCACCAAACTGGAAATCAAA

Figure 5. The nucleic acid sequences of variable domains of anti-ferret CXCR5 and PD-1 antibodies. (**a**) The nucleic acid sequences of variable domain of anti-ferret CXCR5 (clone feX5-C05) heavy chain. (**b**) The nucleic acid sequences of variable domain of anti-ferret CXCR5 (clone feX5-C05) kappa chain. (**c**) The nucleic acid sequences of variable domain of anti-ferret PD-1 (clone fePD-CL1) heavy chain. (**d**) The nucleic acid sequences of variable domain of anti-ferret PD-1 (clone fePD-CL1) kappa chain.

ELISA. ELISAs were performed based on a modified protocol previously described[23]. 96-well MaxiSorp plates (Thermo) were coated with recombinant ferret CXCR5 or PD-1 or control proteins (1 μg/ml at 100 μl/well) overnight at 4 °C. After blocking with 2.5% BSA in PBS, anti-ferret CXCR5 or PD-1 antibodies at different dilutions (starting at 1 μg/ml, four-fold serial dilutions) were added and incubated for two hours at room temperature. Plates were washed with 0.05% Tween 20 in PBS prior to incubation with 1:5000 dilution of HRP-conjugated goat anti-mouse IgG (Sera-Care) for 1 h at room temperature. Plates were washed again and developed using 3,3′,5,5′-Tetramethylbenzidine (TMB) substrate (Sigma) and read at 450 nm using CLARIOstar microplate reader (BMG LABTECH).

FACS. Lymph node cell suspensions from influenza infected ferret were stained with the following panel: live/dead Blue (Thermo Fisher), CD79a PerCP-Cy5.5 (HM47; BioLegend)[24], CD8 AF700 (OKT8; Thermo)[24], CD4 FITC (from CSIRO)[25], BCL6 AF647 (K112-91; BD), BCL6 AF647 (IG191E/A8; BioLegend), CXCR5 BV421 (L138D7; BioLegend), CXCR5 BB515 (RF8B2; BD), CXCR5 PE (2G8, BD); CXCR5 Biotin (in-house), Streptavidin BV421 (BD), PD-1 BV786 (29F.1A12; BioLegend), PD-1 BV421 (EH12.2H7; BioLegend), PD-1 PE (in-house). For BCL6 staining, cells were fixed, permeabilized, and stained using the BD Transcription Factor Buffer kit (BD) according to the manufacturer's instructions. Macaque LN suspensions were stained with Live/dead Aqua (Thermo Fisher), CD4 BV605 (L200; BD), CXCR5 PeCy7 (MU5UBEE, Thermo Fisher), and CD3 BUV737 (SP34-2, BD). All samples were acquired on a BD LSR Fortessa using BD FACS Diva and data was analyzed in FlowJo v10.

Received: 9 June 2020; Accepted: 21 December 2020
Published online: 21 January 2021

References

1. Albrecht, R. A. *et al.* Moving forward: Recent developments for the ferret biomedical research model. *mbio* https://doi.org/10.1128/mBio.01113-18 (2018).
2. Wong, J., Layton, D., Wheatley, A. K. & Kent, S. J. Improving immunological insights into the ferret model of human viral infectious disease. *Influenza Other Respir. Viruses* **13**, 535–546. https://doi.org/10.1111/irv.12687 (2019).
3. Stittelaar, K. J. *et al.* Ferrets as a novel animal model for studying human respiratory syncytial virus infections in immunocompetent and immunocompromised hosts. *Viruses* https://doi.org/10.3390/v8060168 (2016).
4. MacPhail, M. *et al.* Identification of small-animal and primate models for evaluation of vaccine candidates for human metapneumovirus (hMPV) and implications for hMPV vaccine design. *J. Gen. Virol.* **85**, 1655–1663. https://doi.org/10.1099/vir.0.79805-0 (2004).
5. Vigant, F. & Lee, B. Hendra and nipah infection: Pathology, models and potential therapies. *Infect Disord. Drug Targets* **11**, 315–336. https://doi.org/10.2174/187152611795768097 (2011).
6. Cross, R. W. *et al.* The domestic ferret (Mustela putorius furo) as a lethal infection model for 3 species of ebolavirus. *J. Infect. Dis.* **214**, 565–569. https://doi.org/10.1093/infdis/jiw209 (2016).
7. Subbarao, K. & Roberts, A. Is there an ideal animal model for SARS?. *Trends Microbiol.* **14**, 299–303. https://doi.org/10.1016/j.tim.2006.05.007 (2006).
8. Martina, B. E. *et al.* Virology: SARS virus infection of cats and ferrets. *Nature* **425**, 915. https://doi.org/10.1038/425915a (2003).
9. Shi, J. *et al.* Susceptibility of ferrets, cats, dogs, and other domesticated animals to SARS-coronavirus 2. *Science* https://doi.org/10.1126/science.abb7015 (2020).
10. Kim, Y. I. *et al.* Infection and rapid transmission of SARS-CoV-2 in ferrets. *Cell Host Microbe* **27**, 704–709.e702. https://doi.org/10.1016/j.chom.2020.03.023 (2020).
11. See, R. H. *et al.* Severe acute respiratory syndrome vaccine efficacy in ferrets: Whole killed virus and adenovirus-vectored vaccines. *J. Gen. Virol.* **89**, 2136–2146. https://doi.org/10.1099/vir.0.2008/001891-0 (2008).
12. Vinuesa, C. G., Linterman, M. A., Yu, D. & MacLennan, I. C. Follicular helper T cells. *Annu. Rev. Immunol.* **34**, 335–368. https://doi.org/10.1146/annurev-immunol-041015-055605 (2016).
13. Crotty, S. Follicular helper CD4 T cells (TFH). *Annu. Rev. Immunol.* **29**, 621–663. https://doi.org/10.1146/annurev-immunol-031210-101400 (2011).
14. Linterman, M. A. & Hill, D. L. Can follicular helper T cells be targeted to improve vaccine efficacy?. *F1000Research* **5**, 1. https://doi.org/10.12688/f1000research.7388.1 (2016).
15. Nurieva, R. I. *et al.* Bcl6 mediates the development of T follicular helper cells. *Science* **325**, 1001–1005. https://doi.org/10.1126/science.1176676 (2009).
16. Johnston, R. J. *et al.* Bcl6 and Blimp-1 are reciprocal and antagonistic regulators of T follicular helper cell differentiation. *Science* **325**, 1006–1010. https://doi.org/10.1126/science.1175870 (2009).
17. Yu, D. *et al.* The transcriptional repressor Bcl-6 directs T follicular helper cell lineage commitment. *Immunity* **31**, 457–468. https://doi.org/10.1016/j.immuni.2009.07.002 (2009).
18. Meli, A. P. & King, I. L. Identification of mouse T follicular helper cells by flow cytometry. *Methods Mol. Biol.* **1291**, 3–11. https://doi.org/10.1007/978-1-4939-2498-1_1 (2015).
19. von Boehmer, L. *et al.* Sequencing and cloning of antigen-specific antibodies from mouse memory B cells. *Nat. Protoc.* **11**, 1908–1923. https://doi.org/10.1038/nprot.2016.102 (2016).
20. Victora, G. D. & Nussenzweig, M. C. Germinal centers. *Annu. Rev. Immunol.* **30**, 429–457. https://doi.org/10.1146/annurev-immunol-020711-075032 (2012).
21. Kelly, H.G. *et al.* Self-assembling influenza nanoparticle vaccines drive extended germinal center activity and memory B cell maturation. *JCI Insight.* **5**, e136653. https://doi.org/10.1172/jci.insight.136653 (2020).
22. Peng, X. *et al.* The draft genome sequence of the ferret (Mustela putorius furo) facilitates study of human respiratory disease. *Nat. Biotechnol.* **32**, 1250–1255. https://doi.org/10.1038/nbt.3079 (2014).
23. Liu, Y. *et al.* Cross-lineage protection by human antibodies binding the influenza B hemagglutinin. *Nat. Commun.* **10**, 324. https://doi.org/10.1038/s41467-018-08165-y (2019).
24. Liu, W. C. *et al.* Sequential immunization with live-attenuated chimeric hemagglutinin-based vaccines confers heterosubtypic immunity against influenza A viruses in a preclinical ferret model. *Front. Immunol.* **10**, 756. https://doi.org/10.3389/fimmu.2019.00756 (2019).
25. Layton, D. S. *et al.* Development of an anti-ferret CD4 monoclonal antibody for the characterisation of ferret T lymphocytes. *J. Immunol. Methods* **444**, 29–35. https://doi.org/10.1016/j.jim.2017.02.009 (2017).

Acknowledgements

This work was supported by NHMRC Grants APP1149990 and GNT112909. WJ is supported by a Melbourne International Research Scholarship and Melbourne International Fee Remission Scholarship. JAJ, AKW and SJK are supported by NHMRC fellowships.

Author contributions

W.J., A.K.W., J.A.J. and S.J.K. designed the study. W.J., J.W. and H.X.T. performed experiments. P.G.W. provided ferret samples. D.S.L. provided ferret CD4 antibody. W.J., A.K.W., J.A.J., P.G.W. and S.J.K. wrote the manuscript. All authors read and revised the manuscript.

Competing interests

The authors declare no competing interests.

Additional information

Correspondence and requests for materials should be addressed to A.K.W. or J.A.J.

Reprints and permissions information is available at www.nature.com/reprints.

Publisher's note Springer Nature remains neutral with regard to jurisdictional claims in published maps and institutional affiliations.

Open Access This article is licensed under a Creative Commons Attribution 4.0 International License, which permits use, sharing, adaptation, distribution and reproduction in any medium or format, as long as you give appropriate credit to the original author(s) and the source, provide a link to the Creative Commons licence, and indicate if changes were made. The images or other third party material in this article are included in the article's Creative Commons licence, unless indicated otherwise in a credit line to the material. If material is not included in the article's Creative Commons licence and your intended use is not permitted by statutory regulation or exceeds the permitted use, you will need to obtain permission directly from the copyright holder. To view a copy of this licence, visit http://creativecommons.org/licenses/by/4.0/.

© The Author(s) 2021

Chapter 4: Aggregation by peptide conjugation rescue poor immunogenicity of the HA stem

PLOS ONE

RESEARCH ARTICLE

Aggregation by peptide conjugation rescues poor immunogenicity of the HA stem

Wenbo Jiang[1], Emily H. Pilkington[1], Hannah G. Kelly[1], Hyon-Xhi Tan[1], Jennifer A. Juno[1], Adam K. Wheatley[1], Stephen J. Kent[1,2,3]*

1 Department of Microbiology and Immunology, Peter Doherty Institute for Infection and Immunity, University of Melbourne, Melbourne, Victoria, Australia, **2** Melbourne Sexual Health Clinic and Infectious Diseases Department, Alfred Hospital, Monash University Central Clinical School, Carlton, Victoria, Australia, **3** ARC Centre for Excellence in Convergent Bio-Nano Science and Technology, University of Melbourne, Melbourne, Australia

* skent@unimelb.edu.au

Check for updates

OPEN ACCESS

Citation: Jiang W, Pilkington EH, Kelly HG, Tan H-X, Juno JA, Wheatley AK, et al. (2020) Aggregation by peptide conjugation rescues poor immunogenicity of the HA stem. PLoS ONE 15(11): e0241649. https://doi.org/10.1371/journal.pone.0241649

Editor: Victor C. Huber, University of South Dakota, UNITED STATES

Received: July 17, 2020

Accepted: October 16, 2020

Published: November 2, 2020

Copyright: © 2020 Jiang et al. This is an open access article distributed under the terms of the Creative Commons Attribution License, which permits unrestricted use, distribution, and reproduction in any medium, provided the original author and source are credited.

Data Availability Statement: All relevant data are within the manuscript and its Supporting Information files.

Funding: This work was supported by NHMRC grants APP1149990 and GNT112909. WJ is supported by a Melbourne International Research Scholarship and Melbourne International Fee Remission Scholarship. JAJ, AKW and SJK are supported by NHMRC fellowships.

Competing interests: The authors have declared that no conflict of interest exists.

Abstract

Influenza virus infection is a global public health threat. Current seasonal influenza vaccines are efficacious only when vaccine strains are matched with circulating strains. There is a critical need for developing "universal" vaccines that protect against all influenza viruses. HA stem is a promising target for developing broad-spectrum influenza vaccines due to its relatively conserved feature. However, HA stem is weakly immunogenic when administered alone in a soluble form. Several approaches have been employed to improve the immunogenicity of HA stem, including conjugation of HA stem with a highly immunogenic carrier protein or displaying HA stem on a nanoparticle scaffold. Converting a weakly immunologic protein into a multimer through aggregation can significantly enhance its immunogenicity, with some multimeric protein aggregates previously shown to be more immunogenic than their soluble counterparts in animal models. Here, we show that a chemically coupling a peptide derived from the head domain of PR8 HA (P35) with the poorly immunogenic HA stem protein results in aggregation of the HA stem which significantly increases stem-specific B cell responses following vaccination. Importantly, vaccination with this conjugate in the absence of adjuvant still induced robust B cell responses against stem in vivo. Improving HA stem immunogenicity by aggregation provides an alternative avenue to conjugation with exotic carrier proteins or nanoparticle formulation.

Introduction

Seasonal influenza viruses circulate in all geographical regions of the world and cause recurrent disease in humans. Worldwide, these annual epidemics are estimated to cause 1 billion infections, with 3–5 million cases of severe illness and 290,000–650,000 deaths [1]. Influenza viruses undergo continual antigenic evolution allowing mutant viruses to evade host immunity acquired to previous virus strains. Current seasonal influenza vaccines are effective when vaccine strains are matched with circulating strains [2, 3]. However, there is little to no cross-protection against antigenic variants, emerging pandemic or zoonotic outbreak strains [4]. There is therefore tremendous interest in the development of novel "universal" vaccines, that would significantly expand protection to most or all influenza viruses.

HA is the most important surface glycoprotein which mediates viral entry into host cells [5, 6]. Influenza HA can be divided into two domains based on their functions [7]. The head domain contains the receptor-binding site via which the virus binds sialic acid receptors of the target cell, while the stem domain contains fusion peptide which mediates fusion between the viral envelope and the endosomal membrane of the host cell [5]. Unlike the head domain which is highly variable, the stem domain is relatively conserved among influenza viruses [7]. Additionally, anti-stem antibodies have been shown to provide cross-protection against both heterologous and heterosubtypic strains in mice [8, 9]. All these factors make the stem domain an attractive target for universal influenza vaccine. However, soluble stem protein is a poor immunogen which elicits weak humoral and cellular immune responses in vivo [10]. Antibodies are mainly generated against the immunodominant HA head domain in the context of full-length HA [10, 11]. Tan et al. in our group demonstrated that poor intrinsic immunogenicity was responsible for the weak antibody responses targeting HA stem [10].

Immunogen multimerization is an effective strategy for enhancing the immunogenicity of protein antigens [12]. Multimeric antigens can be classified into two major types: highly ordered nanoparticles and amorphous protein aggregates. The ability of nanoparticles to enhance the immunogenicity of protein antigens has been well demonstrated [13]. To overcome the poor immunogenicity of HA stem, Yassine et al. fused the gene encoding ferritin from Helicobacter pylori bacteria to H1 HA stem and expressed nanoparticles of eight trimeric HA stem molecules in their native confirmation around a spherical ferritin core [14]. This ferritin-stem nanoparticle vaccine induced broadly cross-reactive antibody responses and conferred full protection against heterosubtypic H5 virus challenge in mice after sequential immunizations [14].

Protein aggregates are high molecular weight proteins composed of multimers of native or denatured monomers [15]. Although the effect of protein aggregates on the immunogenicity of protein antigens has been assessed in a limited number of studies, experiments conducted in mice have demonstrated that multimeric protein aggregates are more immunogenic than the monomeric forms [16–18]. Hermeling et al. generated recombinant human interferon alpha2a/b (rhIFNα2) aggregates by metal-catalyzed oxidation and showed that the aggregated form increased rhIFNα2-specific antibody responses in wild-type FVB/N mice compared with the native form [17]. They also found that rhIFNα2-specific serum IgG titre is dependent on the level of aggregation [17]. Wei et al. showed that oligomeric aggregates of influenza HA expressed in mammalian cells induced significantly higher levels of neutralizing antibodies in BALB/c mice than monomeric or trimeric HA expressed in the same cell line [19]. Ilyinskii et al. fused a weakly immunogenic model antigen GFP with long polyglutamine (polyQ) domain that triggers protein aggregation and immunized BALB/c mice with plasmids encoding polyQ-GFP or GFP alone [18]. They found that plasmids encoding polyQ-GFP elicited significant higher anti-GFP antibody titre and anti-GFP CTL activity than plasmids encoding GFP alone [18]. Of note, the most widely used aluminium adjuvants also form fibrous loose aggregates of aluminium nanocrystals [20, 21]. Adsorption of antigens to aluminium aggregates enhances vaccine induced immune response [22]. In the present study, we show that conjugation of HA stem with a short HA head peptide rescues the poor immunogenicity of stem protein. We chose a 17-mer peptide from the HA head (termed P35) since we surmised that P35 might constitute a T-helper epitope, although this subsequently was disproven (shown below). Instead of being a T-helper epitope, P35 conjugation induces the formation of stem aggregates, which significantly enhances stem-specific B cell responses in mice.

Materials and methods

Mouse infection and immunization

Mouse studies and related experimental procedures in this study were approved by the University of Melbourne Animal Ethics Committee (#1914874). Female C57BL/6 mice (6–8 weeks old) were anesthetized by isoflurane inhalation prior to infection or immunization. For intranasal influenza infections, mice were instilled with 50μL of 50 TCID50 of A/Puerto Rico/8/34 (PR8) as described previously [10]. For intramuscular vaccinations, 5μg of PR8 HA stem protein [10], HIV gp120 protein (NIH AIDS Reagent Program), hen egg lysozyme (HEL) protein (Sigma), chicken egg ovalbumin (OVA) protein (InvivoGen) or their respective conjugates with peptides (refer to peptide and protein conjugation) with or without Addavax (1:1 ratio; InvivoGen) were injected into both hind quadriceps using a 29G needle. Fourteen days post infection or vaccination, draining lymph nodes (mediastinal lymph nodes (mLN) for infected animals, inguinal lymph nodes (inLN) and iliac lymph nodes (ilLN) for vaccinated animals) and blood were collected for FACS and ELISA analyses.

Antigen stimulations and cell culture

Draining lymph nodes from 5 PR8-infected mice were mashed into single cell suspensions, pooled and cultured in RPMI 1640 supplemented with 10% fetal calf serum and penicillin/streptomycin (RF10). To identify antigen-specific Tfh cells using peptide stimulation [23], cell suspensions were stimulated for 18 hours in RF10 with PR8 HA peptide 11 (P11, LKGIAPLQLGKCNIAGW, 2μg/mL, BEI resources), PR8 HA peptide 35 which is located at positions 192–208 (H3 numbering) (P35, QNLYQNENAYVSVVTSN, 2μg/mL, BEI resources), Concanavalin A (Con A, 5ug/mL, Sigma) or a vehicle (DMSO) control. Cells were cultured in a 48-well plate in 500μl RF10 at a concentration of 2 million cells/ml. At the time of stimulation, anti-CD154 PE antibody (MR1; BioLegend) was added to all culture conditions.

Peptide and protein conjugation

Peptide 11-cysteine (P11C, LKGIAPLQLGKCNIAGWC, GenScript) or peptide 35-cysteine (P35C, QNLYQNENAYVSVVTSNC, GenScript or LifeTein) were conjugated with PR8 HA stem protein [10], HIV gp120 protein (NIH AIDS Reagent Program), HEL protein (Sigma) or OVA protein (InvivoGen) using a commercial cross-linker, sulfosuccinimidyl 4-[N-maleimidomethyl] cyclohexane-1-carboxylate (Sulfo-SMCC, Thermo), according to the manufacturer's instructions. Briefly, proteins were diluted with PBS to 1mg/ml and Sulfo-SMCC were dissolved in distilled water to 5mg/ml immediately before use. 20-fold molar excess of Sulfo-SMCC solution were then added to protein solution and reaction mixture were incubated for 30 minutes at room temperature. Excess Sulfo-SMCC was then removed using desalting columns (Thermo). Peptides were dissolved in DMSO to the desired concentration immediately before use and equal amounts of peptides (peptide: protein = 1:1, m/m) were then added to maleimide-activated proteins and the reaction mixtures were incubated for 30 minutes at room temperature. Excess peptides were then removed using Amicon Ultra Centrifugal Filter (Millipore, 10KD). For some experiments, P35C-stem conjugates were further filtered through Costar Spin-X Centrifuge Tube Filters (Corning, 0.22 μm) and purified by gel filtration using Superose 6 column (GE Life Sciences). The concentration of all peptide-protein conjugates was measured using Qubit 2.0 Fluorometer (Thermo).

Flow cytometry

For detection of antigen-specific GC B cells, freshly isolated LN cell suspensions from individual mice were stained with Aqua Viability Dye (Thermo) and Fc blocked with an anti-CD16/32 antibody (clone 93; BioLegend). Cells were then surface stained with the relevant probes (APC or PE

labelled stem, HEL, OVA or gp120 proteins for baiting antigen-specific GC B cells) [10] and the following antibodies: CD45 APC-Cy7 (30-F11; BD), CD3 BV785 (145-2C11; BioLegend), F4/80 BV785 (BM8; BioLegend), Streptavidin BV785 (BD), B220 BUV737 (RA3-6B2; BD), IgD BUV395 (11-26c.2a; BD), CD38 PE-Cy7 (90; BioLegend), GL7 AF488 (GL7; BioLegend). For detection of Tfh cells *ex vivo*, freshly isolated LN cell suspensions from individual mice were stained with the following panel: Live/dead Red (Thermo), B220 BV605 (RA3-6B2; BD Biosciences), CD3 BV510 (145-2C11; BioLegend), CD4 BUV737 (RM4-5; BD Biosciences), CXCR5 BV421 (L138D7; BioLegend), PD-1 BV786 (29F.1A12; BioLegend). For Ag-specific Tfh identification [23], cells were cultured as described above and then stained with the following panel: Live/dead Red (Thermo), B220 BV605 (RA3-6B2; BD), CD3 BV510 (145-2C11; BioLegend), CD4 BUV737 (RM4-5; BD), CD25 BB515 (PC61; BD), OX40 PeCy7 (OX-86; BioLegend). All samples were acquired on a BD LSR Fortessa using BD FACS Diva and data was analyzed in FlowJo v10.

ELISA

Stem-specific IgG titre of serum from PR8 HA stem or peptide-stem conjugates immunized mice were detected using sandwich ELISA as previously described [24]. Briefly, 0.1μg/ml rabbit anti-His pAb (Genscript) was coated onto MaxiSorp plates (Thermo) overnight at 4˚C. Plates were blocked with 5% skim milk powder in PBS before adding His-tagged PR8 HA stem protein [10]. Serially diluted mouse sera were then added to plates and incubated for 2 h at room temperature. Plates were washed prior to incubation with 1:5,000 dilution of HRP-conjugated goat anti-mouse IgG (Sera-Care) for 1 h at room temperature. Plates were washed and developed using TMB substrate (Sigma), reaction was stopped with 0.16M H_2SO_4 and read at 450nm. Endpoint titers were calculated as the reciprocal serum dilution giving signal 2x background using a fitted curve (4-parameter log regression).

The antigenicity of PR8 HA stem and P35C-stem conjugate was assessed with a panel of anti-HA stem monoclonal antibodies (CR9114, TN1F11, TN1G09, produced in-house) and a negative control antibody VRC01 (produced in-house) as preciously described [24]. Briefly, 96-well MaxiSorp plates (Thermo) were coated with PR8 HA stem and P35C-stem conjugate (2 μg/ml × 100 μl/well) overnight at 4˚C. After blocking with 2.5% BSA in PBS, a panel of anti-HA stem monoclonal antibodies and a negative control antibody at different dilutions (starting at 1 μg/ml, four-fold serial dilutions) were added and incubated for two hours at room temperature. Plates were washed with 0.05% Tween 20 in PBS prior to incubation with 1:10,000 dilution of HRP-conjugated rabbit anti-human IgG (Dako) for 1 h at room temperature. Plates were washed again, developed using 3,3′,5,5′-Tetramethylbenzidine (TMB) substrate (Sigma), stopped with 0.16M H_2SO_4 and read at 450 nm.

Dynamic light scattering and zeta potential

Dynamic light scattering and zeta potential measurements were performed on a Zetasizer Nano ZS (Malvern) instrument and analysed with Zetasizer software. Samples kept on ice were allowed to equilibrate to room temperature prior to analysis, with all measurements taking place at 25˚C. Concentration of all samples was 0.38 mg/mL in PBS for light scattering experiments, and in Milli-Q water (pH 7) for zeta potential experiments to limit salt interference with measurements. Data represent mean values plus/minus standard deviation of three measurements each consisting of 12 runs.

Statistical analysis

Data is presented as mean ± SEM. Statistical significance was assessed by one-way ANOVA and performed using GraphPad Prism version 7 (GraphPad Software). P values less than 0.05

were considered statistically significant and marked with one asterisk, P values less than 0.01 were marked with two asterisks, P values less than 0.001 were marked with three asterisks.

Results

P35-cysteine conjugation improves the immunogenicity of stem

The HA stem is relatively conserved and an attractive target for improved influenza vaccines. However, the HA stem is relatively poorly immunogenic. To study whether the immunogenicity of the HA stem could be improved, we conjugated peptides (P35 and P11) from HA head domain with HA stem proteins and evaluated the immune responses induced by various peptide-stem conjugates in mice. The P35 or P11 peptides and HA stem proteins were coupled with a crosslinker, Sulfo-SMCC. Sulfo-SMCC is a heterobifunctional crosslinker that contains N-hydroxysuccinimide (NHS) ester and maleimide group. The NHS ester reacts with primary amine from N-termimal or lysine of the protein and maleimide group reacts with sulfhydryl from cysteine of the peptide. Therefore, we added a cysteine at the C-terminal of the peptide during peptide synthesis (to produce P11C or P35C peptides). Antigenicity of the stem on peptide-stem conjugate is not altered, which is demonstrated by the similar binding activity of HA stem and P35C-stem with anti-HA stem monoclonal antibodies (CR9114, TN1F11 and TN1G09, S1 Fig). Next, we intramuscularly immunized mice with 5ug stem, or P11C-stem conjugate or P35C-stem conjugate or mixture of 5ug stem plus 5ug free P35C on day 0. Draining lymph nodes (dLNs) and blood were collected on day 14 post immunization.

We first analysed GC B cells for the proportion that were HA stem-specific using fluorescent stem probes [10]. The gating strategy for GC B cells is shown in Fig 1A. As expected, we found that stem was a poor immunogen which elicited negligible stem-specific GC B cell responses (Fig 1B and 1C). The P11C-stem conjugate, or a mixture of stem and free P35C, displayed similarly poor immunogenicity as the HA stem alone. In contrast, a striking proportion of GC B cells were specific for HA stem in the P35C-stem immunized mice (mean 12.9%, range 3.94%-22.9%). We next studied whether the enhanced generation of stem-specific GC B cells translated into the generation of enhanced stem specific antibodies. We found that stem-specific serum IgG was higher in the P35C-stem mice than that of other 3 stem immunized groups (Fig 1D).

We hypothesised that the enhanced stem B cell and antibody response could be due to enhanced total GC B cells or the induction of high levels of Tfh. We therefore analysed the frequency of bulk GC B cells and Tfh cells. We found that the frequency of bulk GC B cells and Tfh cells of P35C-stem immunized mice were similar to those of stem or P11C-stem or stem +P35C immunized mice (Fig 2), suggesting that P35C-stem conjugates did not drive enhanced GC activity. To investigate this further, we assessed whether P11 or P35 were CD4 T cell epitopes in influenza-infected c57BL/6 mice using our recently developed activation-induced marker (AIM) assay [23]. We found that neither P35 nor P11 peptides activated the expression of CD154 or CD25/OX40 markers above that of control in influenza-immune mice, showing they were not significant T-helper epitopes (S2 Fig). Taken together, these data demonstrated that P35C conjugation improves the immunogenicity of stem protein without increasing the frequency of total GC B cells or CD4 T-helper cells or inducing T cell help.

P35C improves the immunogenicity of stem in the absence of adjuvants

The above mouse P35C-stem immunization was done in the presence of a commercial adjuvant, AddaVax. The very high stem-specific GC B cells induced by the conjugated P35C suggested it may be effective in the absence of an adjuvant. To address this question, we immunized four groups of mice with P11C-stem without AddaVax (P11C-stem Ad-), P11C-stem with AddaVax (P11C-stem Ad+), P35C-stem without AddaVax (P35C-stem Ad-) and

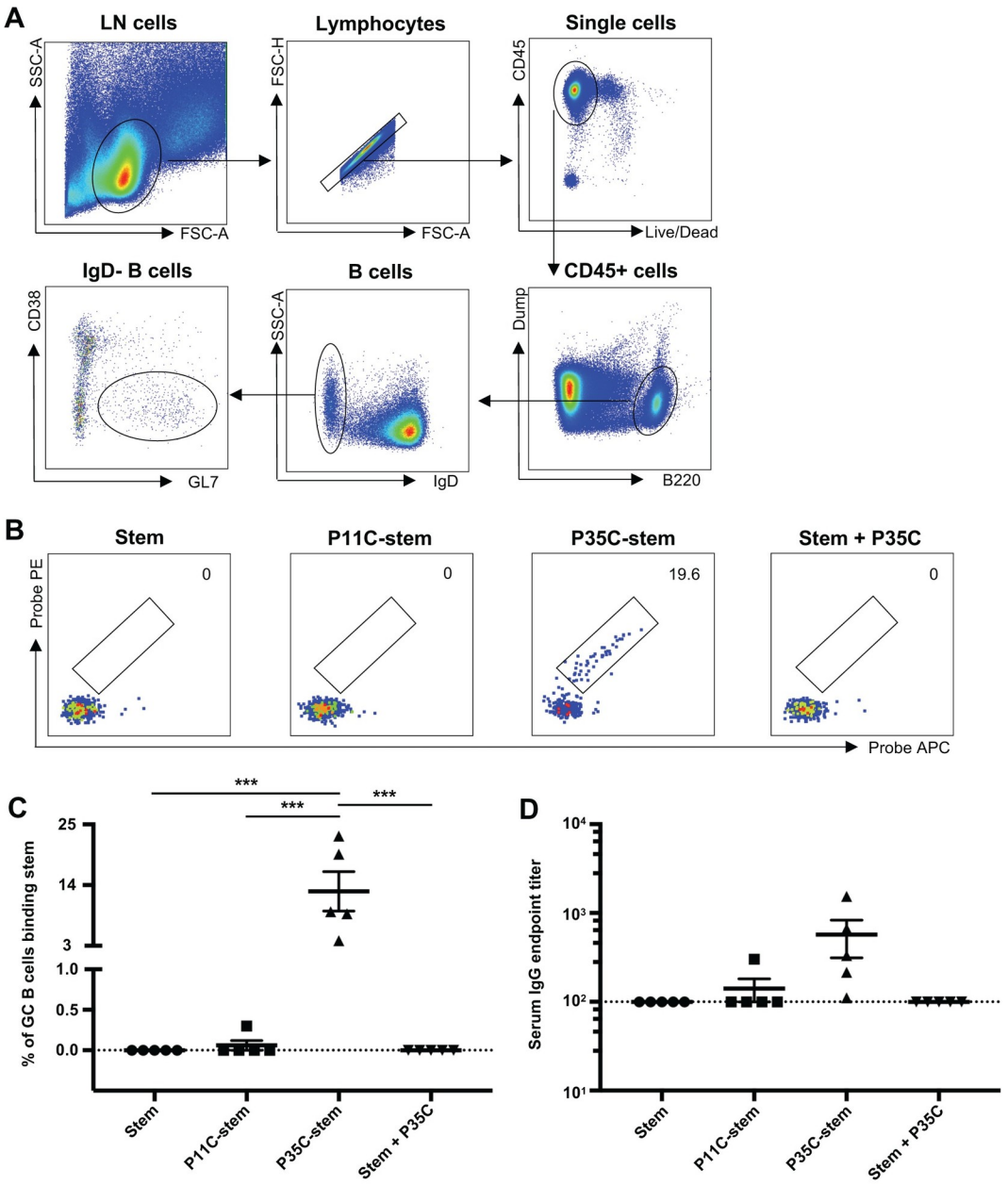


Fig 1. Stem-specific B cell and serological responses in immunized mice. (A) Gating strategy for GC B cells. Lymphocytes were identified by forward scatter area (FSC-A) and side-scatter area (SSC-A). Doublets were excluded by gating on single cells as determined by FSC-A versus FSC-H, and live cells were identified by viability dye exclusion. B cells were identified by B220+ and naïve B cells were excluded by IgD+. GC B cells were identified by GL7+CD38lo. For each step, the parental population is indicated above the plot. (B—C) Representative flow cytometric plots (B) and frequency (C) of GC B cells (B220 +IgD- CD38lo GL7+) from mice (n = 5) immunized with adjuvanted (Addavax) immunogens double stained with PR8 HA stem probes. (D) Serum endpoint total IgG titres of mice (n = 5) immunized with adjuvanted (Addavax) immunogens. Data indicate the mean ± SEM. Statistical significance was assessed by one-way ANOVA.

https://doi.org/10.1371/journal.pone.0241649.g001

P35C-stem with AddaVax (P35C-stem Ad+) on day 0. Draining lymph nodes (dLNs) and blood were collected on day 14 post immunization for FACS and ELISA analyses. As expected, P11C-stem elicited little stem-specific B cell responses regardless of the presence of AddaVax (Fig 3). In contrast, P35C-stem induced significantly higher frequency of stem-specific GC B

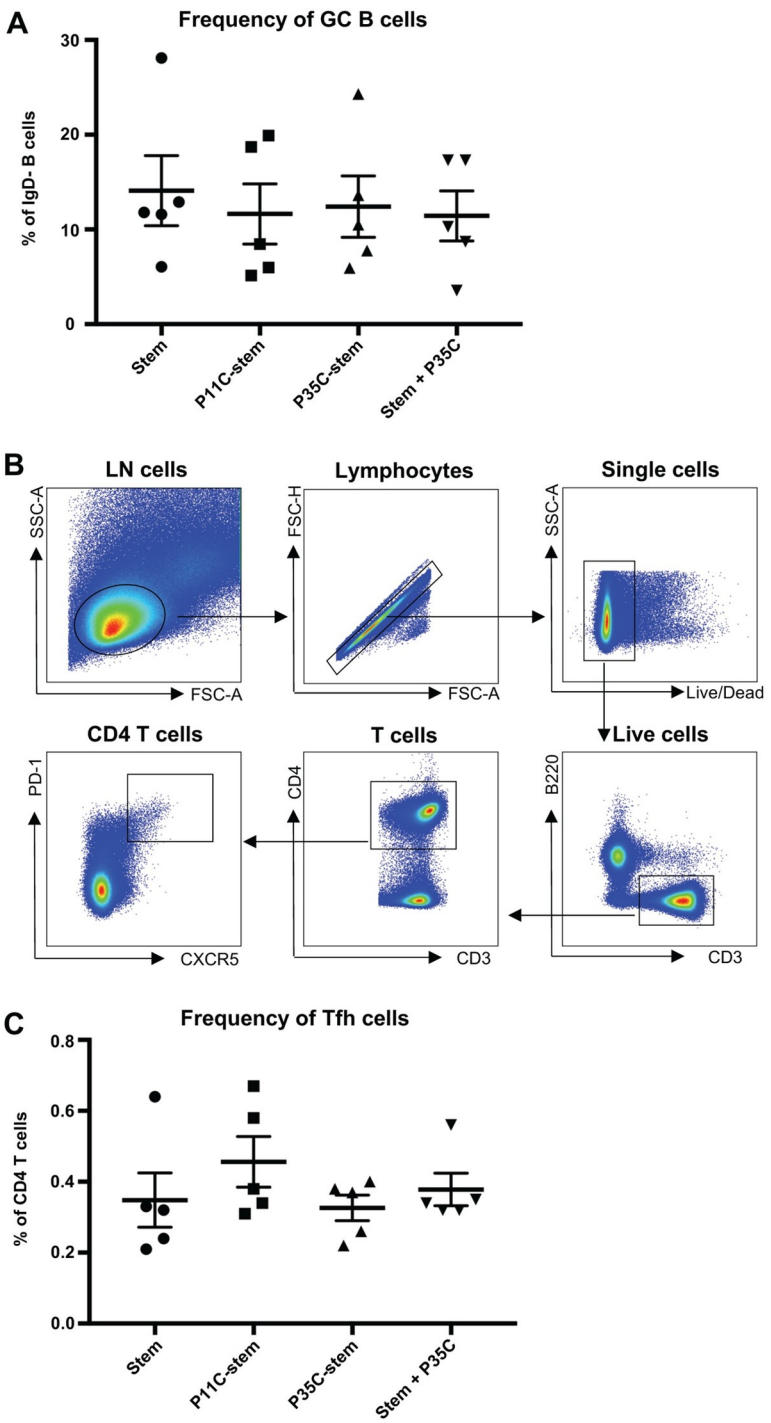


Fig 2. Bulk GC B and Tfh cell responses in immunized mice. (A) Frequency of bulk GC B cells (B220 +IgD-CD38loGL7+) from mice (n = 5) immunized with adjuvanted (Addavax) immunogens. Data indicate the mean ± SEM. (B) Gating strategy for Tfh cells. Lymphocytes were identified by forward scatter area (FSC-A) and side-scatter area (SSC-A). Doublets were excluded by gating on single cells as determined by FSC-A versus FSC-H, and live cells were identified by viability dye exclusion. T cells were identified as CD3+B220- and CD4 T cells were identified as CD3+CD4+. Tfh cells were identified as CXCR5++PD-1++. For each step, the parental population is indicated above the plot. (C) Frequency of bulk Tfh cells (CD4+CXCR5++PD-1++) from mice (n = 5) immunized with adjuvanted (Addavax) immunogens. Data indicate the mean ± SEM.

https://doi.org/10.1371/journal.pone.0241649.g002

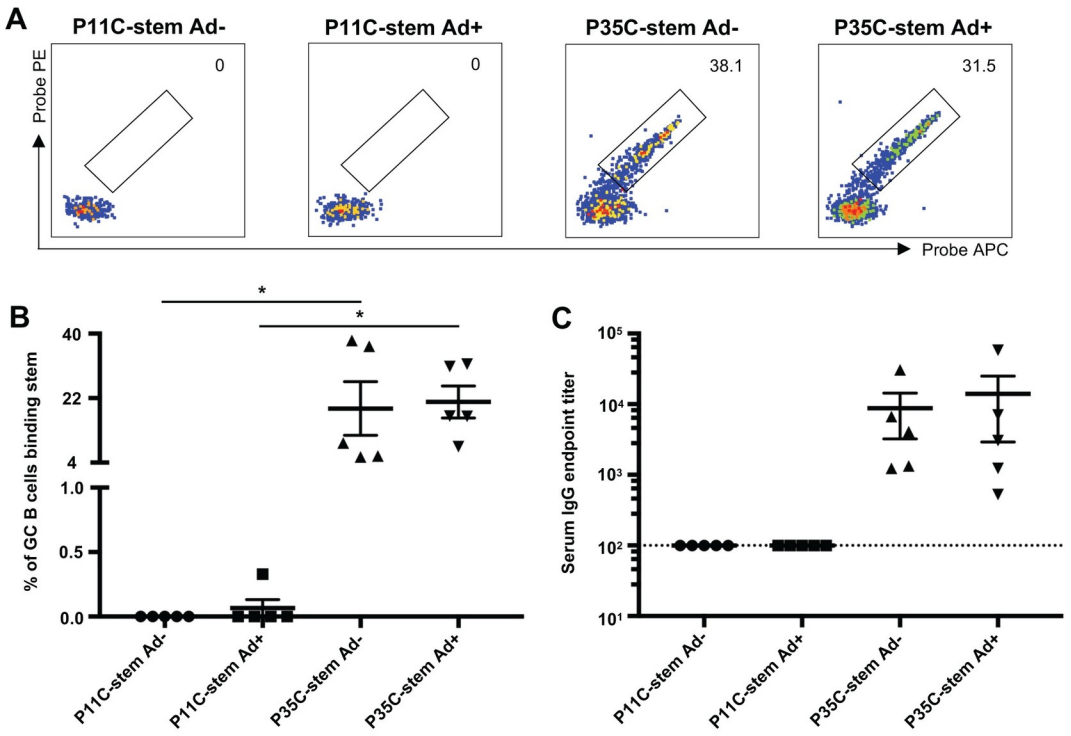


Fig 3. P35C improves the immunogenicity of stem in the absence of adjuvants. (A—B) Representative flow cytometric plots (A) and frequency (B) of stem-specific GC B cells from mice (n = 5) immunized with P11C-stem without Addavax (P11C-stem Ad-) or with Addavax (P11C-stem Ad+) and P35C-stem without Addavax (P35C-stem Ad-) or with Addavax (P35C-stem Ad+). (C) Serum endpoint total IgG titres of mice (n = 5) immunized with P11C-stem without Addavax (P11C-stem Ad-) or with Addavax (P11C-stem Ad+) and P35C-stem without Addavax (P35C-stem Ad-) or with Addavax (P35C-stem Ad+). Data indicate the mean ± SEM. Statistical significance was assessed by one-way ANOVA.

https://doi.org/10.1371/journal.pone.0241649.g003

cells either with or without AddaVax. Stem-specific serum IgG titer of P35C-stem (either with or without AddaVax) immunized mice were higher than that of P11C-stem (either with or without AddaVax) immunized mice. Therefore, P35C-stem enhances stem-specific B cell responses in the absence of adjuvant.

P35C improves the immunogenicity of stem by an aggregation mechanism

We found that P35 is not a CD4 T cell epitope (S2 Fig), and thus the enhanced stem-specific antibody responses is unlikely to be due to Tfh cell help. We therefore assessed whether the P35C-stem conjugates formed protein aggregates, which could provide T cell-independent help to B cells [15]. We filtered P35C-stem through a 0.22um filter and purified it by gel filtration after conjugation. We then immunized mice with gel-filtrated P35C-stem (P35C-stem GF) and unfiltered P35C-stem (P35C-stem). We found that the immunogenicity of gel filtrated P35C-stem significantly decreased compared with normal protocol produced P35C-stem (Fig 4). This suggests that the immunogenic components of P35C-stem were >0.22um and were removed during filtration steps.

We next performed biophysical characterisations of gel-filtrated P35C-stem and unfiltered P35C-stem through dynamic light scattering (DLS) and zeta potential experiments. The hydrodynamic size of gel-filtrated P35C-stem, as determined by the most frequent particle population in solution (hydrodynamic size by Number), was determined to be approximately 9.2 nm, similar to stem alone (10.2 nm); in contrast, the hydrodynamic size of unfiltered

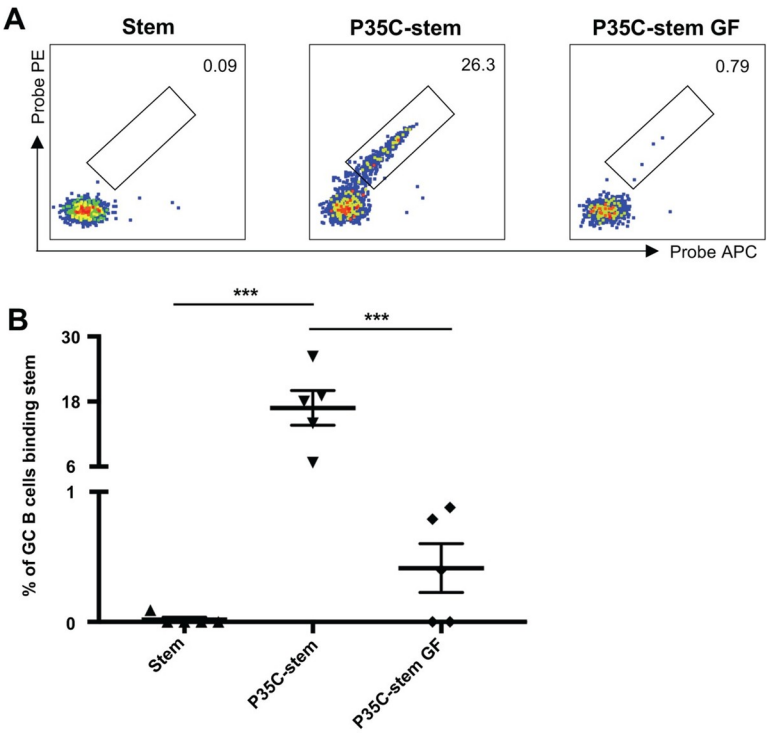


Fig 4. P35C improves the immunogenicity of stem by an aggregation mechanism. Representative flow cytometric plots (A) and frequency (B) of stem-specific GC B cells from mice (n = 5) immunized with adjuvanted (Addavax) PR8 HA stem, P35C-stem or gel filtrated P35C-stem (P35C-stem GF). Data indicate the mean ± SEM. Statistical significance was assessed by one-way ANOVA.

https://doi.org/10.1371/journal.pone.0241649.g004

P35C-stem was >10,000 nm, outside the limit of distribution analysis, and so population peaks could not be resolved (S1 Table). Both samples were polydisperse, but the Z-average hydrodynamic size of the unfiltered P35C-stem (30,290 nm) was determined to be over 750-fold larger than that of the filtered conjugate (39.4 nm). Stem and PC35-stem conjugates were determined to have net negative surface charges by zeta potential analysis (S1 Table). Interestingly, the zeta potential of gel-filtrated P35C-stem was close to neutral at -2.01 mV, while the zeta potential of unfiltered P35C-stem was 10-fold larger at -20.17 mV; this indicates a larger degree of electrostatic repulsion between the unfiltered P35C-stem populations and suggests superior colloidal stability comparative to both the filtrate and stem protein itself (-3.45 mV).

This characterization suggests P35C self-aggregates after conjugation with the HA stem protein to form larger multimers which elicited superior immunity compared to soluble stem proteins.

Generalisability of the enhanced immunogenicity of P35C conjugations to other proteins

The unfiltered P35C-stem was highly immunogenic and we hypothesised that this phenomenon might also be true when other immunogens were conjugated to P35. To assess the generalizability of the application of P35C, we tested another immunogen, hen egg lysozyme (HEL), for conjugation with P35C and mouse immunization. Three groups of C57BL/6 mice were immunized: with HEL protein alone, with the P11C-HEL conjugate or with the P35C-HEL conjugate. Similar to results obtained with the HA stem protein alone, HEL alone elicited little

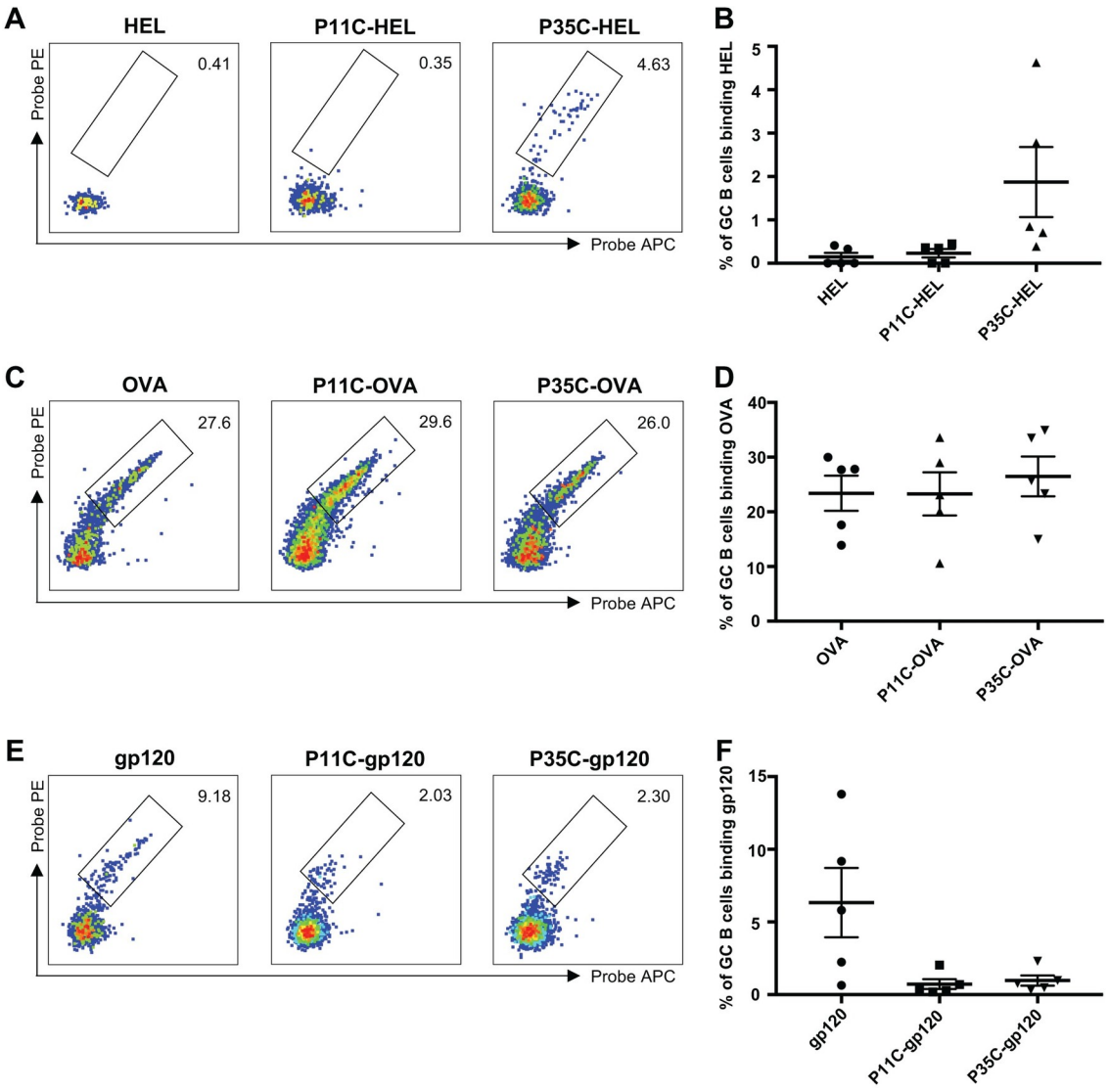


Fig 5. HEL/OVA/gp120-specific B cell responses in immunized mice. (A—B) Representative flow cytometric plots (A) and frequency (B) of GC B cells (B220+IgD–CD38loGL7+) from mice (n = 5) immunized with adjuvanted (Addavax) immunogens double stained with HEL probes. (C—D) Representative flow cytometric plots (C) and frequency (D) of GC B cells (B220+IgD–CD38loGL7+) from mice (n = 5) immunized with adjuvanted (Addavax) immunogens double stained with OVA probes. (E—F) Representative flow cytometric plots (E) and frequency (F) of GC B cells (B220+IgD–CD38loGL7+) from mice (n = 5) immunized with adjuvanted (Addavax) immunogens double stained with gp120 probes. Data indicate the mean ± SEM.

https://doi.org/10.1371/journal.pone.0241649.g005

or no HEL-specific B cell responses (Fig 5A and 5B). The P35C-HEL immunogen, but not the P11C-HEL immunogen, increased the frequency of HEL-specific GC B cells, although it was not statistically significant.

To further probe the ability of P35C conjugation to improve humoral immunity, we selected another well-studied and immunogenic model antigen, OVA, for conjugation with P35C and mouse immunization. C57BL/6 mice were immunized with OVA protein alone or P11C-OVA conjugate or P35C-OVA conjugate. Compared with the HA stem and HEL proteins, OVA was more immunogenic and elicited a strong OVA-specific B cell responses in the absence of peptide conjugation (Fig 5C and 5D). After conjugation with either P35C or the

control P11C peptide, the new immunogens did not significantly increase frequency of OVA-specific GC B cells over their already high levels.

Next, we selected another immunogen, the HIV-1 Env monomer gp120, for conjugation with P35C and mouse immunization. C57BL/6 mice were immunized with gp120 protein alone or P11C-gp120 conjugate or P35C-gp120 conjugate. gp120 alone elicited reasonable gp120-specific B cell responses (Fig 5E and 5F). Surprisingly, gp120-specific GC B cells of P11C-gp120 or P35C-gp120 immunized mice were significantly lower than gp120 alone immunized mice. Since peptide and protein conjugation using Sulfo-SMCC is not site-specific, we surmise that P11C and P35C might block part of the original B cell epitopes of gp120 itself and damage gp120-specific B cell responses.

Discussion

Synthetic oligopeptides have displayed significant adjuvant potential in animal studies recent years [25–28]. Here we showed that conjugation of a short peptide, P35C, improved the immunogenicity of weakly immunogenic HA stem protein in C57BL/6 mice. P35 is 17-amino acid peptide derived from the head domain of PR8 HA. Previous studies demonstrated that glutamine/asparagine (Q/N)-rich domains have a high tendency to form aggregates [29, 30]. P35C is also rich in Q/N-, including two Q and three N and we speculate that this is probably the chemical basis for P35C forming aggregates.

Tan et al. from our group recently demonstrated that HA stem was a poor immunogen which elicited little or no stem-specific antibody response in C57BL/6 mice [10]. In the present study, we found that P35C-stem conjugates significantly enhanced stem-specific antibody responses independent of Tfh cell help. Although P35 is not a strong CD4 T cell epitope in C57BL/6 mice (S2 Fig), we cannot rule out that a weak response below the threshold of detection could be present. To more definitively confirm that the enhanced immunogenicity is T cell-independent, the immunogenicity of stem and P35C-stem could be compared in TCR-deficient mice in future studies. The improved immunogenicity of stem is likely due to P35C induced aggregation of stem proteins since filtration abrogated this improved immunogenicity. Protein aggregates are known to be more efficient in eliciting immune responses than their monomeric forms even in the absence of T-cell help [15, 31]. The enhanced stem-specific antibody responses is probably related to the ability of extensive cross-linking of B-cell receptor by multiple stem proteins displayed on the surface of P35C-stem aggregates [15, 32]. Another possible mechanism would resemble the depot effect of aluminium-containing adjuvants [33–35]. Aggregated stem proteins are trapped within the site of injection and tend to be relatively stabilized against degradation, which allows prolonged release of antigens [25, 27, 32]. The slow release of antigens could provide continual stimulation to B cells directly and/or more durable peptide substrate presented by APC to T cells [10, 27]. In addition, it is possible that aggregated stem proteins promote phagocytosis of antigens by antigen-presenting cells since particulate or aggregated forms of antigens are more efficiently taken up and presented by APC than soluble proteins [18, 28, 36, 37]. Although we showed that P35C-stem improved stem-specific B cell and serological responses, whether the enhanced antibody responses induced by P35C-stem can neutralize the infectivity of live virus and confer protection of mice against influenza virus infection remain to be investigated in future studies.

To investigate whether the enhanced immunogenicity of stem protein by P35C conjugation is generalizable, we tested another immunogen, HEL, for conjugation with P35C and mouse immunization. Our data in groups of 5 mice showed that P35C-HEL conjugates could increase the frequency of HEL-specific GC B cells and HEL-specific serum IgG titre. We also conjugated P35C with HIV gp120 protein and OVA protein and elevated their immune

immunogenicity in mice. We found that P35C-gp120 conjugates or P35C-OVA conjugates did not increase gp120-specific or OVA-specific antibody responses compared with soluble gp120 protein or OVA protein. Possible reasons are: 1) since peptide and protein conjugation using Sulfo-SMCC is not site-specific, P35C might block some of the original B cell epitopes of gp120 or OVA protein; 2) protein aggregation can cover some of the original B cell epitopes of gp120 or OVA protein. Either scenario could limit gp120-specific or OVA-specific B cell responses and offset the enhancement effect of P35C induced aggregation. This is consistent with previous studies that, in some cases, aggregation of a protein antigen did not increase, or even reduced, immunogenicity due to loss of immunogenic epitopes [16].

Conjugation of a highly immunogenic carrier protein with a poor immunogen is an effective strategy to rescue its immunogenicity [38]. However, because of the limited number of potent carrier proteins, conjugate vaccines against various pathogens may be coupled with the same carrier [39]. In addition, repeated immunization is commonly required to induce adequate level of protective immune responses even for the same conjugate vaccine. Pre-existing immunity to the carrier may suppress subsequent immune responses to the same vaccine upon booster immunization or to another vaccine coupled with the same carrier; this phenomenon is termed carrier induced epitopic suppression (CIES) [39, 40]. CIES may happen through competition between carrier-specific and hapten-specific B cells for the antigen or suppression by carrier-induced regulatory T cells [39–41]. Although P35C may also induce anti-P35C immune responses, the level of P35C-specific immune responses will be very low, if any. Thus, use of P35 as a "carrier" for stem protein can probably avoid the potential concern of CIES. In summary, we showed that P35C conjugation rescued the poor immunogenicity of HA stem. P35C conjugation represents a new pathway to boost stem-specific antibody responses without introducing exotic carrier proteins which will elicit anti-carrier responses. Recombinant HA protein vaccine (Flublok) produced in the baculovirus-insect cell system has been licensed for the prevention of seasonal influenza in adults aged 18–49 years [42]. The breadth of the immune responses induced by Flublok is still narrow since the mode of action of Flublok is similar to that of traditional egg-based inactivated vaccines [43]. Stem-based influenza vaccine which can elicit immune responses to a broader range of influenza viruses could be an important supplement to broaden the immunogenicity of current seasonal influenza vaccine, particularly in the case of an emerging pandemic.

Supporting information

S1 Fig. Binding activity of anti-HA stem monoclonal antibodies with PR8 HA stem or P35C-stem. Binding activity of anti-HA stem monoclonal antibodies CR9114 (A), TN1F11 (B), TN1G09 (C) and control anti-HIV-1 gp120 antibody VRC01 (D) with PR8 HA stem (red line) or P35C-stem (blue line) measured by ELISA. Titration curves were generated using sigmoid dose-response of nonlinear fit with GraphPad Prism.
(TIF)

S2 Fig. Activation-induced marker expression of mLN cells from influenza-infected mice following stimulation. (A) Gating strategy to identify CD4 T cells in the mLN. Lymphocytes were identified by forward scatter area (FSC-A) and side-scatter area (SSC-A). Doublets were excluded by gating on single cells as determined by FSC-A versus FSC-H, and live cells were identified by viability dye exclusion. T cells were identified as CD3+B220- and CD4 T cells were identified as CD3+CD4+. For each step, the parental population is indicated above the plot. (B) Representative flow cytometric plots of CD154 expression on CD4 T cells after DMSO, P11, P35, or Con A stimulation for 18 h. (C) Representative flow cytometric plots of

CD25/OX40 expression on CD4 T cells after DMSO, P11, P35, or Con A stimulation for 18 h. (TIF)

S1 Table. Biophysical characterisation of stem protein and P35C-stem conjugates. (DOCX)

Author Contributions

Conceptualization: Wenbo Jiang.

Data curation: Wenbo Jiang, Hannah G. Kelly, Hyon-Xhi Tan.

Formal analysis: Wenbo Jiang.

Funding acquisition: Jennifer A. Juno, Adam K. Wheatley, Stephen J. Kent.

Investigation: Wenbo Jiang, Emily H. Pilkington.

Methodology: Wenbo Jiang, Emily H. Pilkington.

Project administration: Stephen J. Kent.

Resources: Stephen J. Kent.

Supervision: Jennifer A. Juno, Adam K. Wheatley, Stephen J. Kent.

Validation: Wenbo Jiang.

Visualization: Wenbo Jiang.

Writing – original draft: Wenbo Jiang, Emily H. Pilkington.

Writing – review & editing: Emily H. Pilkington, Jennifer A. Juno, Adam K. Wheatley, Stephen J. Kent.

References

1. Krammer F, Smith GJD, Fouchier RAM, Peiris M, Kedzierska K, Doherty PC, et al. Influenza. Nat Rev Dis Primers. 2018; 4(1):3. Epub 2018/06/30. https://doi.org/10.1038/s41572-018-0002-y PMID: 29955068.
2. Chen JR, Liu YM, Tseng YC, Ma C. Better influenza vaccines: an industry perspective. J Biomed Sci. 2020; 27(1):33. Epub 2020/02/16. https://doi.org/10.1186/s12929-020-0626-6 PMID: 32059697; PubMed Central PMCID: PMC7023813.
3. Centers for Disease Control and Prevention. Past seasons vaccine effectiveness estimates. Adjusted vaccine effectiveness estimates for influenza seasons from 2004–2018. https://www.cdc.gov/flu/vaccines-work/past-seasons-estimates.html. Accessed 9 April 2020.
4. Ostrowsky J, Arpey M, Moore K, Osterholm M, Friede M, Gordon J, et al. Tracking progress in universal influenza vaccine development. Curr Opin Virol. 2020; 40:28–36. Epub 2020/04/13. https://doi.org/10.1016/j.coviro.2020.02.003 PMID: 32279026.
5. David M. Knipe PMH. Orthomyxoviridae. Fields Virology, Sixth Edition. 2013.
6. Robert G. Webster ASM, Braciale Thomas J., Lamb Robert A. Structure and replication. Textbook of Influenza, Second Edition. 2013.
7. Pica N, Palese P. Toward a universal influenza virus vaccine: prospects and challenges. Annu Rev Med. 2013; 64:189–202. Epub 2013/01/19. https://doi.org/10.1146/annurev-med-120611-145115 PMID: 23327522.
8. Nachbagauer R, Palese P. Is a Universal Influenza Virus Vaccine Possible? Annu Rev Med. 2020; 71:315–27. Epub 2019/10/11. https://doi.org/10.1146/annurev-med-120617-041310 PMID: 31600454.
9. Sui J, Hwang WC, Perez S, Wei G, Aird D, Chen LM, et al. Structural and functional bases for broad-spectrum neutralization of avian and human influenza A viruses. Nat Struct Mol Biol. 2009; 16(3):265–73. Epub 2009/02/24. https://doi.org/10.1038/nsmb.1566 PMID: 19234466; PubMed Central PMCID: PMC2692245.

10. Tan HX, Jegaskanda S, Juno JA, Esterbauer R, Wong J, Kelly HG, et al. Subdominance and poor intrinsic immunogenicity limit humoral immunity targeting influenza HA stem. J Clin Invest. 2019; 129 (2):850–62. Epub 2018/12/07. https://doi.org/10.1172/JCI123366 PMID: 30521496; PubMed Central PMCID: PMC6355240.

11. Vogel OA, Manicassamy B. Broadly Protective Strategies Against Influenza Viruses: Universal Vaccines and Therapeutics. Front Microbiol. 2020; 11:135. Epub 2020/03/03. https://doi.org/10.3389/fmicb.2020.00135 PMID: 32117155; PubMed Central PMCID: PMC7020694.

12. Snapper CM. Distinct Immunologic Properties of Soluble Versus Particulate Antigens. Front Immunol. 2018; 9:598. Epub 2018/04/06. https://doi.org/10.3389/fimmu.2018.00598 PMID: 29619034; PubMed Central PMCID: PMC5871672.

13. Irvine DJ, Read BJ. Shaping humoral immunity to vaccines through antigen-displaying nanoparticles. Curr Opin Immunol. 2020; 65:1–6. Epub 2020/03/23. https://doi.org/10.1016/j.coi.2020.01.007 PMID: 32200132.

14. Yassine HM, Boyington JC, McTamney PM, Wei CJ, Kanekiyo M, Kong WP, et al. Hemagglutinin-stem nanoparticles generate heterosubtypic influenza protection. Nat Med. 2015; 21(9):1065–70. Epub 2015/08/25. https://doi.org/10.1038/nm.3927 PMID: 26301691.

15. Rosenberg AS. Effects of protein aggregates: an immunologic perspective. AAPS J. 2006; 8(3):E501–7. Epub 2006/10/10. https://doi.org/10.1208/aapsj080359 PMID: 17025268; PubMed Central PMCID: PMC2761057.

16. Wang W, Singh SK, Li N, Toler MR, King KR, Nema S. Immunogenicity of protein aggregates—concerns and realities. Int J Pharm. 2012; 431(1–2):1–11. Epub 2012/05/02. https://doi.org/10.1016/j.ijpharm.2012.04.040 PMID: 22546296.

17. Hermeling S, Schellekens H, Maas C, Gebbink MF, Crommelin DJ, Jiskoot W. Antibody response to aggregated human interferon alpha2b in wild-type and transgenic immune tolerant mice depends on type and level of aggregation. J Pharm Sci. 2006; 95(5):1084–96. Epub 2006/03/23. https://doi.org/10.1002/jps.20599 PMID: 16552750.

18. Ilyinskii PO, Thoidis G, Sherman MY, Shneider A. Adjuvant potential of aggregate-forming polyglutamine domains. Vaccine. 2008; 26(26):3223–6. Epub 2008/05/10. https://doi.org/10.1016/j.vaccine.2008.03.078 PMID: 18467011.

19. Wei CJ, Xu L, Kong WP, Shi W, Canis K, Stevens J, et al. Comparative efficacy of neutralizing antibodies elicited by recombinant hemagglutinin proteins from avian H5N1 influenza virus. J Virol. 2008; 82 (13):6200–8. Epub 2008/04/18. https://doi.org/10.1128/JVI.00187-08 PMID: 18417563; PubMed Central PMCID: PMC2447076.

20. Moyer TJ, Kato Y, Abraham W, Chang JYH, Kulp DW, Watson N, et al. Engineered immunogen binding to alum adjuvant enhances humoral immunity. Nat Med. 2020; 26(3):430–40. Epub 2020/02/19. https://doi.org/10.1038/s41591-020-0753-3 PMID: 32066977; PubMed Central PMCID: PMC7069805.

21. Morefield GL, HogenEsch H, Robinson JP, Hem SL. Distribution of adsorbed antigen in mono-valent and combination vaccines. Vaccine. 2004; 22(15–16):1973–84. Epub 2004/05/04. https://doi.org/10.1016/j.vaccine.2003.10.040 PMID: 15121310.

22. HogenEsch H, O'Hagan DT, Fox CB. Optimizing the utilization of aluminum adjuvants in vaccines: you might just get what you want. NPJ Vaccines. 2018; 3:51. Epub 2018/10/17. https://doi.org/10.1038/s41541-018-0089-x PMID: 30323958; PubMed Central PMCID: PMC6180056 years. D.T.O.H. is an employee of GlaxoSmithKline. C.B.F. is an inventor on patent applications involving combination TLR ligand-aluminum adjuvants and nanoparticle aluminum adjuvants.

23. Jiang W, Wragg KM, Tan HX, Kelly HG, Wheatley AK, Kent SJ, et al. Identification of murine antigen-specific T follicular helper cells using an activation-induced marker assay. J Immunol Methods. 2019; 467:48–57. Epub 2019/02/26. https://doi.org/10.1016/j.jim.2019.02.008 PMID: 30802449.

24. Kelly HG, Tan HX, Juno JA, Esterbauer R, Ju Y, Jiang W, et al. Self-assembling influenza nanoparticle vaccines drive extended germinal center activity and memory B cell maturation. JCI Insight. 2020; 5 (10). Epub 2020/05/22. https://doi.org/10.1172/jci.insight.136653 PMID: 32434990; PubMed Central PMCID: PMC7259527.

25. Rudra JS, Tian YF, Jung JP, Collier JH. A self-assembling peptide acting as an immune adjuvant. Proc Natl Acad Sci U S A. 2010; 107(2):622–7. Epub 2010/01/19. https://doi.org/10.1073/pnas.0912124107 PMID: 20080728; PubMed Central PMCID: PMC2818904.

26. Saenz R, Souza Cda S, Huang CT, Larsson M, Esener S, Messmer D. HMGB1-derived peptide acts as adjuvant inducing immune responses to peptide and protein antigen. Vaccine. 2010; 28(47):7556–62. Epub 2010/08/31. https://doi.org/10.1016/j.vaccine.2010.08.054 PMID: 20800114; PubMed Central PMCID: PMC2963688.

27. Grenfell RF, Shollenberger LM, Samli EF, Harn DA. Vaccine self-assembling immune matrix is a new delivery platform that enhances immune responses to recombinant HBsAg in mice. Clin Vaccine

Immunol. 2015; 22(3):336–43. Epub 2015/01/23. https://doi.org/10.1128/CVI.00714-14 PMID: 25609075; PubMed Central PMCID: PMC4340892.

28. Jones JC, Settles EW, Brandt CR, Schultz-Cherry S. Virus aggregating peptide enhances the cell-mediated response to influenza virus vaccine. Vaccine. 2011; 29(44):7696–703. Epub 2011/08/16. https://doi.org/10.1016/j.vaccine.2011.07.133 PMID: 21839131; PubMed Central PMCID: PMC3190079.

29. Wang X, Das TK, Singh SK, Kumar S. Potential aggregation prone regions in biotherapeutics: A survey of commercial monoclonal antibodies. MAbs. 2009; 1(3):254–67. Epub 2010/01/13. https://doi.org/10.4161/mabs.1.3.8035 PMID: 20065649; PubMed Central PMCID: PMC2726584.

30. Michelitsch MD, Weissman JS. A census of glutamine/asparagine-rich regions: implications for their conserved function and the prediction of novel prions. Proc Natl Acad Sci U S A. 2000; 97(22):11910–5. Epub 2000/10/26. https://doi.org/10.1073/pnas.97.22.11910 PMID: 11050225; PubMed Central PMCID: PMC17268.

31. Sauerborn M, Brinks V, Jiskoot W, Schellekens H. Immunological mechanism underlying the immune response to recombinant human protein therapeutics. Trends Pharmacol Sci. 2010; 31(2):53–9. Epub 2009/12/08. https://doi.org/10.1016/j.tips.2009.11.001 PMID: 19963283.

32. Moyer TJ, Zmolek AC, Irvine DJ. Beyond antigens and adjuvants: formulating future vaccines. J Clin Invest. 2016; 126(3):799–808. Epub 2016/03/02. https://doi.org/10.1172/JCI81083 PMID: 26928033; PubMed Central PMCID: PMC4767337.

33. Ghimire TR. The mechanisms of action of vaccines containing aluminum adjuvants: an in vitro vs in vivo paradigm. Springerplus. 2015; 4:181. Epub 2015/05/02. https://doi.org/10.1186/s40064-015-0972-0 PMID: 25932368; PubMed Central PMCID: PMC4406982.

34. Martinon S, Cisneros A, Villicana S, Hernandez-Miramontes R, Mixcoha E, Calderon-Vargas P. Chemical and Immunological Characteristics of Aluminum-Based, Oil-Water Emulsion, and Bacterial-Origin Adjuvants. J Immunol Res. 2019; 2019:3974127. Epub 2019/06/18. https://doi.org/10.1155/2019/3974127 PMID: 31205956; PubMed Central PMCID: PMC6530223.

35. He P, Zou Y, Hu Z. Advances in aluminum hydroxide-based adjuvant research and its mechanism. Hum Vaccin Immunother. 2015; 11(2):477–88. Epub 2015/02/19. https://doi.org/10.1080/21645515.2014.1004026 PMID: 25692535; PubMed Central PMCID: PMC4514166.

36. Bachmann MF, Jennings GT. Vaccine delivery: a matter of size, geometry, kinetics and molecular patterns. Nat Rev Immunol. 2010; 10(11):787–96. Epub 2010/10/16. https://doi.org/10.1038/nri2868 PMID: 20948547.

37. Kovacsovics-Bankowski M, Clark K, Benacerraf B, Rock KL. Efficient major histocompatibility complex class I presentation of exogenous antigen upon phagocytosis by macrophages. Proc Natl Acad Sci U S A. 1993; 90(11):4942–6. Epub 1993/06/01. https://doi.org/10.1073/pnas.90.11.4942 PMID: 8506338; PubMed Central PMCID: PMC46629.

38. Rappuoli R, De Gregorio E, Costantino P. On the mechanisms of conjugate vaccines. Proc Natl Acad Sci U S A. 2019; 116(1):14–6. Epub 2018/12/24. https://doi.org/10.1073/pnas.1819612116 PMID: 30578318; PubMed Central PMCID: PMC6320500 GlaxoSmithKline group of companies; P.C. is retired and a former employee of the GlaxoSmithKline group of companies.

39. Jegerlehner A, Wiesel M, Dietmeier K, Zabel F, Gatto D, Saudan P, et al. Carrier induced epitopic suppression of antibody responses induced by virus-like particles is a dynamic phenomenon caused by carrier-specific antibodies. Vaccine. 2010; 28(33):5503–12. Epub 2010/03/24. https://doi.org/10.1016/j.vaccine.2010.02.103 PMID: 20307591.

40. McCluskie MJ, Evans DM, Zhang N, Benoit M, McElhiney SP, Unnithan M, et al. The effect of preexisting anti-carrier immunity on subsequent responses to CRM197 or Qb-VLP conjugate vaccines. Immunopharmacol Immunotoxicol. 2016; 38(3):184–96. Epub 2016/04/29. https://doi.org/10.3109/08923973.2016.1165246 PMID: 27121368.

41. Dagan R, Poolman J, Siegrist CA. Glycoconjugate vaccines and immune interference: A review. Vaccine. 2010; 28(34):5513–23. Epub 2010/07/06. https://doi.org/10.1016/j.vaccine.2010.06.026 PMID: 20600514.

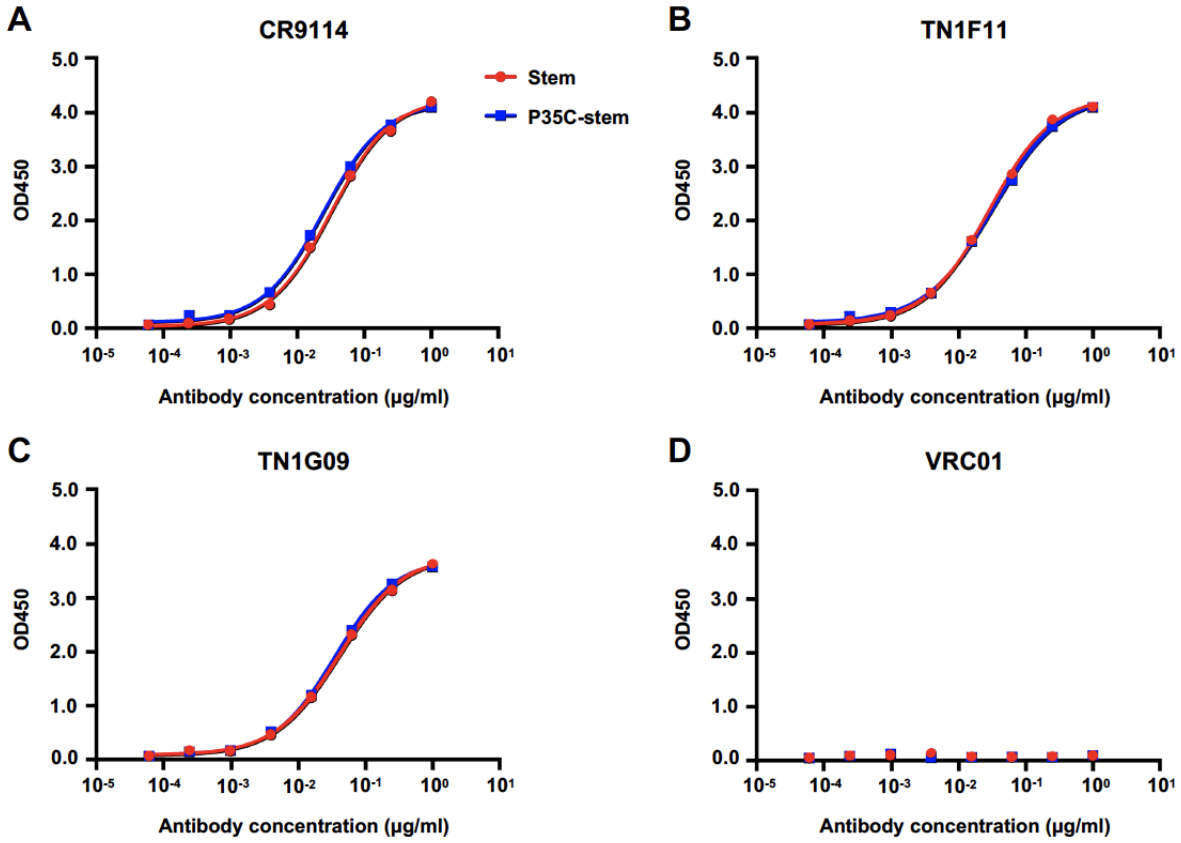
42. Yang LP. Recombinant trivalent influenza vaccine (flublok((R))): a review of its use in the prevention of seasonal influenza in adults. Drugs. 2013; 73(12):1357–66. Epub 2013/08/10. https://doi.org/10.1007/s40265-013-0103-6 PMID: 23928902.

43. Cox MM, Izikson R, Post P, Dunkle L. Safety, efficacy, and immunogenicity of Flublok in the prevention of seasonal influenza in adults. Ther Adv Vaccines. 2015; 3(4):97–108. Epub 2015/10/20. https://doi.org/10.1177/2051013615595595 PMID: 26478817; PubMed Central PMCID: PMC4591523.

Supplemental data for manuscript:

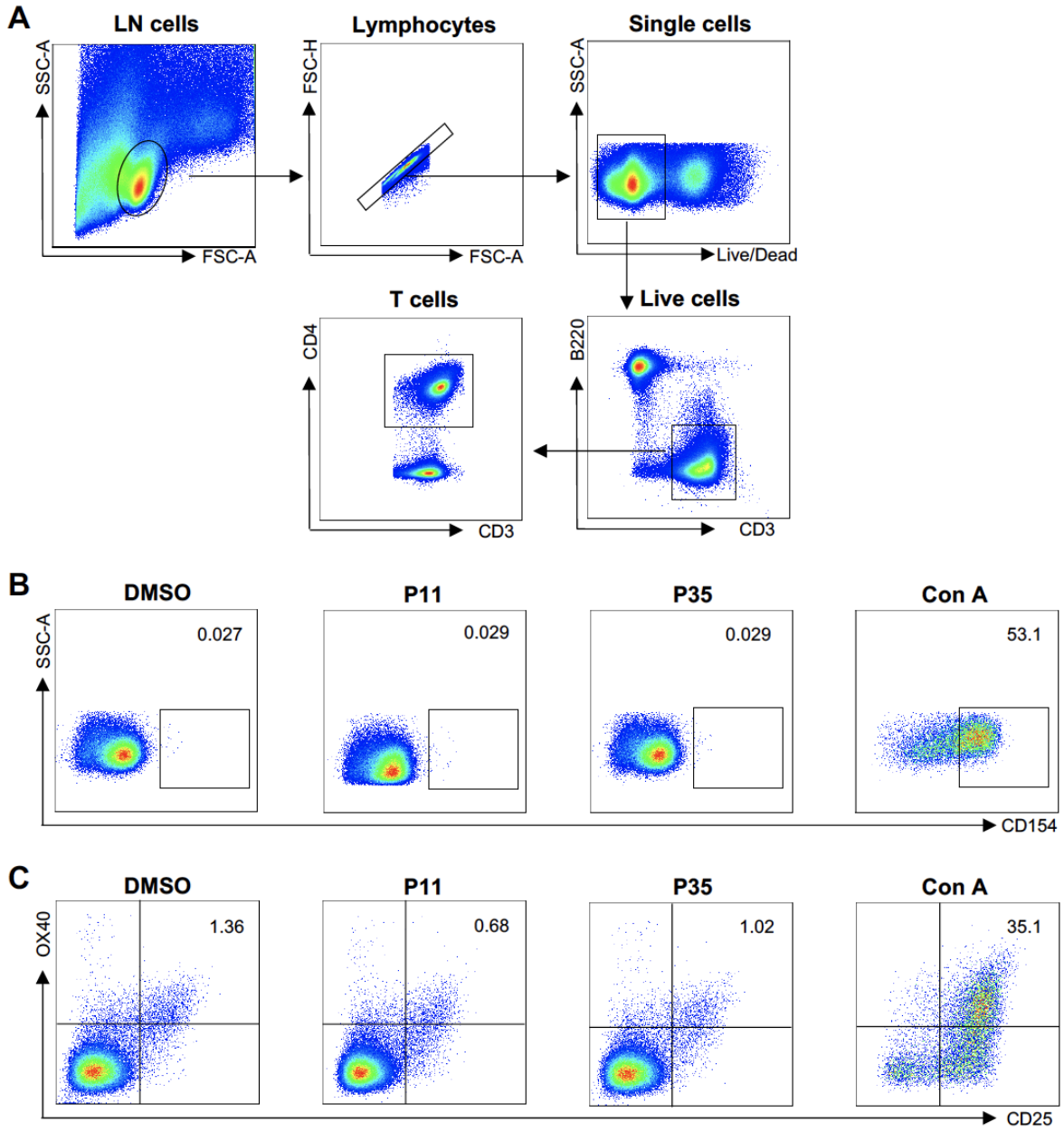
Aggregation by peptide conjugation rescue poor immunogenicity of the HA stem

Wenbo Jiang, Emily H Pilkington, Hannah G Kelly, Hyon-Xhi Tan, Jennifer A Juno, Adam K Wheatley, Stephen J Kent.



S1 Fig. Binding activity of anti-HA stem monoclonal antibodies with PR8 HA stem or P35C-stem.

Binding activity of anti-HA stem monoclonal antibodies CR9114 (A), TN1F11 (B), TN1G09 (C) and control anti-HIV-1 gp120 antibody VRC01 (D) with PR8 HA stem (red line) or P35C-stem (blue line) measured by ELISA. Titration curves were generated using sigmoid dose-response of nonlinear fit with GraphPad Prism.



S2 Fig. Activation-induced marker expression of mLN cells from influenza-infected mice following stimulation.

(A) Gating strategy to identify CD4 T cells in the mLN. Lymphocytes were identified by forward scatter area (FSC-A) and side-scatter area (SSC-A). Doublets were excluded by gating on single cells as determined by FSC-A versus FSC-H, and live cells were identified by viability dye exclusion. T cells were identified as CD3+B220- and CD4 T cells were identified as CD3+CD4+. For each step, the parental population is indicated above the plot. (B)

Representative flow cytometric plots of CD154 expression on CD4 T cells after DMSO, P11, P35, or Con A stimulation for 18 h. (C) Representative flow cytometric plots of CD25/OX40 expression on CD4 T cells after DMSO, P11, P35, or Con A stimulation for 18 h.

S1 Table: Biophysical characterisation of stem protein and P35C-stem conjugates

Sample	**Polydispersity index**	**Hydrodynamic size by Number (nm)**	**Z-average hydrodynamic size (nm)**	**Zeta potential (mV)**
Stem	0.266 ± 0.111	10.2 ± 0.2	145.5 ± 74.6	-3.45 ± 0.345
P35C-stem (filtered)	0.588 ± 0.097	9.2 ± 0.6	39.4 ± 9.6	-2.01 ± 0.919
P35C-stem (unfiltered)	0.733 ± 0.064	>10,000*	30290 ± 2257.8	-20.2 ± 1.79

*unable to resolve due to size exceeding limit (10,000 nm) of distribution analysis model

Chapter 5: General Discussion

Chapter 5: General Discussion

5.1 Integrated findings of this thesis

Influenza disease poses great threat to global public health. Current seasonal influenza vaccines are efficacious only when vaccine strains are matched with circulating strains. There is therefore a critical need to develop "universal" influenza vaccines that elicit broad and potent antibody responses against all influenza viruses. Antibody responses to HA play a central role in defence against influenza virus infection[4]. Tfh cells are crucial for the generation of high-affinity antibody responses[110]. Characterisation of HA-specific Tfh cells is essential to reveal the immunological basis of protective anti-HA antibody responses and to develop novel vaccines for the prevention of influenza infection.

Relatively little is known about HA-specific Tfh cells in important animal models of influenza, such as mice and ferrets. Although mouse Tfh cells have been extensively investigated owing to a wide range of commercially available reagents[113-115], HA-specific Tfh cells are rarely identified in wild type mice following influenza virus infection or HA immunization using conventional intracellular cytokine staining assay. This is because Tfh cells mainly provide contact dependent, selective help to GC B cells as opposed to wholesale cytokine secretion. To identify HA-specific Tfh cells in mice in the context of influenza virus infection and HA immunization, we developed an activation-induced markers (AIM) assay (Chapter 2). We found that HA-specific Tfh cells were clearly detected by quantifying the upregulation of either CD154 or CD25/OX40 following HA peptide pool or whole HA stimulation. The AIM assay provides the opportunity to characterise HA-specific Tfh cells in wild type mice without the need of MHC-II tetramer reagents. With the development of this assay, we were able to probe the immunodominance hierarchy of different Tfh epitopes on HA and investigate the influence

of Tfh responses on humoral immune responses in mice by addition or deletion of Tfh epitopes on HA.

To determine the immunodominance hierarchy of Tfh and conventional CD4 T cell responses, we mapped the Tfh and conventional CD4 T cell epitopes of PR8 HA in PR8 infected C57BL/6 mice. After primary screening using pooled LN cells from multiple mice, we excluded non-stimulatory peptides and selected 14 out of 93 peptides for further confirmation with AIM and ICS assay using LN cells from individual mice (Figure 5.1). We classified the Tfh/CD4 epitopes into major and minor epitopes. The peptides which ranked first of all peptides based on any of the three activation markers (CD154, CD25/OX40 or IFNg) are classified as major epitopes, other positive peptides are classified as minor epitopes. The major and minor Tfh/CD4 T cell epitopes which belong to HA head domain or HA stem protein are shown in Table 5.1. Most of Tfh epitopes, including the most immunodominant epitope Peptide 16, belong to HA head domain. Since C57BL/6 mice have only one major epitope (Peptide 16) and it belongs to HA head domain, we plan to conjugate Peptide 16 (P16) to HA stem protein which lacks immunodominant Tfh epitopes to modulate the immunogenicity of HA stem protein in C57BL/6 mice.

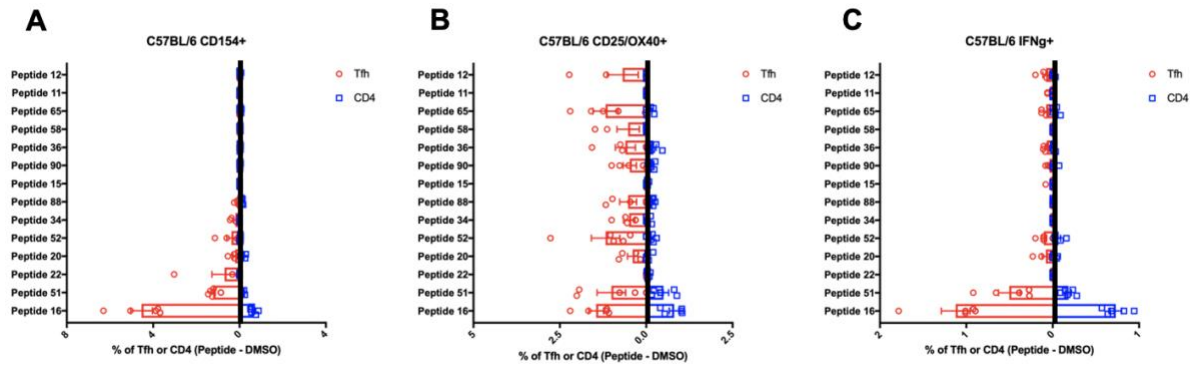


Figure 5.1 Immunodominance hierarchy of Tfh responses and CD4 T cell responses. Immunodominance hierarchy of Tfh (B220-CD3+CD4+CXCR5++PD-1++) responses (red) and CD4 T cell (B220-CD3+CD4+) responses (blue) of mediastinal lymph node-derived cells from A/Puerto Rico/8/1934 (H1N1) virus-infected C57BL/6 mice. Lymph node cells of 5 mice were stimulated with 14 individual peptides which were potentially stimulatory based on primary screening experiment. Antigen-specific responses to each peptide stimulation were measured by cell surface CD154 upregulation (A) or CD25/OX40 upregulation (B) or intracellular IFN-γ upregulation (C).

Table 5.1 Tfh/CD4 T cell epitopes of PR8 HA in C57BL/6 mice.

Epitopes	Epitopes belong to head	Epitopes belong to stem
Major epitopes	P16	No
Minor epitopes	P12, P20, P22, P34, P36, P51, P52	P58, P65

While we were conducting the preliminary experiment to prove our hypothesis that the immunogenicity of HA stem protein in C57BL/6 mice could be rescued by the addition of an immunodominant Tfh epitope from HA head domain, we unexpectedly found that the immunogenicity of HA stem protein in C57BL/6 mice could be improved by the conjugation of a non-immunodominant Tfh epitope, Peptide 35 (P35) (explored in Chapter 4). We hypothesized that either the P35C-stem conjugates would (a) permit strong T-cell dependent

help and/or (b) form protein aggregates, which could provide T cell-independent help to B cells[161]. To evaluate this hypothesis, we filtered P35C-stem through a 0.22um filter and immunized mice with filtered P35C-stem and unfiltered P35C-stem. We found that the immunogenicity of filtered P35C-stem significantly decreased compared with unfiltered P35C-stem. We also found that P35 did not activate the expression of CD154 or CD25/OX40 markers above that of control in influenza-immune mice, showing they were not significant T-helper epitopes. Taken together, these data indicate that P35C improves the immunogenicity of stem by an aggregation mechanism. P35C conjugation represents a new avenue to enhance stem-specific antibody responses without bringing in exotic carrier proteins that will induce anti-carrier responses. Stem-based influenza vaccine which can elicit immune responses to a broader range of influenza viruses could be an important supplement to broaden the immunogenicity of current seasonal influenza vaccine, particularly in the case of an emerging pandemic.

Although mice are widely used for primary screening of influenza vaccine candidates and elucidating the protection mechanisms[75], the predictive value of mouse models for successful vaccination of humans has been questioned[76]. By contrast, ferrets are more reliable animal models for pre-clinical evaluation of the protection efficacy of influenza vaccines. However, ferret Tfh cell responses following influenza vaccine immunization remain largely unexplored owing to the unavailability of suitable immunological reagents. To advance the investigation of ferret Tfh cells, we developed two monoclonal antibodies against ferret CXCR5 and PD-1 using a single B cell PCR-based method (Chapter 3). We found that Tfh cells in lymph nodes from influenza infected ferrets were clearly identified using these antibodies. With these antibodies, we will be able to study the magnitude and quality of ferret Tfh responses in the context of influenza virus infection or vaccination, and the correlation between Tfh responses

and antibody responses. Results from ferret Tfh response studies can provide useful insights regarding how Tfh cells influence vaccine immunogenicity in ferret model. These insights will facilitate the design and evaluation of novel Tfh-targeting vaccines against the infection of influenza and other viruses, including SARS-CoV2.

5.2 Summary of experimental studies

This thesis investigated Tfh responses to influenza virus infection and immunization in mice and ferrets and explored the effects of immunogen multimerization on humoral immunity in the context of limiting Tfh responses to HA stem. In Chapter 2, we developed an assay to identify mouse Ag-specific Tfh cells by evaluating the upregulation of surface activation-induced markers. We showed that stimulation of lymph node cell suspensions from influenza-infected or HA-vaccinated mice with HA peptide pools or HA protein drove upregulation of CD25, OX40, ICOS and CD154 on Tfh cells. We confirmed that Ag-specific Tfh cells were best detected by quantifying the upregulation of either CD154 or CD25/OX40. In Chapter 3, we developed ferret-specific CXCR5 and PD-1 monoclonal antibodies using a single B cell PCR-based method and identified Tfh cells in lymph nodes from influenza infected ferrets using these antibodies. In Chapter 4, we attempted to improve Tfh-dependent antibody responses to HA stem through conjugating a short peptide (P35) derived from influenza HA head domain with the HA stem protein. We found that P35C-stem conjugates significantly increased stem-specific antibody responses in murine immunization studies although without changing the level of Tfh responses. This is likely due to a multimerization of the weakly soluble complex since filtration abrogated this improved immunogenicity. The following discussion integrates the work presented in this thesis with recent literature, with the aim of

highlighting potential future experimental work and outstanding research questions. Specifically, we address the following issues:

- Comparison of CD154 and CD25/OX40 as the makers for identifying Ag-specific Tfh cells;
- The viability of Tfh cells during culture;
- Ferret T cell responses to influenza virus infection and immunization;
- Ferrets as a model for SARS-CoV-2;
- Tfh dependent-enhancement of stem-specific antibody responses;
- Tfh independent-enhancement of stem-specific antibody responses.

5.3 Comparison of CD154 and CD25/OX40 as the makers for identifying Ag-specific Tfh cells

Several cell surface markers are used to identify activation of Tfh since Tfh are difficult to identify with standard intracellular cytokine assays[118,121]. CD154 is a member of the TNF superfamily and is mainly expressed on activated CD4 T cells[183]. CD154 expression on CD4 T cells activates CD40 expressed by B cells, which serves as the second signal for B cell full activation[101]. In GC, Tfh cells provide high-affinity B cells with help signals through the CD154-CD40 interaction, which is critical for antibody affinity maturation[106]. CD25, also called IL-2 receptor α chain (IL-2Rα), is constitutively expressed by regulatory T cells (Tregs) and inducibly expressed by conventional T cells upon activation[184]. CD25, CD122 (IL-2Rβ chain) and CD132 (IL-2Rγ chain) form high-affinity IL-2 receptor complex[184]. IL-2 is known to inhibit Tfh differentiation and differentiating Tfh cells express low levels of CD25 in vivo[118]. However, ex vivo re-stimulation of Tfh cells with peptides can upregulate CD25 expression. This is likely due to supraphysiological amount of peptides used for stimulation or lack of a

negative feedback mechanism to inhibit CD25 expression ex vivo[118]. OX40 (CD134) is a member of the TNFR superfamily and is predominantly expressed on activated CD4 T cells[183,185]. OX40 binds its ligand OX40L expressed by antigen-presenting cells (APCs)[183]. The OX40-OX40L interaction prolongs T cell survival, increases cytokine production and promotes the development of effector and memory T cells[183,185]. Analysis of activation induced expression of CD25 and OX40 are usually combined to effectively differentiate activated Tfh cells from un-activated Tfh cells. By contrast, activation induced expression CD154 is normally used alone due to extremely low level of baseline expression on un-activated Tfh cells.

While both CD154 and the dual expression of CD25 and OX40 can both be used as the makers for identifying Ag-specific Tfh cells, they differ in their sensitivity and the identified cell populations. Our data showed that higher frequencies of Ag-specific Tfh cells were detected by assessing CD154 upregulation than by assessing CD25/OX40 upregulation. In addition, CD154 and CD25/OX40 upregulation appear to identify both common and different subsets of Tfh cells. A portion of CD154 positive Tfh cells were also CD25/OX40 positive, and the remaining CD154 positive Tfh cells were CD25/OX40 negative, and vice versa (Figure 5.2). The question then arises: why do some Tfh cells upregulate CD154 while other Tfh cells upregulate CD25/OX40 upon peptide pool stimulation? What is the difference between the CD154 positive Tfh cells and the CD25/OX40 positive Tfh cells?

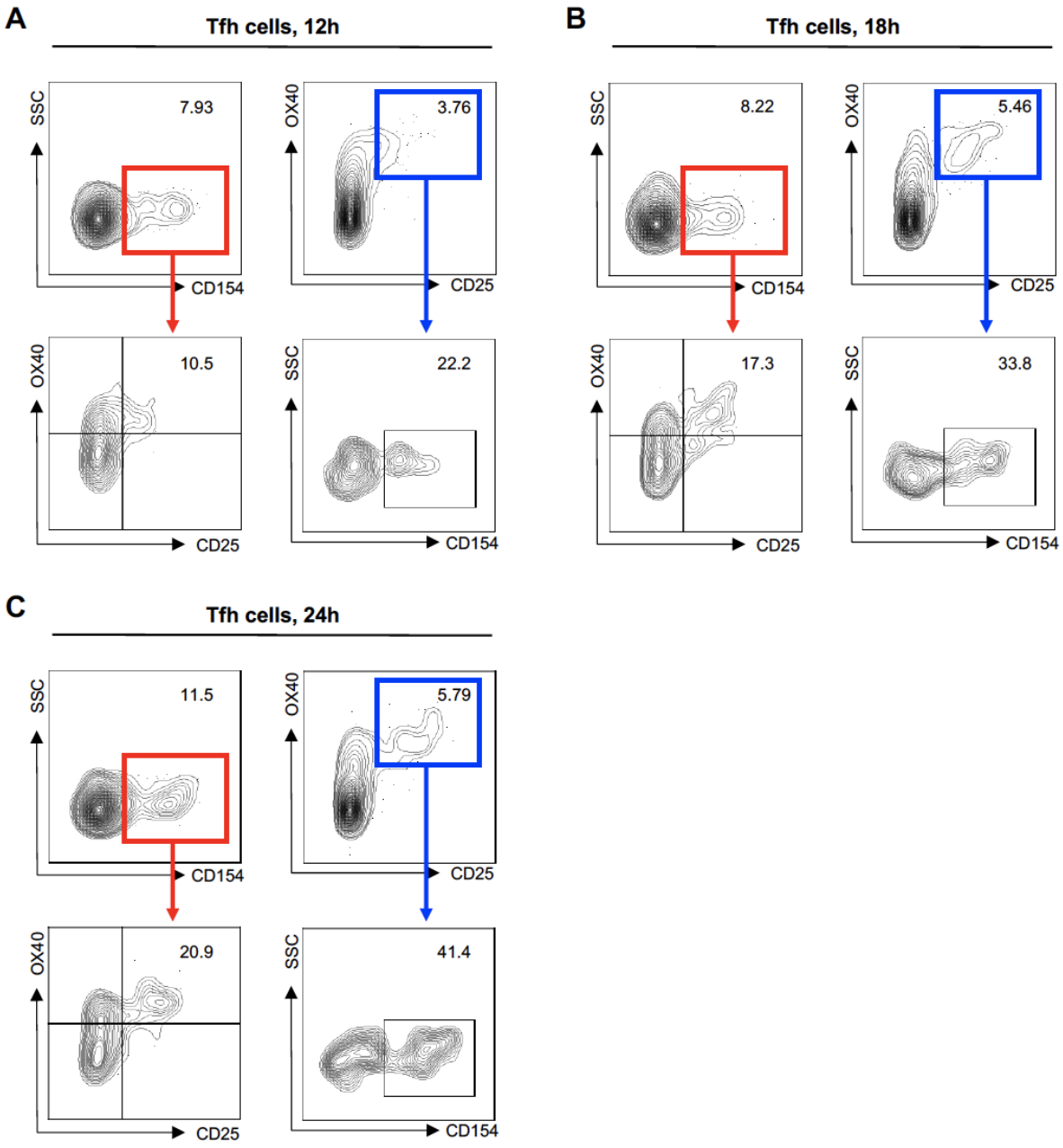


Figure 5.2 Activation-induced CD154 and CD25/OX40 expression identifies both common and distinct populations of antigen-specific Tfh cells. Representative plots of CD154 or CD25/OX40 expression on gated Tfh cells from mLN of influenza infected mice after HA peptide pool stimulation for 12h (A), 18h (B) or 24h (C). Subsequent plots show the representative expression of CD25/OX40 or CD154 within the CD154+ or CD25+OX40++ Tfh cells.

Since we initially observed this phenomenon in samples stimulated with HA peptide pool, we speculate that CD154 and CD25/OX40 may respond to different peptides (epitopes). However, this hypothesis is disproven by the data from single peptide stimulation (Figure 5.3). Several studies have shown that the expression and maintenance of CD25 on CD4 T cells are proportional to TCR affinity and signal strength following virus infection[186,187]. CD4 T cells with low-affinity TCRs expressed less CD25, while CD4 T cells with higher-affinity TCRs expressed more CD25. Thus, the CD154 positive Tfh cells and the CD25/OX40 positive Tfh cells identified following HA peptide pool stimulation in this thesis could represent Tfh cells with different TCR affinity. This hypothesis could be evaluated in future studies by quantifying the binding affinities of TCR: peptide/MHC (pMHC) with purified ectodomains of TCRs and their pMHC ligands using surface plasmon resonance (SPR) technique[188,189] or in situ with membrane anchored TCRs and pMHCs using single-molecule microscopy and fluorescence resonance energy transfer (FRET) technique[190,191].

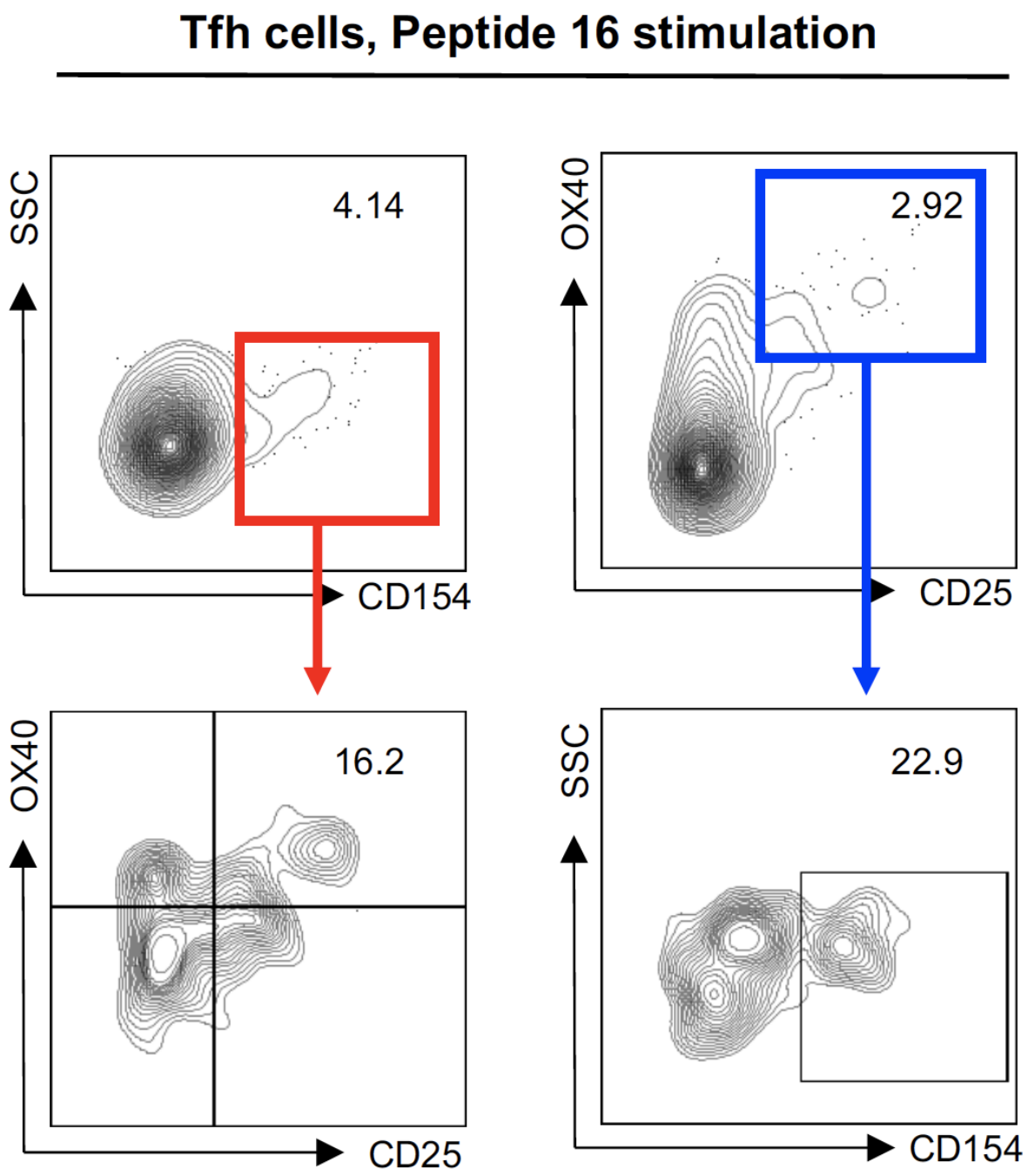


Figure 5.3 Activation-induced CD154 and CD25/OX40 expression following single peptide stimulation. Representative plots of CD154 or CD25/OX40 expression on Tfh cells from mLN of influenza infected mice after CD4 T cell epitope (peptide 16) stimulation for 18h. Subsequent plots show the representative expression of CD25/OX40 or CD154 within the CD154+ or CD25+OX40++ Tfh cells.

Tfh cells are increasingly recognized to be heterogeneous in their phenotype and function[192]. Multiple studies showed that Tfh cells expressed IFN-γ, IL-4, and IL-17, the signature cytokines of Th1, Th2 and Th17[192]. Thus, there is likely to be phenotypically and functionally distinct subsets of Tfh cells. We speculate that the CD154 positive Tfh cells and the CD25/OX40 positive Tfh cells following HA peptide pool stimulation in this thesis may represent different subsets of Tfh cells.

Tfr cells also express Tfh-like phenotypic markers such as CXCR5 and PD-1 as well as transcription factor BCL6[193,194]. Tfh cells identified as CD4+ CXCR5++ PD-1++ may contain a portion of Tfr cells. Recently, Aloulou et al. demonstrated that Tfr cells can be specific for the immunizing antigen[195]. Schoenbrunn et al. showed that Treg cells from human and mouse blood selectively upregulated 4-1BB, but not CD154, after in vitro stimulation[196]. By contrast, conventional CD4 T cells (Foxp3-) mainly upregulated CD154, but not 4-1BB, upon stimulation[196]. The converse expression pattern of 4-1BB and CD154 were used to differentiate antigen-reactive Treg and conventional CD4 T cells[196]. Thus, it is possible that a portion of CD4+ CXCR5++ PD-1++ cells which upregulated CD25/OX40 but not CD154 after HA peptide pool stimulation in this thesis are Tfr cells.

We suggest that it would be informative in future experiments to separately sort CD154 positive Tfh cells and CD25/OX40 positive Tfh cells following HA peptide pool stimulation and perform RNAseq and TCR sequencing to anatomize the difference of these two populations. Dissecting the difference of these two Tfh populations will increase our understanding of the function of Tfh cells and potentially identify the most critical populations of Tfh to support robust antibody responses by vaccination.

5.4 The viability of Tfh cells during culture

Previous studies have highlighted that GC Tfh cells are highly susceptible to apoptosis due to expression of Fas (CD95)[197-199]. Once removed from the GC environment, cell culture of this population can be challenging. A primary consideration in the technical development of a murine AIM assay is therefore to ensure the viability and recovery of Tfh cells following extended cell culture.

To study and potentially improve the viability of Tfh cells, we first compared various types of medium (RPMI 1640, Opti-MEM and AIM-V) for cell culture. We found that the Tfh cell recovery were similar after 18-hour culture with three types of medium. Since serum concentration in medium can significantly affect the cell viability, we next compared RPMI 1640 with different serum concentration (0% (RF0), 10% (RF10) and 20% (RF20)). Compared with the standard RF10 which was normally used for cell culture, we found no significant improvement in Tfh cell recovery after 18-hour culture with RF0 or RF20. It is known that IL-7 could promote T cell survival during culture[200], we then added IL-7 in RF10 medium. However, there was no marked change in Tfh cell recovery for cells cultured for 18 hours with IL-7 containing RF10 in comparison to cells cultured with RF10 alone.

To optimise the detection of Ag-specific Tfh, we determined the kinetics (12h, 18h, 24h) of Tfh cell activation marker expression following HA peptide stimulation (Figure 4A in Chapter 2). Although the upregulation of all activation markers studied was greatest at 24 h post stimulation, the Tfh population was prone to cell death and continually declined as the cell culture time increased. We therefore selected a stimulation time of 18 h in order to achieve a balance between Tfh cell loss and upregulation of surface activation markers.

Murine Tfh cells have been shown to be high expression of purinergic receptor P2X7, an ATP-gated ion channel[201]. Long-lasting P2X7 ion channel opening induces cell death[202]. ADP-ribosylation of P2X7 by ADP-ribosyltransferase 2.2 (ARTC2.2) which uses nicotinamide adenine dinucleotide (NAD) as a substrate results in continuous activation of P2X7 and subsequent cell death[203]. A previous study showed that NAD was released during the preparation of ex vivo cell suspensions from mouse spleen and lymph nodes[203]. NAD–induced cell death (NICD) affects the viability and function of murine primary T cells[203]. Recently, Künzli et al. showed that administration of the ARTC2.2-blocking nanobody prior to euthanizing the mice significantly increases the recovery of Tfh cells from lymphoid organs[204]. We speculate that it could be informative to inject mice with an ARTC2.2-blocking nanobody before sacrifice to improve the in vitro viability of Tfh cells in future experiments.

Furthermore, 2-mercaptoethanol (2-ME) has been long used as a medium supplement to increase the viability of murine lymphocytes during ex vivo culture[205-207]. Future experiments should include 2-ME in the medium during Tfh cell stimulation to further improve the viability of Tfh cells. With higher cell viability, Tfh cells could be stimulated for longer times to obtain higher upregulation of AIM makers, which ultimately should increase the sensitivity and dynamic range of the AIM assay.

5.5 Ferret T cell responses to influenza virus infection and immunization

Most current knowledge regarding ferret immune responses to influenza infection or immunization has been gained from either serological analysis of neutralizing antibody titre measured by HI assay or MN assay[76] or mRNA analysis of immune gene expression measured by qPCR or next-generation sequencing[208,209]. Although serological analyses characterise humoral immune responses to some extent, it cannot be used to analyse cellular immune

responses. Although mRNA analysis can be used for studying ferret cellular immune responses to influenza, data of mRNA levels can correlate poorly with protein levels[81,210]. By contrast, techniques such as flow cytometry and ELISpot can be utilized for direct quantification of immune marker expression. The application of flow cytometry in studying ferret immunological responses has been hampered due to a paucity of commercially available ferret-specific antibodies. Some insights have gained with the identification of a few cross-reactive antibodies and the in-house development of ferret-specific CD4 antibodies[84,211].

DiPiazza et al. characterised the magnitude and hierarchy of Ag-specific CD4 and CD8 T cell responses to different proteins of influenza virus after infection. Spleen cells from influenza infected ferrets at day 10 post-infection were stimulated with peptide pools of HA, NA, NP, M1 and NS1 proteins and IFN-γ secreting cells were quantified by ELISpot assay. For total influenza virus-specific CD4 T cell responses, there were approximately 160 spot-forming units (SFU) per million cells; for total influenza virus-specific CD8 T cell responses, there were approximately 210 SFU per million cells. Importantly, ferret T cell responses to influenza virus infection exhibited different reactivity patterns in individual ferrets, suggesting the MHC heterogeneity in outbred ferrets. For instance, only 2% of the total influenza-specific CD8 T cells was reactive to NA and 51% of the total influenza-specific CD8 T cells were reactive to NS1 in one ferret. By contrast, there was 47% of the total influenza-specific CD8 T cells directing toward NA and 37% of the total influenza-specific CD8 T cells directing toward NS1 in another ferret. Cheng et al. evaluated the Ag-specific antibody and T cell responses induced by live attenuated influenza vaccine (LAIV) and trivalent inactivated influenza vaccine (TIV) in ferrets[211]. The authors showed that LAIV elicited significantly higher level of HA-specific antibody responses compared with TIV. They also showed that LAIV elicited strong influenza virus–specific T-cell responses with 0.45% IFN-γ+ CD4 T cells and 0.35% IFN-γ+ CD8 T

cells. By contrast, TIV induced little influenza virus–specific T-cell responses and the percentages of IFN-γ+ CD4 T cells or CD8 T cells was similar to the that of mock immunized ferrets. The Tfh responses were not evaluated due to the lack of ferret Tfh reagents. Whether the higher-level of antibody responses induced by LAIV correlates with the ability of LAIV to induce Tfh responses remains to be investigated in future.

Our understanding about ferret CD4 and CD8 T cell responses to influenza virus infection and immunization have been improved with utilization of currently commercially available antibodies that cross react with ferret antigens. However, little is known about the function of different subsets of CD4 T cells in ferrets. In particular, our understanding on ferret Tfh responses was heretofore completely lacking. Basic questions, such as what the magnitude and quality of ferret Tfh responses are in the context of virus infection or vaccination, and how Tfh responses correlate with antibody responses following vaccination, remain to be answered. With the ferret-specific CXCR5 and PD-1 antibodies developed in Chapter 3, these questions can now start to be probed.

In addition to antibodies to identify Tfh in ferrets, antibodies against activation markers (such as CD154) are in urgent need to study ferret Ag-specific Tfh cell responses. We have also partially developed a candidate anti-ferret CD154 antibody using the same technologies of mouse immunisation (data not shown). This reagent has been validated to bind to the recombinantly expressed ferret CD154 protein by ELISA but has yet to be validated by flow cytometry. In future experiments, we will perform further validation of this antibody with flow cytometry and, if shown to be specific to CD154 expressed on ferret cells, apply this antibody to identify activated ferret Ag-specific Tfh cells. With an increasing toolbox of ferret immunological reagents available in future, we will be able to perform in-depth

characterisation of the ferret Tfh responses. Results from future ferret Tfh response studies can provide useful insights regarding how Tfh cells influence vaccine immunogenicity. These insights will assist the design and evaluation of novel Tfh-targeting vaccines in the ferret model of human influenza virus infection.

5.6 Ferrets as a model for SARS-CoV-2

In addition to influenza viruses, ferrets are used as the model for studying other respiratory viruses. Martina et al. demonstrated that ferrets are susceptible to experimental infection by the severe acute respiratory syndrome coronavirus that emerged in 2003 (SARS-CoV), and that the virus is efficiently transmitted to co-housed animals[212]. It has now been shown that ferrets are similarly susceptible to the recent pandemic virus severe acute respiratory syndrome coronavirus 2 (SARS-CoV-2)[91,213,214].

Shi et al. intranasally infected ferrets with SARS-CoV-2 viruses isolated from a patient and collected various organs after infection to analyse the viral replication in these organs[91]. Viral RNA and infectious virus were detected in the nasal turbinate of all infected ferrets at day 4 post-infection, but not detected in the lung from day 2 to day 14 post-infection even using intratracheally inoculation. This indicates that SARS-CoV-2 replicates well in the upper respiratory tract, but not in lower respiratory tract of ferrets. Kim et al. also evaluated the replication and shedding of SARS-CoV-2 in different organs of ferrets[213] and most of the results are consistent with Shi's work. Infected ferrets developed fever and shed virus in nasal washes, saliva, blood, urine, and feces which may serve as the vehicle of virus spread from infected individuals to close contacts. Importantly, the authors showed that high level of viral RNA and infectious virus were detected in the lung of infected ferrets at day 4 post-infection. This contradicts Shi's report that no viral RNA or infectious virus was detected in the lung of

infected ferrets. In addition, Kim et al. investigated the transmission mode of SARS-CoV-2 in ferrets. One group of ferrets were inoculated with SARS-CoV-2, other two groups of naïve ferrets were either co-housed in the same cage with infected ferrets (direct contact) or housed in a separate cage (indirect contact). All "direct contact" ferrets ran fever and viral RNA and infectious virus were detected in nasal washes. By contrast, all "indirect contact" ferrets had no fever and viral RNA was only detected in the nasal washes from one third of the ferrets. However, more recently, Richard et al. showed that both viral RNA and infectious virus were detected in throat and nasal swabs from three out of four "indirect contact" ferrets[214]. These data suggest that airborne transmission of SARS-CoV-2 is possible, and even robust in certain circumstances. Although ferrets have not emerged as a preferred model for SARS-CoV-2, they may be useful models for future emerging coronavirus or other respiratory viruses.

Recently, Juno et al. in our group investigated the humoral and circulating Tfh (cTfh) immune responses to spike protein in humans recovered from COVID-19[130]. They found that plasma neutralizing activity positively correlated with the proportion of spike-specific cTfh1 (CCR6−CXCR3+) and cTfh2 (CCR6−CXCR3−), but negatively correlated with the frequency of spike-specific cTfh17 (CCR6+CXCR3−)[130]. Whether this is true in the ferret model of SARS-CoV2 infection or spike immunization remain to be studied. It will be necessary to develop anti-ferret CCR6 and CXCR3 antibodies and interrogate Th1/Th2-like versus Th17-like Tfh responses to spike following SARS-CoV2 infection or spike immunization of ferrets. It could also be feasible to sort ferret Tfh cells (using the surface PD-1 and CXCR5 markers identified in this thesis) and study their gene expression to identify these Tfh subsets. Importantly, this work would be done in draining lymph node tissues to identify lymph node resident Tfh, rather than the cTfh more commonly studied in humans due to tissues access reasons.

5.7 Tfh dependent-enhancement of stem-specific antibody responses

Recently, Nachbagauer et al. showed that vaccination with a chimeric hemagglutinin-based vaccine elicited potent, broad and durable anti-HA stem antibody responses in adults[215]. This corroborates findings in ferrets, where chimeric hemagglutinin-based vaccine induced broadly cross-reactive antibody responses against HA stem[216]. Stem-based influenza vaccines, which can induce immune responses against a broader range of influenza viruses, could be an important supplement to broaden the immunogenicity of current seasonal influenza vaccine, particularly in the case of an emerging pandemic.

The HA stem domain is known to be conserved and immune-subdominant compared with head domain[41]. Tan et al. in our group showed that HA stem immunization elicited little stem-specific antibody responses in C57BL/6 mice[139]. However, vaccination of mice with full-length HA induced much higher level of stem-specific antibody responses. Likewise, stem-specific antibody responses were significantly improved by conjugating it to KLH carrier protein. Analysis of the Ag-specific Tfh cells by AIM assay revealed that full-length HA vaccination elicited high level of head-specific Tfh cells and limited frequency of stem-specific Tfh cells. Similarly, strong KLH-specific Tfh responses were detected in stem-KLH conjugate immunized mice. These data suggest that the poor immunogenicity of stem is at least in part due to its inability to sufficiently induce Tfh cell help and stem-specific antibody responses can be enhanced by conjugating stem with a carrier protein which has potent Tfh epitopes to mimic hapten carrier effect (Figure 5.4 A-B).

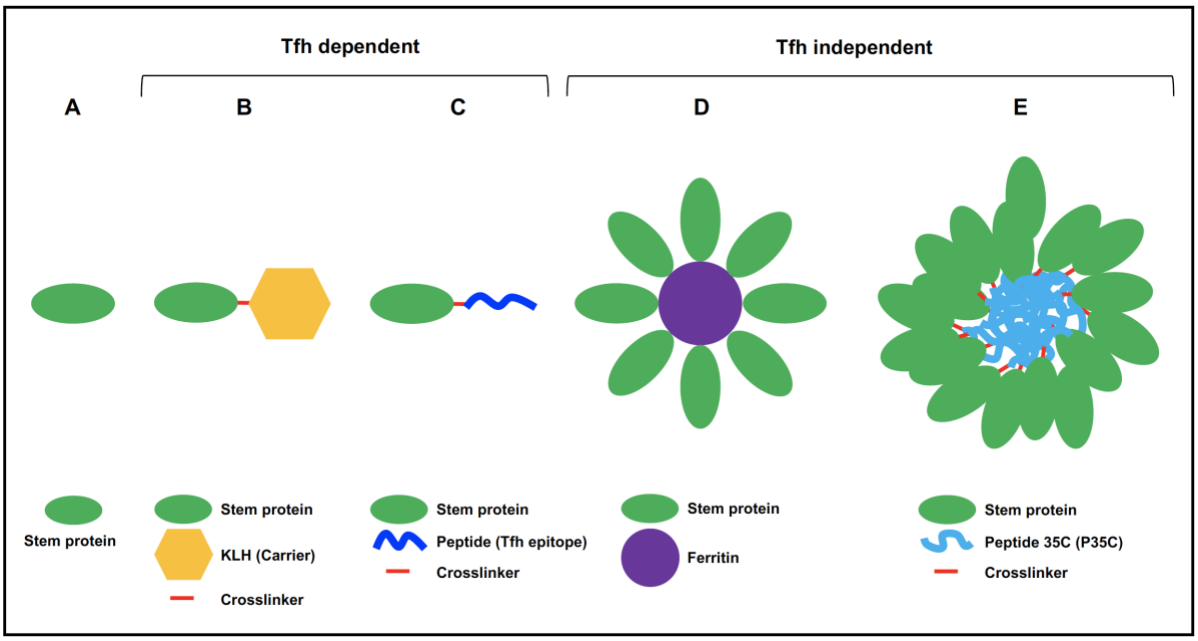


Figure 5.4 Tfh-dependent and -independent approaches to enhance stem immunogenicity. (A) Soluble stem protein which has poor immunogenicity. (B) Enhancing stem immunogenicity by conjugation of stem protein with a highly immunogenic carrier protein (such as KLH) which possesses Tfh epitope(s). (C) Enhancing stem immunogenicity by conjugation of stem protein with a Tfh epitope. (D) Enhancing stem immunogenicity by displaying multiple stem proteins on a ferritin nanoparticle scaffold. (E) Enhancing stem immunogenicity by conjugation of stem protein with P35C which forms aggregates.

An alternative approach is to use only the immunodominant epitope instead of whole carrier protein for conjugation to stem protein. We have determined the immunodominance hierarchy of different Tfh epitopes on HA and identified an immunodominant Tfh epitope, Peptide 16 (Figure 5.1). In future, we plan to conjugate the immunodominant Tfh epitope Peptide 16 from HA head domain to stem protein to rescue its immunogenicity and evaluate the immunogenicity of Peptide 16-stem conjugates in C57BL/6 mice (Figure 5.4C).

5.8 Tfh independent-enhancement of stem-specific antibody responses

5.8.1 Boosting stem-specific antibody responses by ferritin nanoparticles

Converting a weakly immunologic soluble protein to a multimer through particulation or aggregation can significantly enhance its immunogenicity[161,162]. Kelly et al. in our group recently demonstrated that HA-ferritin nanoparticle vaccination elicited higher frequency of HA-specific GC B cells than soluble HA vaccination in mice[217]. Lightsheet microscopy analysis revealed that there was greater deposition of HA-ferritin in draining LNs compared with soluble HA. A higher rate of somatic mutation in heavy chain immunoglobulin genes of HA-specific memory B cells was observed in HA-ferritin immunized mice compared with soluble HA immunized mice. However, the frequency of total Tfh cells was not significantly increased and no ferritin-specific Tfh cells were detected using AIM assay in HA-ferritin immunized mice. These data suggest that HA-ferritin nanoparticle vaccines displaying multimeric HA antigens could enhance HA-specific antibody responses via a B cell–intrinsic mechanism without the dependence on linked recognition of ferritin-specific Tfh cells.

Since HA stem is poorly immunogenic and it has limited Tfh epitopes in C57BL/6 mice (Figure 5.1 and Table 5.1), we plan to use C57BL/6 mice and HA stem as models to explore mechanisms to boost humoral immunity by bypassing limiting Tfh responses using ferritin nanoparticle scaffold in future (Figure 5.4 D).

5.8.2 Boosting stem-specific antibody responses by peptide conjugation

In Chapter 4, we found that P35C-stem conjugates significantly increased stem-specific antibody responses independent of Tfh cell help. Based on the filtration experiment and immunogen size characterization (Figure 4 and S1 Table in Chapter 4), this effect is likely due to P35C induced aggregation of stem proteins since filtration abrogated this improved

immunogenicity. Protein aggregates are known to be more efficient in eliciting immune responses than their monomeric forms even in the absence of T-cell help[161,162]. The enhanced stem-specific antibody response is probably related to the ability of extensive cross-linking of B-cell receptor by multiple stem proteins displayed on the surface of P35C-stem aggregates (Figure 5.4 E)[161,218]. Another possible mechanism would resemble the depot effect of aluminium-containing adjuvants[172-174]. Aggregated stem proteins are trapped within the site of injection and tend to be relatively stabilized against degradation, which allows prolonged release of antigens[218-220]. In addition, it is possible that aggregated stem proteins promote phagocytosis of antigens by antigen-presenting cells since particulate or aggregated forms of antigens are more efficiently taken up and presented by APC than soluble proteins[168,221-223].

Further work is needed to refine this work and more precisely refine the mechanism of enhanced immunogenicity. Although P35 is not a strong CD4 T cell epitope in C57BL/6 mice based on the results of AIM assay (S2 Figure in Chapter 4), we cannot rule out that a weak response below the threshold of detection could be present. To more definitively confirm that the enhanced immunogenicity is T cell-independent, the immunogenicity of stem, P11C-stem and P35C-stem could be compared in TCR-deficient mice. It has been shown that some antigens can stimulate strong BCR signalling or synergetic BCR and TLR signalling, which can bypass the need of T cell help for B cell proliferation[154]. Liao et al. demonstrated that bacteriophage Qβ derived VLP (Qβ-VLPs) induced T-independent antibody responses in TCR-deficient mice[154]. A follow-up study showed that B cell–intrinsic MyD88 signalling promoted initial cell proliferation and differentiation to enhance the germinal centre response to Qβ-VLPs[157]. Thus, it could be informative to vaccinate MyD88 knock-out mice with stem, P11C-stem and P35C-stem to investigate whether the enhanced immunogenicity is TLR signalling-dependent or not.

5.9 Concluding remarks

Influenza virus infection is a global public health threat. Annually seasonal influenza epidemics are estimated to cause 290,000–650,000 deaths worldwide[4]. Current seasonal influenza vaccines are effective when vaccine strains are matched with circulating strains. However, there is little to no cross-protection against antigenic variants, emerging pandemic or zoonotic outbreak strains. There is therefore tremendous interest in the development of novel "universal" vaccines, that would significantly expand protection to most or all influenza viruses. Tfh cells are critical for the generation of high-affinity and long-lasting antibody responses[110]. Characterisation of Tfh cell responses can provide an immunological basis for the development of novel vaccines for the prevention of influenza infection. On the other hand, multimeric antigens have been shown to be more efficient in inducing antibody responses than soluble antigens even without the help of T cells[161,162]. This provides an alternative avenue to boost humoral immunity bypassing limiting Tfh responses.

In this thesis, we first developed and validated an AIM assay to characterize influenza-specific Tfh cells in mice. We showed that the murine AIM assay is robust and sensitive for detecting Ag-specific Tfh cells by assessing the upregulation of CD154 or CD25/OX40. The AIM assay provides the opportunity to quantitate Ag-specific Tfh cells in mice without the reliance on transgenic mice or MHC-II tetramers restricted to specific epitopes. Furthermore, as a live cell assay, Ag-specific Tfh cells could be sorted for downstream applications, such as TCR sequencing or adoptive transfer experiments. We next screened and developed ferret-reactive BCL6, CXCR5 and PD-1 monoclonal antibodies. With these antibodies, we were able to clearly identify Tfh cells in lymph nodes from influenza infected ferrets. The development of

ferret Tfh marker antibodies and the identification of ferret Tfh cells will assist the evaluation of vaccine-induced Tfh responses in the ferret model and the design of novel vaccines against the infection of influenza and other viruses. Finally, we showed that chemically coupling a peptide derived from the head domain of PR8 HA (P35) with the poorly immunogenic HA stem protein resulted in aggregation of the HA stem which significantly increased stem-specific B cell responses independent of Tfh cell help in mice. This suggests that immunogen multimerization could augment antibody responses through a B cell–intrinsic mechanism without the dependence on Tfh cells.

Overall, an increased understanding of Tfh-dependent and -independent mechanisms to boost humoral immune responses will facilitate the development of next-generation vaccines to prevent influenza and other infectious diseases.

Reference

1 Reperant, L. A., Moesker, F. M. & Osterhaus, A. D. Influenza: from zoonosis to pandemic. *ERJ Open Res* **2**, doi:10.1183/23120541.00013-2016 (2016).

2 Kucharski, A. J. *et al.* Estimating the life course of influenza A(H3N2) antibody responses from cross-sectional data. *PLoS Biol* **13**, e1002082, doi:10.1371/journal.pbio.1002082 (2015).

3 World Health Organization. Influenza (Seasonal). https://www.who.int/news-room/fact-sheets/detail/influenza-(seasonal). Accessed 9 April 2020.

4 Krammer, F. *et al.* Influenza. *Nat Rev Dis Primers* **4**, 3, doi:10.1038/s41572-018-0002-y (2018).

5 Putri, W., Muscatello, D. J., Stockwell, M. S. & Newall, A. T. Economic burden of seasonal influenza in the United States. *Vaccine* **36**, 3960-3966, doi:10.1016/j.vaccine.2018.05.057 (2018).

6 Yamayoshi, S. & Kawaoka, Y. Current and future influenza vaccines. *Nat Med* **25**, 212-220, doi:10.1038/s41591-018-0340-z (2019).

7 Morens, D. M., Folkers, G. K. & Fauci, A. S. What is a pandemic? *J Infect Dis* **200**, 1018-1021, doi:10.1086/644537 (2009).

8 Saunders-Hastings, P. R. & Krewski, D. Reviewing the History of Pandemic Influenza: Understanding Patterns of Emergence and Transmission. *Pathogens* **5**, doi:10.3390/pathogens5040066 (2016).

9 Wendel, I., Matrosovich, M. & Klenk, H. D. SnapShot: Evolution of human influenza A viruses. *Cell Host Microbe* **17**, 416-416 e411, doi:10.1016/j.chom.2015.02.001 (2015).

10 David M. Knipe, P. M. H. Orthomyxoviridae. Fields Virology, Sixth Edition. (2013).

11 Short, K. R., Kedzierska, K. & van de Sandt, C. E. Back to the Future: Lessons Learned From the 1918 Influenza Pandemic. *Front Cell Infect Microbiol* **8**, 343, doi:10.3389/fcimb.2018.00343 (2018).

12 Anhlan, D., Grundmann, N., Makalowski, W., Ludwig, S. & Scholtissek, C. Origin of the 1918 pandemic H1N1 influenza A virus as studied by codon usage patterns and phylogenetic analysis. *RNA* **17**, 64-73, doi:10.1261/rna.2395211 (2011).

13 Robert G. Webster, A. S. M., Thomas J. Braciale, Robert A. Lamb. Structure and replication. Textbook of Influenza, Second Edition. (2013).

14 World Health Organization. Influenza (Avian and other zoonotic). https://www.who.int/news-room/fact-sheets/detail/influenza-(avian-and-other-zoonotic). Accessed 9 April 2020.

15 World Health Organization. Standardization of terminology for the influenza virus variants infecting humans. https://www.who.int/influenza/gisrs_laboratory/terminology_variant/en/. Accessed 9 April 2020.

16 World Health Organization. Cumulative number of confirmed human cases of avian influenza A(H5N1) reported to WHO. https://www.who.int/influenza/human_animal_interface/H5N1_cumulative_table_archives/en/. Accessed 9 April 2020.

17 Food and Agriculture Organization of the United Nations. H7N9 situation update. http://www.fao.org/ag/againfo/programmes/en/empres/H7N9/Situation_update.html. Accessed 9 April 2020.

18 Jernigan, D. B. & Cox, N. J. H7N9: preparing for the unexpected in influenza. *Annu Rev Med* **66**, 361-371, doi:10.1146/annurev-med-010714-112311 (2015).

19 Horman, W. S. J., Nguyen, T. H. O., Kedzierska, K., Bean, A. G. D. & Layton, D. S. The Drivers of Pathology in Zoonotic Avian Influenza: The Interplay Between Host and Pathogen. *Front Immunol* **9**, 1812, doi:10.3389/fimmu.2018.01812 (2018).

20 Nunez, I. A. & Ross, T. M. A review of H5Nx avian influenza viruses. *Ther Adv Vaccines Immunother* **7**, 2515135518821625, doi:10.1177/2515135518821625 (2019).

21 Naguib, M. M. *et al.* Global patterns of avian influenza A (H7): virus evolution and zoonotic threats. *FEMS Microbiol Rev* **43**, 608-621, doi:10.1093/femsre/fuz019 (2019).

22 Wu, Y., Wu, Y., Tefsen, B., Shi, Y. & Gao, G. F. Bat-derived influenza-like viruses H17N10 and H18N11. *Trends Microbiol* **22**, 183-191, doi:10.1016/j.tim.2014.01.010 (2014).

23 Ma, W., Garcia-Sastre, A. & Schwemmle, M. Expected and Unexpected Features of the Newly Discovered Bat Influenza A-like Viruses. *PLoS Pathog* **11**, e1004819, doi:10.1371/journal.ppat.1004819 (2015).

24 Joseph, U., Su, Y. C., Vijaykrishna, D. & Smith, G. J. The ecology and adaptive evolution of influenza A interspecies transmission. *Influenza Other Respir Viruses* **11**, 74-84, doi:10.1111/irv.12412 (2017).

25 Lu, L., Lycett, S. J. & Leigh Brown, A. J. Reassortment patterns of avian influenza virus internal segments among different subtypes. *BMC Evol Biol* **14**, 16, doi:10.1186/1471-2148-14-16 (2014).

26 Tan, J., Asthagiri Arunkumar, G. & Krammer, F. Universal influenza virus vaccines and therapeutics: where do we stand with influenza B virus? *Curr Opin Immunol* **53**, 45-50, doi:10.1016/j.coi.2018.04.002 (2018).

27 Bui, C. M., Chughtai, A. A., Adam, D. C. & MacIntyre, C. R. An overview of the epidemiology and emergence of influenza A infection in humans over time. *Arch Public Health* **75**, 15, doi:10.1186/s13690-017-0182-z (2017).

28 A revision of the system of nomenclature for influenza viruses: a WHO memorandum. *Bull World Health Organ* **58**, 585-591 (1980).

29 Hannoun, C. The evolving history of influenza viruses and influenza vaccines. *Expert Rev Vaccines* **12**, 1085-1094, doi:10.1586/14760584.2013.824709 (2013).

30 Su, S., Fu, X., Li, G., Kerlin, F. & Veit, M. Novel Influenza D virus: Epidemiology, pathology, evolution and biological characteristics. *Virulence* **8**, 1580-1591, doi:10.1080/21505594.2017.1365216 (2017).

31 Hatta, M., Kohlmeier, C. K., Hatta, Y., Ozawa, M. & Kawaoka, Y. Region required for protein expression from the stop-start pentanucleotide in the M gene of influenza B virus. *J Virol* **83**, 5939-5942, doi:10.1128/JVI.00180-09 (2009).

32 Jackson, D., Elderfield, R. A. & Barclay, W. S. Molecular studies of influenza B virus in the reverse genetics era. *J Gen Virol* **92**, 1-17, doi:10.1099/vir.0.026187-0 (2011).

33 Nayak, D. P., Balogun, R. A., Yamada, H., Zhou, Z. H. & Barman, S. Influenza virus morphogenesis and budding. *Virus Res* **143**, 147-161, doi:10.1016/j.virusres.2009.05.010 (2009).

34 Reperant, L. A., Rimmelzwaan, G. F. & Osterhaus, A. D. Advances in influenza vaccination. *F1000Prime Rep* **6**, 47, doi:10.12703/P6-47 (2014).

35 Chen, J. R., Liu, Y. M., Tseng, Y. C. & Ma, C. Better influenza vaccines: an industry perspective. *J Biomed Sci* **27**, 33, doi:10.1186/s12929-020-0626-6 (2020).

36 Soema, P. C., Kompier, R., Amorij, J. P. & Kersten, G. F. Current and next generation influenza vaccines: Formulation and production strategies. *Eur J Pharm Biopharm* **94**, 251-263, doi:10.1016/j.ejpb.2015.05.023 (2015).

37 Centers for Disease Control and Prevention. Live Attenuated Influenza Vaccine [LAIV] (The Nasal Spray Flu Vaccine). https://www.cdc.gov/flu/prevent/nasalspray.htm. Accessed 9 April 2020.

38 Jhaveri, R. Live Attenuated Influenza Vaccine: Is Past Performance a Guarantee of Future Results? *Clin Ther* **40**, 1246-1254, doi:10.1016/j.clinthera.2018.07.003 (2018).

39 Tregoning, J. S., Russell, R. F. & Kinnear, E. Adjuvanted influenza vaccines. *Hum Vaccin Immunother* **14**, 550-564, doi:10.1080/21645515.2017.1415684 (2018).

40 Ostrowsky, J. *et al.* Tracking progress in universal influenza vaccine development. *Curr Opin Virol* **40**, 28-36, doi:10.1016/j.coviro.2020.02.003 (2020).

41 Nachbagauer, R. & Palese, P. Is a Universal Influenza Virus Vaccine Possible? *Annu Rev Med* **71**, 315-327, doi:10.1146/annurev-med-120617-041310 (2020).

42 Centers for Disease Control and Prevention. Past seasons vaccine effectiveness estimates. Adjusted vaccine effectiveness estimates for influenza seasons from 2004-2018. https://www.cdc.gov/flu/vaccines-work/past-seasons-estimates.html. Accessed 9 April 2020.

43 World Health Organization. Influenza vaccine viruses and reagents. https://www.who.int/influenza/vaccines/virus/en/. Accessed 9 April 2020.

44 Smith, A. *et al.* A Live Attenuated Influenza Vaccine Elicits Enhanced Heterologous Protection When the Internal Genes of the Vaccine Are Matched to Those of the Challenge Virus. *J Virol* **94**, doi:10.1128/JVI.01065-19 (2020).

45 Koutsakos, M. *et al.* Human CD8(+) T cell cross-reactivity across influenza A, B and C viruses. *Nat Immunol*, doi:10.1038/s41590-019-0320-6 (2019).

46 Vogel, O. A. & Manicassamy, B. Broadly Protective Strategies Against Influenza Viruses: Universal Vaccines and Therapeutics. *Front Microbiol* **11**, 135, doi:10.3389/fmicb.2020.00135 (2020).

47 Clemens, E. B., van de Sandt, C., Wong, S. S., Wakim, L. M. & Valkenburg, S. A. Harnessing the Power of T Cells: The Promising Hope for a Universal Influenza Vaccine. *Vaccines (Basel)* **6**, doi:10.3390/vaccines6020018 (2018).

48 Berthoud, T. K. *et al.* Potent CD8+ T-cell immunogenicity in humans of a novel heterosubtypic influenza A vaccine, MVA-NP+M1. *Clin Infect Dis* **52**, 1-7, doi:10.1093/cid/ciq015 (2011).

49 Lillie, P. J. *et al.* Preliminary assessment of the efficacy of a T-cell-based influenza vaccine, MVA-NP+M1, in humans. *Clin Infect Dis* **55**, 19-25, doi:10.1093/cid/cis327 (2012).

50 Pleguezuelos, O. *et al.* Efficacy of FLU-v, a broad-spectrum influenza vaccine, in a randomized phase IIb human influenza challenge study. *NPJ Vaccines* **5**, 22, doi:10.1038/s41541-020-0174-9 (2020).

51 Sridhar, S. Heterosubtypic T-Cell Immunity to Influenza in Humans: Challenges for Universal T-Cell Influenza Vaccines. *Front Immunol* **7**, 195, doi:10.3389/fimmu.2016.00195 (2016).

52 Kang, J. O. & Chang, J. Challenges in the development of T-cell-based universal influenza vaccines. *Clin Exp Vaccine Res* **6**, 1-3, doi:10.7774/cevr.2017.6.1.1 (2017).

53 Schotsaert, M. *et al.* Natural and long-lasting cellular immune responses against influenza in the M2e-immune host. *Mucosal Immunol* **6**, 276-287, doi:10.1038/mi.2012.69 (2013).

54 El Bakkouri, K. *et al.* Universal vaccine based on ectodomain of matrix protein 2 of influenza A: Fc receptors and alveolar macrophages mediate protection. *J Immunol* **186**, 1022-1031, doi:10.4049/jimmunol.0902147 (2011).

55 Kim, M. C. *et al.* Virus-like particles containing multiple M2 extracellular domains confer improved cross-protection against various subtypes of influenza virus. *Mol Ther* **21**, 485-492, doi:10.1038/mt.2012.246 (2013).

56 Turley, C. B. *et al.* Safety and immunogenicity of a recombinant M2e-flagellin influenza vaccine (STF2.4xM2e) in healthy adults. *Vaccine* **29**, 5145-5152, doi:10.1016/j.vaccine.2011.05.041 (2011).

57 Broecker, F. *et al.* Extending the Stalk Enhances Immunogenicity of the Influenza Virus Neuraminidase. *J Virol* **93**, doi:10.1128/JVI.00840-19 (2019).

58 Kim, K. H. *et al.* Neuraminidase expressing virus-like particle vaccine provides effective cross protection against influenza virus. *Virology* **535**, 179-188, doi:10.1016/j.virol.2019.07.008 (2019).

59 Krammer, F. *et al.* NAction! How Can Neuraminidase-Based Immunity Contribute to Better Influenza Virus Vaccines? *mBio* **9**, doi:10.1128/mBio.02332-17 (2018).

60 Eichelberger, M. C. & Monto, A. S. Neuraminidase, the Forgotten Surface Antigen, Emerges as an Influenza Vaccine Target for Broadened Protection. *J Infect Dis* **219**, S75-S80, doi:10.1093/infdis/jiz017 (2019).

61 Pica, N. & Palese, P. Toward a universal influenza virus vaccine: prospects and challenges. *Annu Rev Med* **64**, 189-202, doi:10.1146/annurev-med-120611-145115 (2013).

62 Sui, J. *et al.* Structural and functional bases for broad-spectrum neutralization of avian and human influenza A viruses. *Nat Struct Mol Biol* **16**, 265-273, doi:10.1038/nsmb.1566 (2009).

63 Ekiert, D. C. *et al.* Antibody recognition of a highly conserved influenza virus epitope. *Science* **324**, 246-251, doi:10.1126/science.1171491 (2009).

64 DiLillo, D. J., Tan, G. S., Palese, P. & Ravetch, J. V. Broadly neutralizing hemagglutinin stalk-specific antibodies require FcgammaR interactions for protection against influenza virus in vivo. *Nat Med* **20**, 143-151, doi:10.1038/nm.3443 (2014).

65 Yassine, H. M. *et al.* Hemagglutinin-stem nanoparticles generate heterosubtypic influenza protection. *Nat Med* **21**, 1065-1070, doi:10.1038/nm.3927 (2015).

66 Impagliazzo, A. *et al.* A stable trimeric influenza hemagglutinin stem as a broadly protective immunogen. *Science* **349**, 1301-1306, doi:10.1126/science.aac7263 (2015).

67 National Institute of Allergy and Infectious Diseases. Dose, safety, tolerability and immunogenicity of an influenza H1 stabilized stem ferritin vaccine, VRCFLUNPF099-00-VP, in healthy adults. https://clinicaltrials.gov/ct2/show/NCT03814720. Accessed 9 April 2020.

68 Krammer, F., Pica, N., Hai, R., Margine, I. & Palese, P. Chimeric hemagglutinin influenza virus vaccine constructs elicit broadly protective stalk-specific antibodies. *J Virol* **87**, 6542-6550, doi:10.1128/JVI.00641-13 (2013).

69 Margine, I. *et al.* Hemagglutinin stalk-based universal vaccine constructs protect against group 2 influenza A viruses. *J Virol* **87**, 10435-10446, doi:10.1128/JVI.01715-13 (2013).

70 Bernstein, D. I. *et al.* Immunogenicity of chimeric haemagglutinin-based, universal influenza virus vaccine candidates: interim results of a randomised, placebo-controlled, phase 1 clinical trial. *Lancet Infect Dis* **20**, 80-91, doi:10.1016/S1473-3099(19)30393-7 (2020).

71 Reneer, Z. B., Jamieson, P. J., Skarlupka, A. L., Huang, Y. & Ross, T. M. Computationally Optimized Broadly Reactive H2 HA Influenza Vaccines Elicited Broadly Cross-Reactive Antibodies and Protected Mice from Viral Challenges. *J Virol* **95**, doi:10.1128/JVI.01526-20 (2020).

72 Giles, B. M. & Ross, T. M. A computationally optimized broadly reactive antigen (COBRA) based H5N1 VLP vaccine elicits broadly reactive antibodies in mice and ferrets. *Vaccine* **29**, 3043-3054, doi:10.1016/j.vaccine.2011.01.100 (2011).

73 Epstein, S. L. Universal Influenza Vaccines: Progress in Achieving Broad Cross-Protection In Vivo. *Am J Epidemiol*, doi:10.1093/aje/kwy145 (2018).

74 Mifsud, E. J., Tai, C. M. & Hurt, A. C. Animal models used to assess influenza antivirals. *Expert Opin Drug Discov* **13**, 1131-1139, doi:10.1080/17460441.2018.1540586 (2018).

75 Margine, I. & Krammer, F. Animal models for influenza viruses: implications for universal vaccine development. *Pathogens* **3**, 845-874, doi:10.3390/pathogens3040845 (2014).

76 Bodewes, R., Rimmelzwaan, G. F. & Osterhaus, A. D. Animal models for the preclinical evaluation of candidate influenza vaccines. *Expert Rev Vaccines* **9**, 59-72, doi:10.1586/erv.09.148 (2010).

77 de Graaf, M. & Fouchier, R. A. Role of receptor binding specificity in influenza A virus transmission and pathogenesis. *EMBO J* **33**, 823-841, doi:10.1002/embj.201387442 (2014).

78 Belser, J. A., Katz, J. M. & Tumpey, T. M. The ferret as a model organism to study influenza A virus infection. *Dis Model Mech* **4**, 575-579, doi:10.1242/dmm.007823 (2011).

79 Wei, C. J. *et al.* Induction of broadly neutralizing H1N1 influenza antibodies by vaccination. *Science* **329**, 1060-1064, doi:10.1126/science.1192517 (2010).

80 Albrecht, R. A. *et al.* Moving Forward: Recent Developments for the Ferret Biomedical Research Model. *MBio* **9**, doi:10.1128/mBio.01113-18 (2018).

81 Wong, J., Layton, D., Wheatley, A. K. & Kent, S. J. Improving immunological insights into the ferret model of human viral infectious disease. *Influenza Other Respir Viruses* **13**, 535-546, doi:10.1111/irv.12687 (2019).

82 Liu, W. C. *et al.* Sequential Immunization With Live-Attenuated Chimeric Hemagglutinin-Based Vaccines Confers Heterosubtypic Immunity Against Influenza A Viruses in a Preclinical Ferret Model. *Front Immunol* **10**, 756, doi:10.3389/fimmu.2019.00756 (2019).

83 Layton, D. S. *et al.* Development of an anti-ferret CD4 monoclonal antibody for the characterisation of ferret T lymphocytes. *J Immunol Methods* **444**, 29-35, doi:10.1016/j.jim.2017.02.009 (2017).

84 DiPiazza, A. *et al.* Flow Cytometric and Cytokine ELISpot Approaches To Characterize the Cell-Mediated Immune Response in Ferrets following Influenza Virus Infection. *J Virol* **90**, 7991-8004, doi:10.1128/JVI.01001-16 (2016).

85 Rutigliano, J. A. *et al.* Screening monoclonal antibodies for cross-reactivity in the ferret model of influenza infection. *J Immunol Methods* **336**, 71-77, doi:10.1016/j.jim.2008.04.003 (2008).

86 Martel, C. J. & Aasted, B. Characterization of antibodies against ferret immunoglobulins, cytokines and CD markers. *Vet Immunol Immunopathol* **132**, 109-115, doi:10.1016/j.vetimm.2009.05.011 (2009).

87 Bentebibel, S. E. *et al.* Induction of ICOS+CXCR3+CXCR5+ TH cells correlates with antibody responses to influenza vaccination. *Sci Transl Med* **5**, 176ra132, doi:10.1126/scitranslmed.3005191 (2013).

88 Herati, R. S. *et al.* Successive annual influenza vaccination induces a recurrent oligoclonotypic memory response in circulating T follicular helper cells. *Sci Immunol* **2**, doi:10.1126/sciimmunol.aag2152 (2017).

89 Moon, J. J. *et al.* Enhancing humoral responses to a malaria antigen with nanoparticle vaccines that expand Tfh cells and promote germinal center induction. *Proc Natl Acad Sci U S A* **109**, 1080-1085, doi:10.1073/pnas.1112648109 (2012).

90 Pardi, N. *et al.* Nucleoside-modified mRNA vaccines induce potent T follicular helper and germinal center B cell responses. *J Exp Med* **215**, 1571-1588, doi:10.1084/jem.20171450 (2018).

91 Shi, J. *et al.* Susceptibility of ferrets, cats, dogs, and other domesticated animals to SARS-coronavirus 2. *Science*, doi:10.1126/science.abb7015 (2020).

92 Karlsson, E. A. *et al.* Influenza virus infection in nonhuman primates. *Emerg Infect Dis* **18**, 1672-1675, doi:10.3201/eid1810.120214 (2012).

93 Krammer, F. The human antibody response to influenza A virus infection and vaccination. *Nat Rev Immunol* **19**, 383-397, doi:10.1038/s41577-019-0143-6 (2019).

94 Wohlbold, T. J. & Krammer, F. In the shadow of hemagglutinin: a growing interest in influenza viral neuraminidase and its role as a vaccine antigen. *Viruses* **6**, 2465-2494, doi:10.3390/v6062465 (2014).

95 Leon, P. E. *et al.* Optimal activation of Fc-mediated effector functions by influenza virus hemagglutinin antibodies requires two points of contact. *Proc Natl Acad Sci U S A* **113**, E5944-E5951, doi:10.1073/pnas.1613225113 (2016).

96 He, W. *et al.* Epitope specificity plays a critical role in regulating antibody-dependent cell-mediated cytotoxicity against influenza A virus. *Proc Natl Acad Sci U S A* **113**, 11931-11936, doi:10.1073/pnas.1609316113 (2016).

97 Jegaskanda, S., Vanderven, H. A., Wheatley, A. K. & Kent, S. J. Fc or not Fc; that is the question: Antibody Fc-receptor interactions are key to universal influenza vaccine design. *Hum Vaccin Immunother* **13**, 1-9, doi:10.1080/21645515.2017.1290018 (2017).

98 Vanderven, H. A. *et al.* What Lies Beneath: Antibody Dependent Natural Killer Cell Activation by Antibodies to Internal Influenza Virus Proteins. *EBioMedicine* **8**, 277-290, doi:10.1016/j.ebiom.2016.04.029 (2016).

99 Abul K. Abbas, A. H. L. a. S. P. B Cell Activation and Antibody Production. Cellular and Molecular Immunology, Ninth edition. (2018).

100 Harwood, N. E. & Batista, F. D. Early events in B cell activation. *Annu Rev Immunol* **28**, 185-210, doi:10.1146/annurev-immunol-030409-101216 (2010).

101 Kenneth Murphy, C. W. The Humoral Immune Response. Janeway's Immunobiology, Ninth Edition. (2017).

102 Victora, G. D. & Nussenzweig, M. C. Germinal centers. *Annu Rev Immunol* **30**, 429-457, doi:10.1146/annurev-immunol-020711-075032 (2012).

103 Victora, G. D. *et al.* Germinal center dynamics revealed by multiphoton microscopy with a photoactivatable fluorescent reporter. *Cell* **143**, 592-605, doi:10.1016/j.cell.2010.10.032 (2010).

104 Gatto, D. & Brink, R. The germinal center reaction. *J Allergy Clin Immunol* **126**, 898-907; quiz 908-899, doi:10.1016/j.jaci.2010.09.007 (2010).

105 Crotty, S. T Follicular Helper Cell Biology: A Decade of Discovery and Diseases. *Immunity* **50**, 1132-1148, doi:10.1016/j.immuni.2019.04.011 (2019).

106 Qi, H. T follicular helper cells in space-time. *Nat Rev Immunol* **16**, 612-625, doi:10.1038/nri.2016.94 (2016).

107 Liu, D. *et al.* T-B-cell entanglement and ICOSL-driven feed-forward regulation of germinal centre reaction. *Nature* **517**, 214-218, doi:10.1038/nature13803 (2015).

108 Kennedy, D. E. *et al.* Novel specialized cell state and spatial compartments within the germinal center. *Nat Immunol* **21**, 660-670, doi:10.1038/s41590-020-0660-2 (2020).

109 Muppidi, J. R. & Klein, U. Directing traffic in the germinal center roundabout. *Nat Immunol* **21**, 599-601, doi:10.1038/s41590-020-0690-9 (2020).

110 Vinuesa, C. G., Linterman, M. A., Yu, D. & MacLennan, I. C. Follicular Helper T Cells. *Annu Rev Immunol* **34**, 335-368, doi:10.1146/annurev-immunol-041015-055605 (2016).

111 Crotty, S. Follicular helper CD4 T cells (TFH). *Annu Rev Immunol* **29**, 621-663, doi:10.1146/annurev-immunol-031210-101400 (2011).

112 Linterman, M. A. & Hill, D. L. Can follicular helper T cells be targeted to improve vaccine efficacy? *F1000Res* **5**, doi:10.12688/f1000research.7388.1 (2016).

113 Nurieva, R. I. *et al.* Bcl6 mediates the development of T follicular helper cells. *Science* **325**, 1001-1005, doi:10.1126/science.1176676 (2009).

114 Johnston, R. J. *et al.* Bcl6 and Blimp-1 are reciprocal and antagonistic regulators of T follicular helper cell differentiation. *Science* **325**, 1006-1010, doi:10.1126/science.1175870 (2009).

115 Yu, D. *et al.* The transcriptional repressor Bcl-6 directs T follicular helper cell lineage commitment. *Immunity* **31**, 457-468, doi:10.1016/j.immuni.2009.07.002 (2009).

116 Tangye, S. G., Brink, R., Goodnow, C. C. & Phan, T. G. SnapShot: Interactions between B Cells and T Cells. *Cell* **162**, doi:ARTN 926.e1
10.1016/j.cell.2015.07.055 (2015).

117 Phetsouphanh, C., Zaunders, J. J. & Kelleher, A. D. Detecting Antigen-Specific T Cell Responses: From Bulk Populations to Single Cells. *Int J Mol Sci* **16**, 18878-18893, doi:10.3390/ijms160818878 (2015).

118 Dan, J. M. *et al.* A Cytokine-Independent Approach To Identify Antigen-Specific Human Germinal Center T Follicular Helper Cells and Rare Antigen-Specific CD4+ T Cells in Blood. *J Immunol* **197**, 983-993, doi:10.4049/jimmunol.1600318 (2016).

119 Zaunders, J. J. *et al.* High levels of human antigen-specific CD4+ T cells in peripheral blood revealed by stimulated coexpression of CD25 and CD134 (OX40). *J Immunol* **183**, 2827-2836, doi:10.4049/jimmunol.0803548 (2009).

120 Keoshkerian, E. *et al.* A novel assay for detection of hepatitis C virus-specific effector CD4(+) T cells via co-expression of CD25 and CD134. *J Immunol Methods* **375**, 148-158, doi:10.1016/j.jim.2011.10.004 (2012).

121 Havenar-Daughton, C. *et al.* Cytokine-Independent Detection of Antigen-Specific Germinal Center T Follicular Helper Cells in Immunized Nonhuman Primates Using a Live Cell Activation-Induced Marker Technique. *J Immunol* **197**, 994-1002, doi:10.4049/jimmunol.1600320 (2016).

122 Reiss, S. *et al.* Comparative analysis of activation induced marker (AIM) assays for sensitive identification of antigen-specific CD4 T cells. *PLoS One* **12**, e0186998, doi:10.1371/journal.pone.0186998 (2017).

123 Bowyer, G. *et al.* Activation-induced Markers Detect Vaccine-Specific CD4(+) T Cell Responses Not Measured by Assays Conventionally Used in Clinical Trials. *Vaccines (Basel)* **6**, doi:10.3390/vaccines6030050 (2018).

124 Pahwa, S. Searching for the origin of the enigmatic circulating T follicular helper cells. *J Clin Invest* **129**, 3048-3051, doi:10.1172/JCI130311 (2019).

125 Ueno, H. Human Circulating T Follicular Helper Cell Subsets in Health and Disease. *J Clin Immunol* **36 Suppl 1**, 34-39, doi:10.1007/s10875-016-0268-3 (2016).

126 He, J. *et al.* Circulating precursor CCR7(lo)PD-1(hi) CXCR5(+) CD4(+) T cells indicate Tfh cell activity and promote antibody responses upon antigen reexposure. *Immunity* **39**, 770-781, doi:10.1016/j.immuni.2013.09.007 (2013).

127 Vella, L. A. *et al.* T follicular helper cells in human efferent lymph retain lymphoid characteristics. *J Clin Invest* **129**, 3185-3200, doi:10.1172/JCI125628 (2019).

128 Koutsakos, M., Nguyen, T. H. O. & Kedzierska, K. With a Little Help from T Follicular Helper Friends: Humoral Immunity to Influenza Vaccination. *J Immunol* **202**, 360-367, doi:10.4049/jimmunol.1800986 (2019).

129 Jennifer A Juno, H.-X. T., Wen Shi Lee, Arnold Reynaldi, Hannah G Kelly, Kathleen Wragg, Robyn Esterbauer, Helen E Kent, C Jane Batten, Francesca L Mordant, Nicholas A Gherardin, Phillip Pymm, Melanie H Dietrich, Nichollas E Scott, Wai-Hong Tham, Dale I Godfrey, Kanta Subbarao, Miles P Davenport, Stephen J Kent, Adam K Wheatley. Immunogenic profile of SARS-CoV-2 spike in individuals recovered from COVID-19. *medRxiv. doi: https://doi.org/10.1101/2020.05.17.20104869* (2020).

130 Juno, J. A. *et al.* Humoral and circulating follicular helper T cell responses in recovered patients with COVID-19. *Nat Med*, doi:10.1038/s41591-020-0995-0 (2020).

131 Zhang, J. *et al.* Circulating CXCR3(+) Tfh cells positively correlate with neutralizing antibody responses in HCV-infected patients. *Sci Rep* **9**, 10090, doi:10.1038/s41598-019-46533-w (2019).

132 Niessl, J. *et al.* Persistent expansion and Th1-like skewing of HIV-specific circulating T follicular helper cells during antiretroviral therapy. *EBioMedicine* **54**, 102727, doi:10.1016/j.ebiom.2020.102727 (2020).

133 Morse, K. *et al.* Association and evidence for linked recognition of type IV secretion system proteins VirB9-1, VirB9-2, and VirB10 in Anaplasma marginale. *Infect Immun* **80**, 215-227, doi:10.1128/IAI.05798-11 (2012).

134 Rappuoli, R., De Gregorio, E. & Costantino, P. On the mechanisms of conjugate vaccines. *Proc Natl Acad Sci U S A* **116**, 14-16, doi:10.1073/pnas.1819612116 (2019).

135 Pollard, A. J., Perrett, K. P. & Beverley, P. C. Maintaining protection against invasive bacteria with protein-polysaccharide conjugate vaccines. *Nat Rev Immunol* **9**, 213-220, doi:10.1038/nri2494 (2009).

136 Niessl, J. & Kaufmann, D. E. Harnessing T Follicular Helper Cell Responses for HIV Vaccine Development. *Viruses* **10**, doi:10.3390/v10060336 (2018).

137 Ueno, H. Tfh cell response in influenza vaccines in humans: what is visible and what is invisible. *Curr Opin Immunol* **59**, 9-14, doi:10.1016/j.coi.2019.02.007 (2019).

138 Kubo, M. & Miyauchi, K. Breadth of Antibody Responses during Influenza Virus Infection and Vaccination. *Trends Immunol* **41**, 394-405, doi:10.1016/j.it.2020.03.005 (2020).

139 Tan, H. X. *et al.* Subdominance and poor intrinsic immunogenicity limit humoral immunity targeting influenza HA stem. *J Clin Invest* **129**, 850-862, doi:10.1172/JCI123366 (2019).

140 He, L. *et al.* Extracellular matrix protein 1 promotes follicular helper T cell differentiation and antibody production. *Proc Natl Acad Sci U S A* **115**, 8621-8626, doi:10.1073/pnas.1801196115 (2018).

141 Hollister, K. *et al.* Insights into the role of Bcl6 in follicular Th cells using a new conditional mutant mouse model. *J Immunol* **191**, 3705-3711, doi:10.4049/jimmunol.1300378 (2013).

142 Cerutti, A., Cols, M. & Puga, I. Activation of B cells by non-canonical helper signals. *EMBO Rep* **13**, 798-810, doi:10.1038/embor.2012.111 (2012).

143 Cerutti, A., Puga, I. & Cols, M. New helping friends for B cells. *Eur J Immunol* **42**, 1956-1968, doi:10.1002/eji.201242594 (2012).

144 Fujii, S. I., Yamasaki, S., Sato, Y. & Shimizu, K. Vaccine Designs Utilizing Invariant NKT-Licensed Antigen-Presenting Cells Provide NKT or T Cell Help for B Cell Responses. *Front Immunol* **9**, 1267, doi:10.3389/fimmu.2018.01267 (2018).

145 Doherty, D. G., Melo, A. M., Moreno-Olivera, A. & Solomos, A. C. Activation and Regulation of B Cell Responses by Invariant Natural Killer T Cells. *Front Immunol* **9**, 1360, doi:10.3389/fimmu.2018.01360 (2018).

146 Tonti, E. *et al.* NKT-cell help to B lymphocytes can occur independently of cognate interaction. *Blood* **113**, 370-376, doi:10.1182/blood-2008-06-166249 (2009).

147 Holderness, J., Hedges, J. F., Ramstead, A. & Jutila, M. A. Comparative biology of gammadelta T cell function in humans, mice, and domestic animals. *Annu Rev Anim Biosci* **1**, 99-124, doi:10.1146/annurev-animal-031412-103639 (2013).

148 Chien, Y. H., Meyer, C. & Bonneville, M. gammadelta T cells: first line of defense and beyond. *Annu Rev Immunol* **32**, 121-155, doi:10.1146/annurev-immunol-032713-120216 (2014).

149 Pang, D. J., Neves, J. F., Sumaria, N. & Pennington, D. J. Understanding the complexity of gammadelta T-cell subsets in mouse and human. *Immunology* **136**, 283-290, doi:10.1111/j.1365-2567.2012.03582.x (2012).

150 Rezende, R. M. *et al.* gammadelta T cells control humoral immune response by inducing T follicular helper cell differentiation. *Nat Commun* **9**, 3151, doi:10.1038/s41467-018-05487-9 (2018).

151 Mond, J. J., Lees, A. & Snapper, C. M. T cell-independent antigens type 2. *Annu Rev Immunol* **13**, 655-692, doi:10.1146/annurev.iy.13.040195.003255 (1995).

152 Bachmann, M. F. & Zinkernagel, R. M. Neutralizing antiviral B cell responses. *Annu Rev Immunol* **15**, 235-270, doi:10.1146/annurev.immunol.15.1.235 (1997).

153 Obukhanych, T. V. & Nussenzweig, M. C. T-independent type II immune responses generate memory B cells. *J Exp Med* **203**, 305-310, doi:10.1084/jem.20052036 (2006).

154 Liao, W. *et al.* Characterization of T-Dependent and T-Independent B Cell Responses to a Virus-like Particle. *J Immunol* **198**, 3846-3856, doi:10.4049/jimmunol.1601852 (2017).

155 Monroe, J. G. & Keir, M. E. Bridging Toll-like- and B cell-receptor signaling: meet me at the autophagosome. *Immunity* **28**, 729-731, doi:10.1016/j.immuni.2008.05.006 (2008).

156 Raval, F. M., Mishra, R., Garcea, R. L., Welsh, R. M. & Szomolanyi-Tsuda, E. Long-lasting T cell-independent IgG responses require MyD88-mediated pathways and are maintained by high levels of virus persistence. *mBio* **4**, e00812-00813, doi:10.1128/mBio.00812-13 (2013).

157 Tian, M. *et al.* B Cell-Intrinsic MyD88 Signaling Promotes Initial Cell Proliferation and Differentiation To Enhance the Germinal Center Response to a Virus-like Particle. *J Immunol* **200**, 937-948, doi:10.4049/jimmunol.1701067 (2018).

158 Bill, R. M. Recombinant protein subunit vaccine synthesis in microbes: a role for yeast? *J Pharm Pharmacol* **67**, 319-328, doi:10.1111/jphp.12353 (2015).

159 Saenz, R. *et al.* HMGB1-derived peptide acts as adjuvant inducing immune responses to peptide and protein antigen. *Vaccine* **28**, 7556-7562, doi:10.1016/j.vaccine.2010.08.054 (2010).

160 Snapper, C. M. Distinct Immunologic Properties of Soluble Versus Particulate Antigens. *Front Immunol* **9**, 598, doi:10.3389/fimmu.2018.00598 (2018).

161 Rosenberg, A. S. Effects of protein aggregates: an immunologic perspective. *AAPS J* **8**, E501-507, doi:10.1208/aapsj080359 (2006).

162 Sauerborn, M., Brinks, V., Jiskoot, W. & Schellekens, H. Immunological mechanism underlying the immune response to recombinant human protein therapeutics. *Trends Pharmacol Sci* **31**, 53-59, doi:10.1016/j.tips.2009.11.001 (2010).

163 Perotti, M. & Perez, L. Virus-Like Particles and Nanoparticles for Vaccine Development against HCMV. *Viruses* **12**, doi:10.3390/v12010035 (2019).

164 Irvine, D. J. & Read, B. J. Shaping humoral immunity to vaccines through antigen-displaying nanoparticles. *Curr Opin Immunol* **65**, 1-6, doi:10.1016/j.coi.2020.01.007 (2020).

165 Kelly, H. G., Kent, S. J. & Wheatley, A. K. Immunological basis for enhanced immunity of nanoparticle vaccines. *Expert Rev Vaccines* **18**, 269-280, doi:10.1080/14760584.2019.1578216 (2019).

166 Wang, W. *et al.* Immunogenicity of protein aggregates--concerns and realities. *Int J Pharm* **431**, 1-11, doi:10.1016/j.ijpharm.2012.04.040 (2012).

167 Hermeling, S. *et al.* Antibody response to aggregated human interferon alpha2b in wild-type and transgenic immune tolerant mice depends on type and level of aggregation. *J Pharm Sci* **95**, 1084-1096, doi:10.1002/jps.20599 (2006).

168 Ilyinskii, P. O., Thoidis, G., Sherman, M. Y. & Shneider, A. Adjuvant potential of aggregate-forming polyglutamine domains. *Vaccine* **26**, 3223-3226, doi:10.1016/j.vaccine.2008.03.078 (2008).

169 Moyer, T. J. *et al.* Engineered immunogen binding to alum adjuvant enhances humoral immunity. *Nat Med* **26**, 430-440, doi:10.1038/s41591-020-0753-3 (2020).

170 Morefield, G. L., HogenEsch, H., Robinson, J. P. & Hem, S. L. Distribution of adsorbed antigen in mono-valent and combination vaccines. *Vaccine* **22**, 1973-1984, doi:10.1016/j.vaccine.2003.10.040 (2004).

171 HogenEsch, H., O'Hagan, D. T. & Fox, C. B. Optimizing the utilization of aluminum adjuvants in vaccines: you might just get what you want. *NPJ Vaccines* **3**, 51, doi:10.1038/s41541-018-0089-x (2018).

172 Ghimire, T. R. The mechanisms of action of vaccines containing aluminum adjuvants: an in vitro vs in vivo paradigm. *Springerplus* **4**, 181, doi:10.1186/s40064-015-0972-0 (2015).

173 He, P., Zou, Y. & Hu, Z. Advances in aluminum hydroxide-based adjuvant research and its mechanism. *Hum Vaccin Immunother* **11**, 477-488, doi:10.1080/21645515.2014.1004026 (2015).

174 Martinon, S. *et al.* Chemical and Immunological Characteristics of Aluminum-Based, Oil-Water Emulsion, and Bacterial-Origin Adjuvants. *J Immunol Res* **2019**, 3974127, doi:10.1155/2019/3974127 (2019).

175 Zapadka, K. L., Becher, F. J., Gomes Dos Santos, A. L. & Jackson, S. E. Factors affecting the physical stability (aggregation) of peptide therapeutics. *Interface Focus* **7**, 20170030, doi:10.1098/rsfs.2017.0030 (2017).

176 Zhao, L. *et al.* Nanoparticle vaccines. *Vaccine* **32**, 327-337, doi:10.1016/j.vaccine.2013.11.069 (2014).

177 Brinkkemper, M. & Sliepen, K. Nanoparticle Vaccines for Inducing HIV-1 Neutralizing Antibodies. *Vaccines (Basel)* **7**, doi:10.3390/vaccines7030076 (2019).

178 Vijayan, V., Mohapatra, A., Uthaman, S. & Park, I. K. Recent Advances in Nanovaccines Using Biomimetic Immunomodulatory Materials. *Pharmaceutics* **11**, doi:10.3390/pharmaceutics11100534 (2019).

179 Qian, C. *et al.* Recent Progress on the Versatility of Virus-Like Particles. *Vaccines (Basel)* **8**, doi:10.3390/vaccines8010139 (2020).

180 Moser, C., Muller, M., Kaeser, M. D., Weydemann, U. & Amacker, M. Influenza virosomes as vaccine adjuvant and carrier system. *Expert Rev Vaccines* **12**, 779-791, doi:10.1586/14760584.2013.811195 (2013).

181 Sliepen, K. *et al.* Presenting native-like HIV-1 envelope trimers on ferritin nanoparticles improves their immunogenicity. *Retrovirology* **12**, 82, doi:10.1186/s12977-015-0210-4 (2015).

182 Kanekiyo, M. *et al.* Self-assembling influenza nanoparticle vaccines elicit broadly neutralizing H1N1 antibodies. *Nature* **499**, 102-106, doi:10.1038/nature12202 (2013).

183 Elias, G., Ogunjimi, B. & Van Tendeloo, V. Activation-induced surface proteins in the identification of antigen-responsive CD4 T cells. *Immunol Lett* **219**, 1-7, doi:10.1016/j.imlet.2019.12.006 (2020).

184 Damoiseaux, J. The IL-2 - IL-2 receptor pathway in health and disease: The role of the soluble IL-2 receptor. *Clin Immunol* **218**, 108515, doi:10.1016/j.clim.2020.108515 (2020).

185 Webb, G. J., Hirschfield, G. M. & Lane, P. J. OX40, OX40L and Autoimmunity: a Comprehensive Review. *Clin Rev Allergy Immunol* **50**, 312-332, doi:10.1007/s12016-015-8498-3 (2016).

186 Kotov, D. I. *et al.* TCR Affinity Biases Th Cell Differentiation by Regulating CD25, Eef1e1, and Gbp2. *J Immunol* **202**, 2535-2545, doi:10.4049/jimmunol.1801609 (2019).

187 Snook, J. P., Kim, C. & Williams, M. A. TCR signal strength controls the differentiation of CD4(+) effector and memory T cells. *Sci Immunol* **3**, doi:10.1126/sciimmunol.aas9103 (2018).

188 Piepenbrink, K. H., Gloor, B. E., Armstrong, K. M. & Baker, B. M. Methods for quantifying T cell receptor binding affinities and thermodynamics. *Methods Enzymol* **466**, 359-381, doi:10.1016/S0076-6879(09)66015-8 (2009).

189 Edwards, L. J., Zarnitsyna, V. I., Hood, J. D., Evavold, B. D. & Zhu, C. Insights into T cell recognition of antigen: significance of two-dimensional kinetic parameters. *Front Immunol* **3**, 86, doi:10.3389/fimmu.2012.00086 (2012).

190 Zhu, C., Jiang, N., Huang, J., Zarnitsyna, V. I. & Evavold, B. D. Insights from in situ analysis of TCR-pMHC recognition: response of an interaction network. *Immunol Rev* **251**, 49-64, doi:10.1111/imr.12016 (2013).

191 Huppa, J. B. *et al.* TCR-peptide-MHC interactions in situ show accelerated kinetics and increased affinity. *Nature* **463**, 963-967, doi:10.1038/nature08746 (2010).

192 Song, W. & Craft, J. T follicular helper cell heterogeneity: Time, space, and function. *Immunol Rev* **288**, 85-96, doi:10.1111/imr.12740 (2019).

193 Fazilleau, N. & Aloulou, M. Several Follicular Regulatory T Cell Subsets With Distinct Phenotype and Function Emerge During Germinal Center Reactions. *Front Immunol* **9**, 1792, doi:10.3389/fimmu.2018.01792 (2018).

194 Xie, M. M. & Dent, A. L. Unexpected Help: Follicular Regulatory T Cells in the Germinal Center. *Front Immunol* **9**, 1536, doi:10.3389/fimmu.2018.01536 (2018).

195 Aloulou, M. *et al.* Follicular regulatory T cells can be specific for the immunizing antigen and derive from naive T cells. *Nat Commun* **7**, 10579, doi:10.1038/ncomms10579 (2016).

196 Schoenbrunn, A. *et al.* A converse 4-1BB and CD40 ligand expression pattern delineates activated regulatory T cells (Treg) and conventional T cells enabling direct isolation of alloantigen-reactive natural Foxp3+ Treg. *J Immunol* **189**, 5985-5994, doi:10.4049/jimmunol.1201090 (2012).

197 Bentebibel, S. E., Schmitt, N., Banchereau, J. & Ueno, H. Human tonsil B-cell lymphoma 6 (BCL6)-expressing CD4+ T-cell subset specialized for B-cell help outside

germinal centers. *Proc Natl Acad Sci U S A* **108**, E488-497, doi:10.1073/pnas.1100898108 (2011).

198 Marinova, E., Han, S. & Zheng, B. Human germinal center T cells are unique Th cells with high propensity for apoptosis induction. *Int Immunol* **18**, 1337-1345, doi:10.1093/intimm/dxl066 (2006).

199 Breitfeld, D. *et al.* Follicular B helper T cells express CXC chemokine receptor 5, localize to B cell follicles, and support immunoglobulin production. *J Exp Med* **192**, 1545-1552 (2000).

200 Rathmell, J. C., Farkash, E. A., Gao, W. & Thompson, C. B. IL-7 enhances the survival and maintains the size of naive T cells. *J Immunol* **167**, 6869-6876, doi:10.4049/jimmunol.167.12.6869 (2001).

201 Iyer, S. S. *et al.* Identification of novel markers for mouse CD4(+) T follicular helper cells. *Eur J Immunol* **43**, 3219-3232, doi:10.1002/eji.201343469 (2013).

202 Georgiev, H. *et al.* Blocking the ART2.2/P2X7-system is essential to avoid a detrimental bias in functional CD4 T cell studies. *Eur J Immunol* **48**, 1078-1081, doi:10.1002/eji.201747420 (2018).

203 Rissiek, B. *et al.* In Vivo Blockade of Murine ARTC2.2 During Cell Preparation Preserves the Vitality and Function of Liver Tissue-Resident Memory T Cells. *Front Immunol* **9**, 1580, doi:10.3389/fimmu.2018.01580 (2018).

204 Kunzli, M. *et al.* Long-lived T follicular helper cells retain plasticity and help sustain humoral immunity. *Sci Immunol* **5**, doi:10.1126/sciimmunol.aay5552 (2020).

205 Ishii, T., Hishinuma, I., Bannai, S. & Sugita, Y. Mechanism of growth promotion of mouse lymphoma L1210 cells in vitro by feeder layer or 2-mercaptoethanol. *J Cell Physiol* **107**, 283-293, doi:10.1002/jcp.1041070215 (1981).

206 Click, R. E. Review: 2-mercaptoethanol alteration of in vitro immune functions of species other than murine. *J Immunol Methods* **402**, 1-8, doi:10.1016/j.jim.2013.11.007 (2014).

207 Lopez-Ocasio, M., Buszko, M., Blain, M., Wang, K. & Shevach, E. M. T Follicular Regulatory Cell Suppression of T Follicular Helper Cell Function Is Context-Dependent in vitro. *Front Immunol* **11**, 637, doi:10.3389/fimmu.2020.00637 (2020).

208 Leon, A. J. *et al.* Sequencing, annotation, and characterization of the influenza ferret infectome. *J Virol* **87**, 1957-1966, doi:10.1128/JVI.02476-12 (2013).

209 Carolan, L. A. *et al.* TaqMan real time RT-PCR assays for detecting ferret innate and adaptive immune responses. *J Virol Methods* **205**, 38-52, doi:10.1016/j.jviromet.2014.04.014 (2014).

210 Maier, T., Guell, M. & Serrano, L. Correlation of mRNA and protein in complex biological samples. *FEBS Lett* **583**, 3966-3973, doi:10.1016/j.febslet.2009.10.036 (2009).

211 Cheng, X. *et al.* Evaluation of the humoral and cellular immune responses elicited by the live attenuated and inactivated influenza vaccines and their roles in heterologous protection in ferrets. *J Infect Dis* **208**, 594-602, doi:10.1093/infdis/jit207 (2013).

212 Martina, B. E. *et al.* Virology: SARS virus infection of cats and ferrets. *Nature* **425**, 915, doi:10.1038/425915a (2003).

213 Kim, Y. I. *et al.* Infection and Rapid Transmission of SARS-CoV-2 in Ferrets. *Cell Host Microbe* **27**, 704-709 e702, doi:10.1016/j.chom.2020.03.023 (2020).

214 Richard, M. *et al.* SARS-CoV-2 is transmitted via contact and via the air between ferrets. *Nat Commun* **11**, 3496, doi:10.1038/s41467-020-17367-2 (2020).

215 Nachbagauer, R. *et al.* A chimeric hemagglutinin-based universal influenza virus vaccine approach induces broad and long-lasting immunity in a randomized, placebo-controlled phase I trial. *Nat Med* **27**, 106-114, doi:10.1038/s41591-020-1118-7 (2021).

216 Nachbagauer, R. *et al.* A universal influenza virus vaccine candidate confers protection against pandemic H1N1 infection in preclinical ferret studies. *NPJ Vaccines* **2**, 26, doi:10.1038/s41541-017-0026-4 (2017).

217 Kelly, H. G. *et al.* Self-assembling influenza nanoparticle vaccines drive extended germinal center activity and memory B cell maturation. *JCI Insight* **5**, doi:10.1172/jci.insight.136653 (2020).

218 Moyer, T. J., Zmolek, A. C. & Irvine, D. J. Beyond antigens and adjuvants: formulating future vaccines. *J Clin Invest* **126**, 799-808, doi:10.1172/JCI81083 (2016).

219 Rudra, J. S., Tian, Y. F., Jung, J. P. & Collier, J. H. A self-assembling peptide acting as an immune adjuvant. *Proc Natl Acad Sci U S A* **107**, 622-627, doi:10.1073/pnas.0912124107 (2010).

220 Grenfell, R. F., Shollenberger, L. M., Samli, E. F. & Harn, D. A. Vaccine self-assembling immune matrix is a new delivery platform that enhances immune responses to recombinant HBsAg in mice. *Clin Vaccine Immunol* **22**, 336-343, doi:10.1128/CVI.00714-14 (2015).

221 Bachmann, M. F. & Jennings, G. T. Vaccine delivery: a matter of size, geometry, kinetics and molecular patterns. *Nat Rev Immunol* **10**, 787-796, doi:10.1038/nri2868 (2010).

222 Kovacsovics-Bankowski, M., Clark, K., Benacerraf, B. & Rock, K. L. Efficient major histocompatibility complex class I presentation of exogenous antigen upon phagocytosis by macrophages. *Proc Natl Acad Sci U S A* **90**, 4942-4946, doi:10.1073/pnas.90.11.4942 (1993).

223 Jones, J. C., Settles, E. W., Brandt, C. R. & Schultz-Cherry, S. Virus aggregating peptide enhances the cell-mediated response to influenza virus vaccine. *Vaccine* **29**, 7696-7703, doi:10.1016/j.vaccine.2011.07.133 (2011).

Appendix

JCI insight

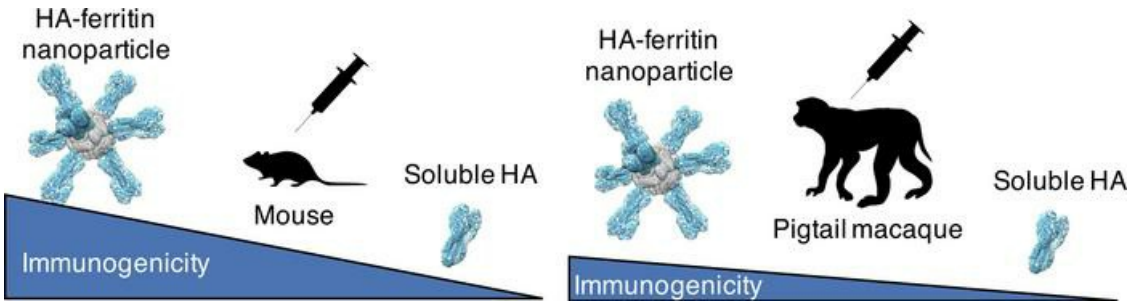
Self-assembling influenza nanoparticle vaccines drive extended germinal center activity and memory B cell maturation

Hannah G. Kelly, … , Stephen J. Kent, Adam K. Wheatley

JCI Insight. 2020;5(10):e136653. https://doi.org/10.1172/jci.insight.136653.

Research Article | Immunology | Vaccines

Graphical abstract



Find the latest version:

https://jci.me/136653/pdf

JCI insight

RESEARCH ARTICLE

Self-assembling influenza nanoparticle vaccines drive extended germinal center activity and memory B cell maturation

Hannah G. Kelly,[1,2] Hyon-Xhi Tan,[1] Jennifer A. Juno,[1] Robyn Esterbauer,[1,2] Yi Ju,[2,3] Wenbo Jiang,[1] Verena C. Wimmer,[4] Brigette C. Duckworth,[5] Joanna R. Groom,[5] Frank Caruso,[2,3] Masaru Kanekiyo,[6] Stephen J. Kent,[1,2,7] and Adam K. Wheatley[1,2]

[1]Department of Microbiology and Immunology, University of Melbourne, The Peter Doherty Institute for Infection and Immunity, Melbourne, Victoria, Australia. [2]ARC Centre of Excellence in Convergent Bio-Nano Science and Technology and [3]Department of Chemical Engineering, University of Melbourne, Parkville, Victoria, Australia. [4]Centre for Dynamic Imaging and [5]Division of Immunology, Walter and Eliza Hall Institute of Medical Research, Department of Medical Biology, University of Melbourne, Parkville, Victoria, Australia. [6]Vaccine Research Center, National Institute of Allergy and Infectious Diseases (NIAID), NIH, Bethesda, Maryland, USA. [7]Melbourne Sexual Health Centre and Department of Infectious Diseases, Alfred Hospital and Central Clinical School, Monash University, Melbourne, Victoria, Australia.

Protein-based, self-assembling nanoparticles elicit superior immunity compared with soluble protein vaccines, but the immune mechanisms underpinning this effect remain poorly defined. Here, we investigated the immunogenicity of a prototypic ferritin-based nanoparticle displaying influenza hemagglutinin (HA) in mice and macaques. Vaccination of mice with HA-ferritin nanoparticles elicited higher serum antibody titers and greater protection against experimental influenza challenge compared with soluble HA protein. Germinal centers in the draining lymph nodes were expanded and persistent following HA-ferritin vaccination, with greater deposition of antigen that colocalized with follicular dendritic cells. Our findings suggest that a highly ordered and repetitive antigen array may directly drive germinal centers through a B cell–intrinsic mechanism that does not rely on ferritin-specific T follicular helper cells. In contrast to mice, enhanced immunogenicity of HA-ferritin was not observed in pigtail macaques, where antibody titers and lymph node immunity were comparable to soluble vaccination. An improved understanding of factors that drive nanoparticle vaccine immunogenicity in small and large animal models will facilitate the clinical development of nanoparticle vaccines for broad and durable protection against diverse pathogens.

Introduction

Engineered nanoparticles present an exciting opportunity in vaccine design allowing for the precise manipulation of antigen presentation and targeting. The immune system has evolved to respond strongly to repetitive antigens displayed on nanoscale structures (1–1000 nm), the size range of most infectious microorganisms (1). Previously, spontaneously forming virus-like particles have been harnessed for highly protective vaccines against human papilloma virus, hepatitis B, and hepatitis E (2). However, because only selected pathogens spontaneously form virus-like particles, engineered nanoparticles offer an opportunity to combine the potent vaccine immunogenicity of virus-like particles with a favorable safety profile for human use.

Engineered nanoparticles carrying vaccine antigens have demonstrated superior immunogenicity over traditional subunit and whole-organism vaccines in experimental disease models of HIV (3), malaria (4), respiratory syncytial virus (5), and tuberculosis (6). For influenza, the self-assembling ubiquitous iron storage protein ferritin has been engineered into protein nanoparticle vaccines, consisting of a ferritin core with 8 trimeric influenza hemagglutinin (HA) spikes on the surface, termed HA-ferritin (7). Vaccination with HA-ferritin in mice and ferrets resulted in serum antibodies of greater magnitude, potency, and breadth compared with those elicited by the licensed inactivated influenza virus vaccine.

Conflict of interest: The authors have declared that no conflict of interest exists.

Copyright: © 2020, American Society for Clinical Investigation.

Submitted: January 22, 2020
Accepted: April 15, 2020
Published: May 21, 2020.

Reference information: *JCI Insight*. 2020;5(10):e136653. https://doi.org/10.1172/jci.insight.136653.

Prototypic candidate vaccines of this kind have now been evaluated in human phase I clinical trials (ClinicalTrials.gov NCT03186781 and NCT03814720). However, the immune mechanisms that underpin the enhanced immunity of nanoparticle-based vaccine platforms are poorly defined (8). Previous studies have demonstrated that compared with monomeric antigens, nanoparticle loading results in improved antigen drainage to lymph nodes (LNs) (9), increased uptake and presentation by follicular dendritic cells (FDCs) (10), and greater induction of follicular helper T cells (T_{FH} cells) (11) and germinal center (GC) responses (9). Recently, the dense glycosylation of HIV envelope antigens displayed on a ferritin nanoparticle was shown to augment immunogenicity through innate recognition via the mannose-binding lectin (MBL) pathway of complement activation (12). However, deglycosylation of the antigen, or the use of MBL-knockout mice, did not completely abrogate the enhanced immunogenicity of nanoparticle delivery, suggesting additional mechanisms contribute to immune enhancement.

In this study, we contrast immune responses to a prototypic ferritin nanoparticle displaying HA versus a formulation of free HA protein analogous to current subunit vaccines. We confirmed enhanced serum antibody titers and GC formation elicited by HA-ferritin, facilitating protective immunity against high-dose influenza challenge. High-dimensional whole-organ imaging demonstrated that antigen deposition and localization in LNs were highly dissimilar between the 2 immunogens. The effect of GC enhancement by HA-ferritin on B cell receptor (BCR) mutation and the role of T_{FH} cells were also examined. Last, we report on the immunogenicity of HA-ferritin in a nonhuman primate model by interrogation of serum antibodies and LN B cell and T_{FH} responses.

Results

Expression of ferritin-based nanoparticles displaying HA from mouse-adapted influenza strain PR8. Ferritin nanoparticles expressing HA from the mouse-adapted influenza strain A/Puerto Rico/08/1934 (PR8) were produced as previously described (7). A gene encoding the ectodomain of PR8 HA was genetically fused to the ferritin gene from *Helicobacter pylori*, expressed using mammalian cell culture and purified using affinity and size exclusion chromatography (Supplemental Figure 1, A and B; supplemental material available online with this article; https://doi.org/10.1172/jci.insight.136653DS1). Expression and self-assembly of particles were confirmed by SDS-PAGE and transmission electron microscopy (TEM) (Supplemental Figure 1, C and D). HA spikes could be visualized protruding from the ferritin core, and the estimated size of about 37 nm was confirmed. Antigenicity of the HA displayed on the ferritin nanoparticles was confirmed intact, based upon binding to monoclonal antibodies reactive against the globular head (TN1F11, 441D6, TN1B09) and stem (CR9114, C179) domains of H1N1 HA (Supplemental Figure 1E). Taken together, PR8 HA-ferritin nanoparticles self-assemble with the native trimeric influenza HA structurally intact.

HA-ferritin elicits enhanced humoral immunity versus soluble antigen. Consistent with previous reports using alternative HA antigens (7), PR8 HA-ferritin nanoparticles were highly immunogenic in mice. C57BL/6 mice were vaccinated intramuscularly with high (3.8 μg HA equivalent) or low (0.38 μg HA equivalent) doses of HA-ferritin nanoparticles or soluble HA, both adjuvanted with AddaVax. Following a single immunization, significantly higher titers of HA-specific serum antibodies were observed for both the high (~6-fold) and low vaccine doses (~32-fold) of HA-ferritin compared with controls immunized with an equivalent dose of soluble HA (Figure 1A). Notably, enhanced immunogenicity from HA-ferritin was conserved following DNA vaccination of mice (Figure 1B), suggesting antigen-loaded nanoparticles remain intrinsically more immunogenic than free antigen whether delivered as exogenous formulations or after de novo generation in vivo.

The protective efficacy of a single vaccination with HA-ferritin nanoparticles versus soluble HA was assessed using intranasal challenge of homologous (PR8) and heterologous (influenza virus A/California/07/2009; CA09) H1N1 influenza viruses (Figure 1C). A single vaccination with either high or low doses of HA-ferritin provided complete protection against low-dose (100 50% tissue culture infectious dose [$TCID_{50}$]), intermediate-dose (500 $TCID_{50}$), and high-dose challenge (2000 $TCID_{50}$) with homologous PR8 virus. In contrast, immunization with soluble HA provided inferior protection, with animals susceptible at intermediate (low-dose soluble HA group) and high (both low and high soluble HA groups) challenge doses. No evidence of cross-strain protection was observed following heterologous challenge with H1N1 CA09. Therefore, vaccination with HA-ferritin nanoparticle vaccines demonstrates superior immunogenicity, dose-sparing effect, and increased protective efficacy.

HA-ferritin vaccination drives enhanced antigen-specific GC reactions. The LNs draining the site of vaccine administration are a key site for the development of protective adaptive immune responses.

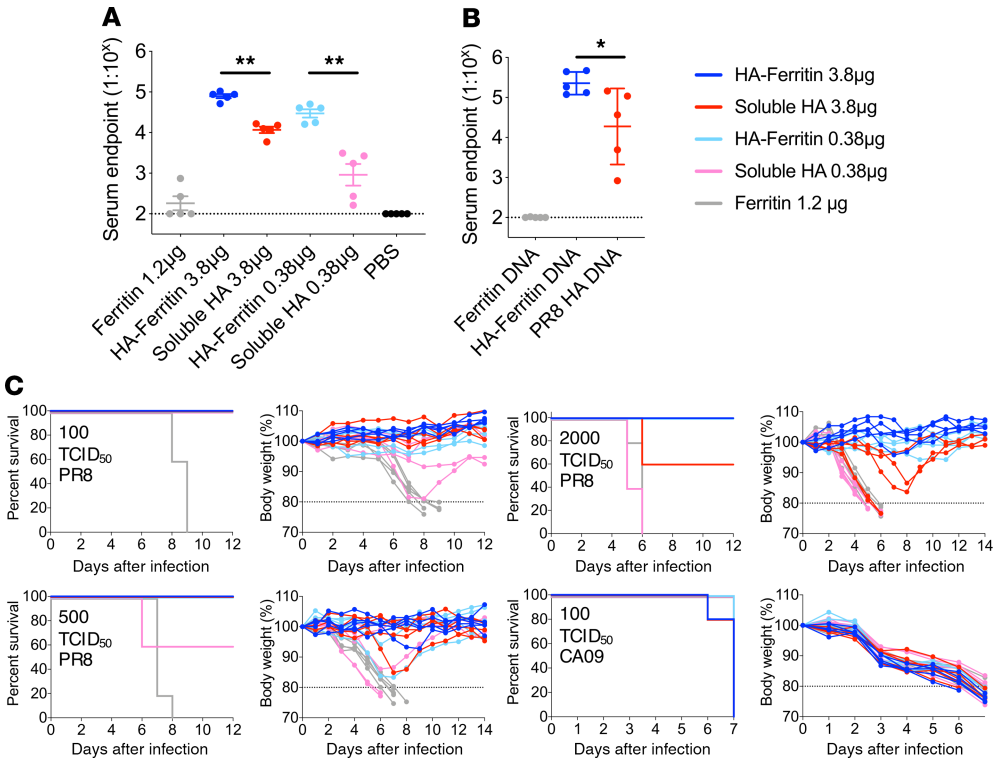


Figure 1. Vaccination with HA-ferritin nanoparticles elicits enhanced antibody titers and protective immunity. C57BL/6 mice (n = 5 mice per group) were vaccinated intramuscularly with high or low doses of HA-ferritin (5 or 0.5 μg) or a molar equivalent of soluble HA (3.8 or 0.38 μg). Control groups received ferritin alone (1.2 μg) or PBS. All vaccines except PBS were adjuvanted with AddaVax. (**A**) HA-specific serum IgG titers were measured by ELISA 14 days after vaccination. Data are representative of 1 of 2 independent experiments. The dashed line indicates detection cutoff (1:100 dilution). (**B**) HA-specific serum IgG titers 14 days after final vaccination in mice vaccinated 3 times at 14-day intervals with 100 μg DNA encoding HA-ferritin, soluble HA, or ferritin. (**C**) Body weight and survival of mice immunized once 14 days before intranasal challenge with PR8 or CA09 influenza strains. The dashed line indicates 20% weight loss. Data represent mean ± SD. *$P < 0.05$, and **$P < 0.01$, determined by a Mann-Whitney U test.

In particular, GCs facilitate somatic hypermutation and affinity maturation of antigen-specific B cells and drive the production of plasma cells secreting high-affinity antibodies. To investigate how nanoparticle vaccination affects GC induction, we first visualized draining LNs in immunized mice 14 days after intramuscular vaccination. Using the GC marker GL7, we observed extensive GC formation following HA-ferritin vaccination compared with limited GCs observed in soluble HA–vaccinated mice (Figure 2A; Supplemental Figure 2). The magnitude and longevity of GC responses in the draining LNs were assessed by flow cytometry. HA-ferritin–immunized animals displayed higher frequencies of GC B cells ($IgD^{-}B220^{+}GL7^{+}CD38^{lo}$) in both draining inguinal and iliac LNs compared with animals vaccinated with the equivalent dose of soluble HA, with these higher relative frequencies maintained over time out to 56 days postimmunization (Figure 2B; gating in Supplemental Figure 3). The antigen specificity of GC B cells was assessed using recombinant PR8 HA probes as previously described (13, 14) (representative staining in Supplemental Figure 3). At 7, 14 (Supplemental Figure 4, A and B), and 56 days after vaccination (Figure 2C), counts of PR8 HA-specific B cells in the GC were significantly or trending higher following low-dose immunization with HA-ferritin compared with soluble HA. Following high-dose vaccination, the counts of PR8 HA-specific B cells were significantly higher in HA-ferritin–vaccinated mice at day 56 but not at day 7 or 14. Therefore, immunization with HA-ferritin drives enhanced GC formation and maintenance, facilitating extended residency of HA-specific B cells within the draining LNs.

HA-ferritin immunization drives increased somatic mutation of HA-specific B cells. Extended GC reactions may facilitate increased somatic mutation of antigen-specific BCRs. To compare the ability of HA-ferritin and soluble HA vaccines to drive maturation of B cell responses, we sequenced heavy chain immunoglobulin genes from HA-specific B cells within the GCs of draining LNs (day 14 or 28 after vaccination)

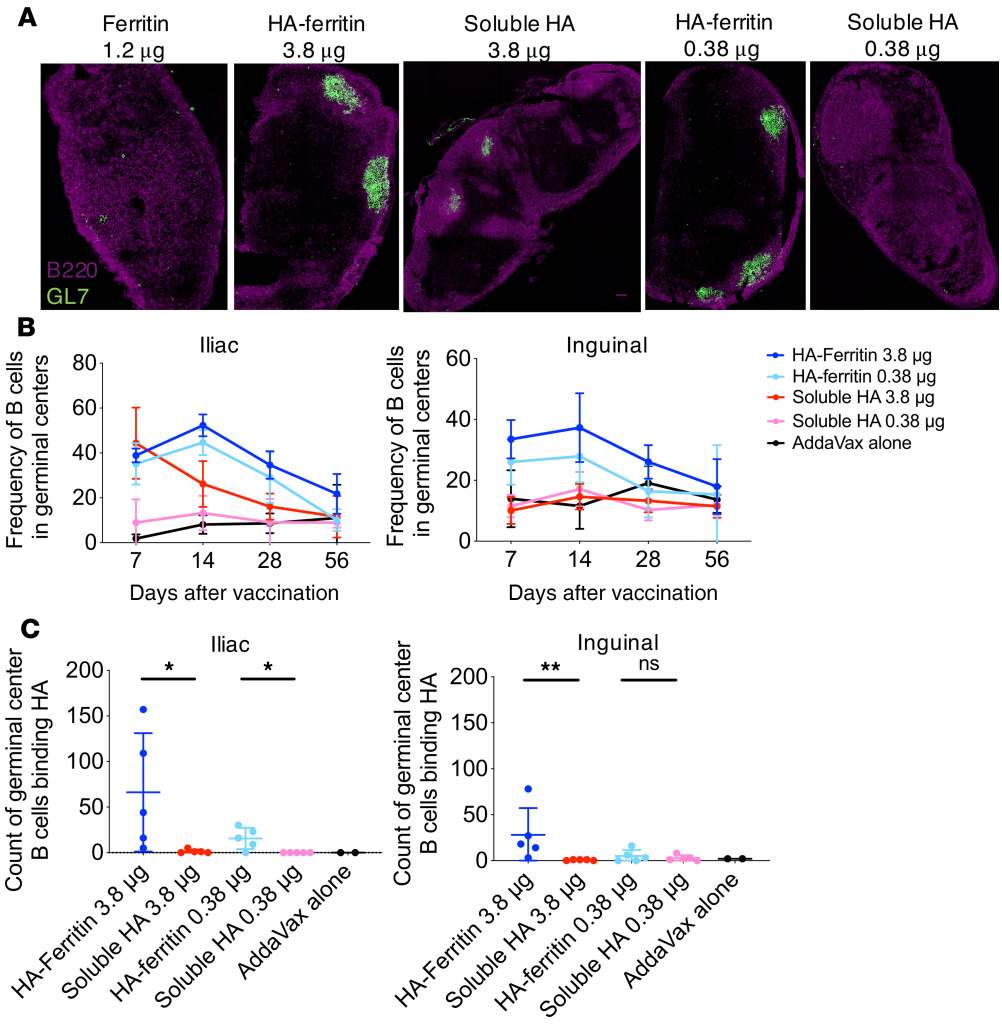


Figure 2. Augmented HA-specific GC responses in the draining LN following HA-ferritin vaccination. (**A**) C57BL/6 (n = 5 mice per group) mice were immunized with HA-ferritin (5 or 0.5 μg) or a molar equivalent of soluble HA (3.8 or 0.38 μg) or 1.2 μg ferritin alone, adjuvanted with AddaVax. After 14 days, draining inguinal LNs were sectioned and stained for GCs (GL7 shown in green and B220 shown in magenta). Images are representative of each treatment group. (**B**) Mice were vaccinated as described for **A** except for AddaVax-alone group n = 2. The proportion of IgD$^-$B220$^+$ cells expressing GL7 in draining iliac (left) and inguinal (right) LNs was quantified by flow cytometry at 7, 14, 28, or 56 days after vaccination. (**C**) The absolute count of GC B cells (B220$^+$IgD$^-$GL7$^+$) in draining iliac (left) and inguinal (right) LNs binding HA at 56 days after vaccination was measured using a probe of biotinylated PR8 HA labeled with streptavidin-PE. Data represent mean ± SD and are representative of 1 of 2 independent experiments. *P < 0.05, and **P < 0.01, determined by a Mann-Whitney U test.

and memory B cells (IgD$^-$GL7$^-$CD38$^+$) isolated from the blood and spleen (day 71 after vaccination). The extent of variable gene mutation in HA-specific B cells was comparable in GCs from both HA-ferritin– and soluble HA–vaccinated mice at both day 14 (mean 2.32% vs. 2.17%) and day 28 (3.56% vs. 3.57%) (Figure 3A). However, within the HA-specific memory B cell population, the degree of somatic mutation observed was significantly elevated following HA-ferritin immunization compared with soluble HA (mean 4.08% vs. 2.83%) (Figure 3B). Therefore, augmented GC activity following HA-ferritin immunization may facilitate increased maturation of antigen-specific B cells, potentiating both quantitative and qualitative improvements to the serological response.

Retention and focused deposition of antigen in GCs following HA-ferritin vaccination. The capacity of antigen-associated glycan to drive interaction with MBL and consequent deposition of ferritin nanoparticles into GCs was recently reported (12). Using lightsheet microscopy, we similarly observed greater accumulation of fluorescently labeled HA-ferritin (Figure 4A; Supplemental Video 1) within draining LNs compared with soluble antigen (Figure 4B; Supplemental Video 2). At 14 days after vaccination, nanoparticles were colocalized with CD35$^+$ FDCs and GCs, identified as pockets of IgD$^-$ cells surrounded by IgD$^+$ B cells. In contrast,

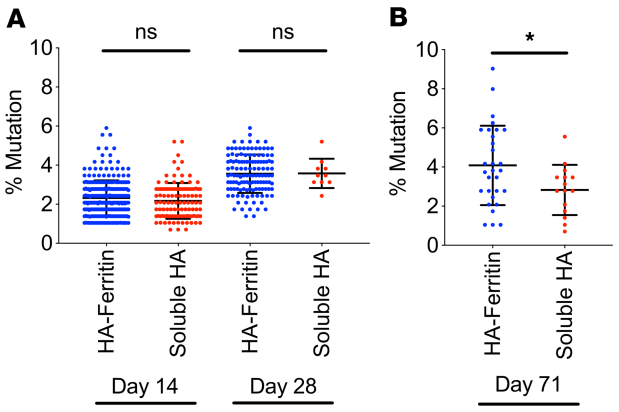


Figure 3. Increased mutation in immunoglobulin genes of memory B cells following HA-ferritin vaccination. C57BL/6 (n = 6 mice per group) mice were immunized with HA-ferritin (5 μg) or a molar equivalent of soluble HA (3.8 μg), both adjuvanted with AddaVax. (**A**) HA-specific GC B cells in draining LNs at days 14 and 28 after vaccination or (**B**) memory B cells in the spleen and blood at day 71 after vaccination were single cell sorted by FACS. Immunoglobulin heavy chain variable domain genes were amplified and sequenced. The mutation rate from germline murine variable domain sequences was determined. Data represent mean ± SD of 10–270 cells. *$P < 0.05$, determined by a Mann-Whitney U test.

GC accumulation of soluble HA antigen was not observed in mice vaccinated with soluble HA, suggesting that focused deposition of antigen underpins augmented GC function following nanoparticle immunization.

Ferritin-specific T_{FH} responses are minimal. T_{FH} cells are antigen-experienced $CD4^+$ T cells that drive the formation and maintenance of GCs (15, 16). Enhanced GC formation following HA-ferritin nanoparticle immunization could potentially be mediated via a differential capacity to recruit T cell help. In particular, T cells specific for epitopes within the *Helicobacter* ferritin core could assist in activation of HA-specific B cells via linked recognition (intermolecular help) (17). The proportion of T_{FH} cells ($CD4^+CXCR5^+PD\text{-}1^+$) in the draining iliac or inguinal LNs, as enumerated by flow cytometry, was similar in animals vaccinated with either soluble HA or HA-ferritin (Figure 5A, gating in Supplemental Figure 5), as were the absolute counts (Supplemental Figure 6). The antigen specificity of T_{FH} cells was examined using an activation-induced marker assay (18) following restimulation of LN homogenates with pools of overlapping peptides spanning either ferritin or HA proteins. Activation of T_{FH}, measured using the canonical B cell helper ligand CD154 (Figure 5B, gating in Supplemental Figure 7), or activation markers CD25 and OX40 (Figure 5C), was not observed in response to stimulation with ferritin peptides. In contrast, stimulation with HA peptides elicited T_{FH} upregulation of CD25 and OX40 in all groups vaccinated with either soluble HA or HA-ferritin. CD154 expression was increased in both high-dose groups and low-dose HA-ferritin but not low-dose soluble HA. These data suggest that linked recognition of ferritin-specific T_{FH} cells by HA-specific B cells is not significant, but increased T_{FH} function may track with the augmented immunogenicity of HA-ferritin at lower vaccine doses.

Lack of HA stem response suggests direct interaction of HA-ferritin with B cells in vivo. The capacity for HA-ferritin to drive the efficient cross-linking of HA-specific BCRs and consequent B cell activation has been established in vitro (19, 20). However, B cell signaling is difficult to directly observe in vivo, and it remains unclear if intact nanoparticles comprise a significant proportion of the immunogenic material interacting with B cells following immunization. We therefore used indirect serological measures to examine the comparative immunogenicity of the 2 domains of HA following HA-ferritin immunization: the nanoparticle-distal globular head and the nanoparticle-proximal stem domain. We hypothesized that direct interaction of B cells with intact nanoparticles displaying the HA array would favor head-specific responses, while the stem-specific responses would remain low or absent because the stem domain is less accessible by BCR binding. This is in contrast to soluble HA, where both the head and stem domains are readily accessible to BCR binding. High-dose soluble HA vaccination elicited serum IgG against stem (Figure 6A) and full-length HA (Figure 6B) detectable from 14 days postvaccination. In contrast, HA-ferritin at both high and low doses elicited negligible serum IgG production against the HA stem despite strong serological responses against full-length HA elicited from 7 days postvaccination. Therefore, HA loading onto nanoparticles mirrors the steric constraints of HA trimers on influenza virions (21) and suggests that structurally intact nanoparticles are directly recognized by B cells in vivo.

Enhanced immunogenicity of HA-ferritin is not observed in pigtail macaques. We investigated whether the enhanced immunogenicity of HA-ferritin observed in mice translated to nonhuman primate immunization models. Pigtail macaques were intramuscularly immunized with a single dose of 15 μg HA-ferritin or an equimolar amount of soluble HA, adjuvanted with AddaVax. Serum IgG responses against full-length HA were

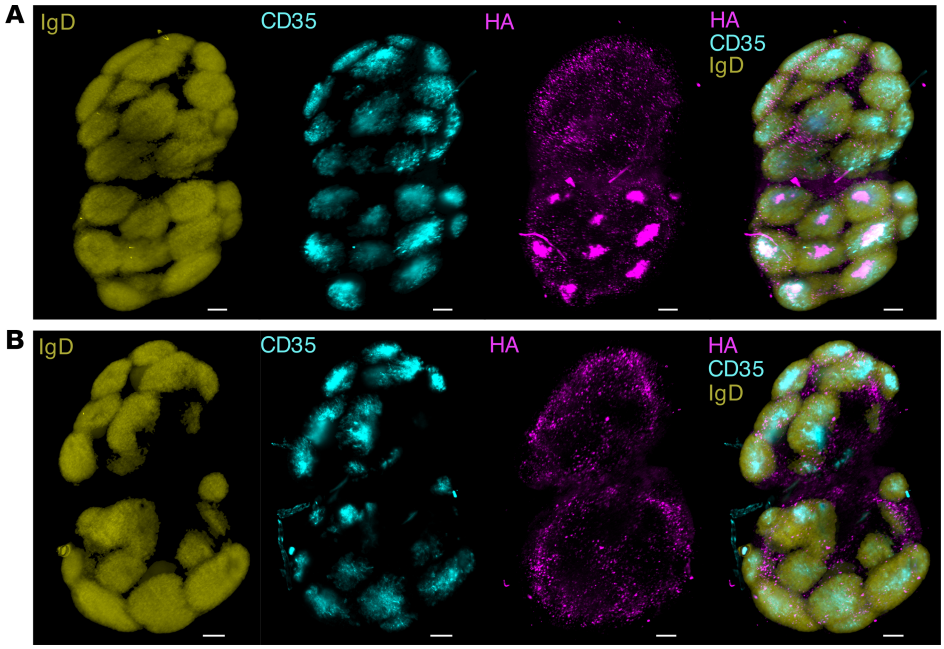


Figure 4. Increased deposition of HA-ferritin in GCs. C57BL/6 mice (n = 2 mice per group) were immunized with Alexa Fluor 647–labeled HA-ferritin (5 μg) (**A**) or a molar equivalent of Alexa Fluor 647–labeled soluble HA (3.8 μg) (**B**), adjuvanted with AddaVax. After 14 days, draining inguinal LNs were stained (IgD, to identify B cells, yellow; CD35, a marker of FDCs, blue), cleared and imaged by lightsheet microscopy. Images are maximum intensity projections of Z-stacks and are representative of each treatment group. Scale bar: 200 μm.

comparable between the 2 groups at 21 days after vaccination (Figure 7A). Stem HA antibodies were similarly low between the 2 vaccine groups (Supplemental Figure 8A). The HA inhibition (HAI) titers against PR8 virus at 21 days after vaccination were generally low, although they did appear higher in 3 of 5 HA-ferritin–vaccinated animals (Supplemental Figure 8B). T_{FH} and GC B cell responses in draining LNs were examined at 21 days postvaccination. No significant changes in the frequency of T_{FH} cells ($CD4^+CXCR5^+PD\text{-}1^+$) (Figure 7B, gating in Supplemental Figure 9) or the proportion of T_{FH} cells expressing transcription factor Bcl6 and proliferation marker Ki-67 (Figure 7C) were observed between draining LNs versus nondraining axillary LNs in either HA-ferritin or soluble HA groups. Similarly, the frequency of GC B cells ($CD20^+IgM^-IgD^-IgG^+Bcl6^+Ki\text{-}67^+$) was generally unchanged following vaccination with either HA-ferritin or soluble HA (Figure 7D, gating in Supplemental Figure 10). Notably, HA-specific GC B cells were detected in the draining LNs of 3/5 animals vaccinated with HA-ferritin versus 0/5 animals immunized with soluble HA (Figure 7E, representative staining in Supplemental Figure 10). Overall, while a proportion of pigtail macaques showed increased frequencies of HA-specific GC B cells upon HA-ferritin immunization, we did not observe any significant enhancement in serum IgG, GC, or T_{FH} responses compared with animals vaccinated with soluble HA.

Discussion

Numerous nanoparticle-based vaccines are currently in clinical development as improved immunization platforms against infectious diseases (reviewed in ref. 8). However, the precise immune mechanisms underpinning the enhanced immunogenicity of many particulate vaccines remain unclear. Previously, self-assembling HA-ferritin nanoparticles were shown to augment neutralizing and cross-reactive antibody responses against influenza virus in ferret and mouse models (7). Similarly, we find ferritin nanoparticle display of HA from PR8 dramatically increased HA-specific serum antibody titers and consequent protective efficacy in mice compared with immunization with free HA equivalents. In addition, we demonstrate augmented and longer-lasting GC reactions within draining LNs, focused deposition of antigen in GCs of draining LNs, and greater BCR mutation in memory B cells following HA-ferritin immunization but no improvement in HA-specific T_{FH} responses. The improved serological outcomes elicited by ferritin nanoparticle vaccines in our murine model appear linked to the capacity to drive greater involvement of antigen-specific B cells in GCs, facilitating improved affinity maturation and/or expanded plasma cell differentiation.

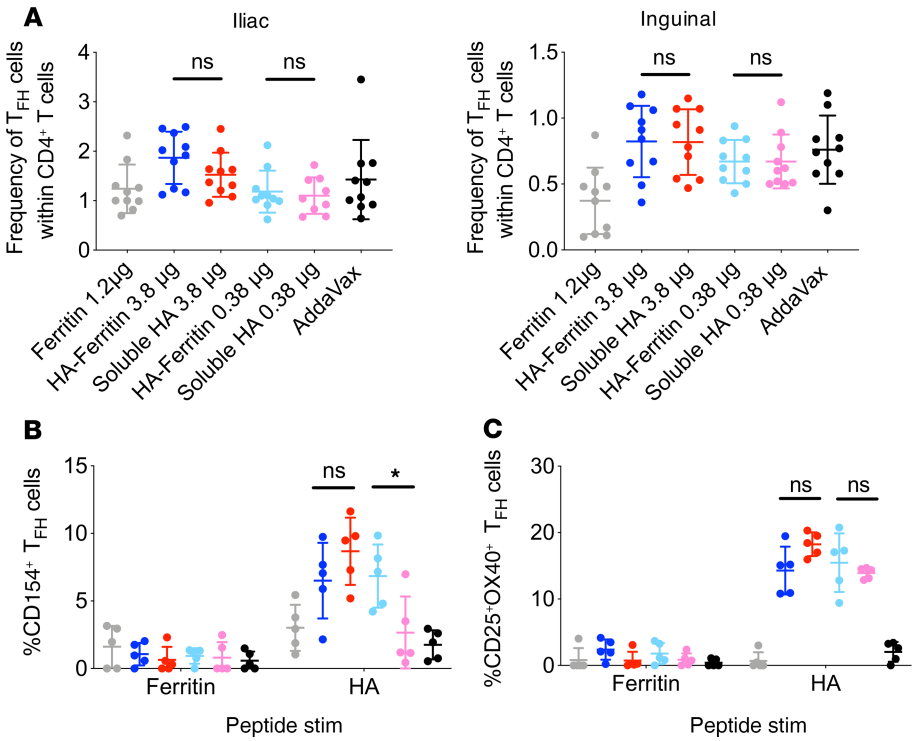


Figure 5. Superior immunity of HA-ferritin is not driven by ferritin-specific T_{FH} cells. (**A**) C57BL/6 (n = 10 mice per group) mice were immunized with HA-ferritin (5 or 0.5 μg) or a molar equivalent of soluble HA (3.8 or 0.38 μg), or 1.2 μg ferritin alone, adjuvanted with AddaVax. Fourteen days following vaccination, draining iliac (left) and inguinal (right) LNs were harvested. The proportion of T_{FH} cells (identified as $CXCR5^+PD\text{-}1^+$) within the $CD4^+$ T cell population was determined by flow cytometry. Data shown are combined from 2 independent experiments. Fourteen days after mice were vaccinated as in **A**, inguinal and iliac LNs were harvested and pooled for each mouse (n = 5 mice per group). Lymph node suspensions were cultured for 18 hours with pools of overlapping peptides spanning HA or ferritin proteins (final concentration of each peptide, 2 μg/mL) or DMSO alone. Antigen specificity was determined by the proportion of T_{FH} cells positive for ligand CD154 (**B**) or activation markers ($CD25^+OX40^+$) (**C**) following subtraction of DMSO background. Data represent mean ± SD. *$P < 0.05$, determined by a Mann-Whitney U test.

Critically, the heightened immunogenicity imparted by HA-ferritin was not recapitulated in immunized nonhuman primates, highlighting the potential technical and immunological complexities when extrapolating data from murine studies to higher-order primate models.

Other studies have reported increased GC activity following nanoparticle vaccination (10, 12, 22). A number (or combination) of discrete mechanisms could contribute to this effect. The high antigenic density and particulate nature of nanoparticle vaccines can facilitate increased antigen delivery to draining LNs following immunization, increasing both spatial and temporal opportunities for activation of naive B and T cells and the initiation of GC reactions. Coating with natural IgM (9, 23) or complement activation via classical (24), alternative (25), and MBL (12) pathways can increase retention of nanoparticles by GC-resident FDCs. Here, we showed concentration of HA-ferritin in draining LNs with GC-resident FDCs, which we failed to detect for soluble HA. Previously, glycosylation patterns on ferritin-based nanoparticles were shown to be critical for immunogenicity and concentration in GCs (12). However, complete deglycosylation of ferritin particles reduced the serum IgG response by only 2- to 3-fold, suggesting other factors are also important. In the present study, both soluble HA and HA-ferritin were expressed using the same mammalian Expi293 cells, presumably allowing comparable glycosylation patterns. Further, that the superior immunogenicity of HA-ferritin over soluble HA is maintained following DNA vaccination suggests factors beyond glycosylation are likely to contribute.

The activity of antigen-specific T_{FH} cells could contribute to augmented GC function. We find that despite increased frequencies of GC B cells following HA-ferritin vaccination, the proportion of T_{FH} cells was comparable after vaccination with either HA-ferritin or soluble HA antigen. This is consistent with other reports using ~40-nm self-assembling protein nanoparticles (12) and ~25-nm virus-like particles (26)

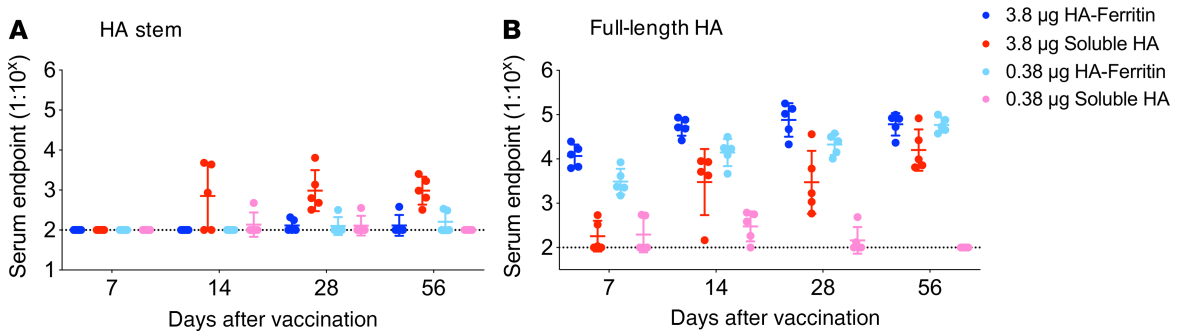


Figure 6. HA-stem response hindered by particulate display of antigen. C57BL/6 mice (n = 5 mice per group) were vaccinated intramuscularly with high or low doses of HA-ferritin (5 or 0.5 μg) or a molar equivalent of soluble HA (3.8 or 0.38 μg). All vaccines were adjuvanted with AddaVax. Serum IgG titers against stem HA (**A**) or full-length HA (**B**) were measured by ELISA at 7, 14, 28, or 56 days after vaccination. Data represent mean ± SD and are representative of 1 of 2 independent experiments. The dashed line indicates detection cutoff (1:100 dilution).

but in contrast to the T_{FH} expansion observed following vaccination with antigen conjugated to ~200-nm lipid vesicles (11, 22) or 130-nm synthetic poly(lactic-co-glycolic acid) particles (4). In terms of specificity, we detected few T_{FH} cells specific for the *Helicobacter* ferritin core, suggesting that linked recognition of ferritin plays a small or no role in supporting increased HA-specific B cell responses following immunization with HA-ferritin in our model. In response to HA peptides, expression patterns of activation markers CD25 and OX-40 were largely consistent between vaccine groups, while CD154 expression was substantially higher following low-dose HA-ferritin vaccination compared with soluble HA. Costimulatory molecule CD154 (CD40L) directly engages CD40 on B cells, promoting maintenance of established GC responses (27). Therefore, at low doses, HA-ferritin vaccines may maintain a superior capacity to promote T_{FH} activation and the provision of T cell help.

Multimeric BCR engagement via direct interaction of intact nanoparticles with B cells contributes to potent B cell activation and consequent GC differentiation (28). The ability of HA-ferritin nanoparticles to potently stimulate BCR cross-linking in vitro has previously been demonstrated using engineered B cell lines expressing HA-specific BCR (19, 29), an effect not observed with free HA protein alone (20). However, BCR engagement and signaling are difficult to demonstrate in vivo, as is determining that antigen-loaded nanoparticles are conformationally intact upon presentation to B cells in draining LNs. As an indirect measure of this, we assessed the comparative immunogenicity of the 2 domains of HA, the globular head comprising the trimer apex and the C-terminal stem domain. We find in comparison with free HA trimers, epitopes in the HA stem are poorly targeted in the polyclonal antibody response following HA-ferritin immunization. This is consistent with other studies where HIV envelope (Env) antigen loaded onto nanoparticles sterically blocks epitopes located proximal to the nanoparticle surface, reducing antigenicity in vitro (30) and immunogenicity in vivo (30, 31). In the present study, the serological evidence indirectly suggests that naive B cells are primed by intact nanoparticles in vivo. Further in-depth interrogation of nanoparticle–B cell interactions in LNs is warranted, likely requiring the use of technologies such as Nur77-EGFP transgenic mice (32) or similar as sensors of BCR signaling in vivo. In the case of influenza vaccination, a reduced immune response to the highly conserved HA stem may limit the potential of a nanoparticle as a "universal" vaccine. This necessitates creative solutions to antigen display, such as nanoparticles displaying only stabilized stem (29).

Although ferritin-based nanoparticle vaccines are highly protective in rodent models (7), there have been few studies that have advanced into large and/or outbred animal models. HA-ferritin conferred greater protection than standard trivalent inactivated vaccines (TIVs) in a ferret model of influenza infection, although the antigenic integrity and glycosylation of HA in TIV are unclear (7). There are mixed results in the context of HIV. Ferritin nanoparticles displaying HIV Env trimers do appear more immunogenic than soluble trimers in rabbits immunized using a DNA prime-protein boost approach, though less pronounced compared with mice (33). However, alternative Env immunogens (ConM SOSIP) on ferritin show no advantage over soluble trimers in terms of serum antibody induction in rabbits (30), although there is some evidence of increased early antibody responses following priming (34). HIV-ferritin nanoparticles are clearly immunogenic in rhesus macaques (34) although lacking a direct comparison to soluble protein. Immunization of cynomolgus macaques with ferritin nanoparticles displaying Epstein-Barr virus antigen shows superior immunogenicity compared with the soluble antigen counterpart (35, 36).

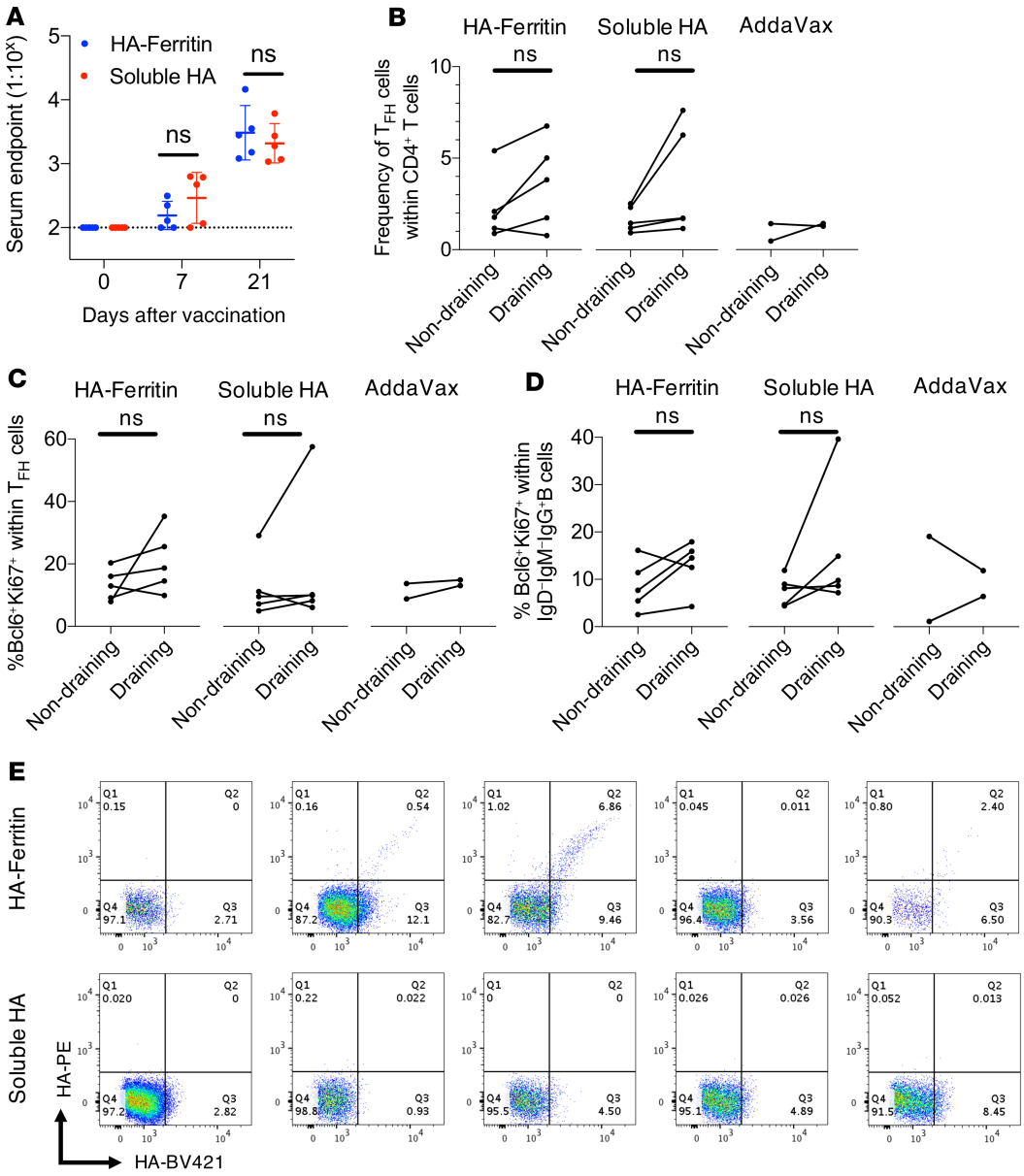


Figure 7. Enhanced immunogenicity of HA-ferritin over soluble HA does not translate to nonhuman primates. Pigtail macaques (n = 5) were vaccinated once intramuscularly with HA-ferritin (15 μg) or a molar equivalent of soluble HA (11.25 μg), both adjuvanted with AddaVax. A control group received AddaVax alone (n = 2). (**A**) Serum IgG titers against HA were measured by capture ELISA at 0, 7, and 21 days after vaccination. The dashed line indicates detection cutoff (1:100 dilution). Data represent mean ± SD. (**B**) At day 21, draining and nondraining LNs were harvested. The proportion of T_{FH} cells (identified as $CXCR5^+PD\text{-}1^+$) within $CD4^+$ T cells and (**C**) their expression of transcription factor Bcl6 and proliferation marker Ki-67 were determined. (**D**) The proportion of $CD20^+IgM^-IgD^-IgG^+$ B cells involved in LN GCs (identified as $Bcl6^+Ki\text{-}67^+$). (**E**) Flow cytometry plots showing HA specificity of these GC B cells in draining LNs measured using dual probes of biotinylated PR8 HA labeled with streptavidin-fluorophores. Data collected from 1 experiment. Analyzed using a Mann-Whitney U test (**A**) or Wilcoxon's matched-pairs signed-rank test (**B**–**D**).

While the differences in antigen-binding, serum antibody titers are minor, the neutralizing capacity of antibodies are vastly different, even in the context of preexisting immunity. In the present study, serum antibody titers against HA were comparable in soluble- and nanoparticle-vaccinated macaques, although HAI titers appeared modestly higher in HA-ferritin–vaccinated animals, possibly indicative of some qualitative improvements in the serological response. However, frequencies of GC B cells and T_{FH} cells in macaque LNs were consistent between HA-ferritin– and soluble HA–immunized animals, in sharp contrast to the highly reproducible and pronounced enhancement of GC activity seen in mice.

A number of factors could contribute to the divergent responses to HA-ferritin vaccines observed in our studies using mice and macaques. First, the pigtail macaques used in this study are an outbred population and express polymorphic MHC, BCR, and FcR alleles with unknown influences on vaccine immunogenicity. In humans, heterogeneity in MHC-II molecules that present influenza-derived peptides results in variable immunity against influenza (37). Similarly, we previously established the differential immunogenicity of the HA stem domain in BALB/c versus C57BL/6 mice may be partially a function of distinct MHC-II genetics (14). Increasing experimental group sizes in outbred animals may be necessary to observe statistically significant differences. However, given the significant costs and logistical challenges of nonhuman primate studies, these questions may ultimately best be answered by detailed analysis from human clinical trials either planned or underway (ClinicalTrials.gov NCT03186781, NCT03814720).

Second, the mechanisms of innate cell recognition of HA-ferritin in primates need further clarification. In mice, the immunogenicity of ferritin nanoparticles displaying viral antigens was recently reported to be heavily influenced by MBL recognition of glycosylated antigen (12). However, in humans, MBL is highly polymorphic, with 23 known MBL haplotypes (38), correlating with 1000-fold variations in serum MBL concentration (39). In contrast to MBL-knockout mice, which are more susceptible to influenza (40), *S. aureus* (41), and nematode (42) infections, adult humans with MBL deficiency do not suffer from increased morbidity or mortality from infectious diseases (43), illustrating potential redundancy in innate immune pathways in humans. Higher-order primates, including macaques, express the same MBL-2 gene as humans but lack polymorphisms and express MBL-1, a pseudogene in humans (44). It is therefore currently unclear if the dominant role of MBL, or other critical pathways of innate immune recognition modulating nanoparticle vaccine immunogenicity in mice, is recapitulated in some or all primate species.

Third, the dose and timing of vaccination and experimental assessment may contribute to apparent vaccine immunogenicity between species. In the present study, macaques received a 15-μg HA-equivalent dose, equal to the dose delivered in human seasonal influenza vaccinations. However, given macaques are naive whereas humans has extensive preexisting immunity, it is unclear if differential outcomes between soluble and nanoparticle delivery may have become apparent with higher dose immunizations or after assessment at alternative time points given cell metabolism and proliferation in macaques are slower than in mice (45). Alternatively, booster immunization may be required to more sensitively detect the differential immune outcomes of HA-ferritin versus soluble HA or could further be enhanced by modifying antigen delivery duration through osmotic pumps or escalating doses, which has been shown to enhance the magnitude and quality of GC and T_{FH} responses in rhesus macaques (46). At a technical level, we note that complex lymphatic drainage patterns and clustering of LNs make accurate identification of the principal antigen draining node problematic in macaques, resulting in an underestimation of the immune readout. In rhesus monkeys, nanoparticle vaccination in the deltoid muscle drains only sporadically to the axillary LNs, while subcutaneous administration showed more consistent drainage to the axillary LNs (47), potentially allowing for more accurate quantification of GC responses in future trials.

In summary, our data suggest that within mice, increased LN deposition of HA-ferritin, and likely heightened BCR cross-linking in vivo, can drive extended GC activity that increases the quantity and quality of protective serum antibody responses. However, in nonhuman primates similarly immunized, we see no systemic enhancement of immunogenicity of a ferritin-based influenza vaccine, suggesting important unresolved differences exist between rodent and primate models of immunization. A greater mechanistic understanding into nanoparticle vaccine recognition by innate and adaptive immunity, nanoparticle vaccine trafficking and deposition in vivo, and any relevant differences that exist between animal immunization models is required to clarify the potential of nanoparticle platforms as next-generation human vaccines for influenza and other important pathogens.

Methods

Design and expression of ferritin nanoparticles. The development of recombinant ferritin and HA-ferritin nanoparticles was previously described in detail (7). Briefly, a gene encoding the ectodomain of HA from A/Puerto Rico/08/1934 modified with a Y98F substitution to eliminate sialic acid binding was fused to a modified gene encoding *H. pylori* nonheme iron–containing ferritin (GenBank NP_223316) using a Ser-Gly-Gly linker. This fusion construct was subcloned into a mammalian expression vector. DNA was purified using EndoFree Plasmid Mega Kit (QIAGEN). Ferritin and HA-ferritin nanoparticles were expressed by transient transfection of Expi293F (Life Technologies, Thermo Fisher Scientific) suspension cultures

insight.jci.org https://doi.org/10.1172/jci.insight.136653

and purified using ion exchange chromatography with HiTrap Q HP column (GE Healthcare) or lectin *Galanthus nivalis* agglutinin (EY Laboratories, Inc.), respectively. Nanoparticle preparations were further purified using size exclusion chromatography using Superose 6 PG XK 16/70 column (GE Healthcare), with correct expression confirmed by SDS-PAGE.

Transmission electron microscopy. Purified nanoparticles were negatively stained with 1% uranyl acetate (Polysciences) in Milli-Q water (MilliporeSigma), and TEM images were recorded on a FEI Tecnai TF20 instrument with an operation voltage of 200 kV.

Antigenicity ELISA. MaxiSorp plates (Nunc) were coated overnight with the purified nanoparticles. After blocking with 5% skim milk powder in PBS, serial dilutions of human mAbs (produced in-house) specific for the head or stem of HA were added. Plates were washed before adding an HRP-conjugated anti-human IgG (P0214, DAKO) at 1:30,000. Plates were washed and developed using TMB substrate (MilliporeSigma) and read at 450 nm.

HA protein synthesis and purification. Recombinant full-length (13) and stem-only (14) PR8 HA protein with ablated sialic acid binding were prepared as previously described and used as either flow cytometry probes or an immunogen. Briefly, HA genes were synthesized (GeneArt) and subcloned into mammalian expression vectors. HA protein was expressed by transient transfection of Expi293 (Life Technologies, Thermo Fisher Scientific) suspension cultures and purified by polyhistidine-tag affinity chromatography and gel filtration. For use as flow cytometry probes, proteins were biotinylated using BirA (Avidity) and stored at –80°C. Before use, biotinylated HA proteins were labeled by the sequential addition of streptavidin-conjugated to phycoerythrin (PE) (Life Technologies, Thermo Fisher Scientific) or BV421 (BD) and stored at 4°C.

Mouse immunizations and viral challenge. All mice were female C57BL/6 aged 6–8 weeks at the start of experiments. Mice were anesthetized by isoflurane inhalation before infection or immunization. Groups of 5 mice were immunized with either 5 or 0.5 μg of HA-ferritin nanoparticles (corresponding to 3.8 and 0.38 μg of HA, respectively); 3.8 or 0.38 μg of soluble trimeric HA; 1.2 μg ferritin nanoparticles; 100 μg DNA plasmid encoding HA-ferritin fusion, HA or ferritin, or PBS. All immunizations were given intramuscularly into both hind quadriceps using a 29-gauge needle. All protein vaccines were formulated with AddaVax (InvivoGen) at a 1:1 ratio except PBS-only controls. Blood samples were collected by cardiac puncture 14 days after immunization and serum frozen. For viral challenge experiments, mice were intranasally instilled with 50 μL of the specified $TCID_{50}$ dose of A/Puerto Rico/08/1934 (PR8) or A/California/04/2009 (CA09). The mice were observed for clinical signs of infection and weight measurements were recorded daily.

Macaque studies. Twelve pigtail macaques (*Macaca nemestrina*) recycled from previous HIV vaccination studies were randomized for use in this study. Each experimental group contained 1 female with the remainder being male, aged between 21 and 36 months. Before any procedure the animals were anesthetized intramuscularly with ketamine. Animals were immunized in the right deltoid muscle with 1 dose of HA-ferritin (15 μg) or a molar equivalent of soluble HA (11.25 μg) formulated 1:1 v/v with AddaVax (Invitrogen, Thermo Fisher Scientific). Serial blood samples were collected and serum isolated. At necropsy 21 days after vaccination, draining and nondraining LNs were collected and homogenates were cryopreserved.

Mouse serum antibody ELISA. Overnight 2 μg/mL HA protein was coated onto MaxiSorp plates (Nunc). Plates were blocked with 5% skim milk powder in PBS before adding serially diluted mouse sera in duplicate. Plates were washed before addition of an HRP-conjugated anti-mouse IgG (474-1806, KPL) at 1:10,000 dilution. Plates were washed and developed using TMB substrate (MilliporeSigma); reaction was stopped with 0.16 M H_2SO_4 and read at 450 nm. Endpoint titers were calculated as the reciprocal serum dilution giving signal 2 times background using a fitted curve (4-parameter log regression).

Macaque serum antibody capture ELISA. Overnight 0.1 μg/mL rabbit anti-His polyclonal antibody (GenScript) was coated onto MaxiSorp plates (Nunc). Plates were blocked with 5% skim milk powder in PBS before adding His-tagged full-length or stem HA protein. Serially diluted macaque sera were added in duplicate. Plates were washed before addition of an HRP-conjugated anti-macaque IgG (1B3, Kerafast) at 1:8000. Plates were washed and developed using TMB substrate (MilliporeSigma); reaction was stopped with 0.16 M H_2SO_4 and read at 450 nm. Endpoint titers were calculated as the reciprocal serum dilution giving signal 2 times background using a fitted curve (4-parameter log regression).

Confocal microscopy. LNs were harvested into O.C.T. Embedding Compound (Tissue-Tek, Sakura Finetek) 14 days after vaccination, snap-frozen, and cryosectioned into 7-μm slices (Leica). Dried sections were fixed in acetone for 10 minutes before blocking with 5% (w/v) BSA and 2% normal goat serum. Cell staining was

insight.jci.org https://doi.org/10.1172/jci.insight.136653

performed using the following antibodies: B220 BV480 (RA3-6B2, BD), GL7 Alexa Fluor 488 (GL7, BioLegend), and CD35 BV421 (8C12, BD). Slides were mounted with ProLong Diamond Antifade Mountant (Life Technologies, Thermo Fisher Scientific). Images were recorded on a ZEISS Laser Scanning Confocal (LSM710) with 20×/0.8 NA air objective at 1 Airy unit, located at the Biological Optical Microscopy Platform at the University of Melbourne. Postprocessing of images was performed with FIJI (version 1.0).

Lightsheet microscopy. Methods are described in detail elsewhere (48). Fat-excised LNs were harvested into PLP buffer (1% paraformaldehyde, 2 mg/mL $NaIO_4$, 0.1 M lysine, 0.05 M phosphate buffer) and fixed 4–6 hours. LNs were transferred into blocking buffer containing 1% normal goat serum, 1% BSA, and 0.3% Triton X-100 in PBS and incubated overnight at room temperature (RT). LNs were then incubated 1:100 with IgD–Alexa Fluor 488 (11-26c.2a; BioLegend) and CD35 BV421 (8C12; BD) in blocking buffer for 3 days at RT. LNs were washed with PBS containing 0.2% Triton X-100 and 0.5% 1-thioglycerol for 24 hours. LNs were cleared for 24 hours at RT in 86% Histodenz (MilliporeSigma), 0.5% 1-thioglycerol, 0.1% Triton X-100, and 40% *N*-methylacetamide. The clearing solution was replaced and LNs were cleared for a further 24 hours. The cleared LNs were embedded in 2% low-melting agarose and 1:10,000 Fluoresbrite YG Calibration beads (1 μm, Polysciences) inside sawn-off 1-mL syringes and submerged in clearing solution for 3 days before imaging. The refractive index of the clearing solution was matched throughout the protocol. Nodes were imaged on a ZEISS Z.1 lightsheet microscope with a 5×/0.16 air objective. The XY resolution was 1.31 μm, the Z resolution was 5 μm, and the lightsheet thickness was 10.7 μm. Images were processed using Imaris (Bitplane).

Lymphocyte homogenates. Mouse LNs and spleens and macaque LNs were harvested into RF10 media (RPM I1640, 10% FCS, 1× penicillin-streptomycin-glutamine; Life Technologies, Thermo Fisher Scientific). Single-cell suspensions were prepared by mechanical homogenization through a 70-μm cell strainer. Mouse spleen cells and anticoagulant-collected mouse blood were then treated with Pharm Lyse (BD) to lyse red blood cells before subsequent use. Macaque LN homogenates were suspended in 90% FCS with 10% DMSO and stored in liquid N_2.

Flow cytometry detection of HA-specific murine B cells. Single-cell suspensions were stained with Aqua viability dye (Thermo Fisher Scientific) and Fc blocked with CD16/32 antibody (93; BioLegend). Cells were then surface stained with a PR8 HA probe and the following antibodies: B220 BUV737 (RA3-6B2; BD), IgD BUV395 (11-26c.2a; BD), CD45 Cy7-APC (30-F11; BD), GL7 Alexa Fluor 488 (GL7; BioLegend), CD38 Cy7/PE (90; BioLegend), streptavidin BV786 (BD), CD3 BV786 (145-2C11; BioLegend), and F4/80 BV786 (BM, BioLegend). Cells were washed twice and fixed with 1% formaldehyde (Polysciences). Flow cytometry data were acquired on a BD LSRFortessa using BD FACSDiva, analysis was performed using FlowJo v10, and statistical assessment was performed in GraphPad Prism.

Sequencing of antigen-specific antibodies and calculation of mutation rate. Murine immunoglobulin heavy chains were sequenced as previously described (49). Briefly, single-cell suspensions of lymphocytes were stained with Aqua viability dye (Thermo Fisher Scientific) and Fc blocked with CD16/32 antibody (93; BioLegend). Cells were then surface stained with a PR8 HA-PE and PR8 HA-BV421 probes and the following antibodies: IgD PerCP-Cy5.5 (11-26c2a; BD), F4/80 BV786 (BM8; BioLegend), CD3 BV786 (145-2C11; BioLegend), streptavidin- BV786 (BD), CD45 APC-Cy7 (30-F11; BD), B220 BV650 (RA3-6B2; BD), GL7 Alexa Fluor 488 (GL7; BioLegend), and CD38 PE-Cy7 (90; BioLegend). Single, class-switched, dual probe–positive GC or memory B cells were sorted into 96-well PCR plates using a BD FACSAria and stored at –80°C. mRNA was reverse-transcribed using random hexamers, and recombined heavy chain genes were amplified by nested PCR and sequenced (Macrogen). Mutations in the variable domains relative to C57BL/6 germline immunoglobulin genes were calculated using IMGT (www.imgt.org).

HAI assays. HAI assays were performed as previously described (50) using PR8 virus. Briefly, macaque immune sera were pretreated with receptor-destroying enzyme (RDE II, Denka Seiken), and HAI assays were performed using 4 hemagglutinating units per well and 1% turkey red blood cells. HAI titers are expressed as the reciprocal of the highest dilution of serum at which hemagglutination was completely inhibited. Titers less than 20 were assigned as 10.

Activation-induced marker assay to detect murine T_{FH} responses. Based on published protocols used to identify antigen-specific T_{FH} cells (18), freshly isolated LN cells were cultured in RF10 medium for 18 hours at 37°C with peptide pools (2 μg/peptide/mL) spanning *H. pylori* ferritin (GenScript) or PR8 HA (BEI Resources). Peptide pools were generated from a peptide array of 17-mers overlapping by 11 amino acids, suspended in DMSO. Anti-CD154 BV650 (MR1, BioLegend) was added during stimulation. After stimulation, cells

insight.jci.org https://doi.org/10.1172/jci.insight.136653

were recovered and stained with blue viability dye (Thermo Fisher Scientific), CD3 BV510 (145-2C11; BioLegend), CD25 BB515 (PD61; BD), PD-1 BV786 (29F.1A12; BioLegend), CXCR5 BV421 (L138D7; BioLegend), CD4 BUV737 (RM4-5; BD), OX-40 PE/Cy7 (OX-86; BioLegend), ICOS PerCP-eFluor 710 (15F9; Life Technologies, Thermo Fisher Scientific), B220 BV605 (RA3-6B2; BD), and F4/80 PE-CF594 (T45-2342; BD) before being washed, fixed, and acquired on a BD LSRFortessa using BD FACSDiva. Flow data were analyzed in FlowJo v10, and statistical assessment was performed in GraphPad Prism.

Identification of antigen-specific macaque B cells and T_{FH} cell activation. To identify antigen-specific B cells and activated T_{FH} cells, defrosted LN cell suspensions were stained with PR8 HA-PE and PR8 HA-BV421 probes along with the following surface panel: CD14 BV510 (M5E2; BioLegend), CD16 BV510 (3G8; BioLegend), streptavidin BV510 (BD), Live/Dead Aqua (Thermo Fisher Scientific), CD4 BV605 (L200; BD), IgG BV786 (G18-145; BD), CXCR5 PE-Cy7 (MU5UBEE; Invitrogen, Thermo Fisher Scientific), CD20–Alexa Fluor 700 (2H7; BD), PD-1 APC Fire (EH12-2H7; BioLegend), IgD–Alexa Fluor 488 (polyclonal; Southern Biotech), IgM BUV395 (G20-127; BD), and CD3 BUV737 (SP34-2; BD). For Bcl6–Alexa Fluor 647 (IG191E/A8; BioLegend) and Ki-67 BV650 (B56; BD) staining, cells were fixed, permeabilized, and stained using the BD Transcription Factor Buffer Kit according to the manufacturer's instructions. Samples were acquired on a BD LSRFortessa using BD FACSDiva. Flow data were analyzed in FlowJo v10, and statistical assessment was performed in GraphPad Prism.

Statistics. Data are presented as mean ± SD unless otherwise stated. Statistical significance was assessed by Mann-Whitney *U* test or Wilcoxon's matched-pairs signed-rank test (Figure 7, B–D) and performed using Prism version 7 (GraphPad). *P* values less than 0.05 were considered statistically significant and marked with 1 asterisk. *P* values less than 0.01 were marked with 2 asterisks.

Study approval. Mouse studies were approved by the University of Melbourne Animal Ethics Committee (number 1714104). Macaque studies (*Macaca nemestrina*) were approved by the Commonwealth Scientific and Industrial Research Organisation Animal Health Animal Ethics Committee (number 1833).

Author contributions

HGK, HXT, JAJ, SJK, and AKW designed the study. HGK, HXT, RE, WJ, and AKW performed experiments. VCW, BCD, and JRG facilitated lightsheet microscopy. YJ and FC facilitated TEM. MK provided ferritin expression constructs and facilitated protein purification methods. HGK, HXT, SJK, and AKW wrote the manuscript. All authors read and revised the manuscript.

Acknowledgments

The authors acknowledge the facilities and the scientific and technical assistance of the Biological Optical Microscopy Platform, the University of Melbourne. We also thank the expertise of Melbourne Cytometry Platform, specifically Vanta Jameson and Sarvy Taghavi. TEM analyses were conducted using the facilities at Bio21 Advanced Microscopy Facility, the University of Melbourne. HAI assay reagents and advice were provided by Paul Whitney, World Health Organization Collaborating Centre for Reference and Research on Influenza, Melbourne, and Mingyang Wang, Department of Microbiology and Immunology, The Peter Doherty Institute for Infection and Immunity, the University of Melbourne. The following reagent was obtained through BEI Resources, NIAID, NIH: Peptide Array, Influenza Virus A/Puerto Rico/8/1934 (H1N1) Hemagglutinin Protein, NR-18973. This study was supported by the ARC Centre of Excellence in Convergent Bio-Nano Science and Technology Project CE140100036 (to SJK and FC), an NHMRC program grant APP1149990 (to SJK), and NHMRC project grants GNT1129099 and GNT1162760 (to AKW). JAJ, FC, SJK, and AKW are supported by NHMRC fellowships.

Address correspondence to: Stephen J. Kent or Adam K. Wheatley, Department of Microbiology and Immunology, Doherty Institute, 792 Elizabeth St., Melbourne, Victoria, Australia 3000. Phone 61.383449939; Email: skent@unimelb.edu.au (SJK). Phone: 61.383440764; Email: awheatley@unimelb.edu.au (AKW).

1. Gause KT, Wheatley AK, Cui J, Yan Y, Kent SJ, Caruso F. Immunological principles guiding the rational design of particles for vaccine delivery. *ACS Nano*. 2017;11(1):54–68.
2. Donaldson B, Lateef Z, Walker GF, Young SL, Ward VK. Virus-like particle vaccines: immunology and formulation for clinical translation. *Expert Rev Vaccines*. 2018;17(9):833–849.
3. Ingale J, et al. High-density array of well-ordered HIV-1 spikes on synthetic liposomal nanoparticles efficiently activate B cells.

Cell Rep. 2016;15(9):1986–1999.
4. Thompson EA, et al. TLR-adjuvanted nanoparticle vaccines differentially influence the quality and longevity of responses to malaria antigen Pfs25. *JCI Insight*. 2018;3(10):120692.
5. Marcandalli J, et al. Induction of potent neutralizing antibody responses by a designed protein nanoparticle vaccine for respiratory syncytial virus. *Cell*. 2019;176(6):1420–1431.e17.
6. Yu F, et al. Nanoparticle-based adjuvant for enhanced protective efficacy of DNA vaccine Ag85A-ESAT-6-IL-21 against Mycobacterium tuberculosis infection. *Nanomedicine*. 2012;8(8):1337–1344.
7. Kanekiyo M, et al. Self-assembling influenza nanoparticle vaccines elicit broadly neutralizing H1N1 antibodies. *Nature*. 2013;499(7456):102–106.
8. Kelly HG, Kent SJ, Wheatley AK. Immunological basis for enhanced immunity of nanoparticle vaccines. *Expert Rev Vaccines*. 2019;18(3):269–280.
9. Link A, Zabel F, Schnetzler Y, Titz A, Brombacher F, Bachmann MF. Innate immunity mediates follicular transport of particulate but not soluble protein antigen. *J Immunol*. 2012;188(8):3724–3733.
10. Hu X, et al. Immune response of a novel ATR-AP205-001 conjugate anti-hypertensive vaccine. *Sci Rep*. 2017;7(1):12580.
11. Pardi N, et al. Nucleoside-modified mRNA vaccines induce potent T follicular helper and germinal center B cell responses. *J Exp Med*. 2018;215(6):1571–1588.
12. Tokatlian T, et al. Innate immune recognition of glycans targets HIV nanoparticle immunogens to germinal centers. *Science*. 2019;363(6427):649–654.
13. Whittle JR, et al. Flow cytometry reveals that H5N1 vaccination elicits cross-reactive stem-directed antibodies from multiple Ig heavy-chain lineages. *J Virol*. 2014;88(8):4047–4057.
14. Tan HX, et al. Subdominance and poor intrinsic immunogenicity limit humoral immunity targeting influenza HA stem. *J Clin Invest*. 2019;129(2):850–862.
15. Mesin L, Ersching J, Victora GD. Germinal center B cell dynamics. *Immunity*. 2016;45(3):471–482.
16. Song W, Craft J. T follicular helper cell heterogeneity: time, space, and function. *Immunol Rev*. 2019;288(1):85–96.
17. Mitchison NA. T-cell-B-cell cooperation. *Nat Rev Immunol*. 2004;4(4):308–312.
18. Jiang W, et al. Identification of murine antigen-specific T follicular helper cells using an activation-induced marker assay. *J Immunol Methods*. 2019;467:48–57.
19. Corbett KS, et al. Design of nanoparticulate group 2 influenza virus hemagglutinin stem antigens that activate unmutated ancestor B cell receptors of broadly neutralizing antibody lineages. *mBio*. 2019;10(1):e02810-18.
20. Villar RF, et al. Reconstituted B cell receptor signaling reveals carbohydrate-dependent mode of activation. *Sci Rep*. 2016;6:36298.
21. Andrews SF, et al. Immune history profoundly affects broadly protective B cell responses to influenza. *Sci Transl Med*. 2015;7(316):316ra192.
22. Moon JJ, Suh H, Li AV, Ockenhouse CF, Yadava A, Irvine DJ. Enhancing humoral responses to a malaria antigen with nanoparticle vaccines that expand Tfh cells and promote germinal center induction. *Proc Natl Acad Sci U S A*. 2012;109(4):1080–1085.
23. Phan TG, Grigorova I, Okada T, Cyster JG. Subcapsular encounter and complement-dependent transport of immune complexes by lymph node B cells. *Nat Immunol*. 2007;8(9):992–1000.
24. Tavano R, et al. C1q-mediated complement activation and C3 opsonization trigger recognition of stealth poly(2-methyl-2-oxazoline)-coated silica nanoparticles by human phagocytes. *ACS Nano*. 2018;12(6):5834–5847.
25. Chen F, et al. Complement proteins bind to nanoparticle protein corona and undergo dynamic exchange in vivo. *Nat Nanotechnol*. 2017;12(4):387–393.
26. Liao W, Hua Z, Liu C, Lin L, Chen R, Hou B. Characterization of T-dependent and T-independent B cell responses to a virus-like particle. *J Immunol*. 2017;198(10):3846–3856.
27. Vinuesa CG, Linterman MA, Yu D, MacLennan IC. Follicular helper T cells. *Annu Rev Immunol*. 2016;34:335–368.
28. Bachmann MF, Jennings GT. Vaccine delivery: a matter of size, geometry, kinetics and molecular patterns. *Nat Rev Immunol*. 2010;10(11):787–796.
29. Yassine HM, et al. Hemagglutinin-stem nanoparticles generate heterosubtypic influenza protection. *Nat Med*. 2015;21(9):1065–1070.
30. Brouwer PJM, et al. Enhancing and shaping the immunogenicity of native-like HIV-1 envelope trimers with a two-component protein nanoparticle. *Nat Commun*. 2019;10(1):4272.
31. Brinkkemper M, Sliepen K. Nanoparticle vaccines for inducing HIV-1 neutralizing antibodies. *Vaccines (Basel)*. 2019;7(3):E76.
32. Mueller J, Matloubian M, Zikherman J. Cutting edge: an in vivo reporter reveals active B cell receptor signaling in the germinal center. *J Immunol*. 2015;194(7):2993–2997.
33. Sliepen K, et al. Presenting native-like HIV-1 envelope trimers on ferritin nanoparticles improves their immunogenicity. *Retrovirology*. 2015;12:82.
34. Sliepen K, et al. Structure and immunogenicity of a stabilized HIV-1 envelope trimer based on a group-M consensus sequence. *Nat Commun*. 2019;10(1):2355.
35. Bu W, et al. Immunization with components of the viral fusion apparatus elicits antibodies that neutralize Epstein-Barr virus in B cells and epithelial cells. *Immunity*. 2019;50(5):1305–1316.e6.
36. Kanekiyo M, et al. Rational design of an Epstein-Barr virus vaccine targeting the receptor-binding site. *Cell*. 2015;162(5):1090–1100.
37. Luckey D, Weaver EA, Osborne DG, Billadeau DD, Taneja V. Immunity to influenza is dependent on MHC II polymorphism: study with 2 HLA transgenic strains. *Sci Rep*. 2019;9(1):19061.
38. Boldt AB, et al. Phylogenetic nomenclature and evolution of mannose-binding lectin (MBL2) haplotypes. *BMC Genet*. 2010;11:38.
39. Minchinton RM, Dean MM, Clark TR, Heatley S, Mullighan CG. Analysis of the relationship between mannose-binding lectin (MBL) genotype, MBL levels and function in an Australian blood donor population. *Scand J Immunol*. 2002;56(6):630–641.
40. Chang WC, et al. Lack of the pattern recognition molecule mannose-binding lectin increases susceptibility to influenza A virus infection. *BMC Immunol*. 2010;11:64.
41. Shi L, et al. Mannose-binding lectin-deficient mice are susceptible to infection with Staphylococcus aureus. *J Exp Med*.

2004;199(10):1379–1390.
42. Carter T, et al. Mannose-binding lectin A-deficient mice have abrogated antigen-specific IgM responses and increased susceptibility to a nematode infection. *J Immunol*. 2007;178(8):5116–5123.
43. Dahl M, Tybjaerg-Hansen A, Schnohr P, Nordestgaard BG. A population-based study of morbidity and mortality in mannose-binding lectin deficiency. *J Exp Med*. 2004;199(10):1391–1399.
44. Verga Falzacappa MV, Segat L, Puppini B, Amoroso A, Crovella S. Evolution of the mannose-binding lectin gene in primates. *Genes Immun*. 2004;5(8):653–661.
45. Althaus CL. Of mice, macaques and men: scaling of virus dynamics and immune responses. *Front Microbiol*. 2015;6:355.
46. Cirelli KM, et al. Slow delivery immunization enhances HIV neutralizing antibody and germinal center responses via modulation of immunodominance. *Cell*. 2019;177(5):1153–1171.e28.
47. Havenar-Daughton C, et al. Rapid germinal center and antibody responses in non-human primates after a single nanoparticle vaccine immunization. *Cell Rep*. 2019;29(7):1756–1766.e8.
48. Li W, Germain RN, Gerner MY. Multiplex, quantitative cellular analysis in large tissue volumes with clearing-enhanced 3D microscopy (C_e3D). *Proc Natl Acad Sci U S A*. 2017;114(35):E7321–E7330.
49. von Boehmer L, et al. Sequencing and cloning of antigen-specific antibodies from mouse memory B cells. *Nat Protoc*. 2016;11(10):1908–1923.
50. Kristensen AB, et al. Antibody responses with Fc-mediated functions after vaccination of HIV-infected subjects with trivalent influenza vaccine. *J Virol*. 2016;90(12):5724–5734.